3D Evaluation of Thermal-Hydraulic Parameters and Hydrogen Distribution inside Nuclear Power Plant Containment due to LB-LOCA

By Muhammet Enis Kanik

Supervisors:
Dr. Omid Noori-Kalkhoran & Prof. Massimiliano Gei

Advisor:
Dr. Kevin Fernandes-Cosials

Thesis submitted to Cardiff University for the degree of Doctor of Philosophy

School of Engineering
Cardiff University
June 2023

Table of Contents

List of Figures

List of Tables

Acknowledgements

The author of this thesis would like to express his appreciation to the Ministry of Education of the Turkish Republic for his fully-funded PhD studentship and their generous support during his education and this thesis.

The author of this thesis would like to express his sincere gratitude to his main supervisor, Dr. Omid Noorikalkhoran, for his constructive and motivating approach during the challenging times experienced throughout the thesis period. In addition, the author would like to thank Professor Massimiliano Gei for his kind and supportive attitude and Dr. Kevin Fernandez-Cosials for sharing his wisdom and knowledge about GOTHIC simulation.

The author would like to appreciate Advance Research Computing at Cardiff (ARCCA) team at Cardiff University, especially their Senior programmer, Mr. Thomas Green, to provide high-performance computing resources and advice for this research.

The author also would like to thank Zachry Nuclear Engineering, Inc, NC, United States and their senior consultant Dr Jeffrey W. Lane for providing GOTHIC code and their generous support during the project.

List of Contributions

Papers in Referred Journals

1. Muhammet Enis Kanik, Omid Noori-kalkhoran, Kevin Fernández-Cosials, Massimiliano Gei. “Full scope 3D analysis of a VVER-1000 containment pressurization during a LB-LOCA by employing AutoCAD and GOTHIC code”.
Published In: Progress in Nuclear Energy Journal 152 (2022)
DOI: https://doi.org/10.1016/j.pnucene.2022.104376.

2. Muhammet Enis Kanik, Omid Noori-kalkhoran, Kevin Fernández-Cosials, Massimiliano Gei.“ 3D Analysis of Hydrogen Distribution and Its Mitigation Using Passive Autocatalytic Recombiners (PARs) Inside VVER-1000 Containment”
Published in: Energies Journal, MDPI publication, 2023, 16(18), 6612
DOI: https://doi.org/10.3390/en16186612

Papers in Review

3. Muhammet Enis Kanik, Omid Noori-kalkhoran, Kevin Fernández-Cosials, Massimiliano Gei. “3D analysis of spray effect on long-term depressurization of VVER-1000 containment during LB-LOCA”.
Published in: Progress in Nuclear Energy Journal (Accepted for publication)

Abstract

Containment as the last barrier of defence in depth prevents uncontrolled releases of radioactive materials to the environment. Analysing the containment stability/integrity in nuclear accidents and the reliability of engineered safety features in reducing the thermal/pressure loads on the containment is a key step in safety assessment of nuclear power plants. Moreover, combustion of generated hydrogen during an accident might pose a risk to the containment safety. 3D evaluation of thermal-hydraulic parameters and hydrogen distribution considering their mitigation methods inside a VVER-1000/V446 containment during a large-break loss of coolant accident were considered in this research. To achieve this goal, in the first step, 3D model of VVER-1000/V446 containment was built in detail by using AutoCAD. Then, the geometry of the containment has been transferred from AutoCAD to a containment analysis code, GOTHIC, and the model has been finalized. In addition, the main 3D model has also been modified to a great extent (installing 80 passive autocatalytic recombiners and locating hydrogen sources) to evaluate the performance of hydrogen removal system inside the containment on keeping the hydrogen concentration below the flammability limit. 2D profiles of relevant parameters as well as 3D temperature and average volumetric hydrogen concentration contours are presented as the outcome of this study. The results were validated against the results of final safety analysis report. In this manuscript, chapter 1 will provide basic information about key concepts in nuclear safety and introduce past works related to the topic of the study. Chapter 2 will give detailed information about the case stusy reactor studied, particularly about the containment, and explain accident considered scenarios in simulations. Chapter 3 informs about the hydrogen in nuclear power plants. Chapter 4 provide information about the modelling procedures in detail. Finally, chapter 5 will present the results and discuss the simulation outcomes.

List of Abbreviations

AOO	Anticipated Operational Occurrence
BDBA	Beyond Design Basis Accident
BWR	Boiling Water Reactor
CFD	Computational Fluid Dynamics
CPS	Control and Protection System
CSS	Containment Spray System
CVCS	Chemical and Volume Control System
DBA	Design Basis Accident
DECL	Double-Ended Cold Leg
ECCS	Emergency Core Cooling System
ECR	Emergency Control Room
ESF	Engineered Safety Feature
FA	Fuel Assembly
FSAR	Final Safety Analysis Report
HA	Hydraulic Accumulator
HPIS	High-Pressure Injection System
HRS	Hydrogen Removal System
IRWST	In-Containment Refuelling Water Storage Tank
LB-LOCA	Large Break Loss of Coolant Accident
LOCA	Loss of Coolant Accident
LP	Lumped Parameter
LPIS	Low-Pressure Injection System
LWR	Light Water Reactor
MCP	Main Circulation Pipeline
MCR	Main Control Room
NB	Nominal Diameter
NPP	Nuclear Power Plant
PAR	Passive Autocatalytic Recombiner
PSA	Probabilistic Safety Assessment
PWR	Pressurized Water Reactor
RCC	Reactor Collecting Chamber
RCP	Reactor Coolant Pump

RCS	Reactor Coolant System
RHRS	Residual Heat Removal System
RNG	Radioactive Noble Gases
RPC	Reactor Pressure Chamber
SB-LOCA	Small Break Loss of Coolant Accident
TMI-2	Three Mile Island Unit 2

CHAPTER 1

INTRODUCTION

1.1 Nuclear Safety

The starting point of the nuclear reactor era was the experiment of Fermi and his associates that achieved the first man-made self-sustaining nuclear chain reaction in the experimental reactor “Chicago Pile-1” in 1942. The research reactor used natural uranium with graphite as the neutron moderator (Allardice and Trapnell, 1946). Fermi and his team realized some safety concepts while building the world’s first nuclear reactor which were used in designing LWRs decades later (Sehgal, 2012):

- Nuclear fission reactions produce high levels of radioactivity which puts the people exposed to it at a significant risk. This meant some protective measures like shielding, remote siting and containment should be considered.
- Some systems are needed to control the operation of the reactor such as control rods to ensure safety.

Through the experiences accumulated on the operation of civilian nuclear reactors, post-accident analyses and the several large-scale separate-effect and integral-effect research facilities, nowadays, nuclear safety could be defined in the latest IAEA glossary by its three important aspects (IAEA, 2019):

I. The achievement of normal operation without any excessive exposure to the workers and any excessive amount of radioactivity released to the environment.
II. Prevention of incidents and accidents.
III. Mitigation of the accident consequences if the prevention measures could not stop the accident to occur.

In this chapter, first, the defence-in-depth concept will be introduced. Before going into details about the concept, accident terminology in nuclear power plants will be clarified. Next, two safety assessment methodologies will be clarified in detail. Then, engineered safety features (ESFs) will be explained. At the end of the chapter, the literature survey part will introduce the past studies that have been made relevant to the context of this thesis.

1.1.1 Plant States and Relevant Terminologies

Before going into details about nuclear safety, the classification of the plant states and relevant accident terminologies need to be clarified. Figure 1-1 shows the different plant states in the order in which the severity of the plant condition increases from left to right. A nuclear power plant is in normal operation, which means an operation within specified operational limits and conditions during states like startup, power operation, shutting down, refuelling, maintenance etc. Some abnormal operations that are expected to occur at least once during an operational lifetime of a plant such as loss of normal electrical power or turbine trip which are called “anticipated operational occurrences (AOOs)” in accident terminology. Those abnormal operations do not develop into accident conditions and lead to any significant damage to the important items for safety since they are anticipated in the design stage and measures are taken already to prevent them. Accident conditions are more severe than AOOs, they define a state which is the result of a more significant deviation from normal operational states, though less frequent, in comparison to AOOs. Accident conditions include design basis accidents (DBAs) and design extension conditions. DBAs are postulated events that are considered in the design stage of the plant according to established design criteria and conservative methodology. If an initiating event develops into a DBA, damage to the fuel and radioactive material release are kept within authorized limits. A beyond-design basis accident (BDBA) leads to a more severe condition than a DBA. The most serious of all the accident types in a nuclear power plant happens if an initiating event progresses beyond the design criteria, induces a significant core degradation, and turns into a severe accident (IAEA, 2019). Severe accidents are also contemplated in the design and operation of a plant, even some regulatory authorities prescribe that these accidents should be taken into account in the plant design stage (IAEA, 2000). The categorization of accident types in nuclear power plants according to severity could be seen in Figure 1-2. It should be noted that although the naming in the categorization has evolved through time by IAEA, the corresponding phenomena remain the same. The severity of the accident increases while moving towards the centre from the periphery.

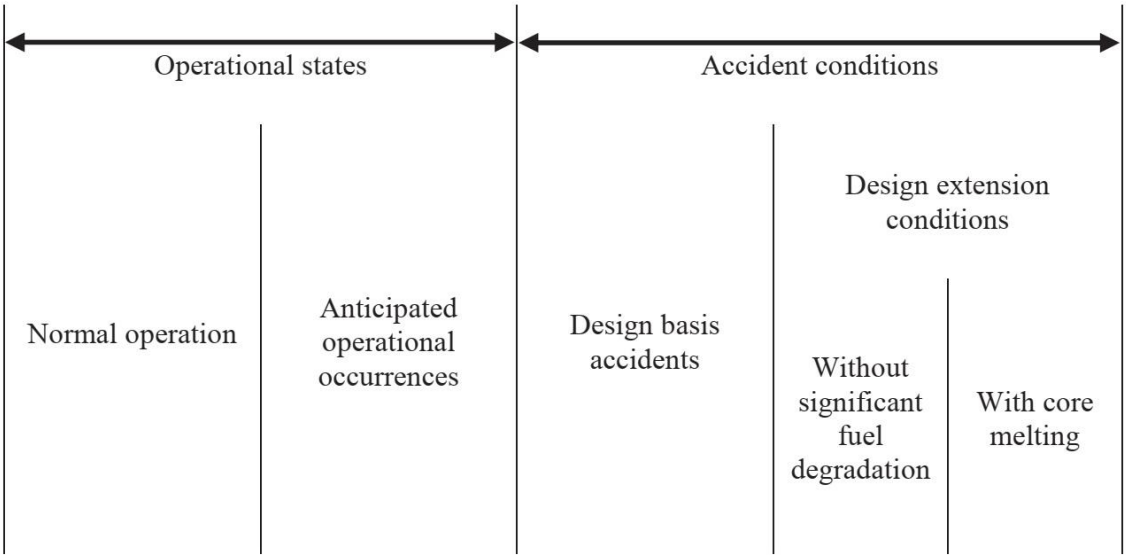

Figure 1-1. Plant States (IAEA, 2019).

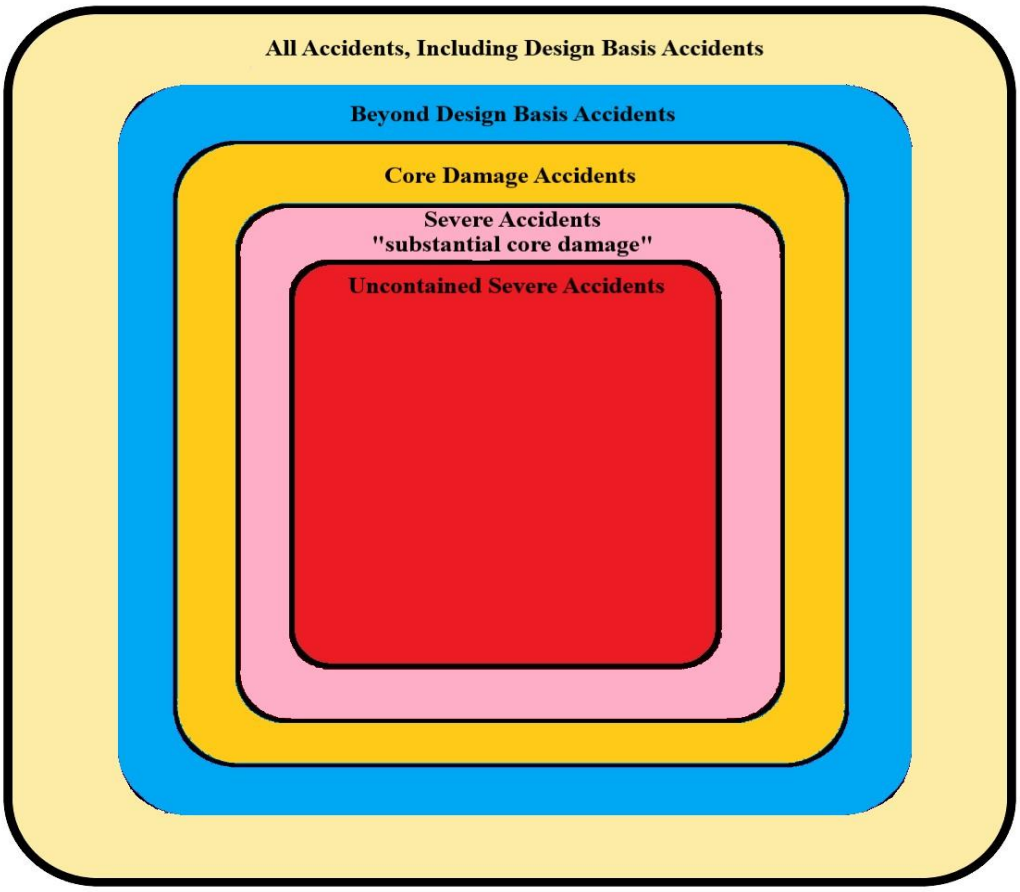

Figure 1-2. Categorization of nuclear accidents in terms of severity, reproduced from (NRC, 1997).

1.1.2 Defence-in-Depth Strategy

Defence-in-depth strategy is a key concept in nuclear safety which puts several successive barriers to confine the radioactive substances to prevent any excessive radioactive release to workers, the public and the environment. These barriers in light water reactors (LWRs) are the fuel matrix, the fuel cladding, the boundary of the reactor coolant system, and, finally, the containment (IAEA, 1996). A fuel pellet leaks only a small amount of gaseous fission products. Metal cladding confines the volatile fission products released from the pellets and some tubes could release some fission products through the cracks on the cladding. There are some filters to decontaminate the water on the reactor coolant system to reduce the radioactivity of the coolant. Leak-tight containment isolates radioactive substances effectively from the environment. The defence-in-depth strategy aims to maintain the integrity of these physical barriers from external and internal events to protect the public and the environment.

Measures are categorized into five levels of defence. The first four levels of defence aim to keep the integrity of successive barriers and limit the consequences of the failures whereas the fifth level is related to off-site emergency planning to limit exposure to external radioactive release. Although the employment of defence-in-depth strategies may be different in each country and the plant design should be considered in implementation, the approach at each level is similar.

Level 1: Prevention of abnormal operation and failures

The defence-in-depth concept, in general, consists of two important objectives to achieve. The main objective in this level is accident prevention. If the objective of the prevention could not be achieved and the initiating event progresses into a more severe condition, the goal is to limit the consequences of the accident in later stages. This level prioritizes minimizing deviations from normal operating conditions through provisions for the design of systems and components and operating personnel. Quality assurance in the design of equipment, systems and components of the plant with appropriate safety margins to ensure resistance to any operational anomaly or providing instructions and adequate training to operating personnel are included in this level of protection.

Level 2: Control of abnormal operation and detection of failures

If an initiating event deviates the plant status from normal operation to abnormal operation, the failure should be controlled by inherent plant features and systems to prevent the progression of the failure to a more severe condition. The aim is to return plant status to normal operation limits as soon as possible. Automatic control systems act as diagnostic tools to correct any operating malfunctions before reaching reactor protection limits, for example, power-operated relief valves, automatic limitation systems on coolant level, pressure and temperature and on reactor power or process control function systems that warn about failures in the control room. Periodic monitoring and testing of the quality and compliance of systems and components by taking into account design limits to detect any deterioration that might pose a risk to plant safety are also considered at this level (IAEA, 1996).

Level 3: Control of accidents within the design basis

Even though the measures are taken in the first two levels of protection to prevent any failure to progress, accidents occur. ESFs and protection systems are included in this level to keep the accident progression within the design basis limit, in other words, prevent the core damage to confine radioactive substances within the containment. ESFs are designed by considering postulated accidents that produce loads to threaten the containment and component integrity. Such postulated accidents are considered in the design stage can be break of a reactor coolant pipe or in a main steam or feedwater line or loss of control of criticality in a control rod withdrawal. Emergency operating procedures are also defined at this level to protect the barriers, notably containment, in such postulated accidents (IAEA, 1996).

Two important concepts that are considered in the design stage are redundancy and diversity, especially for the components, systems and equipment in levels 2 and 3 of protection. Redundancy is a term which means the use of two or more similar systems in parallel. If one of the systems fails, the other systems continue operating to keep the plant status as intended. Redundancy is commonly employed in nuclear power plants and is essential for safety systems such as emergency core cooling or shutdown control. Sometimes, all the components of a redundant system could stop functioning if one failure leads to another or multiple failures are triggered by the effect of a common source. For instance, several components of the same detector type might fail to the same thermal stress during a loss of coolant accident (LOCA). This is called a common-mode failure. Many common-mode failures could be predicted, and appropriate measures could be taken beforehand. However, in some cases,

they occur unexpectedly and are recognized after the failure emerged. The term called diversity is a way to minimize such failures, which is using two different and independent systems or components to achieve the same result in a nuclear power plant. An illustration of those two concepts, redundancy and diversity, could be seen in the electric power supply system of nuclear power plants. Operating instruments need direct current which is supplied by two independent storage batteries. Whereas alternating current is required to operate valves, pumps and air blowers which are supplied by the generator of the plant connected to two separate busbar sets. When the plant is shut down or the generator does not function as intended, two independent offsite power sources are also available. Whether all the onsite and offsite electrical power fails, alternating current is provided to the plant by onsite diesel generators (Glasstone and Sesonske, 1994).

The concept of defence-in-depth strategy extended further to include core melt accidents that are not considered in the design stage of the nuclear power plant after the Three Mile Island Unit 2 (TMI-2) accident in the United States in 1979. The accident and the probabilistic safety assessments (PSAs) showed that severe accidents should also be considered for plant safety. These developments resulted in an additional level of protection in the defence-in-depth strategy (Jacquemain, 2015).

Level 4: Control of severe conditions including prevention of accident progression and mitigation of the consequences of a severe accident

It is assumed that the first three levels of the defence-in-depth strategy ensure that core integrity could be achieved, and radioactive materials are confined within the core. However, there is still a risk that an accident could develop into severe plant conditions and core melting occurs. The fourth level includes provisions to decrease both the likelihood of an accident which leads to significant core damage and the magnitude of the radioactive release to the environment of such an accident to a degree as low as reasonably achievable. Both controlling the development of the accident and the mitigation of the possible consequences of the accident if it nevertheless occurs are two key objectives at this level (IAEA, 1996).

In the original designing phase of a nuclear facility (Level 1-3), severe plant conditions are not taken into account since the probability of such kinds of transients is very low. Examples that could result in severe plant conditions could be given as an extremely unlikely event such as a flood followed by a tsunami or multiple failures, such as the complete loss of all trains of a safety system. The thermal inertia of the plant allows the implementation of

additional measures and procedures by delaying the accident progression. Emergency procedures include both preventive and mitigatory measures and the objectives of these procedures are (IAEA, 1996):

- To monitor the main characteristics of plant status and maintain the reactor subcriticality.
- To recover heat removal from the core and maintain long-term core cooling.
- To ensure containment integrity by removing heat from the system and if further accident progression and consequent severe core damage could not be avoided, prevention of thermal-mechanical loads that could lead to containment failure.
- Recapturing control of the plant if it is possible and if severe accident progression could not be stopped, delaying the degradation of the plant status, and implementing on-site and off-site emergency response.

The protection of the containment is the most important part of the objective to mitigate the consequences of a severe accident in Level 4. The containment structure is designed to withstand pressure and has very strict permissible leakage rules under specific conditions. Some systems and components that are designed to maintain containment integrity under severe plant conditions such as containment coolant system, hydrogen recombiners and containment inerting system in boiling water reactors (BWRs) (to dilute the containment atmosphere with nitrogen) for preventing hydrogen explosions within the containment. Operators have a crucial role in actuating and taking decisive actions about such systems and components in emergency status. Therefore, the preparation and training of the staff for severe plant conditions are crucial for implementing the emergency procedures effectively (IAEA, 1996). The on-site emergency plan is prepared as a managerial provision to protect personnel working at the site during an accident and to mitigate the off-site consequences of that accident. When the plan is launched, emergency response teams of the plant are mobilized to contain the accident and prevent radioactive release into the environment (Jacquemain, 2015).

Level 5: Mitigation of the radiological consequences of significant external releases of radioactive materials

Even though the above-mentioned measures are expected to limit the consequences of a severe accident, radioactive releases might occur, and the defence-in-depth strategy should take into account off-site emergency plans. Off-site emergency plans include collecting and

assessing information about the exposure levels expected to occur after the release and short-term and long-term protective intervening actions. The responsible authorities take such kind of actions with the guidance of the operating organization and the regulatory body. The readiness of the organization for the implementation of both on-site and off-site emergency plans is also checked and maintained periodically (IAEA, 1996). Examples of measures that are taken at this level are evacuation, shelters, taking of potassium iodide tablets and restriction on food consumption etc. The off-site emergency plan is prepared considering the site specifications in detail (Jacquemain, 2015).

After describing each level of protection in the defence-in-depth strategy, an overview of the levels and the corresponding plant states which are explained in section 1.1.1 is illustrated in Figure 1-3. The first row demonstrates which defence-in-depth strategy is used at a particular level, prevention and mitigation of the accident are the two objectives that are mentioned here. The second row provides information about which plant state corresponds to each level and is listed from left to right according to the severity of the conditions. Normal operation is the first in the order and poses no challenge to the safety of the nuclear facility. The challenges start with AOOs and are counteracted by normal plant systems in Level 2. The third category of operational plant states corresponds to more severe challenges, including DBAs. ESFs take a supplementary role in the protection of the plant to the safety provided by normal plant systems. The fourth level is where the severity increased to a level beyond design basis and the fifth level deals with the necessity of mitigating the consequences of a radioactive release.

Through the sixth row to the end of the diagram, it could be seen that normal plant actions are adequate to respond to events encountered in the first two levels. Complex operating states demand specific procedures and features starting from level 3 and beyond, including accident management on the upper level of severity in conditions.

For example, an accident which is beyond design basis at a lesser severity degree including damage to the reactor core with extensive distortion and failure of the cladding but not melting of the fuel would release some radioactive substances into the primary coolant circuit. The consequences of this release would extend the scope of detailed provisions of emergency operating procedures in Level 3. Then, the operating staff would use the more suggestive ultimate operating procedures to mitigate the radioactive release in the primary coolant circuit to bring the plant back to a more controlled and cooled state. The procedures

would utilize normal plant systems, ESFs and special design features of the plant. Mitigation of this severe condition would be so effective that no significant release beyond confinement occurs which means there would be no need to implement off-site emergency measures (IAEA, 1999).

The relation between barriers and levels of protection in the defence-in-depth concept could be seen in Figure 1-4. The radioactive material which is at the centre of the figure is enclosed by three successive physical barriers: fuel matrix, fuel cladding and the boundary of the primary coolant system. If the objective of the first level which is the prevention of deviation from normal operation could not be achieved, then the second level steps in to respond to and control any abnormal operation to ensure the continued integrity of the first three barriers. The third level of protection is there to prevent the evolution of the failure in the second level to further into DBA with the help of ESFs and protection systems. Moreover, the prevention of the accident progression to a severe accident and preserving radioactive materials within the containment are key tasks to be fulfilled by the third level of protection. The fourth barrier is confinement, and the integrity of the last barrier is the main objective of the fourth level through accident management. Finally, the fifth level aims to mitigate the consequences of radioactive release to the environment (IAEA, 1999).

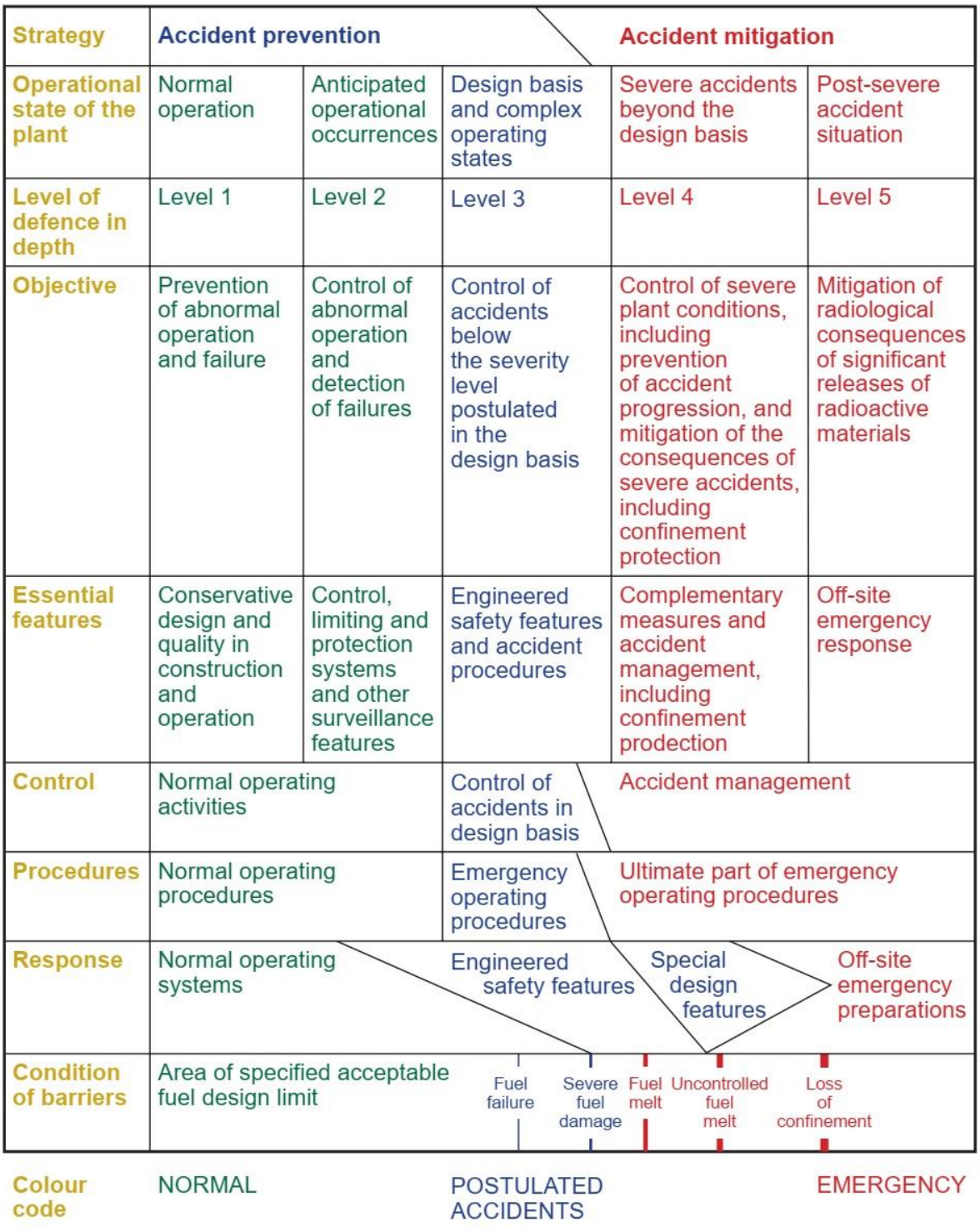

Figure 1-3. The overview of the defence-in-depth strategy (IAEA, 1999).

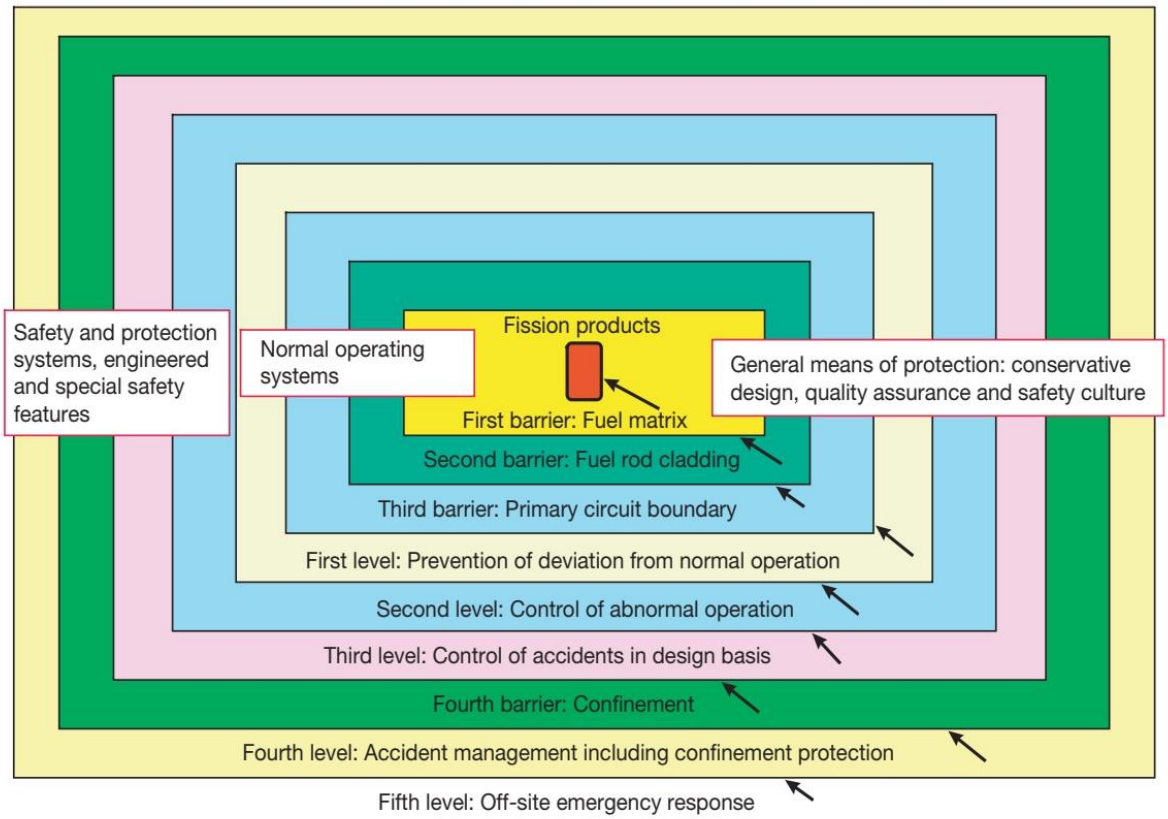

Figure 1-4. The interrelationship between barriers and levels of protection in defence-in-depth (IAEA, 2005a).

1.1.3 Safety Assessment

Safety assessment is a systematic process that is accomplished throughout the design process and the lifetime of the plant to ensure that all the relevant safety requirements are met by the proposed or actual design. Safety assessment covers formal safety analysis that includes the evaluation of the potential hazards related to the plant operation (IAEA, 2019). It includes a review of the structures, systems and components whether they could fail or not and identifies the consequences of those failures. The objective of the assessment is to investigate whether there is an underlying design weakness of the plant. The safety analysis report prepared for licensing provides information about a description of the plant sufficient for independent assessment of its safety features. The report includes detailed information about the major features of the systems, specifically systems used in cooling, containment of radioactive substances, reactor control and shutdown and ESFs. It describes the limiting set of DBAs, shows the results, and justifies the selection of the plant. If the review of the safety analysis report by regulatory authorities is approved, it demonstrates that the report responds to all safety questions sufficiently (IAEA, 1999).

Safety assessment examines possible challenges to the levels of protection in defence-in-depth. An essential element of a safety assessment is to judge whether and to what extent the safety functions (controlling the power, confining the radioactive materials, and cooling the fuel) are ensured by the levels of defence (IAEA, 1996). There are two complementary methods that have been developed to assess the safety features of the plant; deterministic and probabilistic.

1.1.3.1 Deterministic Method

An essential component of the defence-in-depth strategy is a plant design that provides an effective means to perform safety functions in normal, abnormal and accident conditions. The design is built upon deterministic assumptions and procedures without explicit consideration of probabilities. In the deterministic method, postulated events are chosen to include a range of related possible initiating events that could challenge plant safety to set design parameters for ESFs. Analyses are made to examine the effectiveness of the safety functions and whether they could control or mitigate as intended. Conservative assumptions are made at all steps of the calculations of the accidental sequences to demonstrate that the plant meets the safety requirements and that the results regarding potential radioactive releases to the environment are at acceptable levels (IAEA, 1996).

The radiological consequences of a postulated accident scenario should be investigated by taking into account the different pathways of radioactive materials to the environment (via air or underground water) and to people (by irradiation or by inhaling or ingesting the radionuclides) (IAEA, 1996).

1.1.3.1.1 Categorization of Initiating Events

An initiating event is defined as an identified event which leads to AOOs or accident conditions (IAEA, 2019). It could be seen as a “triggering agent” which leads to a progression of subsequent events resulting in a deviation from normal plant operation. Either AOO or an accident could develop from an initiating event depending on the circumstances. The development of a comprehensive list of initiating events is a complicated task due to the many possible cause that might trigger a deviation from normal operation. Therefore, the use of operational experience, engineering judgement, probabilistic and deterministic analysis of accidents are required for the task. There are different ways of grouping initiating events, each categorization provides different event lists (IAEA, 2002). Grouping by principal effect

leading to potential degradation of fundamental safety functions provides these event categories considered typically in the reactor design (NRC, 1979):

I. Increase in heat removal by the secondary system (e.g., feedwater system malfunctions that result in a decrease in feed water temperature),
II. Decrease in heat removal by the secondary system (e.g., feedwater piping break),
III. Decrease in flow rate in the reactor coolant system (e.g., reactor coolant pump shaft break),
IV. Reactivity and power distribution anomalies (e.g., a spectrum of rod ejection accidents),
V. Increase in reactor coolant inventory (e.g., inadvertent operation of emergency core cooling system (ECCS) during power operation),
VI. Decrease in reactor coolant inventory (e.g., LOCAs caused by the spectrum of postulated piping breaks within the reactor coolant pressure boundary)
VII. Radioactive release from a subsystem or component (e.g., radioactive liquid/gas waste system leak or failure),
VIII. Anticipated transients without scram (e.g., inadvertent control rod withdrawal).

Each category on the event list is typically subdivided into several more specific events, and one example of those specific events is given above next to each category. Several variations for each individual event are analysed by considering various plant operational states at the time of the accident (IAEA, 2002). Among various variations from the same set of initiating events, only the one which causes the most serious consequences is selected to be investigated (bounding case). It may also be that one accident is the worst for one consequence and another one is worse for another consequence (e.g., peak reactor pressure or peak fuel cladding temperature), in this instance, both should be studied (Petrangeli, 2006). The event sets are chosen above because they affect the state of the reactor and can lead to additional complications in operations. For example, an increase in heat removal by the secondary system in a pressurized water reactor (PWR) would lead to low temperature for the primary coolant, which would add reactivity to the core and increase power. A decrease in heat removal in the secondary system would result in higher pressure in the vessel of a PWR. A decrease in the core water inventory might be through a small-break LOCA (SB-LOCA) which complicated the transient experienced by the TMI-2 reactor and developed into an accident. The SB-LOCA can continue for a considerable time to become a complex transient.

The response and actions of the operator can change the course of the transient to a more demanding or stable state for the reactor (Sehgal, 2012).

Grouping by principal cause of the initiating events considered in the reactor design leads to the categories listed below (IAEA, 1995):

I. Reactivity anomalies due to control rod malfunctions,
II. Reactivity anomalies due to boron dilution or cold water injection,
III. Coastdown of the main circulation pumps,
IV. Loss of primary system integrity (LOCAs),
V. Interfacing systems LOCA,
VI. Loss of integrity of the secondary system,
VII. Loss of power supply,
VIII. Malfunctions in the primary systems,
IX. Malfunctions in the secondary systems,
X. anticipated transients without scram,
XI. Accidents in fuel handling,
XII. Accidents in auxiliary systems,
XIII. Accidents due to external events.

Grouping by frequency of the occurrence of an event is another way to classify initial events. A typical subdivision is given in Table 1-1. The probabilistic values given in the table are illustrative, not representing the actual calculated probabilities (outcome of Level 1 PSA). Starting with initial events that lead to AOOs, the frequency is between 10^{-2} and 1, which means occurrence is expected within a lifespan of a plant. As it can be seen by the comparison between occurrence and acceptance criteria, the severity of the consequences and the frequency of an initiating event is inversely proportional. The table ends with severe accidents which are very unlikely to occur posing a threat to the containment integrity and demanding an emergency response.

Table 1-1. Representative subdivision of events according to occurrences (IAEA, 2002).

Occurrence (1/reactor year)	Characteristics		Terminology	Acceptance Criteria
10^{-2} - 1 (Expected in the life of the plant)	Expected	Anticipated Operational Occurrences	Anticipated transients, transients, frequent faults, incidents of moderate frequency, abnormal conditions, upset conditions	No additional fuel damage
10^{-4} - 10^{-2} (Chance greater than 1% over the life of the plant)	Possible	DBAs	Infrequent incidents, infrequent faults, limiting faults, emergency conditions	No radiological impact at all or no radiological impact outside the exclusion area
10^{-6} - 10^{-4} (Chance less than 1% over the life of the plant)	Unlikely	BDBAs	Faulted conditions	Radiological consequences outside exclusion area within limits
Less than 10^{-6} (Very unlikely)	Remote	Severe accidents	Faulted conditions	Emergency response needed.

1.1.3.1.2 Acceptance Criteria

Acceptance criteria are used to judge the acceptability of the results of safety analysis. It includes (IAEA, 2002):

a) Setting numerical limits on the values of predicted parameters,
b) Setting conditions for plant states during and after an accident,
c) Setting performance requirements on systems,
d) Setting requirements on the need for actions by the operator.

Acceptance criteria are most commonly applied to licensing calculations; however, they may also be applied to the results of severe accident analyses, typically in terms of doses to the

public or the prevention of substantial damage to the containment. The range and conditions of applicability of each specific criterion must be clearly specified. Basic (high-level) acceptance criteria are usually defined as limits set by a regulatory body, for example, maximum doses to the public. Specific acceptance criteria may be developed by the designer or owner and approved by the regulatory body, or they may be set by the regulatory body itself. They are chosen to be sufficient but not necessarily to meet the basic acceptance criteria. Generally, they are used to confirm that there are adequate safety margins beyond the authorized limits to allow for uncertainties and to provide integrity of barriers in defence in depth. An example of a specific acceptance criterion would be a limit on the cladding temperature in a PWR during a LOCA (IAEA, 2002).

Acceptance criteria differ according to the conditions related to the accident, for example, the frequency of the initiating event, the reactor design and the plant conditions. Different criteria are generally needed to assess the vulnerability of individual barriers and various aspects of the accident. More stringent criteria apply for events with a higher frequency of occurrence, as indicated in Table 1-1. For example, a 'no substantial containment damage' criterion is set for all DBAs, while a 'no cladding damage' criterion would only be set for frequent accidents and AOOs. Similarly, a 'no boiling crisis' criterion is applicable for anticipated operational occurrences, while a 'cladding temperature less than 1204°C' criterion is used for LOCAs (IAEA, 2002). As a typical example for DBAs, the following criteria should be met in a design basis LOCA in an LWR by the requirement of the NRC according to 10 CFR 50.46 (NRC, 2022):

- The calculated maximum fuel cladding temperature following the accident should not exceed 1204°C.
- The calculated total oxidation of the cladding, as a result of the interaction of the hot zircaloy with steam, shall nowhere exceed 0.17 times the total cladding thickness before oxidation.
- The calculated total amount of hydrogen gas generated by the chemical reaction of zirconium in the cladding with liquid water and steam shall not exceed 1% of the hypothetical amount that would be generated if all the cladding material surrounding the fuel pellets, in other words, within the active core, were to react.
- Calculated changes in the geometry, e.g., in fuel rod diameters and spacing, shall be such that the core remains amenable to cooling.

- After the successful initial operation of the ECCS, the calculated core temperature shall be maintained at an acceptably low value for the extended period of time required by the decay of the long-lived radioactivity remaining in the core.

The temperature of the fuel rod cladding increases to a maximum in the reflood stage after a LOCA. The integrity of the cladding must be preserved so that it does not disintegrate under the thermal stress subsequently imposed when the very hot fuel rods are quenched. Embrittlement of zircaloy, which could lead to disintegration, is a function of the temperature and degree of oxidation. The first and second criteria are intended to eliminate the possibility of embrittlement and melting of the cladding (Glasstone and Sesonske, 1994).

The third criterion limits the amount of hydrogen gas produced by the zirconium-steam reaction. The aim is to keep the concentration of the hydrogen gas in the containment atmosphere well below the combustible level. Local swelling or ballooning of the cladding caused by the expansion of contained fission-product gases could affect the flow of coolant water through the core. The fourth criterion ensures that the core will remain coolable during the reflood stage despite changes in its internal geometry. The objective of the fifth criterion is self-explanatory (Glasstone and Sesonske, 1994). Calculations also should have a conservative approach and put some safety margins to meet the criteria under a DBA scenario such as (Glasstone and Sesonske, 1994):

- The calculation of stored heat in the fuel is based on a pre-accident reactor power level of 102 percent of the maximum operating power, with the highest allowed peaking factor and the lowest estimated thermal conductance between the fuel pellets and the cladding.
- Heat transfer during blowdown must be calculated using NRC-approved realistic models having an extensive experimental basis.
- The fission-product decay heat is taken to be 20 percent greater than in the American Nuclear Society standard. The calculation of the heat generation rate from the zirconium-water reaction using the Baker-Just relationship is also conservative.
- The peak cladding temperature of 1204°C refers to the hottest region of the hottest fuel rod. This criterion ensures that there would be very little damage to the reactor core.

1.1.3.1.3 Safety Margin

The safety margin of operating reactors is defined as the difference or ratio in physical units between the limiting value of an assigned parameter (exceeding the value that leads to the failure of a system or component) and the actual value of that parameter in the plant. The existence of such margins assure that nuclear power plants always operate safely in all modes of operation. The most important safety margins are related to physical barriers against the release of radioactive material, such as fuel matrix and fuel cladding (typically limited values are a departure from nucleate boiling ratio, fuel temperature, fuel enthalpy, clad temperature, clad strain, clad oxidation), reactor coolant system (RCS) boundary (pressure, stress, material condition), containment (pressure, temperature) and maximum public dose. The safety margin is usually understood as the difference in physical units between the regulatory acceptance criteria and the results provided by the calculation of the relevant plant parameter. Calculations by complex computer codes are used to judge the values of safety margins. To achieve this justification, a best estimate or a conservative approach is used. Conservative approach has a deliberate pessimism regarding selected acceptance criteria which do not have a separate treatment of uncertainties, whereas best-estimate approach is free of deliberate pessimism regarding selected acceptance criteria, more realistically depicts the plant behaviour and covers Uncertainty Analysis. The limiting value is generally referred as the safety limit or the acceptance criterion. The safety limits are limits for which the plant is designed based on accepted codes and standards. The regulatory acceptance criteria could be more restrictive or the same as safety limits depending on the national policy. For the purpose of evaluating safety margins, regulatory acceptance criteria should be taken as a reference. Regulatory body may specify requirements of the minimum safety margin depending on the parameters and events considered in the assessment of safety margins (IAEA, 2003). Figure 1-5 shows the safety margins concept with the relationship between limits and calculation results of two different approaches.

In the past the margins to acceptance criteria have been determined by conservative evaluation model calculations. During the recent years a rising trend in computational reactor safety analysis is to replace these conservative calculations by best estimate calculations. In case of best estimate calculations, it is necessary to make an uncertainty analysis of the code results when determining the safety margin. Qualified computer codes are needed for this purpose, which are validated by pre- and post-test calculations of appropriate experiments,

experiences from other plants and benchmark calculations on national and international levels (IAEA, 2003).

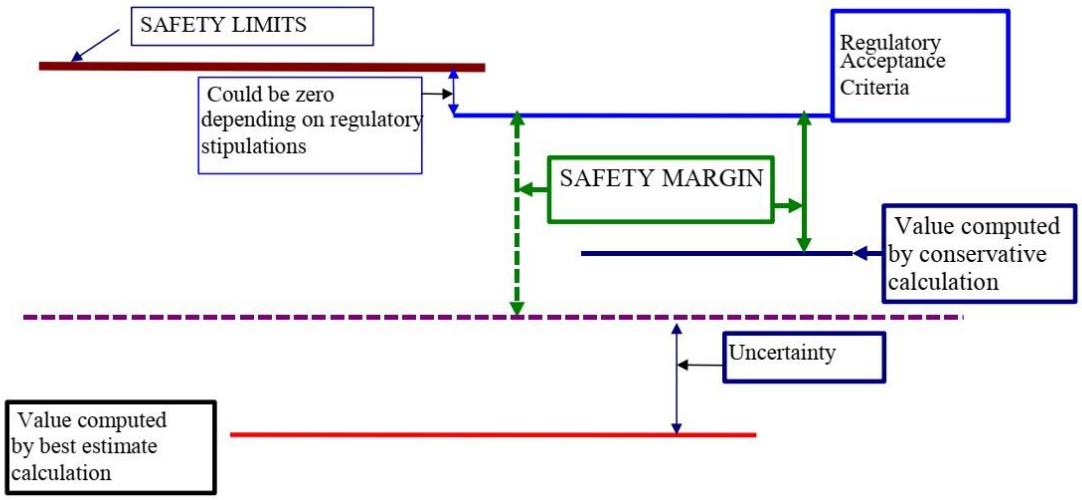

Figure 1-5. The Safety Margins (IAEA, 2003).

1.1.3.1.4 Computer Codes

This section covers the general view of the code types used in AOO and DBA analysis. The codes related to containment and hydrogen combustion analysis will be explained in detail in Chapter 3.

Complex computer codes are used for the analysis of the performance of nuclear power plants. The ranging of these codes includes specialized reactor physics codes and containment analysis codes. These codes have a strong and secure basis in terms of accuracy since many have been widely accepted and used in applications related to reactor safety in various countries (IAEA, 2002). Computer codes can be categorized by the component or system being analysed into the following six types for anticipated transients and DBAs (IAEA, 2002):

- reactor physics codes which model the core neutronic behaviour,
- fuel behaviour codes which illustrate the behaviour of individual fuel rods,
- thermohydraulic codes, including system codes, subchannel codes, porous media codes and computational fluid dynamics (CFD) codes, which typically model reactor vessel and other coolant system structures such as pumps, valves and accumulators.

- containment analysis codes which are generally used for the lumped parameter containment models, however some utilizes multi-dimensional capabilities to analyse containment behaviour.
- atmospheric dispersion and dose codes,
- structural analysis codes which model the behaviour of the vessel, piping and containment structures by considering the mechanical properties of the materials under various accident conditions.

On the next section, containment analysis codes will be explained in detail due to the relevance of the content to this thesis.

1.1.3.1.4.1 Containment Analysis Codes

The containment is the final barrier in the defence-in-depth strategy, it is designed to mitigate radioactive release into the environment if the reactor vessel is breached. Therefore, preventing containment failure is the most important goal of severe accident management strategies.

LOCA is one of the DBA types where coolant at high pressure and temperature inside the reactor coolant system leaks into the containment atmosphere through a pipe break. This accident leads to containment pressurization and a rapid temperature increase in the containment that might exceed its design values. Such an accident might result in the loss of the containment integrity and radioactive leakage into the environment. Therefore, TH parameters of a containment atmosphere during a DBA need to be investigated as a safety assessment procedure. To implement this assessment mainly two types of codes can be employed.

In lumped parameter codes, some regions inside the containment are defined as control volumes and the spatial differences of thermohydraulic parameters such as temperature or fluid density are not considered within that control volume. Conservation equations are solved for those control volumes by only taking account of time-dependent behaviour. In other words, average values of thermohydraulic parameters within each control volume are considered in the conservation equations and they are solved for each time step by numerical methods for each control volume separately. The determination of thermal-hydraulic parameters such as temperature within a region inside the control volume, therefore, is not possible. The only information that could be taken by the solution of these codes is the

average parameters of the control volume. They have been the most widely used computer codes up to now in both severe accident and safety design analysis. Therefore, many experiments that have been performed serve a good validation base for those codes and they demand less computational cost and run relatively faster (IAEA, 2011).

Another type of containment analyses codes that has been used in the field is computational fluid dynamics (CFD) codes. In CFD codes, the momentum equations are solved within some discreet regions by using the method of finite elements. Spatial variations are also considered. Nodalization is finer which leads to a higher accuracy rate as well. However, the time investment to model the actual geometry of a complex system like the containment building with lots of instruments and equipment inside is quite large. Moreover, the computational time is longer, and it demands a more powerful computational system to perform the simulation compared to lumped parameter codes (IAEA, 2011).

1.1.3.2 Probabilistic Method

The United States Nuclear Regulatory Commission (NRC) (the continuation of the Atomic Energy Commission (AEC)) was established in 1974 and one of the earliest tasks of the commission was to sponsor a study of the public risk from nuclear reactors to compare it to other industrial and natural risks. The study was conducted by the Professor Norman C. Rasmussen of the Massachusetts Institute of Technology (MIT) and published in 1975 with the title Reactor Safety Study (NRC, 1975). This report, which has the reference number WASH-1400, was the first comprehensive PSA (Jacquemain, 2015).

PSAs conduct a systematic investigation of the numerous possibilities of event combinations and accident sequences following an initiating event. They comprise a set of technical analyses for evaluating the risks at a plant by considering accident frequencies and their consequences. They provide an overall view of reactor safety by taking into account equipment resistance. There are three main types of PSAs categorized according to the consequences considered in the assessment (Jacquemain, 2015):

- Level 1 PSA: used to identify sequences resulting in core melt and quantify the frequencies.
- Level 2 PSA: used to assess the significance and frequency of the radioactive releases to the environment.

- Level 3 PSA: used to assess probabilities of consequences on the public with regards to dosimetry and contamination (even including the frequencies of health effects such as cancer)

The Rasmussen report is the first example of a Level 3 PSA, and it is still considered as a reference for an approach to deal with core melt accidents (Jacquemain, 2015). The report used detailed and comprehensive fault and event tree methods to predict accident scenarios developed into radioactive release into the environment, harming the public health living near the plant and the land contamination around the site of the plant. A typical BWR and a PWR were selected for the probabilistic analyses (Sehgal, 2012). Table 1-2 shows the consequences of early fatalities, early illness, total property damage in billions of dollars, decontamination area and relocation area in square miles with respect to various probabilities ranging from 1 in 20000 to 1 in a billion. The maximum probability in the table is chosen as 1 in 20000 since it is the calculated probability of a core melt in a light water reactor per year which is very small (Sehgal, 2012).

The main two aspects of the PSA are frequency (probability) and severity (consequences) since the multiplication of those two concepts defines the risk. The probability concept is examined through the fault and event tree methodology. An event tree is a technique for the quantitative risk (or probability) assessment of an accident. Following an initiating event, the event tree progresses with the various consequences of the event through possible options. Event trees are quite similar in essence to the decision trees commonly used in business decisions (Glasstone and Sesonske, 1994). An outline of the event tree could be seen in Figure 5 demonstrates a progression of events starting from a large pipe break (large break loss of coolant accident (LB-LOCA)). P_1 is the probability of the occurrence of the pipe break. The decision following this initial event is whether the electric power is available or not to supply the active ESFs. If power is not available (including auxiliary power) then active safety features will not operate and lead to a core degradation, including a significant amount of radioactive release to the environment. The probability of such kind of scenario occurring as indicated at the bottom of the outline equals to $P_1 \times P_2$. If electric power is available, the next branch is about whether the ECCS will function or not. The probability of failure is P_3 and the probability of the system available equals to (1-P_3). The subsequent branches check whether the fission product removal system or containment integrity fails or not. The overall probability of a chain of events is the product of the possibilities of each event composing the chain, listed on the rightmost in Figure 1-6. The third probability from

the below includes terms like (1-P_4) and (1-P_5) that are not shown in the probability formula list in Figure 1-6 since the failure probabilities like P_3, P_4 and P_5 are very small so the values of (1-P) are considered as unity (Glasstone and Sesonske, 1994). The fault tree is a logic diagram to determine the probability of the initiating failure. The probabilities of failures such as P_2 and P_3 (failures of electric power and ECCS respectively) are set through the fault tree analysis by examining the electrical and mechanical systems of the plant and components. The fault trees could have a huge size with many branches since the functioning of a safety system might rely on numerous components. The consequences of the events also need to be assessed just like probabilities. To achieve this goal, models that simulate the physical processes that occurred through an event progression need to be designed. The researchers of the Rasmussen Report developed a code for estimating source term. Different scenarios of containment failure were considered, and various metrologies were assumed for the area near the plant studied in the model (Sehgal, 2012).

PSAs are subject to limitations and have some inherent flaws. First, the human factor is very difficult to quantify in a PSA because of the unpredictability of human actions. Human error contributes to the plant risk substantially even if the overall reliability of the plant technology has been improved by decreasing the influence of human error through the enhanced man-machine interface and automation. Stress factor in accident conditions also contributes to unpredictability and make the probabilistic assessment more difficult. Another limiting effect could be seen in the evaluation of hazards. Most PSAs do not include external events, earthquakes or flooding because of tsunamis, as initiators. These hazards are difficult in nature and could threaten multiple safety systems simultaneously unlike the internal events localized at a specific region of a plant. The contribution of those hazards is specific to the site and the plant. The methods currently used to evaluate the effect of those hazards have large uncertainties (IAEA, 1992). Uncertainties about the fault and event tree methodology are also placing error limits on the results. For example, a double-ended pipe break in the primary coolant system of a reactor could only be estimated due to the lack of experience of the event. Moreover, a component is regarded as failed or available in an event or fault tree but there are some situations that the component undergoes a partial failure, in other words, it is operative but not at full efficiency (Glasstone and Sesonske, 1994).

The probabilistic method is in a more supplementary role to the deterministic method in a safety analysis. The integration of the two methodologies might provide better insights into system performance, interactions and weaknesses in the design, reliability, and selection of

accident scenarios. The deterministic approach could also provide conservatism to deal with the uncertainties within the probabilistic approach with an adequate safety margin (IAEA, 2016).

Table 1-2. Early consequences of reactor accidents for one reactor with the probabilities, extracted from WASH-1400 (NRC, 1975).

Probability per Reactor-Year	Early Fatalities	Early Illness	Total Property Damage $\$10^9$	Decontamination Area (Square Miles)	Relocation Area (Square Miles)
One in 20,000	<1.0	<1.0	<0.1	<0.1	<0.1
One in 1,000,000	<1.0	300	0.9	2000	130
One in 10,000,000	110	3000	3	3200	250
One in 100,000,000	900	14000	8	-	290
One in 1,000,000,000	3300	45000	14	-	-

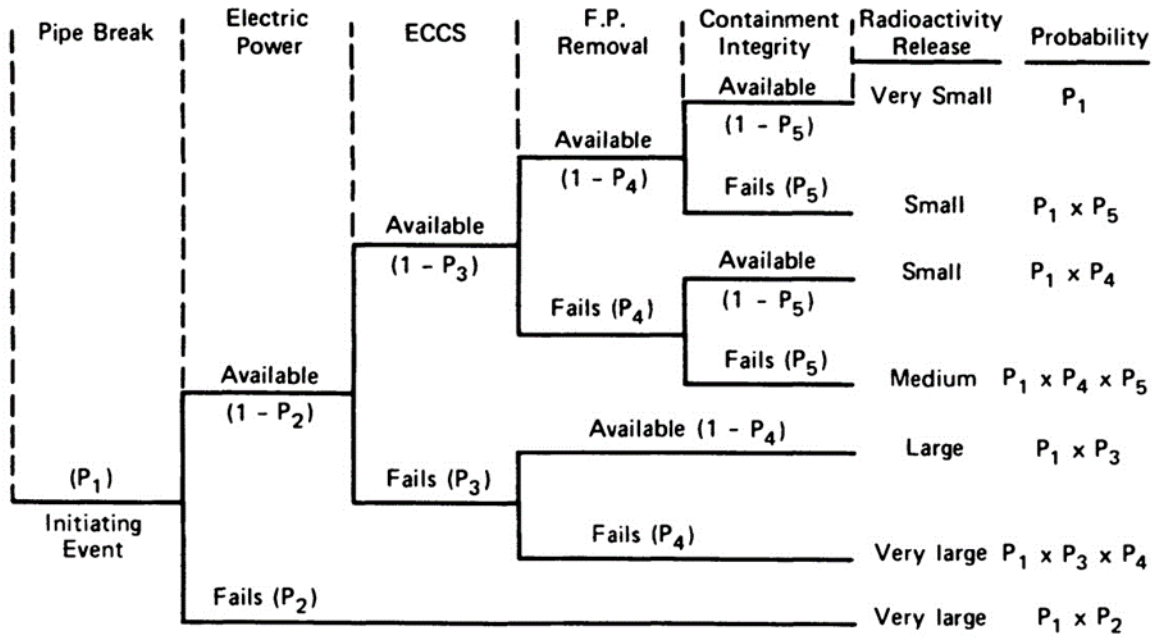

Figure 1-6. Simplified LB-LOCA event tree (Glasstone and Sesonske, 1994).

1.1.4 Engineered Safety Features

ESFs are designed to prevent or limit the radioactive release to the environment when a highly unlikely transient or accident that is too severe to be accommodated by the reactor protection system occurs. The major ESFs are (Glasstone and Sesonske, 1994):

I. ECCS to supply water to the reactor core in the event of a LOCA,
II. The containment vessel (or structure) to provide a barrier to confine the radioactive materials that might be released from the reactor core,
III. the cleanup system for removing part of the radioactivity and heat that may be present in the containment atmosphere,
IV. hydrogen control to prevent the formation of a combustible gas mixture involving hydrogen inside the containment.

1.1.4.1 Emergency Core Cooling System

If a break sufficiently large enough occurs in the primary coolant circuits of a water-cooled reactor, the system pressure will drop and the ECCS will start to function. This system comprises several independent subsystems which could be actuated in sequence as depressurization goes on. The subsystems provide water into the core to cool down when the flow of primary coolant is considerably decreased or lost. The supplied water is taken from different sources, with larger volumes allocated to flood the core during the later stages of

depressurization. Redundancy of equipment and flow paths is provided to ensure the safety of the operation (Glasstone and Sesonske, 1994).

In PWRs, the high-pressure injection system (HPIS) actuates when the reactor system pressure suffers a moderate drop, from the normal operating pressure of 15.5 MPa to around 11 MPa. A decline in the pressure to that extent could occur after a small break in the primary coolant circuit of the reactor or if the pressurizer relief valve failed to close after the normal pressure had been restored following an overpressure condition. The HPIS would then rapidly compensate for the loss of coolant (water or steam). This ECCS subsystem uses the same pumps as the chemical and volume control system (CVCS). It injects borated water into the cold leg of the reactor coolant system. A slow-acting backup system might be included to inject borated water into the hot leg of the reactor coolant system (Glasstone and Sesonske, 1994).

Following a large break, the system pressure would drop rapidly and then another ECCS subsystem, the accumulator injection system, would be actuated. The accumulators are two or more independent tanks having cool borated water stored under nitrogen gas at a pressure of about 1.4 to 4.1 MPa depending on the system design. The tanks are connected through check valves to the reactor cold legs or sometimes directly into the upper part of the downcomer system of the reactor vessel. When the primary system pressure decreases below the pressure in the accumulator approximately 20 to 25 s following a large break, the check valves would open automatically, and borated water would be injected into the reactor vessel rapidly. The accumulator tanks act on a passive principle since they can function without pumps which need electric power to operate (Glasstone and Sesonske, 1994).

As the pressure drops more, a low-pressure injection system (LPIS) is actuated. The system uses the pumps and heat exchangers of the residual heat removal system. If the offsite power fails, there would be plenty of time for the emergency diesel generators to start. Details of the systems vary among reactor designs, but usually, the system takes the water initially from the refuelling storage water tank and then, if necessary, from the sump at the bottom of the containment (Glasstone and Sesonske, 1994). A flow diagram of a typical PWR for ECCS could be seen in Figure 1-7 with all the subsystems mentioned.

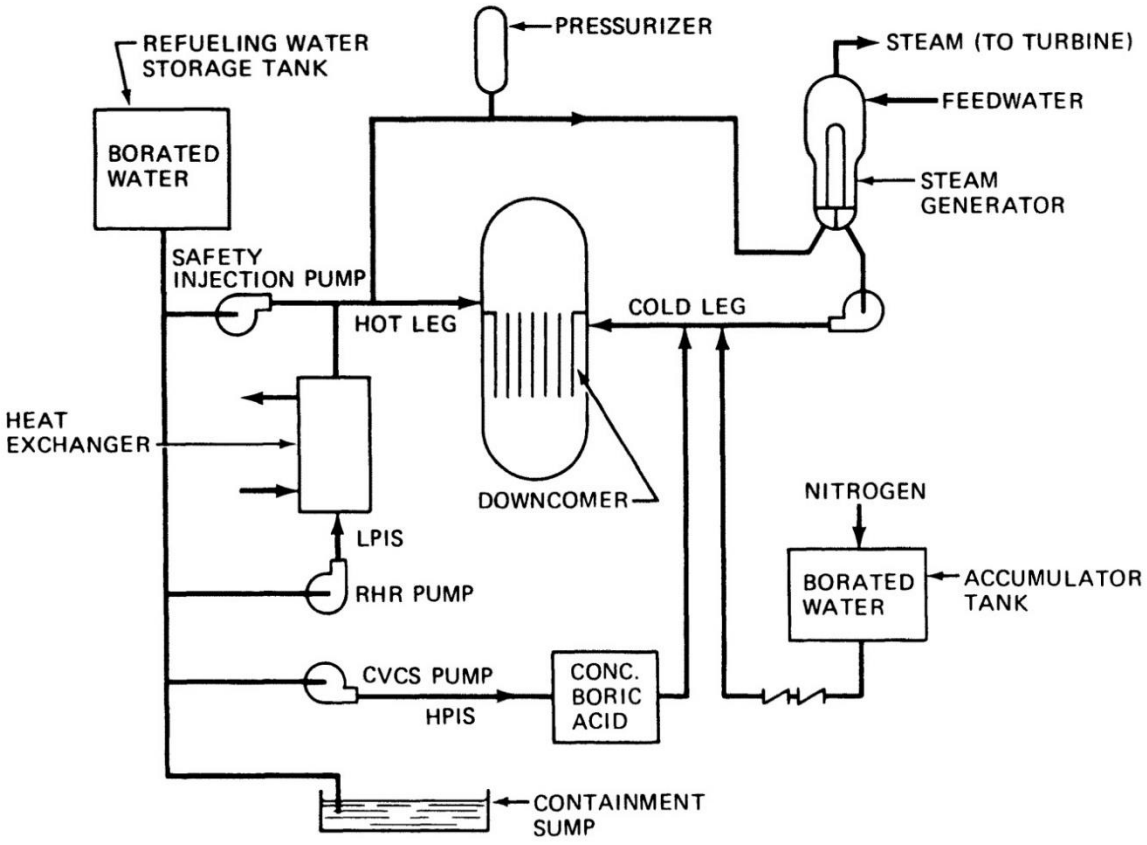

Figure 1-7. Flow diagram for ECCS of a typical PWR (Glasstone and Sesonske, 1994).

1.1.4.2 Containment Systems

A containment structure enclosing the reactor primary system acts as the final barrier to radioactive material release to the environment in the defence-in-depth design of the reactor safety systems. Even if containment design in LWRs is traditionally based on holding the pressure caused by the release of the primary coolant in a LOCA and withstanding the impact of internally generated missiles, margins are such that considerably higher pressures can be accommodated before failure (Glasstone and Sesonske, 1994). The primary functions of a containment system (containment structure and its various subsystems such as containment heat removal or spray system) which must be fulfilled in the context of LOCA could be listed as follow (Oslick, 1976):

a) withstand the pressure build-up within the containment structure from the postulated LOCA and maintain its structural integrity indefinitely after the LOCA,
b) operate in conjunction with the ECCS to limit energy releases from the LOCA to prevent pressure build-up in the containment structure above its design limit,

c) limit offsite releases of radioactive materials during and following a LOCA to below regulatory limits,
d) reduce pressure and temperature in the containment structure following a LOCA to enable recovery,
e) provide protection for the reactor coolant system from external environmental effects.

Containment structures for PWRs (the type of reactor relevant to the context of this thesis) differ from plant to plant, but they are commonly cylindrical (around 37 m diameter) with a domed top (roughly 61 m). They are usually made of reinforced concrete (about 1.07 m thickness) with an internal steel liner (roughly 38 mm thickness). The entire primary coolant system is enclosed along with elevated injection tanks as it is shown in Figure 1-8. A spherical design is shown in Figure 1-9. The spherical design provides additional operating floor area and efficient placement of auxiliary and maintenance activities in comparison to a cylindrical design of equivalent free volume. An in-containment refuelling water storage tank (IRWST) provides water for both safety injection and severe accident core debris cooling as shown in Figure 1-9. Sphere diameters range from around 40 m for a 2600-MW(t) plant to around 60 m for a plant rated at 3800 MW(t). Corresponding free volumes are approximately 57,000 and 96,000 m^3, respectively (Glasstone and Sesonske, 1994).

In case of a complete loss of coolant, nearly all the heat content of the coolant and fuel before the accident would be released to the containment atmosphere. The volume and strength of the containment are designed to withstand the maximum containment temperature and pressure that would be expected from the steam produced by the flashing of all the water in the primary circuit and from the effects of the ECCS. Typically, the calculated maximum pressure is about 280 kPa, the containment structure is therefore designed to withstand 310 kPa and is tested at 350 kPa. The leakage rate should not exceed 0.1 per cent of the containment volume per day at the design pressure. Spherical containments may be designed for pressures as high as 500 kPa (Glasstone and Sesonske, 1994).

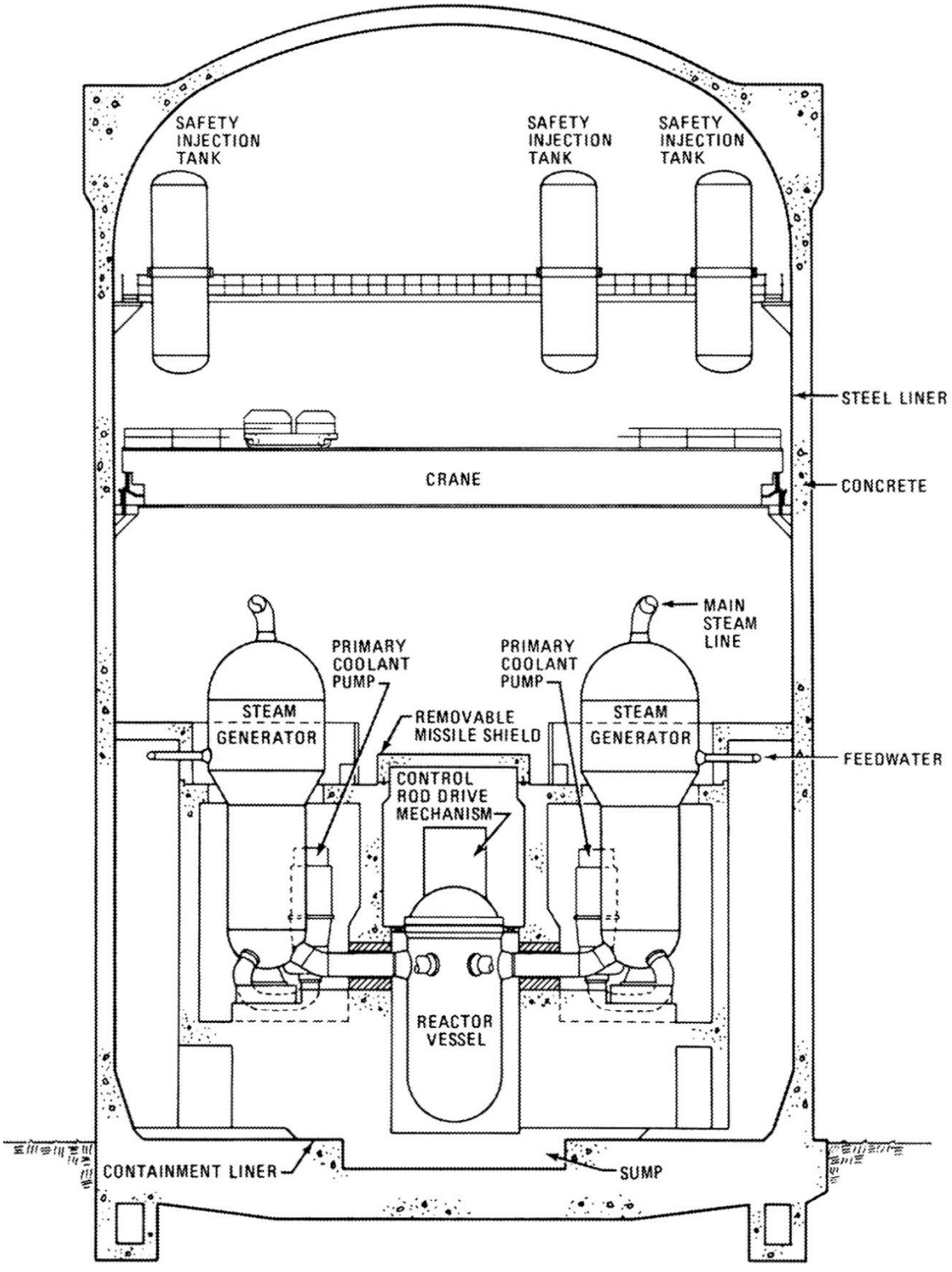

Figure 1-8. A typical cylindrical PWR containment (Glasstone and Sesonske, 1994).

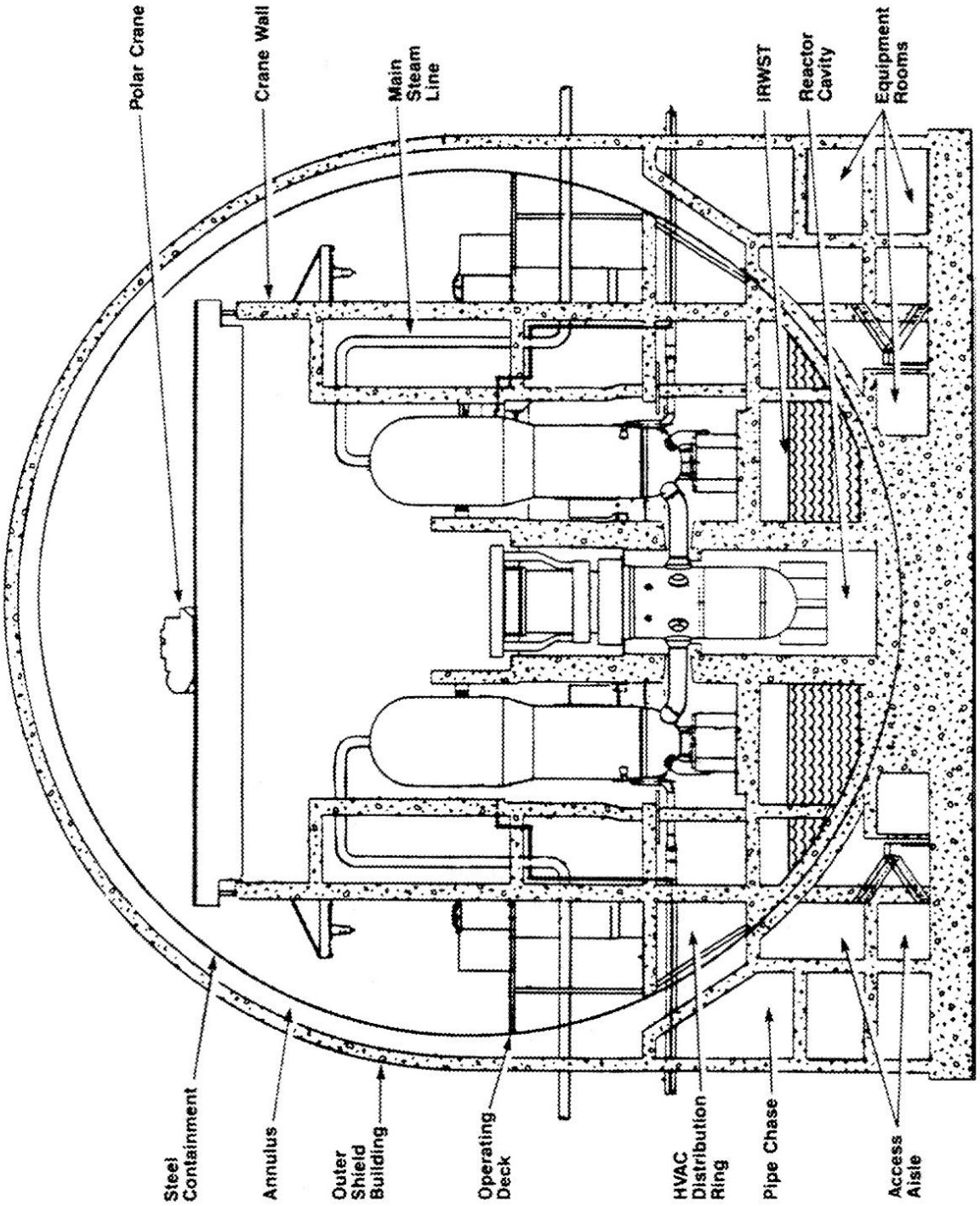

Figure 1-9. A typical spherical PWR containment (Glasstone and Sesonske, 1994).

The containment spray system (CSS) provides water through the nozzles of a spray header near the top of the structure to cool the containment atmosphere and decrease the pressure by condensing part of the steam after a LOCA. The water collected in the containment sump can be recirculated through the heat exchangers of the residual heat removal system (RHRS) to provide continuous cooling of the containment atmosphere. CSS also serve to remove some

of the radioactivity from the atmosphere. Sodium hydroxide or alkaline sodium thiosulfate in the water facilitates the removal of radioiodines which are generally the determining factor in the environmental hazard of a large radioactive release. The radioactivity level in the containment atmosphere would also be reduced by using blowers to circulate the air through iodine absorbers and particulate filters in some PWR designs (Glasstone and Sesonske, 1994).

1.1.4.2.1 Containment Failure Modes

In case of a containment failure, the way it fails can have a significant impact on offsite releases. If containment leaks slowly, then large fractions of the radionuclides may still be retained inside the containment or surrounding buildings. Gravitational settling of radioactive aerosols inside the containment or surrounding buildings or from sprays or other systems removing the radionuclides from the containment atmosphere might provide retention of radioactive substances. Contrarily, a large rupture of the containment can result in the rapid transport of radionuclides to the environment with minimal retention (NRC, 1997).

Rasmussen's classification of the possible containment failure modes is still used today. The five main modes are shown in Figure 1-10 (Jacquemain, 2015):

- mode α: steam explosion in the vessel or reactor pit caused by an interaction between the corium and the coolant, inducing loss of containment integrity,
- mode β: initial or fast-induced loss of containment integrity,
- mode γ: hydrogen explosion in the containment, leading to loss of its integrity,
- mode δ: slow overpressurisation of the containment, leading to loss of its integrity,
- mode ε: basemat melt-through by the corium, leading to basemat breach.

Mode V, that is bypasses of the containment by outgoing pipes, evaluated separately, since it is not directly related to the behaviour of the containment building. Containment bypass involves failure of the reactor coolant system boundary in such a manner that a path is created to the outside without going through containment (Jacquemain, 2015).

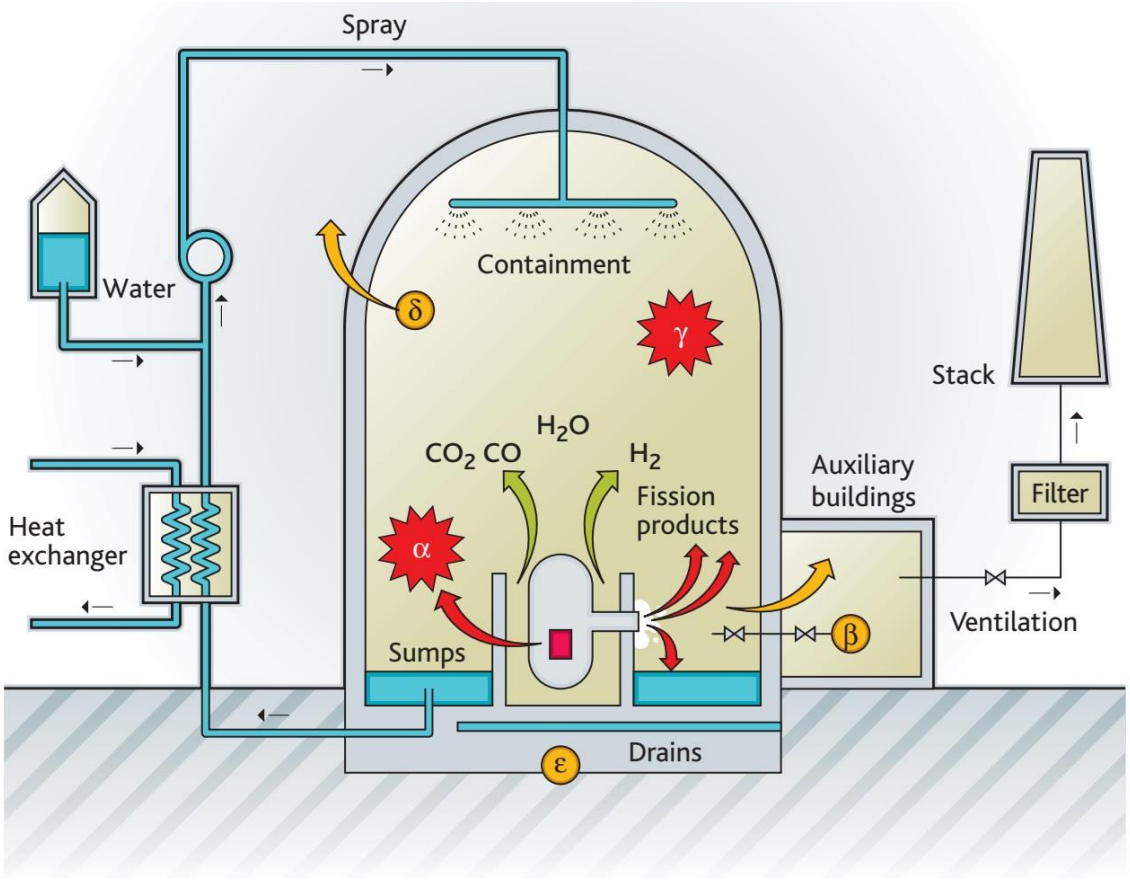

Figure 1-10. Possible containment failures according to the Rasmussen Report (Jacquemain, 2015).

Direct leaks can occur if automatic isolation of containment penetrations fails or if the integrity of the containment hatches is lost during an accident progression. Initial containment failure (mode β) is very important as it can allow radioactivity to be released directly to the environment from the very start of an accident (Jacquemain, 2015).

A steam explosion (mode α) may occur when hot, fragmented corium interacts with water present in either the vessel lower head or the reactor pit (if the vessel is melted through). The mechanical energy of a steam explosion in the vessel could cause the vessel to burst and generate missiles that could threaten the integrity of the containment and particularly the vessel head (Jacquemain, 2015).

Mode δ corresponds to loss of containment integrity from overpressure due to heating of the containment atmosphere resulting from inadequate removal of the heat generated by the fission products and to the progressive formation of a significant amount of gases during erosion of the basemat concrete by corium. Steam from the water used to cool the corium to slow its progress might be added to these gases. If the containment atmosphere is not cooled,

its internal pressure will rise inexorably and could lead to a loss of containment integrity after a period of 24 hours (Jacquemain, 2015).

Mode γ is about hydrogen explosions. Combustion of all the hydrogen produced mainly by oxidation of the zircaloy cladding would produce a pressure pulse that could threaten the containment integrity. Corium could melt through the basemat after the vessel failure following a severe accident and radioactive materials could escape through the containment through soil and water (Jacquemain, 2015).

1.2 Literature Survey

1.2.1 Research in Brief

In this research thesis, 3D evaluation of short-term and long-term thermal-hydraulic (TH) parameters and hydrogen distribution inside containment of a VVER-1000/V446 nuclear power plant are conducted during an LB-LOCA and its progression by using the GOTHIC code (EPRI, 2018a). To assess the mitigation methods, the effects of the CSS on TH parameters, hydrogen distribution and in addition, mitigation of the hydrogen risk through passive autocatalytic recombiners (PARs) are also investigated. Moreover, sensitivity analysis of spray temperature and spray droplet diameter on long-term depressurization is examined. To achieve these goals, in the first step, as-built 3D structure of VVER-1000/V446 containment was modelled in detail by using AutoCAD. The AutoCAD model has been processed to be prepared for GOTHIC 3D input. Meanwhile, an equivalent GOTHIC lumped parameter (LP) model is also prepared to validate the modelling procedure and results against the reactor's final safety analysis report (FSAR). 2D profiles and 3D contours of thermal-hydraulic parameters and hydrogen distribution with and without installed ESFs (CSS and PARs) are also presented as outcomes.

1.2.2 Past Studies on Thermal-hydraulic Parameters within Containment during an Accident

Several studies have been published to analyse the containment thermal-hydraulic response in recent years. The employed analysis methods could be classified into three main groups:

I. simulation through nuclear codes which employed an LP methodology such as CONTAIN (Williams et al., 1997) and MELCOR (Humphries et al., 2017),

II. developing TH models through Multiphysics equations by employing a programming language like MATLAB (Mathworks, 2022) or FORTRAN (Sun Microsystems, 2001),

III. employing 3D/CFD codes such as GASFLOW (Nichols et al., 1998) and ANSYS-CFX (Stubley, 2009).

Starting from the studies of containment analysis utilizing LP approach codes, German containment code system COCOSYS (Allelein et al., 2008) was used for the simulation of passive containment cooling of AP1000 during an LB-LOCA and the results were validated against Westinghouse's in-house WGOTHIC code and MELCOR code results. The peak pressure value of the containment during the LOCA was conservatively calculated by COCOSYS. The difference between COCOSYS results and the results achieved by WGOTHIC and MELCOR was only around 0.1 – 0.2 bar. In addition, a best estimate calculation was made taking into account the plumes above the steam generator compartments that yielded a peak pressure result 0.8 bar lower than the WGOTHIC result (Broxtermann and Allelein, 2013). In a study that analyses a simulation of a station blackout event in a two-looped pressurized water reactor with passive safety systems, MAAP (EPRI, 2013), MELCOR and ASTEC (Chatelard et al., 2014) codes produced similar thermal-hydraulic results for the containment, Passive containment filtered venting system and PARs were used merely without any recovery option to evaluate the capability of these passive systems to mitigate the consequences of the severe accident (Šadek et al., 2017). MELCOR was used in a study to validate a containment input model for a CANDU-6 plant by comparing the results with integrated leakage rate tests. The analysis was made for the atmosphere stabilization and the main test phases. Although the results showed reasonable agreement with the measurements of temperature and the vapour pressure, they also showed obvious deviations in the pressure and the local temperatures in the middle and lower regions (Kim et al., 2018).

Some of the past studies developed the TH model by imposing conservation equations to simulate containment pressurization. Firstly, Noorikalkhoran et al. studied VVER-1000 containment pressurization by developing a single-cell model of the containment in MATLAB by employing discretized conservation equations. They also simulated an LB-LOCA containment pressurization for short-term and long-term transients using CONTAIN code and compared the results of all the models to the final safety analysis report (FSAR). The results show that CONTAIN could predict the TH response of the containment

reasonably well (Noori-Kalkhoran et al., 2014a, 2014b). Two years later, the same group developed a multicell model of VVER-1000 containment by considering the effects of nodalization and spatial location of cells. It was demonstrated that the modified model improved the results and provide more resolution about the overall distribution of the TH parameters (Noori-Kalkhoran et al., 2016).

Utilising CFD codes, in 2016, Zhu et al. evaluated the COCOSYS and ANSYS CFX performance on the prediction capability by simulation results of a simplified enclosure based on generic containment. The simulation considered separate effect plume due to a heat source by taking into account two boundary conditions, adiabatic and convection. COCOSYS overestimated the average temperature in comparison to CFX results for the adiabatic boundary condition, whereas COCOSYS results of the average temperature in the convection boundary condition were underestimated compared to CFX results. The temperature stratification phenomenon was well depicted by the CFX as could be seen in Figure 1-11, whereas COCOSYS could not match the same performance (Zhu et al., 2016). In 2018, a heat and mass transfer model is developed for spray cooling in ANSYS CFX and validated against experimental data by simulations in THAI containment. A full three-dimensional geometrical mesh of THAI was used for all simulations. Simulation results show a good agreement with experimental data for the polydisperse spray configuration (Kaltenbach and Laurien, 2018). Moreover, Li et al. developed a dynamic film model of containment to investigate thermal-hydraulic parameters such as velocity and temperature fields with the implementation of the passive containment cooling system in GASFLOW-MPI. They confirmed their model by comparing it to experimental data of separate effect test Experiments on a Falling Film Evaporation facility and an integral test facility (Li et al., 2019).

GOTHIC is a general-purpose thermal-hydraulic analysis code that could be applied to nuclear power plant systems, containment and confinement buildings by providing LP and 3D geometry options as a hybrid code. Unlike standard CFD codes, it utilizes the porous media approach to define 3D geometries in modelling to produce time and resource-efficient results. In 2010, condensation phenomena inside international reactor innovative and secure (IRIS) is investigated by using models built in RELAP5 and GOTHIC codes. Containment behaviour is examined in terms of drywell temperature and pressure response, heat transfer coefficient (HTC) and steam volume fraction distribution, and internal recirculating mass flow rate during an SB-LOCA. The research demonstrates that RELAP5 is capable of the correct depiction of containment-related phenomena even if some flaws could be observed

such as a marked overestimation of internal natural recirculation (Papini et al., 2011). In 2015, Ozdemir et al. made an analysis that utilizes the capability of GOTHIC code to model drywell, wetwell and connecting vent system of the Fukushima Daiichi Unit 1 building that can predict the 3-dimensional flow patterns and the temperature and gas distributions. The model also contains leakage to the surrounding reactor building and the wetwell vent to the stack. MAAP5 Baseline Scenario of the reactor unit is used to provide input to the GOTHIC model for the steam, H2 and CO release and heat transfer from the RPV to the containment. The results show a good agreement with the recorded data of the Fukushima accident (Ozdemir et al., 2015). Bocanegra et al. developed three subdivided GOTHIC models with different mesh sizes and one GOTHIC LP model to simulate an LB-LOCA in a PWR containment. They compared those different models in terms of containment thermal-hydraulic parameters and discussed the discrepancies between models. The temperature and velocity distributions show a high dependence on the three-dimensional phenomena. However, the pressure trend is similar in all models with small differences in the values (Bocanegra et al., 2016). In another study, an LB-LOCA scenario has been simulated for AP1000 containment building by using the 3D capabilities of the GOTHIC code. The pressure and temperature response of the containment were analysed. To attain the boundary conditions for the GOTHIC model, the LOCA mass and energy release data were received from a TRACE model of the AP1000 reactor (Fernández-Cosials et al., 2017a). Jimenez et al. evaluated equipment and instrumentation environmental qualification criteria based on LP model calculations by using a GOTHIC model of a PWR-W containment in a LOCA scenario. Since equipment and instrumentation Environmental Qualification in containment is based on pressure and temperature enveloping profiles calculated with LP models, the aim of the study was to provide more detailed results by developing a 3D model. These enveloping profiles were the solution in a single cell that represents a large volume in LP models, whereas volumes were subdivided into thousands of cells in 3D models and could provide a more accurate solution (Jimenez et al., 2017). Recently, a new 3D modelling methodology was proposed and applied to Trillo Nuclear Power Plant during an LB-LOCA using the GOTHIC code. The methodology suggested using Computer Aided Design (CAD) tools to manage the geometry of the model, rather than using the GOTHIC code graphical user interface. The 3D results of the thermal-hydraulic parameters were compared to lumped parameter results and sensitivity analyses were performed (Fernández-Cosials et al., 2019).

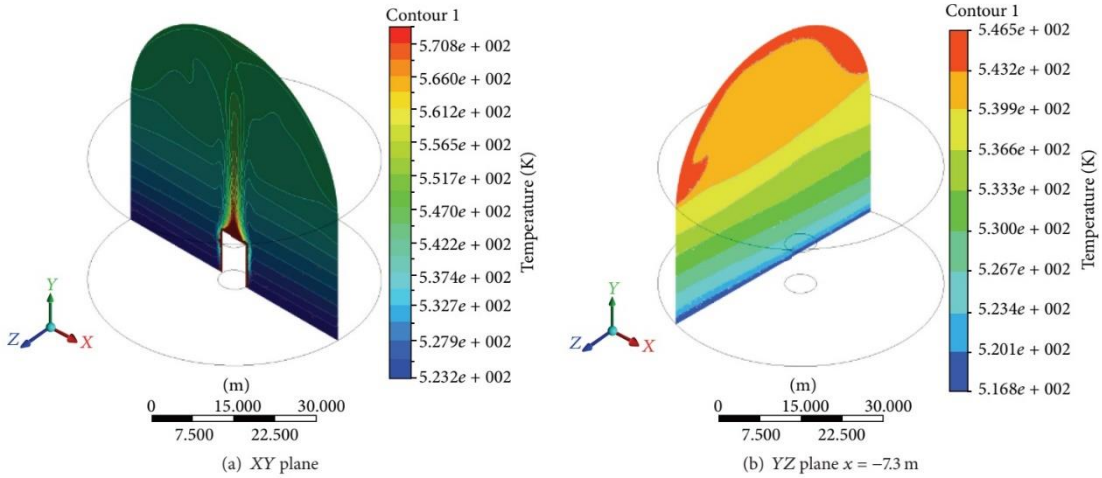

Figure 1-11. Contour map of the enclosure demonstrating the thermal stratification at upper points in CFX calculations at 10106 sec (Zhu et al., 2016).

1.2.3 Past Studies on Hydrogen Distribution within Containment during an Accident

Utilizing the LP codes, in 2013, the MELCOR code was used for performing calculations of a station blackout accident for VVER-1000 containment by modelling two different versions: the containment with 8 already installed PARs and the containment with additional 15 new PAR units. The reason for adding additional new PAR units was related to the changing of the reactor fuel in Kozloduy plant with a new one that increased the amount of zirconium in the reactor core. Oxygen starvation due to the recombination reaction was observed with the model that contains additional units. The calculations of the two models ensured that the hydrogen concentration would be below the flammability limits in the containment during the accident scenario (Vryashkova, 2013). Saghafi et al. conducted an analysis of determining the optimum PAR configuration in a Westinghouse-type PWR by using the MELCOR code. An LB-LOCA without ECCS actuation was selected as the bounding case for the study after the PSA results. 40 different PAR configurations were examined in a Westinghouse-type PWR to find the optimal configuration with a minimum number of PARs in the containment. The obtained configuration was equally effective for hydrogen risk mitigation with a 36% reduction in the number of PARs compared to the base case design (Saghafi et al., 2017). Noorikalkhoran et all, simulated VVER-1000/V446 containment response to an LB-LOCA scenario by using MELCOR and CONTAIN codes. In addition, they judged the effectiveness of the spray system to mitigate the consequences of the accident. Hydrogen distribution was

also simulated by MELCOR and CONTAIN codes and implementation of PAR installation into the model and the assessment of the PAR performance on mitigation of hydrogen risk were made in the MELCOR code. They also provided validation for their results against FSAR (Noori-kalkhoran et al., 2019).

Most of the open-source and commercial CFD codes are not capable of performing simulations of severe accident sequences in full-scale containments of nuclear power plants within reasonable computational times due to the lack of specific nuclear safety models and code validations. Contrarily, GASFLOW has an extensive verification and validation base, and it has been widely used for hydrogen safety analysis of various nuclear reactor types in recent studies (Xiao et al., 2016). Two different German PWR types were modelled in GASFLOW to analyse steam and hydrogen distributions considering mitigation of the hydrogen combustion risk by PARs. The accident scenario involved a postulated BDBA triggered by an LB-LOCA at a low release location from a rupture of the surge line from the hot leg of the primary loop to the pressurizer. The results were compared to the results of two LP codes and demonstrated the differences between the LP and CFD approaches to the same phenomena (Royl et al., 2000). A study was carried out to investigate the hydrogen distribution in a VVER440/213 containment in the event of a medium break LOCA (MB-LOCA) which progresses into a BDBA. The spatial distribution of TH parameters and gas concentrations were obtained from GASFLOW calculations. The results were compared to CONTAIN LP results which showed qualitatively similar trends. Quantitatively speaking, differences in the pressure histories and total amount of steam in the containment are observed (Kostka et al., 2002). GASFLOW was used to investigate hydrogen distribution in a station blackout scenario on Advanced Power Reactor 1400 (APR1400) containment. The source term data regarding hydrogen and steam were taken from a MAAP calculation. The accident scenario included hydrogen and steam transport from the reactor vessel to IRWST through the pilot-operated safety relief valves of the pressurizer, condensation of the steam in the IRWST water due to its subcooling and the release of the dry hydrogen to the free volume of the IRWST and to the annular compartments through the vent holes of the IRWST. The control of the hydrogen concentration is found difficult for the base design of APR1400. In addition, design modifications are proposed and evaluated with GASFLOW in terms of the hydrogen mitigation strategy. Figure 1-12 shows the hydrogen cloud and plume formed during the accident in the containment (Kim et al., 2005). In 2009, Kim et al. investigated the hydrogen distribution and characteristics of the gas mixture involving hydrogen inside the

OPR1000 containment following an SB-LOCA. The conclusion of the study was that flame acceleration due to the hydrogen concentration above the limit was not possible for OPR1000 containment due to the steam amount inside the gas mixture during accident progression (Kim et al., 2009). Qinshan-II nuclear power plant was examined in terms of hydrogen risk by utilizing GASFLOW in a study carried out in 2009. The effect of the spray system on hydrogen distribution was investigated in three modes: without the spray system, direct and both direct and recirculation spray. It was observed that hydrogen risk increased significantly in direct spray mode, whereas recirculation spray had a minor effect on the results. A new PAR model has been developed in GASFLOW to simulate more realistically the phenomena behind the operation of the system. It was also noted that the spray modes did not have a significant effect on the efficiency of the PARs. The results were also validated against experimental data (Xiong et al., 2009). Recently, the advanced parallel version of the GASFLOW sequential code, GASFLOW-MPI, was used for the first time to analyse the hydrogen explosion at Fukushima Unit 1 reactor. Gas dispersion in the containment, the formation of hydrogen-steam-air mixture by considering the stratification phenomenon and the prediction of the pressure loads to the containment and internal structures were examined in the study (Xiao et al., 2017).

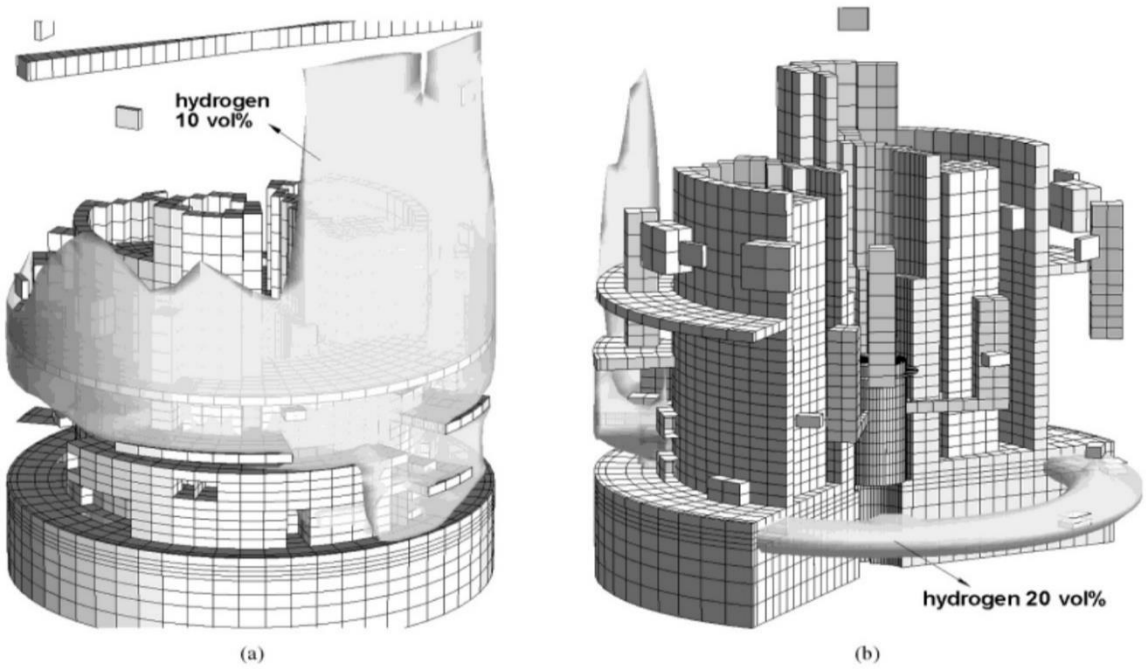

Figure 1-12. GASFLOW results showing the hydrogen distribution in APR1000 at 2400 seconds: (a) 10 vol% hydrogen cloud is developed around the operating deck and (b) 20 vol% hydrogen plume is shown at the left IRWST vent hole (Kim et al., 2005).

As an example of studies employing other CFD codes, a hydrogen release scenario inside a garage based on experiments performed by CEA in the GARAGE facility (France) has been simulated with and without PAR installation to evaluate whether the PAR system could be useful to decrease hydrogen concentration, outside of containment, inside a typical surrounding of hydrogen or fuel cell applications. The in-house code REKO-DIREKT was implemented in the CFD code ANSYS-CFX to model the PAR operation. The study demonstrated that the PAR works efficiently by reducing the hydrogen concentration and promoting mixing inside the garage. The result of the simulation could be seen in Figure 1-13 (Reinecke et al., 2013). In. 2014, VVER440/V230 containment was modelled to evaluate steam and hydrogen distribution and mitigate the hydrogen risk by PAR installations. ANSYS-FLUENT was used to obtain the three-dimensional distribution of the relevant parameters (Philipov and Filipov, 2014). In 2014, A CFD-based model was developed in ANSYS-FLUENT to simulate hydrogen distribution in the containment in severe accident progression. The model was validated against the experimental data obtained from three different facilities: THAI, PANDA and TOSQAN (Visser et al., 2014). Recently, Park et al. investigated a 3D detailed simulation of hydrogen behaviour using FRAMATOME PAR and NIS PAR in the THAI project by employing ANSYS-FLUENT code. To reduce the calculational cost, PAR performance was simulated by applying the hydrogen removal rate correlation equation to the catalyst region. It was demonstrated that TH parameters, gas velocity entering the PAR, hydrogen distribution and hydrogen removal rate were similar to the experimental data (Park et al., 2022).

GOTHIC employs a coarser mesh due to the inherent qualities of its subdividing process and porous approach. Therefore, GOTHIC does not cause the problem of demanding computational time and cost unlike CFD codes yet still provides three-dimensional results like the other CFD codes. For this reason, GOTHIC has been used widely in hydrogen risk analysis recently. In 2015, the GOTHIC code is used to simulate hydrogen distribution in a spherical PWR containment in case of fast release of hydrogen-steam mixture from hot-leg creep rupture during a postulated total station blackout. The mitigation strategy included only the dilution resulting from the large free volume of the containment and the high value of the design pressure. The flammability limit was evaluated using Shapiro Diagram (Papini et al., 2015). Two years later, Lopez-Alonso et al. analysed the location, size and number of the PARs to minimise the hydrogen risk in a PWR-KWU containment type during a station blackout scenario. The PAR configuration decreased the likelihood of hydrogen combustion

in all the containment compartments at the end of the simulation. The study demonstrated that the PAR configuration could lead to a reduction between 30–45% of the final hydrogen concentration in comparison to the unmitigated scenario (Lopez-Alonso et al., 2017). In the same year, a PWR-W GOTHIC model was created to simulate hydrogen distribution in the event of a station blackout accident. The venting and spraying strategy and their impact on hydrogen risk are assessed in a sensitivity analysis. Moreover, a new parameter Tau to estimate the hydrogen risk was introduced d(Fernández-Cosials et al., 2017b). The GOTHIC code was utilized to evaluate the effectiveness of the PARs installed in the Gösgen NPP in Switzerland during a station blackout scenario. The PAR modelling approach was validated by simulation of two experiments performed in the frame of the OECD/NEA and THAI project. The results show that PARs could not prevent the formation of a stratified cloud of hydrogen (10% molar concentration), however, they can mitigate the accumulated hydrogen once it formed as could be seen in Figure 1-14 (Papini et al., 2019). In 2021, the analysis of a preventive venting strategy to limit hydrogen risk following a station blackout accident was made for a GOTHIC BWR-6 Mark III containment model. The analysis showed that an appropriately planned venting strategy could mitigate the hydrogen risk (Díez Álvarez-Buylla et al., 2021).

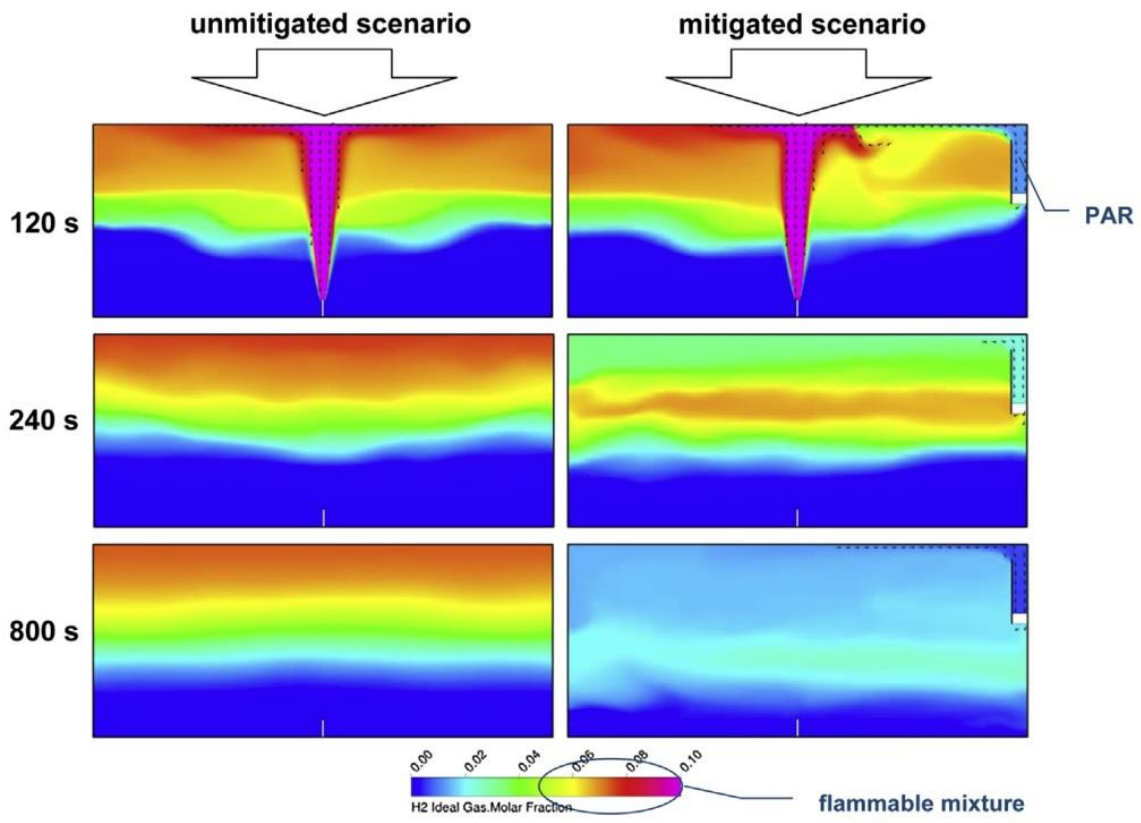

Figure 1-13. Hydrogen concentration fields for (a) unmitigated and (b) mitigated scenario (Reinecke et al., 2013).

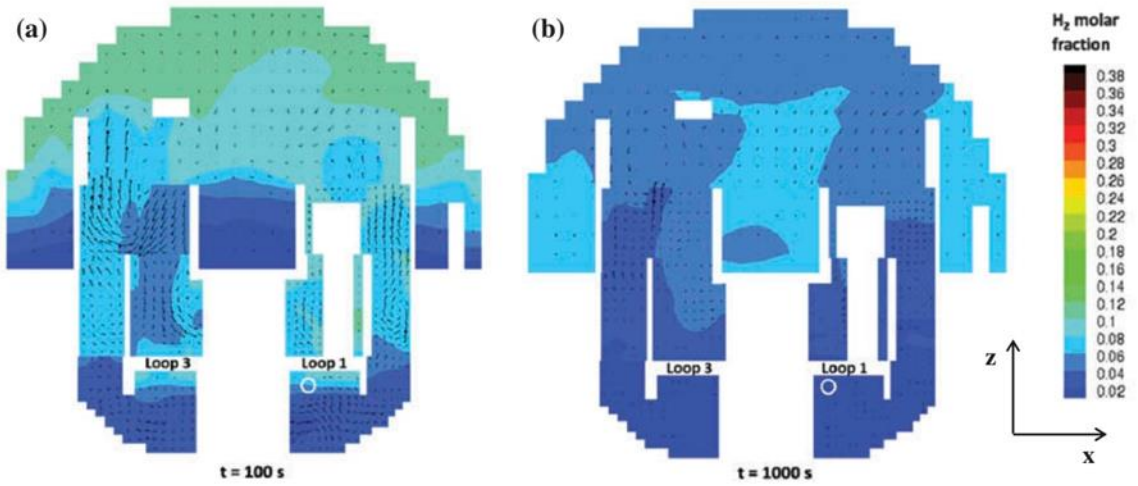

Figure 1-14. Two-dimensional demonstration of formed hydrogen fields (mitigated scenario) (Papini et al., 2019).

CHAPTER 2

CASE STUDY

2.1 VVER 1000/V446 Nuclear Power Plant

The VVER (water-cooled water-moderated power reactor) is a pressurised LWR of Soviet Union design. It operates on the same principles of a Western PWR reactor and uses similar technological systems. The primary coolant is pressurised water. The coolant heats up in the reactor core and steam is produced on the secondary side of the steam generators.

VVER-type reactor development was started by OKB "GIDROPRESS" in 1955. The first reactor of 210 MW electrical power was commissioned at Unit I of Novovoronezh NPP in 1964. Several basic engineering solutions developed for the first VVER provides the originality of the design and most of them became traditional features for subsequent VVER generations (Ryzhov et al., 2010). Such solutions could be listed here (Ryzhov et al., 2010):

I. A hexagonal grid for the arrangement of fuel assemblies (FAs) in the reactor core and correspondingly the shape of fuel assemblies is hexahedral. The fuel rods in the fuel assembly are arranged in a triangular grid,
II. The material for fuel rod cladding is zirconium–niobium alloy,
III. Opportunity for transportation of all large-sized equipment by railway to allow a complete manufacturing process under factory conditions,
IV. The reactor vessel material is high-strength alloyed carbon steel that is serviceable in high neutron radiation fluxes,
V. The bottom part of the reactor vessel which contains the core has no nozzles or any other holes,
VI. The reactor vessel is manufactured of solid-forged shells without longitudinal welds,
VII. Control and protection system (CPS) drives, outlets of temperature and power control systems are arranged on the removable upper head unit of the reactor,
VIII. An original design of horizontal-type steam generators with a tube sheet in the form of two cylindrical heads,
IX. The material of steam generator heat exchanger tubes is austenitic stainless steel.

VVER-1000 reactors were started to be developed by OKB Gidropress in 1966. The first reactor with an electrical power of 1000 MW was built at Novovoronezh NPP Unit 5 in 1980. In the design, the traditional engineering solutions of VVER were used with the modernization from the experience acquired in the design, manufacture, and operation of the previous VVER models. The intention at design stage included an improvement in economic

efficiency of the NPP construction and ensuring operational safety in agreement with the regulatory documents at that time. An instantaneous double-ended guillotine break of the main coolant pipeline was considered as the maximum design basis accident. Containment of prestressed concrete enclosed the reactor plant (Ryzhov et al., 2010).

2.1.1 Reactor Vessel and Internals

The reactor of VVER-1000/V446 is a vertical high-pressure vessel which consists of a core barrel with a core baffle, protective tube unit (PTU), fuel assemblies (FA) forming the core, and control rods connected to extension shafts of the drive displacement units. The reactor top head with drives moving control rod core axial is placed on the vessel flange, as could be seen in Figure 2-1.

The reactor vessel is made of several solid-forged shells, inter-welded, with elliptic bottom and flange, tightly sealed with two rod gaskets and tightened with 54 M170 studs. There are two vessel shells, each vessel shell has four nozzles with a nominal diameter of 850 mm, connected with pipelines of the reactor coolant circuit to four primary loops. Each shell also has two nozzles with a nominal diameter of 300 mm connected to the accumulators of the ECCS. The four outlet nozzles are placed above four inlet nozzles with a distance of 1800 mm between their centres.

The core barrel is made as a welded cylindrical shell that supports the bottom and flange and rests on the vessel shoulder. The elliptic bottom of the core barrel together with 163 supports and spacing grid form a structure for support and spacing of FAs. The core baffle, working as a displacer and the filter, is located in the core barrel at the core level. The core baffle consists of several massive rings mechanically connected with one another and with the core barrel bottom. The coolant passes through the longitudinal channels and cools the core baffle metal effectively. The metal of the core baffle and core barrel reduces fast neutron fluence that hits on the vessel during the assigned service life up to permissible value. A protective tube unit is placed on the FA cap from above, it is pressed to the core barrel flange with the elastic component that sets between the protective tube unit shoulder and the top head of the vessel. PTU lower slab is attached with FA spring-loaded heads providing spacing to FAs and preventing vibration. Forces from FA spring-loaded heads are transferred through the protective tube unit and compressed elastic component to the top head of the vessel. CPS control rods and in-core instrumentation system detectors are placed in the protective tubes.

The upper unit structurally combines the elliptic top cover, CPS nozzles, control rod drives, nozzles for in-core instrumentation system detectors output and air vent nozzle.

Coolant is forcedly supplied into the reactor through input nozzles using reactor coolant pumps. Next, the coolant goes down along the annular gap between the vessel and the core barrel to lower plenum, then into the core through the orifices of the bottom of the core barrel. Passing through the core the coolant is heated up due to nuclear reactions in the fuel and goes out of the core into the protective tube unit shell-side through the punched lower slab of the protective tube units. The coolant then leaves the reactor through perforations in the shells of the protective tube units, the core barrel and the hot leg nozzles of the vessel.

Systems of reactivity control are based on the use of two independent principles:

- mechanical displacement of CPS absorber rods in the core,
- change of boric acid concentration in the coolant.

The in-core instrumentation system detectors help with the measurement of power distribution on the core volume during normal operation, if necessary, power distribution and operational parameters connected with it can be changed by the motion of CPS control rods. Emergency protection of the reactor can bring the core to subcritical state from any power level at any permissible initial position of CPS absorber rods and maintain subcriticality of the core in case of reactivity release in accident conditions. The control rods are moved by the pitch electromagnetic drive of the ShEM-3 type at a rate of 2 cm/s.

The slow change of reactivity under normal operating conditions is provided by the feed and blowdown system by a change of boron concentration in the coolant. This system provides withdrawal of part of the coolant from the primary circuit with the current boric acid concentration and, supplies borated concentrate (39.5 - 44,5 g/dm^3 H_3BO_3, in standard conditions) to the circuit by using make-up pumps instead of the removed coolant. During reactor operation at power, borated regulation and CPS control rods enable to compensate changes of reactivity connected with fuel bum-up, transients on xenon, and also to make changes in the reactor power level (AEOI, 2003).

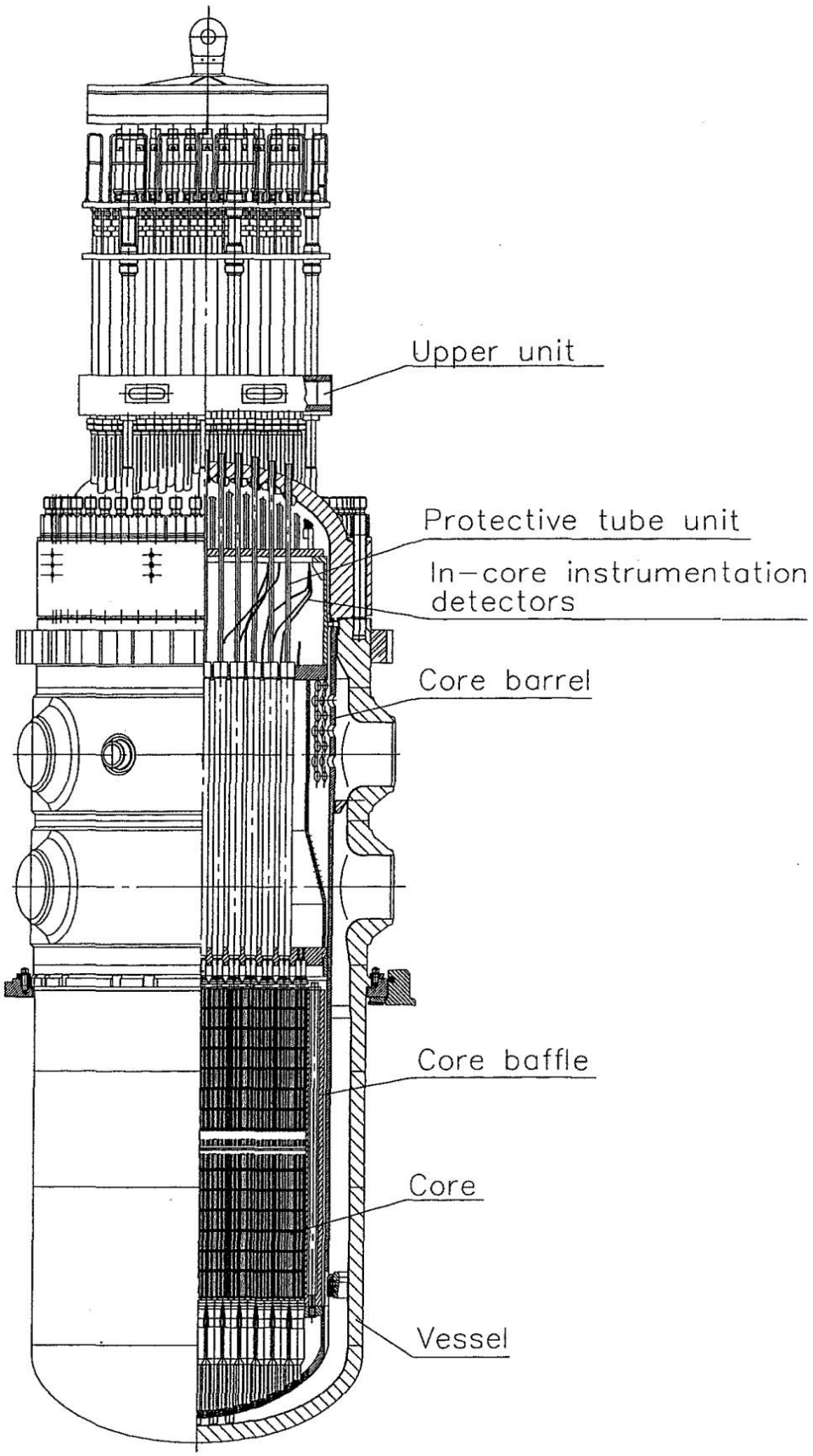

Figure 2-1. VVER-1000/V446 reactor with its internals (AEOI, 2003).

2.1.2 Reactor Core

The core of reactor VVER-1000 (V-446) is intended for heat generation and its transfer from the fuel rods surface to the coolant throughout the design fuel loading without exceeding the allowable limits of the fuel rods damage. The core in VVER-1000 (V-446) consists of 163 FA, in accordance with the core map, CPS absorber rods are moved, and burnable absorber rod bundles are arranged. CPS absorber rods are intended for quick termination of the nuclear reaction in the core, keeping the power at the assigned level. It provides power change from one level to another, axial power fuel flattening, and prevention and suppression of xenon oscillations. Burnable absorber rod bundles are intended for power field flattening over the core radius, decrease of multiplication coefficient at the beginning of fuel bum up cycle and provision of reactor operation within the range of coolant negative temperature coefficients of the reactivity (AEOI, 2003).

The VVER-1000 reactor core comprises 163 hexagonal FAs. The lattice pitch is 23.6 cm. The fuel rods are also arranged in a hexagonal structure inside FAs. The FA consists of three components: the cap, fuel rod bundle and tailpiece as could be seen in Figure 2-2. The FA cap is designed to perform the following functions (AEOI, 2003):

I. to ensure detachable engagement with the fuel rod bundle,
II. to ensure the required compression force of the reactor core assembly by considering thermal expansions of the reactor internals and fuel assemblies,
III. to protect the fuel rod bundle ends from mechanical damage during assembly re-loading,
IV. to interact with the grip device of the fuel handling equipment,
V. to stabilize coolant flow out of the core,
VI. to damp drop of the CPS absorption rods with the drive extension shaft during reactor scram.

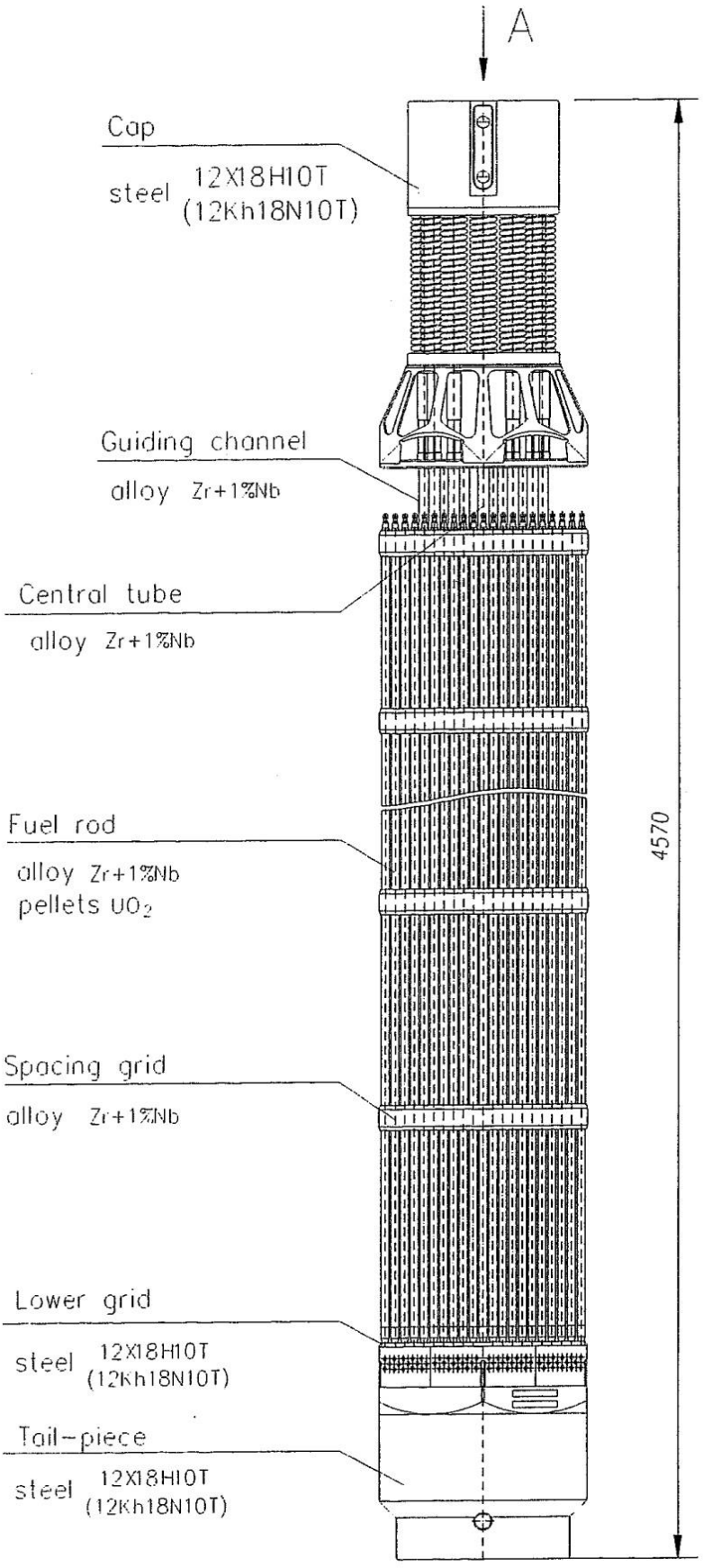

Figure 2-2. VVER-1000/V446 Fuel Assembly (AEOI, 2003).

The fuel rod bundle comprises 331 rod positions. The typical arrangement includes a tube with water at the centre, one position is used for in-core measurements, guide tubes of movable CPS absorber rods are placed into 18 positions, and the 311 positions are filled with fuel rods. Six of the fuel rods can contain burnable absorbers. The pattern could be seen in Figure 2-3 (Ryzhov et al., 2010).

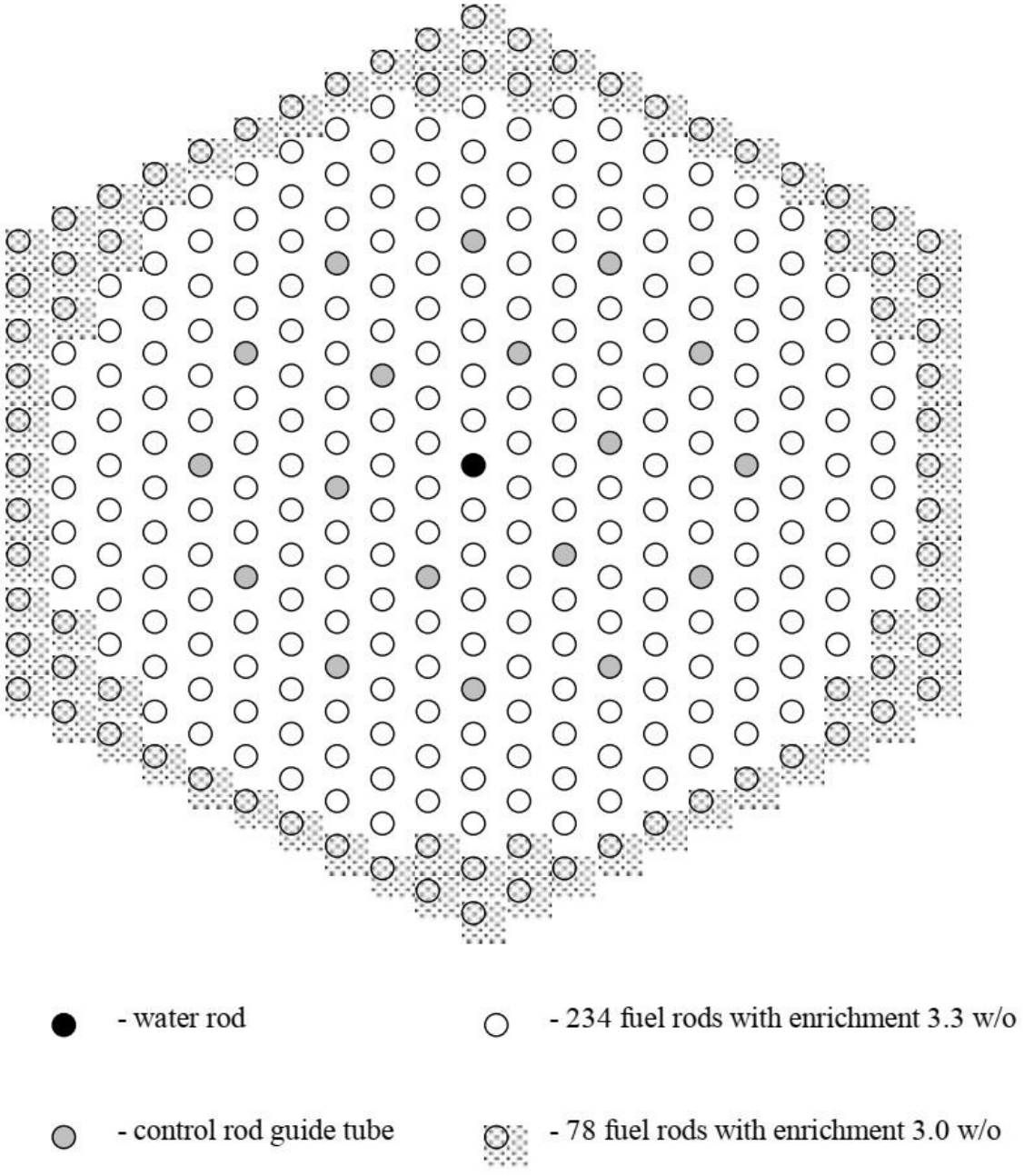

Figure 2-3. VVER-100/v446 Fuel assembly configuration (Ivanov et al., 2002).

CPS control rods includes 18 absorbing elements. The absorbing material used is boric carbide B_4C and dysprosium titanate (Dy_2O_3 TiO_2). Application of dysprosium titanate in the absorbing element lower part is contributed to expand the CPS AR service life with sufficient

efficiency of reactor scram to be remained. Boric carbide density should not be less than 1.7×10^3 kg/m^{3}and dysprosium titanate density should not be less than 4.9×10^3 kg/m^3.

The fuel rod structure consists of the following components: upper plug, cladding, lower plug, fuel stack made up of UO_2 pellets and a catch (Figure 2-4).

The fuel rod contains a tube with an outside diameter 9.1×10^{-3} m and end-pieces of zirconium alloy filled with the pellets of sintered UO_2. Material of fuel rod cladding is the alloy Zr1%Nb. The fuel rod plenum is filled with helium at pressure (2,0 ± 0,25) MPa to prevent cladding from in-service collapsing. Fuel rods are pressurized by welding. There is a gas receiver in the upper part of the fuel rod to collect any gas released during operation (AEOI, 2003).

Zr1%Nb alloy which is used as the cladding material in the core (as in Figure 2-2 and Figure 2-4) is one of the most prominent differences between VVER and western PWRs. In western PWRs, the cladding material is ZrSn alloy. The Zr1%Nb alloys have good operational experience at low temperatures, where they are more resistant to oxidation than Zircaloy. The VVER fuel cladding at the end of the cycle has a much thinner oxide layer and produces much less hydrogen than the PWR cladding of the western design. Therefore, the Zr1%Nb cladding appears to have significant ductility even at high burnups. The VVER cladding produces slightly more hydrogen at high temperatures, and the material becomes brittle at lower oxidation rates (OECD/NEA, 1999).

18 control rods inside a FA assemble a cluster. Control rod clusters are arranged into 10 groups, each group moves together. Control rod clusters are placed in 85 FA at the first fuel charge. Starting from the second fuel charge, the number increases to 103. The time passed for a control rod drop at reactor scram is not more than 4 s. The reactor core and the arrangement of control rod groups on it are demonstrated in Figure 2-5. The outermost layer consists of reflectors. The design characteristics of the core, fuel assembly and fuel rod could be seen in Table 2-1.

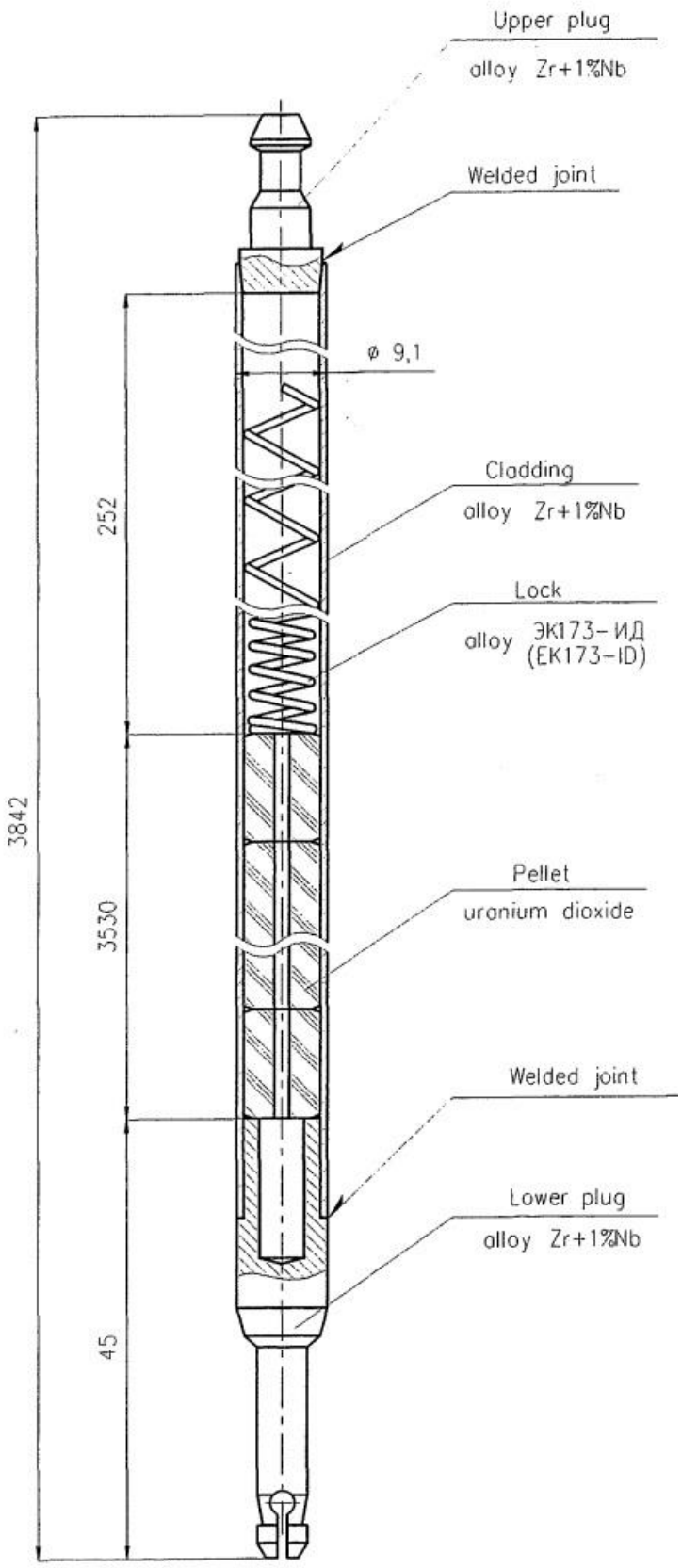

Figure 2-4. Fuel Rod of VVER-1000/V446 (AEOI, 2003).

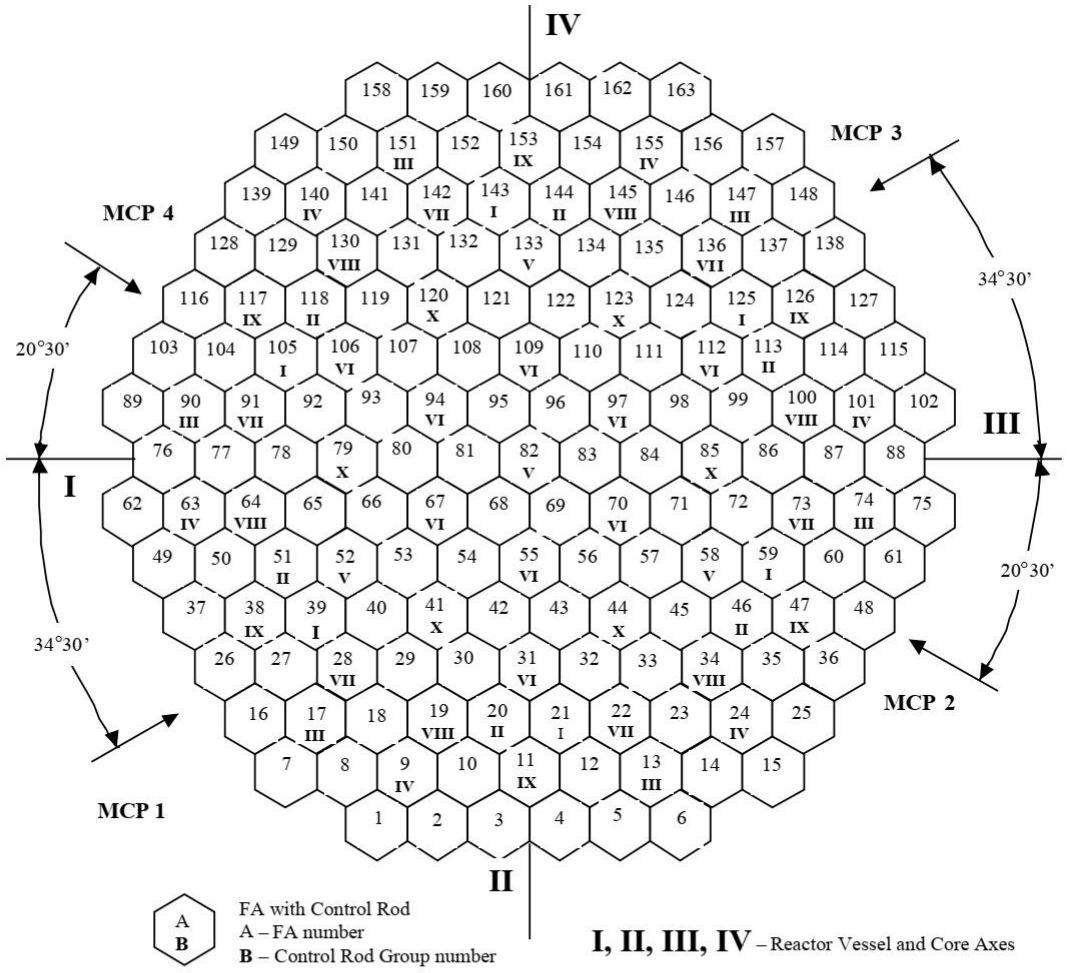

Bank	No rods	Purpose
I	6	Safety
II	6	Safety
III	6	Safety
IV	6	Safety
V	4	Parth-lenght
VI	9	Safety
VII	6	Safety
VIII	6	Safety
IX	6	Safety
X	6	Regulating

Figure 2-5. The arrangement of control rods inside the core (Ivanov et al., 2002).

Table 2-1. Features of the VVER-1000 core, fuel assembly and fuel rod (AEOI, 2003).

Characteristics	Value
Core:	
nominal thermal power, MW	3000
number of FAs with burnable absorber pcs.	163
number of FA, pcs	Up to 42
nominal reactor cycle with UO_2, kg	around 79840
FA pitch, cm	23.6
core height in the working state, cm	355
core equivalent diameter, cm	316
average linear heat rate, W/cm	166.7
average fuel power density, kW/kgU	42.6
coolant flowrate, m^3/h	84000
The temperature at the reactor inlet, °C	291
water-uranium ratio (geometrical)	1.97
Fuel Assembly:	
FA form in a plan	hexagonal
arrangement of fuel rods	triangle
fuel rod pitch, mm	12.75
number of fuel rods in the fuel assembly, pcs.	312
nominal dimensions "for wrench", mm	23.4
uranium dioxide mass in the fuel assembly, kg	around 490
The number of guide channels, pcs.	18
The number of spacer grids, pcs.	15
measuring channel, pcs.	1
The central channel, pcs.	1
Fuel Rod:	
uranium dioxide mass in the fuel rod, kg	1575
cladding material	Zr1%Nb alloy
cladding outside diameter, mm	9.1

cladding inside diameter, mm	7.73
fuel pellet material	UO_2
fuel pellet outside diameter, mm	7.57
hole diameter in the fuel pellet, mm	1.5
fuel pellet height, mm	11
fuel pellet density, g/cm^3	Btw 10.4 - 10.7

2.1.3 Reactor Coolant System

The reactor cooling system for the VVER-1000 reactor plants under normal operating conditions (primary side) comprises four circulation loops. Each circulation loop is composed of a reactor coolant pump (RCP) and a steam generator. Each loop has two pipeline sections which are distinguished as hot and cold legs. The pipe section from the reactor outlet nozzle-to-steam generator collector is the hot leg. The pipe sections from the steam generator outlet nozzle to the RCP inlet nozzle and the RCP outlet nozzle to the reactor inlet nozzle compose the cold leg. The connection between the hot leg of the fourth circulation loop and the pressurizer is made by a 426 × 40 mm surge line. The connection between the hot leg of the third circulation loop and the pressurizer is made by a 219 × 20 mm line and it is an injection line.

The material selected for the RCP is 10GN2MFA alloy structural steel. The internal pipe surface is clad with corrosion-resistant 04X20N10G2B stainless steel not prone to intergranular corrosion by the coolant (Ryzhov et al., 2010). The primary circuit system layouts are demonstrated in Figure 2-6 and Figure 2-7. The thermal-hydraulic features of the primary system are listed in Table 2-2.

The main steady-state conditions of the reactor plant operation are:

- operation with four loops at nominal power,
- operation with three and two loops at 67 % of power (three loops), 50 % (two opposite loops), 40 % (two adjacent loops);
- natural circulation of the reactor coolant system with removal of residual heat from the core following the reactor shutdown due to trip of all RCP sets.

Under operation with three or two loops (RCP sets are tripped in inoperative loops and steam generators of these loops are connected to steam header by steam), the

temperature mode of operating loops is practically identical to the case of operation with all four loops. Through the loops with RCP sets tripped, the reverse coolant flow takes place from the reactor inlet plenum into the reactor outlet plenum through the steam generator. Temperature of coolant in reverse flow in the section of the inoperative loop from the reactor inlet nozzles to the steam generator is equal to the temperature of coolant entering the reactor from operating loops, and in the section from the steam generator to the reactor outlet nozzles is practically equal to saturation temperature at steam pressure in the main steam header.

Natural circulation is used for the removal of residual heat from the core after the reactor shutdown due to the loss of all RCP sets. The possibility of these conditions is supported by the calculation analysis and tests at the forerunner unit with the standard WWER-1000 reactor. Power removed from the core by the natural circulation of coolant is 10 % of the nominal. that is considerably higher than the probable value of residual heat. With the indicated power the coolant at the outlet of the most-powered fuel assemblies of the core is subcooled to the saturation temperature of not less than 5°C (AEOI, 2003).

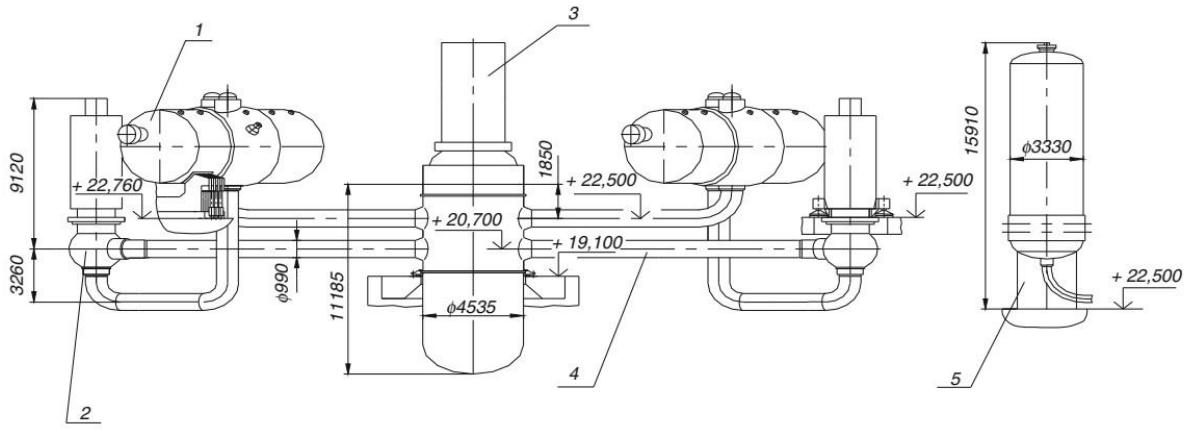

Figure 2-6. The first layout of the primary circuit, 1. Steam generator, 2. Reactor coolant pump, 3. Reactor, 4. Main coolant pipeline, 5. Pressurizer. (Ryzhov et al., 2010).

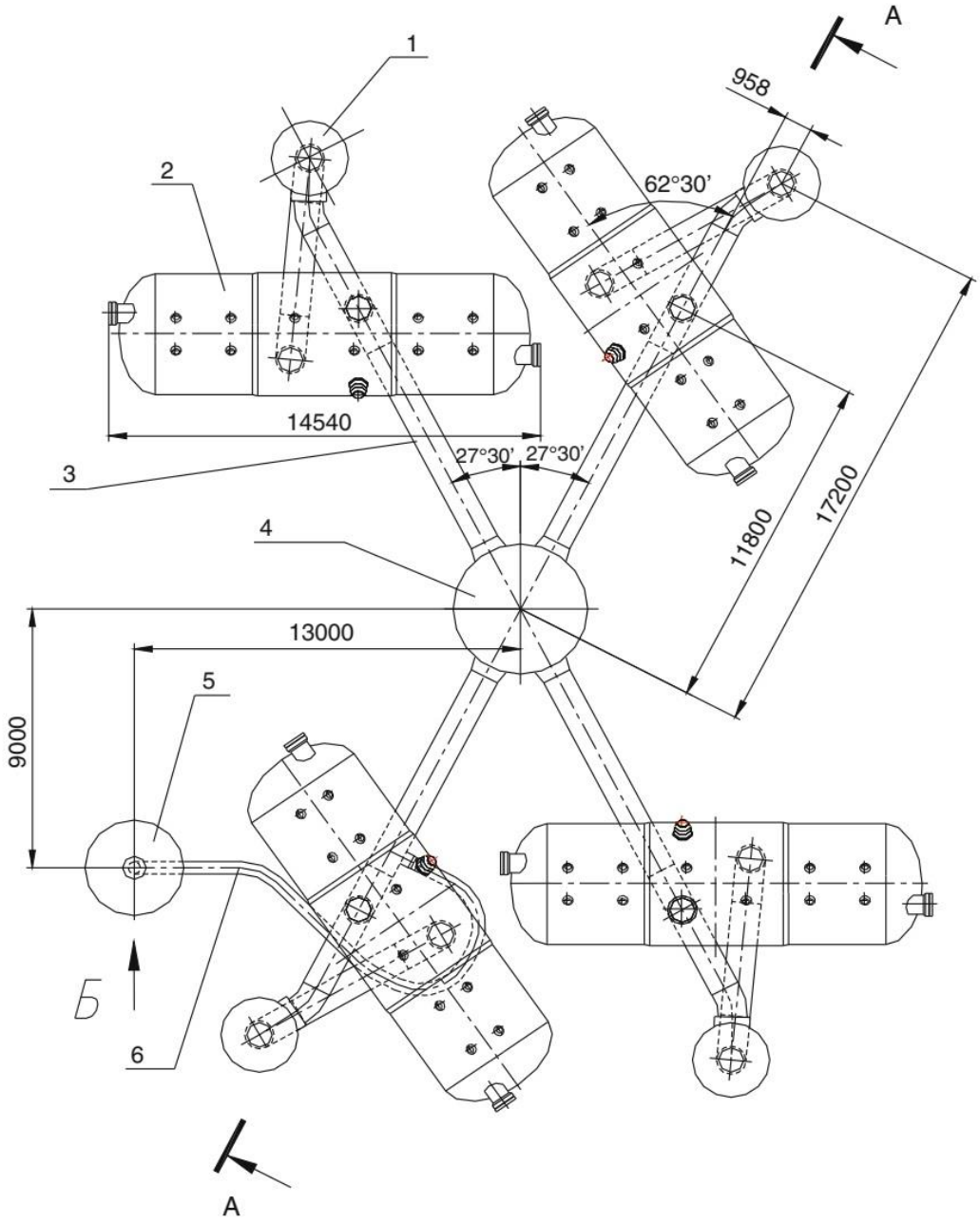

Figure 2-7. The second layout of the primary circuit, 1. Reactor coolant pump, 2. Steam generator, 3. Main coolant pipeline, 4. Reactor, 5. Pressurizer, 6. Surge line (Ryzhov et al., 2010).

Table 2-2. Thermal-hydraulic characteristics of the primary system (AEOI, 2003).

Parameter	Value
Nominal thermal reactor power, MW	3000
The flow rate through the reactor, m^3/h	84800
Operating pressure, MPa	15.7
Coolant temperature at the reactor inlet, °C	291
Coolant temperature at the reactor outlet, °C	321
Coolant enthalpy at the reactor inlet, kJ/kg	1290
Coolant enthalpy at the reactor outlet, kJ/kg	1460
Coolant density at the reactor inlet, kg/m^3	743
Coolant density at the reactor outlet, kg/m^3	675
The number of loops, pcs.	4
Steam pressure in the steam generator header, MPa	6.28
The temperature of the main feedwater in the steam generator, °C	220
The steam capacity of the steam generator, t/h	1470
Steam moisture at the steam generator outlet, %	maximum 0.2

2.1.4 Steam Generators

The steam generators used in the VVER-100 are of the PGV-1000M type. It is a single-vessel recuperative heat exchanger with a horizontal alignment which guarantees that the heat transfer surfaces are submerged. The heat transfer surface in the steam generator design enables the contact of the primary coolant with the secondary coolant. The vessel of the steam generator contains forged shells, stamped elliptic bottoms, and forged nozzles that are joined by welding. The vessel design provides easy access to inspect the internal structures from the secondary side (Ryzhov et al., 2010).

The heat transfer surface consists of 10978 U-tubes, 16 × 1.5 mm in size, that are arranged in coils and positioned in a staggered order horizontally. The coils are connected to primary-side collectors. The U-tube ends are hydraulically expanded over the collector wall thickness and

are argon-arc welded onto the inside surface of the collectors. The material used for the U-tubes is austenitic steel. The primary-side collectors are designed to distribute the coolant in the heat exchange tubes, collect, and evacuate it. The internal surface of the collector is covered with two layers of corrosion-resistant cladding (Ryzhov et al., 2010). The steam generator used in VVER-1000 could be seen in Figure 2-8.

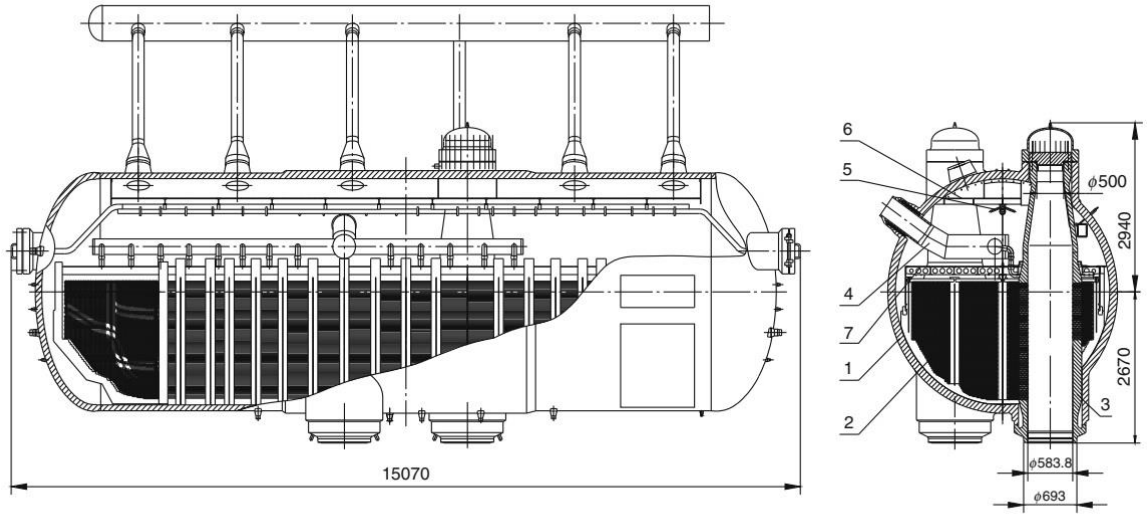

Figure 2-8. The steam generator of VVER-1000. 1. Vessel, 2. Heat transfer surface, 3. Primary-side collectors, 4. Main feedwater distribution devices, 5. Emergency feedwater distribution devices, 6. Steam-receiving perforated plate, 7. Submerged perforated plate (Ryzhov et al., 2010).

2.1.5 The Pressurizer

The pressurizer is a vertical vessel connected to the hot leg of the primary circuit loop as could be seen in Figure 2-9. The pressurizer is equipped with a spray system and electrical heaters to keep the pressure of the primary circuit at constant. The spray system is placed at the top of the pressurizer and is designed for injecting water into the steam volume to provide steam condensation and consequent pressure drop (IAEA, 2005b). The water source lines that supply the spray system are (Ryzhov et al., 2010):

- The RCP discharge line under normal operating conditions and under AOOs,
- The discharge line of the high-pressure emergency injection pumps under DBA and BDBA conditions.

Electric heaters, placed in the lower part of the pressurizer, are designed for water heating and consequent pressure increase in the primary circuit. They are also used for coolant heating during reactor start-up (IAEA, 2005b).

The pressurizer vessel is made of carbon steel with austenitic cladding on the internal surfaces to increase the resistance to corrosion. The pressurizer is connected to the hot leg of the main coolant pipeline through the lower nozzle of the surge line with a nominal diameter of 350 mm (Ryzhov et al., 2010). Table 2-3 provides the main parameters of the pressurizer.

Table 2-3. Main parameters of the pressurizer (IAEA, 2005b; Ryzhov et al., 2010).

Parameter	Value
Pressure, MPa	15.7
Temperature, °C	346
Total Volume, m^3	79
Water volume under nominal conditions, m^3	55
Steam volume under nominal conditions, m^3	24
Electric heaters power, kW	2520 ± 190
Quantity of electric heaters, pcs.	28

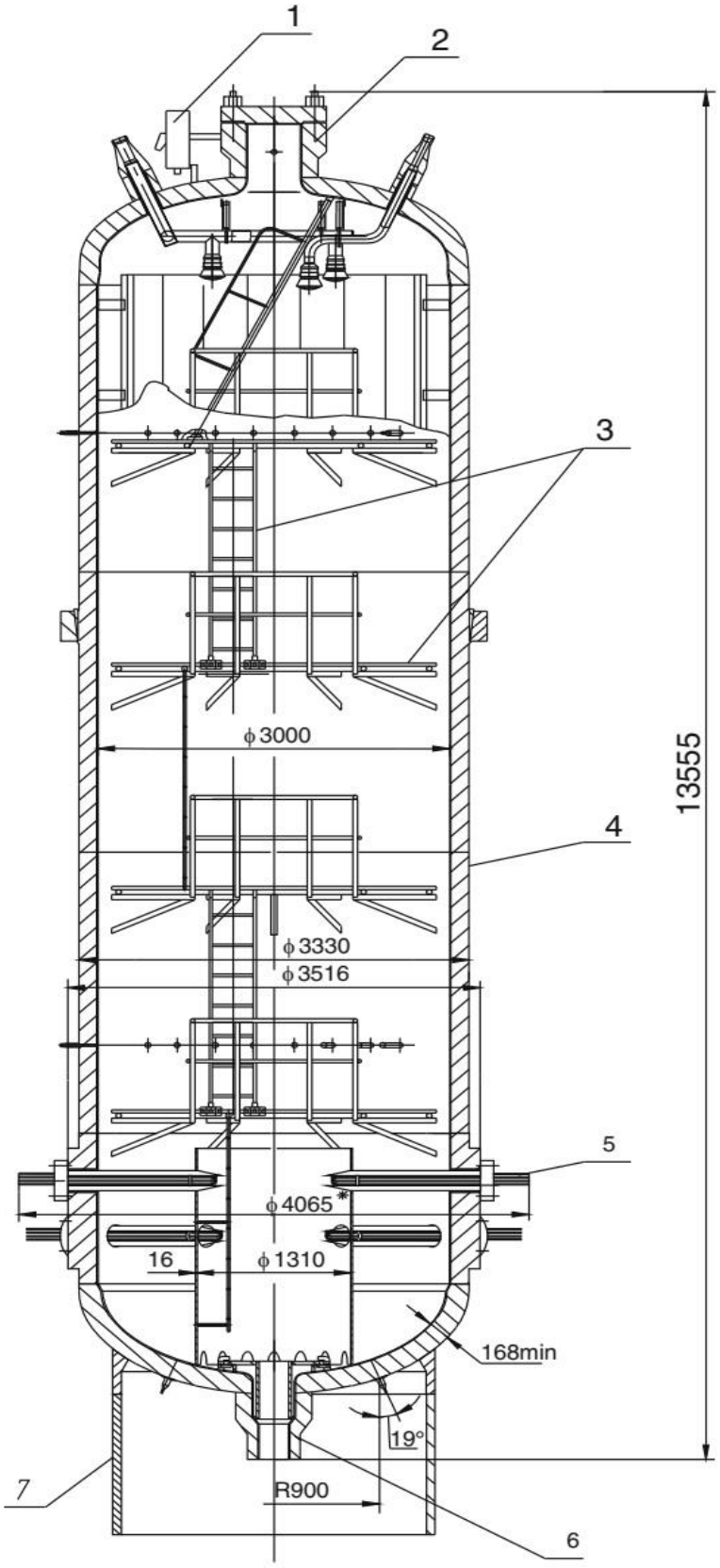

Figure 2-9. The pressurizer (Ryzhov et al., 2010). 1. Surge Bottle, 2. Neck, 3. Internals, 4. Vessel, 5. Tubular electric heater unit, 6. Nozzle, 7. Support.

2.2 VVER-1000/V446 Containment

The containment design consists of two layers: the outer cylindrical reinforced concrete layer and the inner spherical steel layer as seen in Figure 2-10. Negative pressure is retained between two layers to collect any leakage in an emergency. The secondary cylindrical concrete containment acts as a protective shell for the reactor building from the outside effects. It is also used as biological protection against ionizing radiation. The inner spherical steel containment comprises the main system components and some of the auxiliary instruments. The radius of the inner containment is 28 m. The parameters of the design and structure of the containment are listed in Table 2-4.

The outer protective containment is of a cylindrical shape with a spherical dome. It is made of cast-in-situ reinforced concrete. The containment thickness at the top is 1750 mm, whereas at the bottom it is 2000 mm. Its diameter as per the outer edges is 62.8 m. Its total height is 60.4 m. The gap between the outer concrete and inner steel containment in their dome part is 1650 mm. This allows them to operate independently in all modes, including an aircraft crash on the outer containment. In points of the annulus civil constructions supporting the outer containment, there are envisaged technical facilities reducing the transfer of dynamic loads to the inner constructions from specific effects on the outer containment. The outer containment is provided with necessary number of doors and gates required by process and fire safety regulations.

The outer containment is made of concrete, grade Bn-250 with a density of 2.35 kg/m^3. This complies with the requirements of biological protection. The inner surface of the containment is coated with a protective epoxy layer. Due to insignificant negative pressure formed in the annulus, the lack of leakage from the annulus to the environment is ensured by the natural density of the containment concrete.

With the purpose to protect the secondary protective containment from overpressure all pipelines with high parameter materials running through them (temperature higher than 150 °C) and the break of them which can result in a pressure increase in the secondary protective containment, are located within the steel containment (AEOI, 2003).

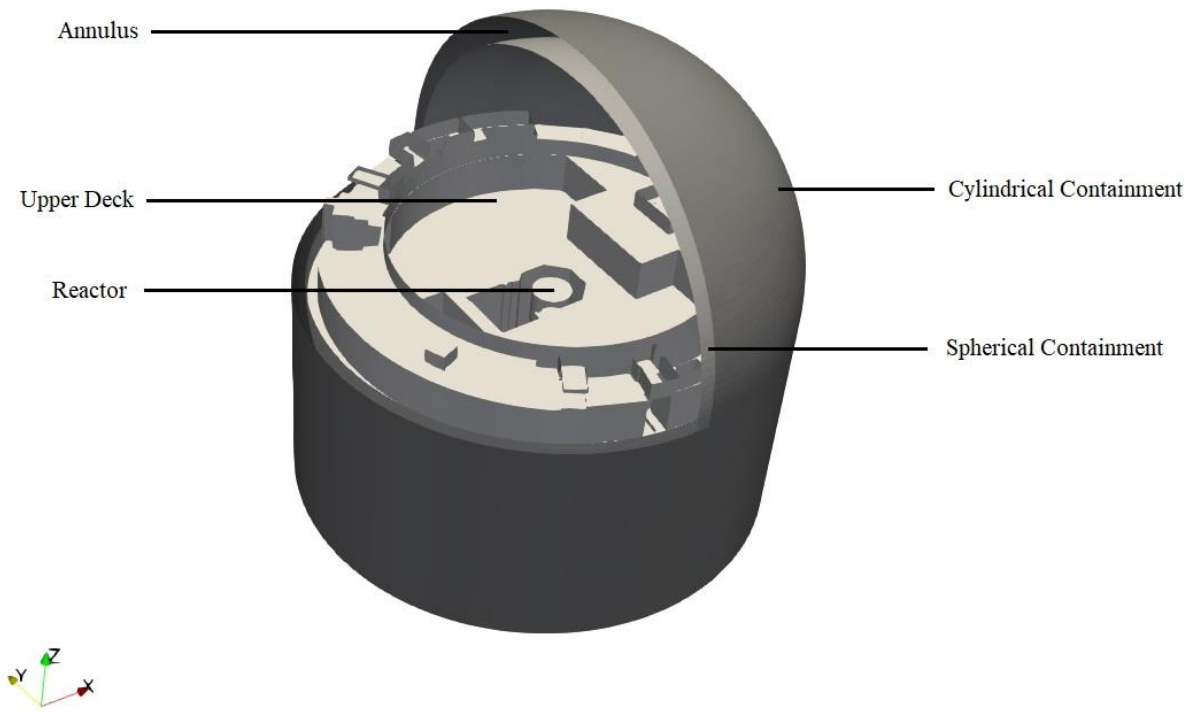

Figure 2-10. Simplified version of the VVER-1000 containment showing the annulus and the two-containment system.

The pipelines of the secondary circuit cross the double protective containment and run through the space between the steel containment and concrete protective containment with the purpose to avoid increase of parameters due to break of pipelines. Break of the pipelines with low parameter materials running through them (temperature not higher than 150 °C) in annulus is not dangerous with respect to increasing pressure in this space and the performance of its functions. For the creation of rarefaction inside the annulus during accidents and loss of power, a ventilation system is provided. During normal operation of the plant, the ventilation system is on standby. The system is activated automatically at pressure increase in the rooms of the hermetic containment above 0.03 MPa (overpressure) or by an interlock of the stepped load on the diesel generator during power loss. The ventilation system also provides removal of radioactive materials coming through loose seals of the steel protective containment in the annulus and discharge from a vent pipe through filters. The safety systems are located within the spherical containment as well as the other systems containing radioactive materials. All systems are made from welded structures except pipe joints, requiring flange coupling for maintenance and repair (AEOI, 2003).

Table 2-4. Structural and design parameters of VVER-1000 containment (AEOI, 2003).

Parameter	Value
Structural Parameters:	
Inner steel diameter (m)	56
Inner steel thickness (m)	1.65
Outer reinforced concrete shell thickness (m)	1.75
Containment free volume (m^3)	71040
Design parameters:	
Maximum internal pressure at 150 °C (MPa)	0.46
Maximum pneumatic test pressure at a temperature of up to 60 °C (MPa)	0.51
Peak temperature (in separate compartment) (°C)	Up to 206 °C for up to 5 minutes
Maximum (averaged over the volume) temperature (°C)	150

The detailed representation could be examined in side and front view plans of the containment, Figure 2-11 and Figure 2-12, respectively. The elevation of the spherical containment at the bottom is -5 meters. At the elevation of 23 meters, the xy plane cuts through the spherical containment centre. The rooms that start with the AO code are placed in the spherical containment. Auxiliary rooms that are between spherical and cylindrical containment have a BO code before their number. The upper deck is at an elevation of 21.5 meters. Two of the circulation loops with RCPs (number 25) and steam generators (number 30) and the reactor core (number 24) could be observed in Figure 2-11. The bubbler tank (number 29), the pressurizer (number 26) and the reactor core could be seen in Figure 2-12. The two pools that are located on the left side of Figure 2-12, are the fuel pool (leftmost) and the inspection well reactor pressure vessel internals. The following view plans are from

elevations -6 m, -1.5 m, 2 m, 6 m, 9 m, 10.5/12 m, 16.4 m, 21.5 m and finally 26.8 m, provided through Figure 2-13 to Figure 2-21.

Figure 2-11. The side view (yz plane cut through the center) of the VVER-1000/V446 containment. (This space is intentionally blank for security reasons).

Figure 2-12. The front view (xz plane cuts through the center) of the VVER-1000/V446 containment. (This space is intentionally blank for security reasons).

Figure 2-13. The view plan of the containment at -6 m. (This space is intentionally blank for security reasons).

Figure 2-14. The view plan of the containment at -1.5 m. (This space is intentionally blank for security reasons).

Figure 2-15. The view plan of the containment at 2 m. (This space is intentionally blank for security reasons).

Figure 2-16. The view plan of the containment at 6 m. (This space is intentionally blank for security reasons).

Figure 2-17. The view plan of the containment at 9 m. (This space is intentionally blank for security reasons).

Figure 2-18. The view plan of the containment at 10.5/12 m. (This space is intentionally blank for security reasons).

Figure 2-19. The view plan of the containment at 16.4 m. (This space is intentionally blank for security reasons).

Figure 2-20. The view plan of the containment at 21.5 m. (This space is intentionally blank for security reasons).

Figure 2-21. The view plan of the containment at 26.8 m. (This space is intentionally blank for security reasons).

2.3 VVER-1000/V446 Containment Engineered Safety Features

2.3.1 Containment Spray System (CSS)

CSS is designed for operation under emergency conditions arising from leakage of the primary coolant system and leakage of the secondary side inside the containment. Under normal operating conditions the system does not operate and is in the standby mode. The system elements during operation are subject to periodic tests. The system performs the reduction function of pressure, temperature and radioactive iodine isotope concentration inside the steel containment during emergency conditions.

The CSS design has been developed proceeding from conditions of a DBA, involving reactor coolant system large breaks (LB-LOCA) inside the steel containment by making allowance for the following principles:

I. single failure principle,
II. redundancy principle,
III. separation principle,
IV. automatic response principle.

The system efficiency permits maintaining the pressure within the steel containment in case of design-basis accidents within design values, time required for pressure reduction does not exceed 24 hours, while standards in terms of releases and content of radioactive products in the environment do not be exceeded.

Power supply of the CSS mechanisms is provided by a normal operation power supply system and an emergency power supply system. In case of loss of power, the system is fed by the emergency power supply system.

CSS consists of two spray headers located at the top of the containment approximately 2 meters below the steel layer (Figure 2-22). Each header comprises 10 to 11 nozzles to cover all the containment volume below effectively with the spray water jets. Boric acid solution (16 g of H_3BO_3 per 1 kg H_2O) is supplied to each spray header in the amount of 83.3 kg/s by the borated water tanks of the residual heat removal system until the water in the sump reaches the necessary head pressure to feed the spray system itself. CSS is in standby mode initially. The actuation of the system starts as soon as the pressure difference reaches 0.03

MPa inside the containment following a LOCA or a secondary side rupture. In case of a signal on loss of normal power at any moment of the accident the pumps in the CSS are switched over to the emergency power supply system and are actuated according to the program of stepped startup of the diesel generators. The spray temperature is not a fixed value but rather between 20-60 °C, since the water temperature in the sump is not constant. The solution that is sprayed also includes iodine-binding reagents to keep the radioactive products below the limit. The spray headers are located in the spherical volume of the containment at elevations 48.5 and 49.0 m, with this arrangement, the falling height of thin-dispersed droplets is about 27 m.

All pipelines of the CSS have been manufactured from steel of 08X18H10T grade. The valves have been manufactured from austenitic-class stainless steel. All joints are welded joints. The materials have been considered for compatibility with the components of the containment spray system with respect to the boric acid solution (AEOI, 2003).

2.3.2 Containment Vessel Isolation System (CVIS)

The function of CVIS consists of isolating the pipelines, systems containing process fluids (primary coolant, high- and low-pressure nitrogen, air, etc.) penetrating the containment vessel to ensure that no uncontrolled release of radioactivity from the containment can occur, particularly following a radiation release type accident. The requirements of the system could be listed like this:

I. compliance with the design requirements for designing the equipment for safety class 2,
II. To provide one barrier at least for isolation assuming a single failure,
III. permitting isolation of the containment in the time required.

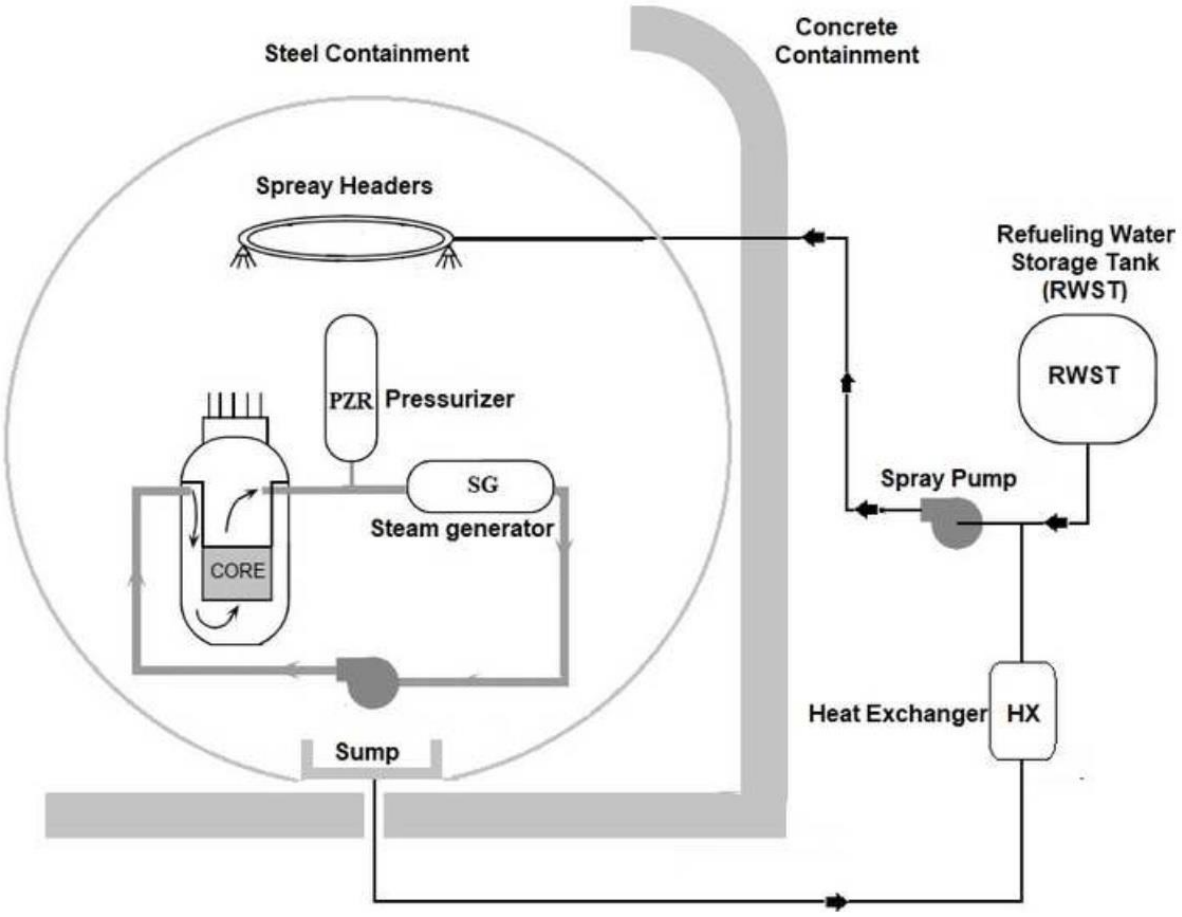

Figure 2-22. The Layout of Containment Spray System.

All the isolation valves withstand threshold leakage within reasonable limits. Total leakage through all the valves in a penetration is less than 60 % of the maximum permissible leakage in the containment. The main portion of the leak goes into the annulus and is discharged into the atmosphere after being filtered.

Signals for the containment isolation received from the reactor protection systems are the first condition for actuation of the valves with electric drive and pneumatic drive in the systems, which are not required for technical safety means or for the system relating to safety.

Signals for the containment isolation are executed by at least two levels of emergency conditions for isolating specific systems:

- signal on pressure increase within the containment up to 0.0003 MPa initiating closing of the ventilation systems in the containment is the signal for the first phase of isolation,

- signal of the second phase of isolation is generated by overpressure in the containment up to 0.03 MPa, initiating closing of localizing valves of systems, which do not have safe shutdown function or safety function in case of emergency.

All the isolating valves have positioning sensors in order to make it possible to exercise continuous control over the progress from the main control room and emergency control room (AEOI, 2003).

2.3.3 Hydrogen Removal System (HRS)

The HRS is designed to control the concentration of hydrogen that may be released within the containment vessel atmosphere following a LOCA (detailed information about hydrogen mitigation systems, especially PARs could be found in section 3.5.). In DBAs, the HRS maintains indoor hydrogen concentrations inside the containment below flame-propagation limits, in the design range of the parameters of containment atmosphere. In the HRS, which ensures hydrogen-related safety in the containment, passive catalytic hydrogen recombiners are used, which are located in the places where accumulation of hydrogen is possible.
Under design basis accidents, hydrogen monitoring system ensures the monitoring of the volumetric hydrogen concentrations and defines the hydrogen safety/hydrogen danger status within the compartments of the containment and presents the information to operative personnel.

The system is designed proceeding on the following principles:

I. single-failure principle,
II. redundancy principle,
III. separation principle,
IV. principle of system’s automatic actuation.

Under DBA conditions, deflagration burning, even local, is ruled out. The design limit is not more than 2 % of hydrogen concentration by volume on the average over the volume inside the containment under DBAs (24 h). The design limit for the post-accident period (for 30 days) is not more than 0.5 % of hydrogen concentration by volume on the average over the volume inside the containment.
Following a LOCA, hydrogen gas may accumulate within the containment vessel from various sources. If a sufficient amount of hydrogen is generated, it may react with oxygen present in the containment vessel atmosphere at rates rapid enough to lead to high temperatures and significant over pressurization of the containment vessel. The lower

flammability limit for hydrogen in air saturated with water vapour at room temperature and atmospheric pressure is assumed to be 4 per cent. The components of the HRS have been designed so that they will operate successfully to maintain the maximum hydrogen concentration in the containment at or below 2 % by volume during LOCA and below 0.5% by volume in the post-accident period. The limit equal to 2 per cent by volume was selected to reflect a reasonable limit to avoid problems like nonuniform mixing etc. The concentration of 2 per cent by volume is not reached.
The hydrogen monitoring system is in function under all operating conditions including accident conditions.

The hydrogen monitoring system is designed to**:**

- **a)** present information to the operating personnel on the status of the hydrogen-air-vapour mixture in the containment with regard to the safety design limits,
- **b)** monitor the functional capability of the HRS in performing its designated function.

The hydrogen monitoring system generates an alarm signal to the main control room (MCR) and emergency control room (ECR) when the volumetric hydrogen concentration of 2 % is reached within the containment.

The operation of the HRS is based on the passive principle, so it does not require the signal from the system of monitoring the hydrogen concentration or power supply for its operation. On the other hand, the hydrogen monitoring system should be powered from a 2nd group normal and emergency power supply system (AEOI, 2003).

The HRS employs RVK-500 recombiners to dispose hydrogen through flameless catalytic burning. It is manufactured by CJSC INPK RET, Russia. The catalyst unit of RVK-500 recombiner includes 696 catalytic cylindrical rods. The height of each rod is 64 mm, and the diameter is 5 mm (Avdeenkov et al., 2022). Mechanically, a PAR includes a unit of catalysts, comprising a set of catalytically active components, convection section, having a protective housing, and a cantilever to fasten it to the embedded part. The platinum group metals are used as the catalyst (AEOI, 2003). An RVK-500 unit could be seen in Figure 2-23 and the characteristics of the recombiner are listed in Table 2-5.

Figure 2-23. An RVK-500 unit (Avdeenkov et al., 2022). 1. PAR framework, 2. Catalyst unit comprises a set of catalytic frames, 3. Catalyst rods combined in frames.

The operating principle of the hydrogen concentration sensor used in hydrogen monitoring system is based on the property of a conductor made of a palladium-silver alloy to absorb hydrogen from the steam-gas mixture being analysed, and to change its resistance as hydrogen is absorbed. The amount of absorbed hydrogen is proportional to its partial pressure and, hence, its volumetric concentration. The change in the electric resistance is proportional to the amount of absorbed hydrogen. Thus, knowing the change in the resistance and the pressure of the steam-gas mixture, one can determine the hydrogen concentration (AEOI, 2003).

Table 2-5. The parameters of RVK-500 recombiner (AEOI, 2003).

Characteristic	Value
Height, mm	950
Width and Length, mm	226 × 334
Mass, kg, maximum	25
Specific capacity for recombined hydrogen, kg/(m^2s) (capacity related to the area of the convective section of the shell at 0.2 MPa and 100 °C):	
when the volumetric concentration of hydrogen is 3 %	0.001
when the volumetric concentration of hydrogen is 5 %	0.0022
when the volumetric concentration of hydrogen is 8 %	0.0046

Under normal operating conditions negligible quantity of hydrogen, being escaped due to possible coolant leakage, and generated due to spent fuel cooling pond water radiolysis, may be available inside leak-tight compartments. Taken from the experience results, hydrogen volumetric concentration inside the leak-tight compartments does not exceed 0.3 %, and there is no need for the operation of the HRS. Thus, HRS is in standby (ready-to-operate) mode during normal operation. The HRS comes into action under the following conditions (AEOI, 2003):

I. when the steam-gas medium in the containment has a temperature of above 20 °C, and the volumetric concentration of hydrogen is not less than 0.45 %,
II. when the steam-gas medium in the containment has a temperature of above 20 °C, and the volumetric concentration of oxygen is more than 0.45 %.

The total number of PARs and hydrogen detectors that are installed inside the containment were selected as 80 and 32, respectively. HRS capacity, specified by the number of PARs, was matched on the base of hydrogen generation inside the containment during the DBA associated with coolant leakage caused by rupture of a pipeline of maximum nominal

diameter 850 mm. This particular accident is characterized with availability of full spectrum of potential hydrogen sources, located both inside and outside the reactor vessel, with adherent specific features, such as intensity and length of existence within both accident, and post-accident period of time. Moreover, in determining HRS capacity, it is considered that PAR numbers should be 20 % more than its design number by taking into account the redundancy principle, based on the experience gained and the items listed (AEOI, 2003):

I. not more than 10 % of system devices in each compartment are allowed to be damaged by missiles,
II. 5 % increase is accepted for the purpose of reducing the ambiguity in the degree of environment non-uniformity inside the containment.

2.4 The Accident Scenario

In this section, the first subsection will give information about the variant that were selected in this thesis for the analysis of the containment response in terms of TH parameters. The second part introduces the variant for the hydrogen distribution analysis, which is the same variant, with the consideration of the hydrogen sources and their contributions to the overall hydrogen release following the onset of the accident. The hydrogen distribution analysis considered in FSAR is a DBA accident, this thesis examines the same accident for comparison purposes between models in FSAR and in this thesis.

2.4.1 Determination of Mass and Energy Release of the Postulated Accident

In case of a postulated leak in primary or secondary circuit, coolant mass and energy release results in air pressure and temperature increase inside internal containment. Reached values of temperatures and peak pressures depend on various factors, such as rupture point, leak size, etc. Basing on the results of calculations of mass and energy releases from the reactor unit under pipelines ruptures, the accident with main circulation pipeline (MCP) rupture at the reactor inlet (under which maximum release of energy in the form of steam takes place) was selected for the analysis as an accident determining maximum pressure in containment.

Mass and energy yield analysis for the postulated accidents with the loss of the primary circuit coolant is performed for the following design-basis accidents:

- rupture of the main circulation pipeline at the reactor inlet (nominal diameter (NB) 850 mm),
- rupture of the main circulation pipeline at the reactor outlet (NB 850 mm),
- rupture of injection pipeline from pressurizer (NB 179 mm),
- rupture of pipeline with equivalent NB 100 mm diameter at the reactor inlet,
- rupture of pipeline with equivalent NB 50 mm diameter at the reactor inlet.

The main task of analysing the above mentioned off-normal modes consists in the determination of the maximum mass and energy release from the viewpoint of substantiation of the containment. It is conservatively assumed that the leakage is located directly near the reactor vessel, as a much faster and deeper depressurization of the primary circuit takes place in this case.

To take account of leakage location effect on the mass and energy release during the analysis of the mode with the main circulation pipeline rupture at the reactor inlet (NB 850 mm), two variants are considered: Main coolant pump line rupture at the reactor inlet and at the RCP suction. When analysing the modes with main coolant pump line rupture at the reactor outlet (NB 850 mm) two variants are as well considered: rupture of a loop with and without pressurizer. To take account of the effect produced by the proportionality of water distribution from ECCS pumps between the reactor chambers two variants of supply are considered: proportional distribution of water from ECCS pumps between the reactor chambers and complete leakage of water. Conditions and parameters of mass and energy release under which both maximum and minimum energy release to the containment are determined. When choosing the scenario of occurrence of accidents with the pipeline ruptures and the total number of possible combinations of operating channels of emergency safety systems in the course of an accident, the main purpose of the calculations was taken into account, namely, achievement of the maximum (or minimum, if necessary) steam generation under the containment.

In total, there are six variations of ruptures at the primary circuit with break size NB 850 mm considered in the analysis as explained above:

- Variant 1 : Rupture at the reactor inlet, uniform distribution from ECCS.
- Variant 2 : Rupture at the reactor inlet, the water injected by ECCS into RPC.
- Variant 3 : Rupture at the reactor outlet, loop with pressurizer.
- Variant 4 : Rupture at the reactor outlet, loop without pressurizer.

- Variant 5 : Rupture at RCP suction.
- Variant 6 : Rupture at the reactor inlet (for calculation of minimum pressure inside the containment.)

Analysis of mass and energy release for the postulated accidents with the loss of coolant is conducted according to the TETCH-M-97 program in FSAR. TETCH-M-97 program simulates all main components and systems of plants with VVER-type reactors: reactor, steam generators, pressurizer, RCP, RHRS (hydraulic vessels and pumps), control and protection systems etc.

To obtain the maximum pressure under the reactor containment the following heat sources were taken into account in the course of mass and energy release analysis.

Composition of the heat sources accounted:

1. primary circuit coolant,
2. water supplied by ECCS pumps,
3. residual power density heat,
4. energy, accumulated in the core,
5. energy, accumulated in the primary circuit metal structures,
6. secondary circuit heat.

The input data for calculations and the assumptions are chosen so that to ensure the conservatism of the results of calculations of the accidents being discussed from the standpoint of obtaining maximum (and minimum, if necessary) releases of mass and energy into the containment.

The reactor is assumed to be operating at a core power level of 3120 MW with the conservative zero moderator coefficient. The initial fuel temperature is calculated with account for fuel densification effects. The initial volume of primary side coolant corresponds to the high water level in the pressurizer (the nominal level plus measurement error). The TECH-M-97 computer code calculates heat exchange between the coolant and the metal of the reactor and other components in the primary and secondary circuits considering their different thickness. When calculating the heat transfer, the influence of the varying water level at the metal surfaces of reactor chambers is considered. Summary information about the basic initial data to conduct calculations of mass and energy release under the postulated ruptures of the primary circuit is in Table 2-6. All six variants are compared within the list.

The four loops of the reactor primary circuit with the position of the break point for the variant 2 is depicted in Figure 2-24. It should be noted that Variant 6 in Table 2-6 is designed for evaluation of the minimum pressure value in the steel containment, so the initial parameters were accepted with respect to deviations to a low value and the quantity of ECCS channels in the case is maximized. It provides the minimum steam outflow from the reactor to the steel containment volume during the accident.

In this thesis, the LOCA selected to examine containment response and hydrogen concentration is variant 2, a large break (NB=850mm) double-ended guillotine-type break at the reactor inlet. This double-ended cold leg (DECL) LOCA transferred the maximum energy into the containment among other variants, and consequently, it was selected as the worst-case scenario to simulate in FSAR as well.

The first phase of a LOCA transient is the blowdown phase which starts with the break and continues through mass and energy discharges driven by the pressure difference between the primary circuit and the containment atmosphere. The reactor coolant level decreases until the pressure of the reactor coolant system reaches an equilibrium with the containment pressure. In the second phase, the phase of the repeated flooding of the core, an ECCS train injects water into the core from hydraulic accumulators (HAs) which is activated when the pressure of the reactor reduced below the pressure of the gas in HAs to cover dehydration of the core. Meanwhile, supplied water from two ECCS trains discharges through the break, removes heat from the containment atmosphere by the heat transfer of droplets released and fills the sump. This phase ends when the reactor core is completely quenched. The third phase involves the long-term cooldown of the core with heat removal from the metal structures of the primary and secondary sides (AEOI, 2003).

The mass and energy of steam and water releases of the two break sources (since it is a double-ended accident, there are two break sources) in variant 2 could be seen in Figure 2-25 to Figure 2-28 with short-term (0<time<200 seconds) and long-term (200<time<10^5 s) perspectives. The data set ends at 17060 seconds when the reactor coolant inventory is completely discharged which means no more injection of mass and energy into the system could be observed after that point.

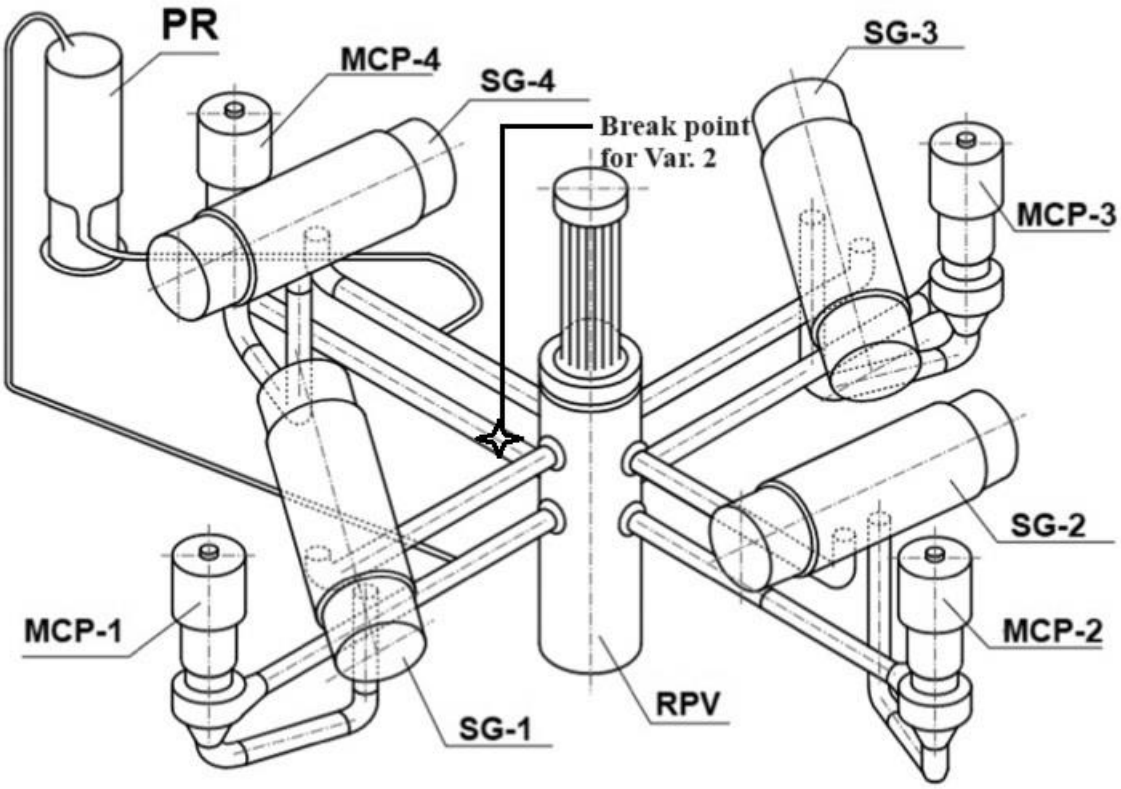

Figure 2-24. The loops of the reactor primary circuit, showing the location of the break at the reactor inlet of the loop 4, in Variant 2. MCP= Main Coolant Pump, SG = Steam Generator, PR = Pressurizer, RPV = Reactor Pressure Vessel.

Table 2-6. Parameters of 6 different LOCAs with NB 850 mm break, considered (AEOI, 2003). HA = Hydraulic Accumulator, RCC = Reactor Collecting Chamber and RPC = Reactor Pressure Chamber.

Name of parameter	Variants 1 and 2 (calculation of Pmax)	Variants 3 and 4 (calculation of Pmax)	Variant 5 (calculation of Pmax)	Variant 6 (calculation of Pmin)
Initial power, MW	3120	3120	3120	2880
The initial pressure in the primary circuit, MPa	16.0	16.0	16.0	15.4

The initial pressure in the secondary circuit, MPa	6.37	6.37	6.37	6.17
Place of rupture	reactor inlet (loop 4)	reactor outlet variant 3 - loop from pressurizer variant 4 - loop 4	rupture at the RCP suction (loop 4)	reactor inlet (loop 4)
Number of HA of ECCS (design), pcs.	3	3	3	4
Pump connection circuit (design)	hot and cold lines of loop 2 RCC/RPC variant 1 - 0.5/0.5 (uniform) variant 2 - 0.0/1.0 (water only supplied to RPC)	hot and cold lines of loop 2	hot and cold lines of loop 2	hot and cold lines of loops 1-4
Water temperature in ECCS tanks, °C	60	60	60	30
ECCS water temperature under operation from the sump, °C	55	55	55	55

Water reserve in ECCS tanks (calculated), m^3	395	395	395	1580
Number of high pressure coolant pumps (design)	1	1	1	4
Number of low pressure coolant pumps (design)	1	1	1	4

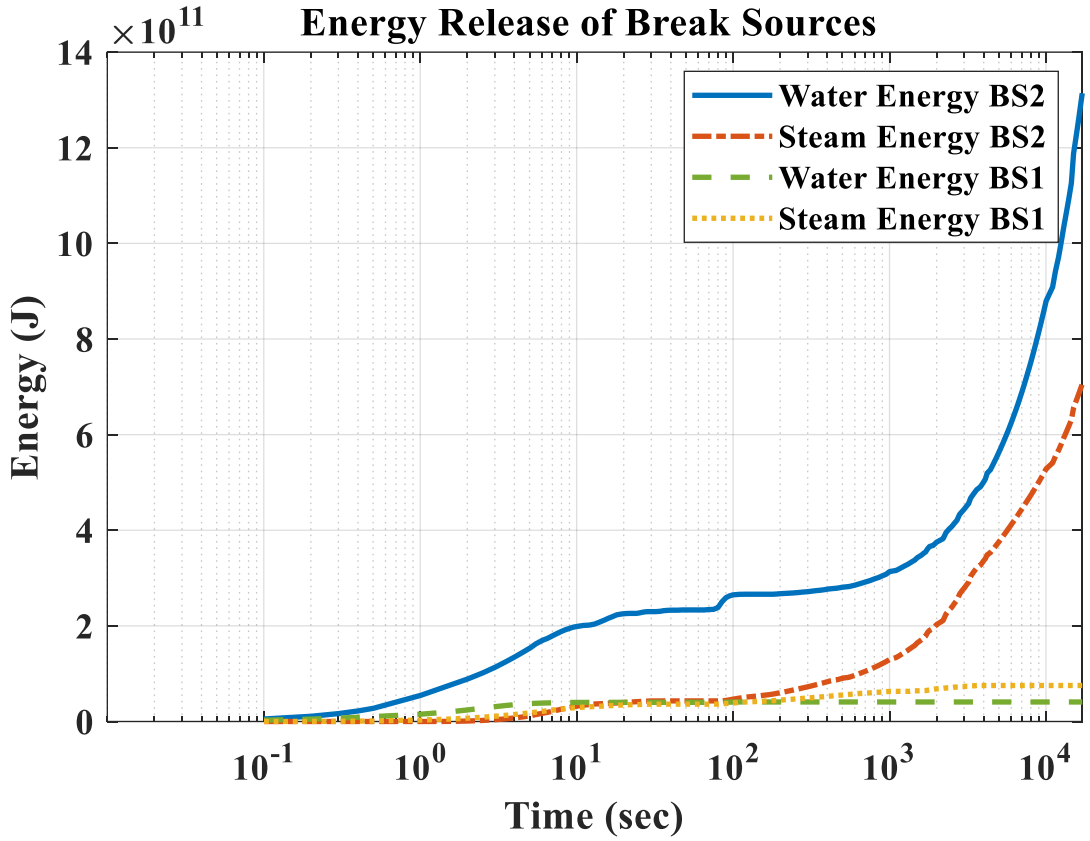

Figure 2-25. The long-term energy data of the two break sources during the LOCA.

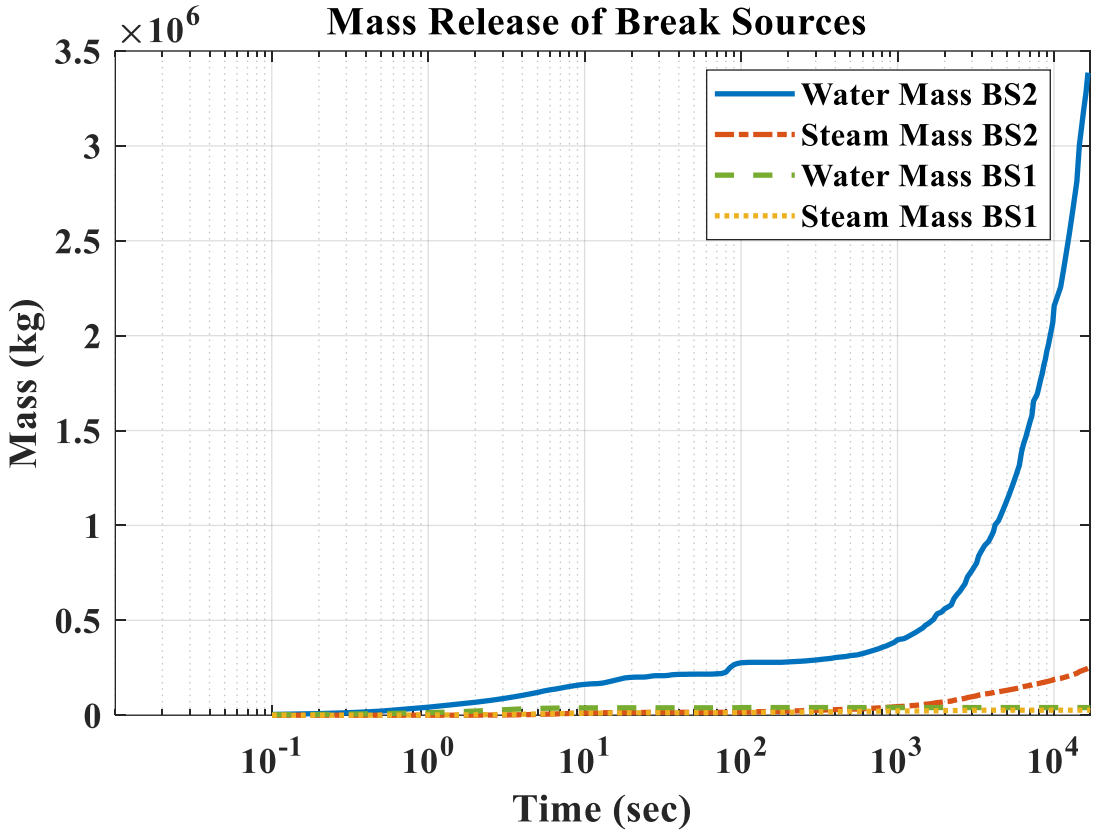

Figure 2-26. The long-term mass data of the two break sources during the LOCA.

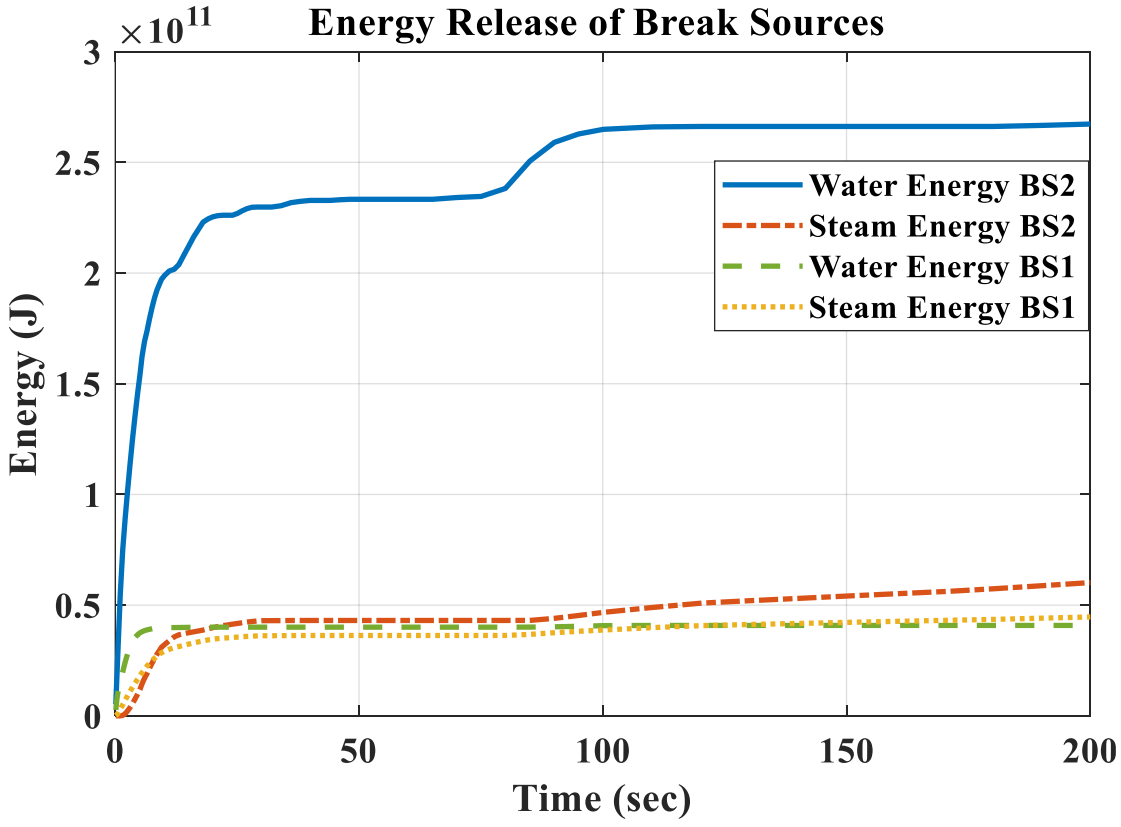

Figure 2-27. The short-term energy data of the two break sources during the LOCA.

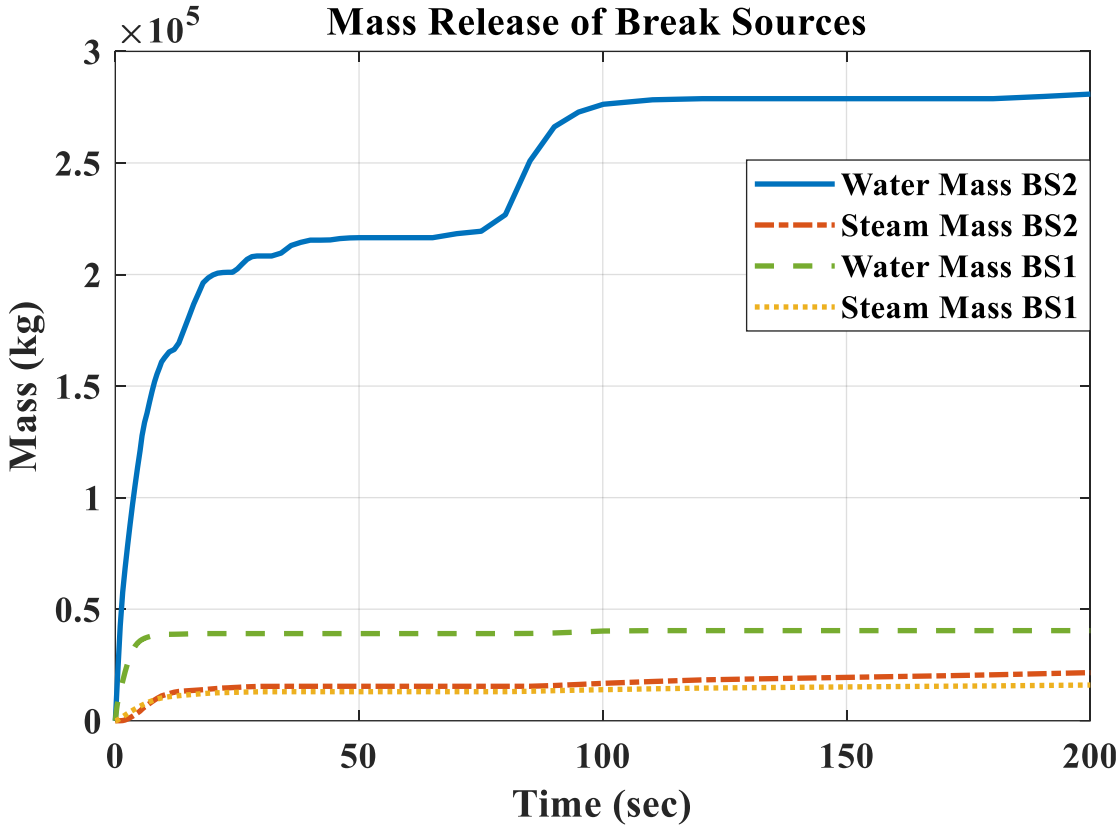

Figure 2-28. The short-term mass data of the two break sources during the LOCA.

2.4.2 The Hydrogen Release during the Postulated Accident

The variant 2 is also used for the postulated DBA since it leads to the greatest release of hydrogen into the containment compartments among the other variants. The main processes resulting in the formation of hydrogen during a LOCA are the following:

I. interactions of the zirconium claddings of the fuel elements with steam,
II. radiolytic decomposition of the coolant solutions during the accident and in the post-accident period,
III. corrosion of metals and metal coatings due to the exposure to coolant and spray solutions.

Below is a list of the hydrogen sources, which have been considered in the analysis:

a) hydrogen dissolved in the primary coolant system,
b) steam-zirconium reaction,

c) radiolysis of the coolant in the primary system,
d) radiolysis of the coolant in the fuel pool,
e) radiolysis of the coolant in the containment sump,
f) radiolysis of steam in the containment atmosphere,
g) decomposition of hydrazine-hydrate,
h) corrosion of protective metal coatings,
i) radiolysis of polymeric varnish and paint coatings,
j) hydrogen existing in the containment atmosphere under normal operating conditions.

Each of the above-listed sources has been analysed in detail, and calculations of the amount of hydrogen formed have been performed.

Before going into the details about the hydrogen sources, the basic assumptions used in the calculation procedures are introduced as follows:

- the amount of zirconium that has reacted with the formation of hydrogen amounts to 1% of the total mass of the zirconium claddings of fuel elements during a design-basis LOCA (which is in consonance with the requirement of the NRC according to 10 CFR 50.46 mentioned in section 1.1.3.1.2),
- The formation of hydrogen due to the interaction of zirconium claddings of fuel elements with steam takes place instantaneously.
- The main dose-forming fission products in the containment atmosphere are radioactive noble gases (RNG).
- The energy of gamma-radiation and beta-radiation of RNG is completely absorbed by the steam in the containment atmosphere.
- In the calculations of the radiolytic formation of hydrogen in the primary system and in the fuel pool, only the energy of gamma-radiation of the fission products is considered.
- The intensity of gamma-radiation in the primary system and in the fuel pool comprises 50 % of the power of the heat released from the core and the spent fuel.
- The portion of the energy of gamma-radiation absorbed by the coolant in the primary system and in the fuel pool amounts to 10 %.
- 100 % of the energy of gamma-radiation and beta-radiation of the fission products is absorbed by the coolant which accumulated in the sump.

- The radiation-chemical yield of hydrogen and oxygen resulting from the radiolytic formation of hydrogen in the primary circuit and fuel pool is G(H2) = 2G(O2) = 0.45 molecules/100 eV and G(H2) = 2G(O2) = 1 molecule/100 eV in the sump.
- Radiolytic formation of oxygen was not considered.
- The contribution of the radiation energy of transuranium isotopes was not considered.

The results of the calculations of hydrogen formation inside the containment during the LB-LOCA for each source are presented in accordance with the above-listed items:

a) The hydrogen dissolved in the primary system coolant:

The amount of the hydrogen instantaneously released into the containment volume is 2.3 kg.

b) Steam-zirconium reaction:

The amount of the hydrogen released into the containment volume due to the steam-zirconium reaction is 12.5 kg. In the calculations of the amount of hydrogen formed during steam-zirconium reaction, the following initial data have been assumed:

- the total mass of the zirconium cladding of fuel elements is 23400 kg,
- Moreover, the total mass of spacing grids, central channels of fuel assemblies and neutron flux control channels, which is 5100 kg of zirconium, was considered.
- Thus, the mass of zirconium taken into account in calculating the hydrogen formation is 285 kg of zirconium (1% of the total Zr mass of 28500 kg).

c) Radiolysis of the coolant in the primary system:

The amount of hydrogen released into the containment volume in the course of radiolytic decomposition of the coolant in the primary system due to the power of residual heat released in the core is 12,5 kg by the moment the LOCA has ended (first 24 h), and by the end of the post-accident period (30 days), it is 102.2 kg. In the calculations of the amount of hydrogen formed in the process of radiolytic decomposition of the coolant in the primary system, the following initial data have been adopted: the design thermal power amounts to 3120 MW.

d) Radiolysis of coolant in the fuel pool:

The amount of hydrogen released into the containment volume in the process of radiolytic decomposition of the coolant in the fuel during LB-LOCA amounts to 1.8 kg by the moment the LOCA has ended and 44.5 kg by the end of the post-

accident period. In the calculations of the amount of hydrogen formed in the process of radiolytical decomposition of the coolant in the fuel pool, the following initial data have been adopted: the power of heat releases from the spent fuel determined by summation over the groups of fuel assemblies amounts to 3.78 MW, and it is constant over the time period (31 days).

e) Radiolysis of the coolant in the sump:

The amount of hydrogen released into the containment volume in the process of radiolytic decomposition of the coolant solution in the sump amounts to 15.91 kg by the moment the LOCA has ended, and 94.88 kg by the end of the post-accident period. In the calculations of the amount of hydrogen formed, the following initial data have been adopted:

- the intensities of gamma-radiation and beta-radiation of the fission products have been determined from the condition of the loss of leak tightness of 1176 fuel elements out of the total number of 163 fuel assemblies (each containing 312 fuel elements, see Table 2-1) in the core,
- The chemical elements that released as fission products into the containment has been adopted in the following proportion: radioactive noble gases (RNG) – 100 %, halogens 50 %, others (Cs, Rb, Ru, Te, Ba, Ce etc.) – 1 %,
- fission products within the 1 % are distributed in the following proportion: cesium (Cs) – 70 % and others (Rb, Ru, Te, Ba, Ce etc.) 30 %,
- the composition of the halogens is almost entirely determined by the iodine isotopes,
- the chemical forms of iodine are represented by the following compounds: molecular iodine (I2) – 90 %, cesium iodide (CsI) – 1 %, organic compounds of iodine – 5 % (they are mainly represented by methyl iodide, CH3I), molecular iodine (adsorbed on aerosols) 4 %.

f) Radiolysis of steam in the containment atmosphere:

The amount of hydrogen released into the containment volume in the process of radiolytic decomposition of steam in the containment atmosphere during LB-LOCA amounts to 0.72 kg by the moment the accident has ended. At this point, the radiolytic decomposition of steam in the containment atmosphere is practically

complete. In the calculations of the amount of hydrogen formed, the following initial data have been adopted:

- the radiation-chemical yield of hydrogen is G(H2) = 1 molecule/100 eV,
- the density of steam is 2.46 kg/m^3. It is constant during the first 8 hours after the accident, the initial parameters of the atmosphere in the containment volume in the accident (T = 150 °C and P = 0.46 MPa) are assumed during that period,
- It is not considered that the density of steam will be considerably reduced to the values determined by the post-accident parameters 24 hours later after the accident has occurred. Thus, the conservatism is built in the calculations of hydrogen formation in the process of radiolytic decomposition of steam in the containment atmosphere.

g) Decomposition of hydrazine-hydrate:

Hydrazine hydrate ($N_2H_4 \cdot H_2O$) is one of the types of hydrazine that acts as an oxygen scavenger to reduce corrosion effect of the oxygen dissolved in water (Tsubakizaki et al., 2009). The amount of the hydrogen formed in the process of decomposition of hydrazine hydrate is 53.8 kg. the total content of hydrazine-hydrate amounts to 527.2 kg was used in the calculation.

h) Corrosion of metal and metallized protective coatings:

The amount of hydrogen formed due to corrosion of the metal and metallized protective coatings is negligibly small since the galvanized surfaces with an area no greater than 500 m^2 and the coating layer thickness of 90 μm is coated with protective varnish-paint enamels that prevent the spray solution from contacting with the metallized coating surface. Furthermore, the design does not employ aluminum instead it uses stainless steel for various locations such as protective sheaths of pipelines and vent ducts.

i) Radiolysis of polymeric varnish-paint coatings:

The amount of hydrogen formed due to the radiolytic decomposition of protective polymeric varnish and paint coatings is virtually zero because the fraction of the energy of gamma radiation from fission products absorbed by the layer of protective polymeric varnish and paint coatings with a thickness of 200 μm is 10^{-7}.

j) The presence of hydrogen in the containment atmosphere under normal operating conditions:

The sources determining the presence of hydrogen in the containment atmosphere under normal operating conditions of the power unit are non-controlled leaks of the reactor coolant and radiolysis of the coolant in the fuel pool. The volumetric concentration of hydrogen under normal operating conditions does not exceed 0.3% according to the data obtained from measurements at in-service Russian VVER-1000 reactors. As a result, the initial amount of hydrogen in the containment atmosphere is calculated as 19.3 kg.

The results of the calculations of the amount of hydrogen formed by individual sources are summarized in Table 2-7 which also provides information about the total amount of hydrogen which is generated inside the containment (AEOI, 2003). Figure 2-29 shows the generated hydrogen profiles according to the sources considered in the accident scenario. For comparison purposes, the total amount of hydrogen produced before its triggered combustion 9 hours and 30 minutes later from the onset of the accident was around 350 kg in the TMI-2 severe accident (Henrie and Postma, 1987) which produced larger total hydrogen amount in comparison to the DBA scenario here (~ 105 kg of hydrogen at the same time duration following the accident) since the latter only considers 1% of the total zirconium in the core to react with steam (as explained in section 1.1.3.1.2.).

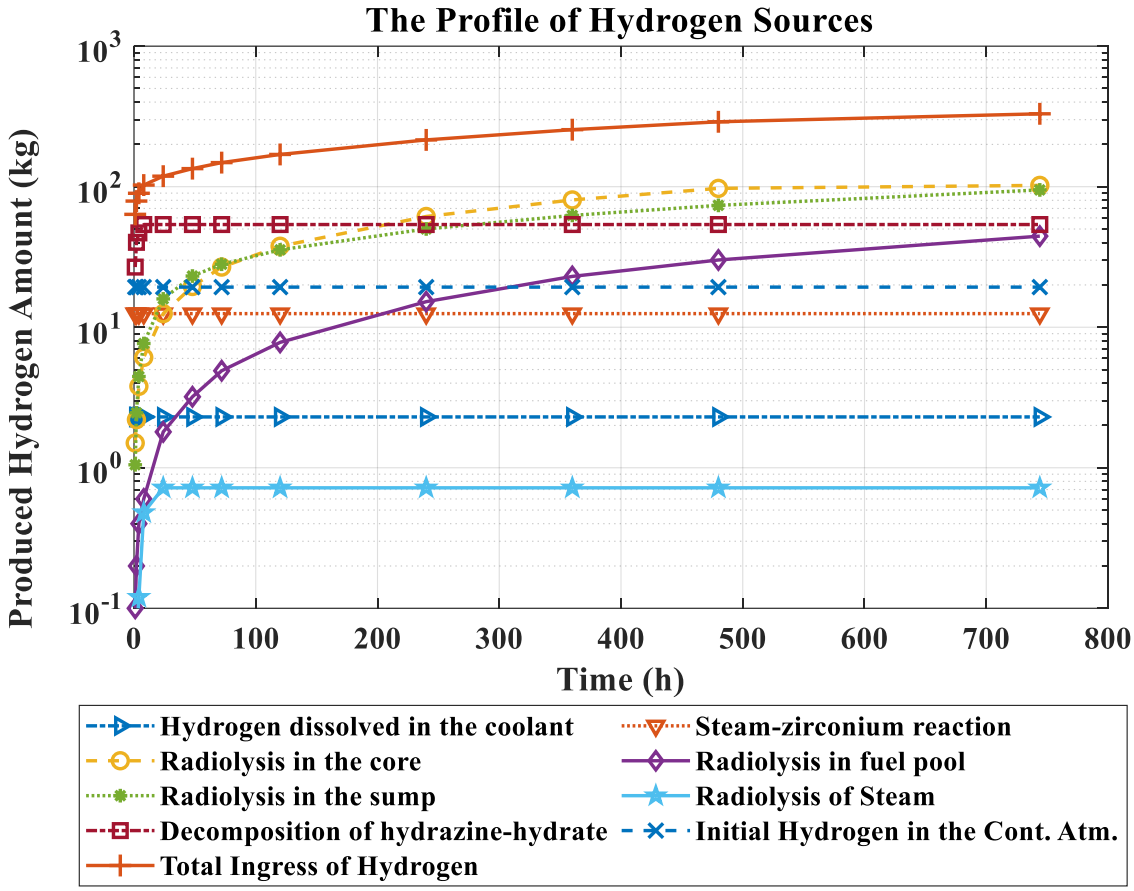

Figure 2-29. The profile of hydrogen sources.

Table 2-7. Individual hydrogen sources and their contribution to the overall amount of hydrogen inside the containment with respect to time (AEOI, 2003).

Hydrogen formation by different sources and total mass, in kg	Time h/days											
	1	2	4	8	24	48	72	120	240	360	480	744
	-	-	-	-	1	2	3	5	10	15	20	31
Hydrogen dissolved in the coolant	2.3	2.3	2.3	2.3	2.3	2.3	2.3	2.3	2.3	2.3	2.3	2.3
Steam-Zirconium Reaction	12.5	12.5	12.5	12.5	12.5	12.5	12.5	12.5	12.5	12.5	12.5	12.5
Radiolysis in the core	1.5	2.2	3.8	6.1	12.5	19.5	26.8	37.7	61.4	80.5	97.3	102.2
Radiolysis in the fuel pool	0.1	0.2	0.4	0.6	1.8	3.2	4.9	7.8	15.2	23	30.1	44.5
Radiolysis in the sump	1.05	2.46	4.46	7.66	15.91	23.14	28.07	35.54	50.04	62.47	73.66	94.88
Radiolysis of steam	0.03	0.06	0.12	0.48	0.72	0.72	0.72	0.72	0.72	0.72	0.72	0.72
Decomposition of hydrazine hydrate	26.8	40.2	46.9	53.8	53.8	53.8	53.8	53.8	53.8	53.8	53.8	53.8
Hydrogen in the containment atmosphere at normal operation	19.3	19.3	19.3	19.3	19.3	19.3	19.3	19.3	19.3	19.3	19.3	19.3
Total generated hydrogen	63.58	79.04	89.78	102.74	118.83	134.46	148.39	169.66	215.26	254.59	289.68	330.20

CHAPTER 3
HYDROGEN IN NUCLEAR POWER PLANTS

3.1 Introduction

In this section, basic hydrogen properties will be discussed briefly and some previous examples of hydrogen related accidents in nuclear industry will be given to stress the importance of managing the amount of hydrogen released during an accident. The following sections will provide information about the hydrogen generation and hydrogen distribution inside the containment, hydrogen combustion and finally the mitigation techniques for hydrogen risk in a nuclear power plant during an accident.

Hydrogen generation could occur at rates from 0.1 to 5 kg/s for a typical PWR following a severe accident (Kljenak et al., 2012). However, hydrogen generation is estimated to occur at rates 1 to 50 g/s in a DBA (Bachellerie et al., 2003) in which there is a limitation that set at 1204 °C for the maximum fuel cladding temperature at any point in the core. In severe accident scenarios, the contribution of water radiolysis might be regarded as negligible. However, for DBA analysis of hydrogen risk they could be considered due to the two orders of magnitude difference in the hydrogen production rate. All in all, the section which discusses the hydrogen generation will only consider water radiolysis and steam-zirconium reaction (only the reaction of 1% of the total zirconium in the core, see section 1.1.3.1.2) considering DBA conditions. More comprehensive explanation of hydrogen sources within the context of severe accidents will be provided in Appendix I.

The hydrogen atom comprises a nucleus that contains a single proton and an electron. The hydrogen molecule is formed of two hydrogen atoms bounded together. Hydrogen is not toxic for humans and does not act as a corrosive medium. The risk comes from the presence of a large amount of hydrogen in a containment is the possibility of its combustion. In 1979, at the TMI-2 nuclear power plant in Pennsylvania (USA), one of the turning points in the history of civilian use of nuclear power, an intense hydrogen deflagration happened on the second day of an SB-LOCA (Henrie and Postma, 1987). Approximately 350 kg of hydrogen was produced because of the zirconium-water reaction during the accident. Subsequent hydrogen combustion caused a pressure peak at around 2.8 bar, 9 hours and 50 minutes after the initiation of the accident, but the containment did not fail due to its design pressure limit being around 5 bar (Figure 3-1). Analyses that were made after the accident suggested that the hydrogen produced during the accident was mixed over the containment atmosphere uniformly. How the hydrogen deflagration was triggered is not known clearly today but the likely explanation of the cause could be given with an electric spark. After the TMI-2

accident, the phenomenon of hydrogen combustion in nuclear power plants was examined in more detail, the prevention and the mitigation of hydrogen explosion following an accident in particular (Kljenak et al., 2012).

In 2011, an earthquake with magnitude 9.0 on the Richter scale hit on the Fukushima nuclear power plant. The plant shut down automatically and did not receive any visible structural damage during the earthquake. However, the plant was without its off-site power supply since the AC electric power lines in the area were damaged because of the earthquake. Emergency diesel generators supplied electricity to the plant operation until a gigantic tsunami arrived and flooded the lower parts of the reactor buildings including the location of the generators. A tsunami with around 5 meters maximum height was considered in the design stage of the plant. However, the tsunami wave that hit the reactor buildings after the earthquake was around 14 meters in height. The damaged diesel generators stopped working and this led to a long-duration station blackout accident (Figure 3-2) (Sehgal, 2012). The accident progressed and hydrogen explosions occurred in three units out of a total of six units, inflicting substantial damage to the facilities and primary and secondary containment structures. The hydrogen explosions in units 1 and 3 stemmed from the accumulation of hydrogen gas within the primary containment due to the zirconium-water reaction in the reactor and the subsequent transport of that hydrogen gas to the secondary containment. It is believed that the reason for hydrogen accumulation in unit 4 is an inverse flow of hydrogen gas mixture through a standby gas treatment system from unit 3 (NEA/CSNI, 2014).

In the light of these two accidents, hydrogen in nuclear power plants poses a significant threat to the confinement of radioactivity within the reactor building. Large quantities of hydrogen could be produced through various sources and released into the containment atmosphere during an accident progression. Hydrogen is a highly flammable gas that could react with oxygen and generate thermo-mechanical loads higher than the design limits of the containment structure. Produced hydrogen gas mainly by zirconium oxidation mixes with air and steam and forms a gas mixture which could be flammable depending on the composition of the mixture, pressure and temperature following an accident. Since containment is the final barrier that prevents radioactive releases into the environment, hydrogen released into the containment should be investigated carefully by taking into account any combustion risk with an ignition source.

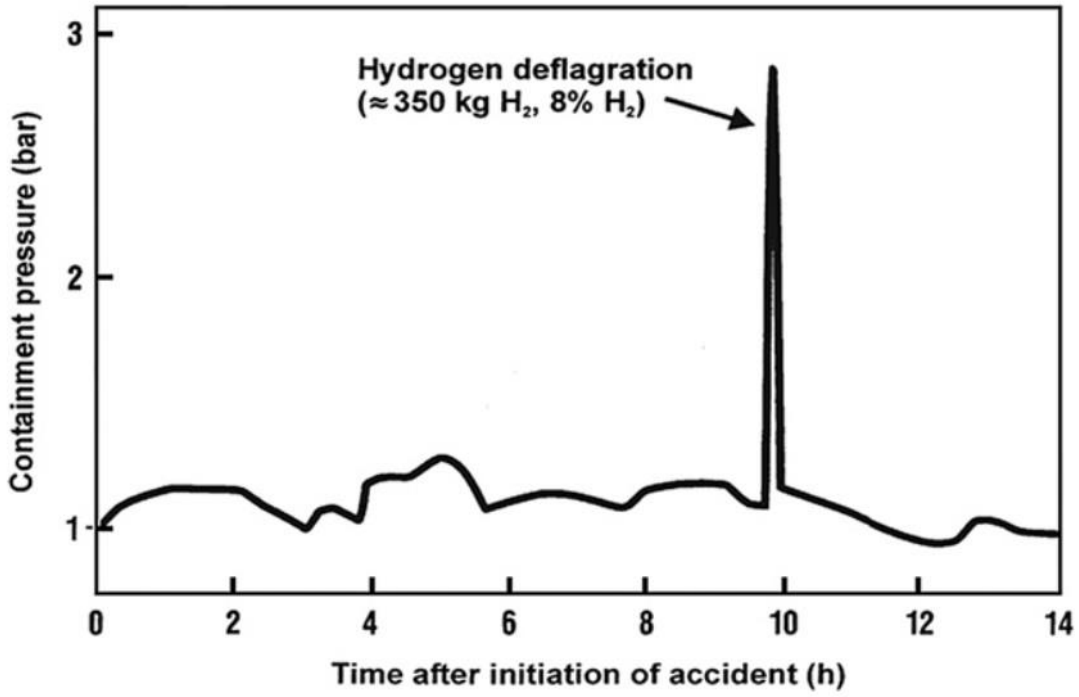

Figure 3-1. Containment pressure with respect to time in the course of TMI-2 accident (Henrie and Postma, 1987).

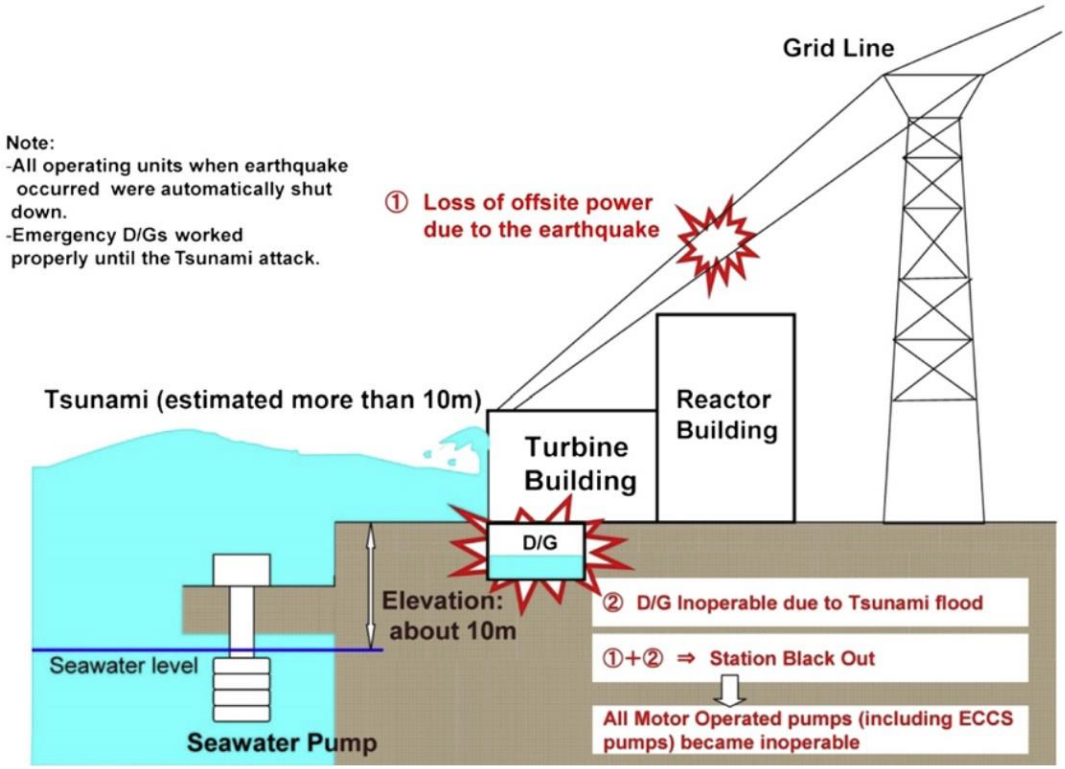

Figure 3-2. The cause of the station blackout event in the Fukushima nuclear plant (Sehgal, 2012).

Hydrogen has a molar mass of 2.016 g/mol. It is much lighter than other gases likely to be found in the atmosphere of a nuclear power plant containment during an accident because of this property. Therefore, when hydrogen is part of a heterogeneous atmosphere in a closed compartment, it is likely to accumulate in the upper parts due to its buoyancy.

The dynamic viscosity of hydrogen at 0 °C is 8.4×10^{-6} Pa·s, which is lower than the dynamic viscosity of saturated steam at 1 bar: 12×10^{-6} Pa·s, and around half of the dynamic viscosity of air at 0 °C: 12×10^{-6} Pa·s. This lower dynamic viscosity means that when hydrogen is flowing upward, air entrainment would be less intensive than in a comparable situation with steam, but not fundamentally different in case of a severe accident.

The diffusivity of hydrogen in air at a pressure of 1 atmosphere and temperature of 25 °C is 0.41×10^{-4} m^2/s, though the diffusivity of steam in the air at the same conditions is 0.26×10^{-4} m^2/s. Thus, greater diffusion of hydrogen than of steam may be expected during an accident progression inside the containment. This could provide help in predicting the formation of regions with high hydrogen concentration where hydrogen ignition and subsequent combustion are more likely (Kljenak et al., 2012).

3.2 Hydrogen Generation

3.2.1 Zirconium Oxidation

Following a LOCA, when the core is uncovered, zirconium fuel cladding reacts with steam and is oxidized at high temperatures. The reaction is strongly exothermic and rapid, it intensifies the process of core degradation by further increasing the temperature rise in the core (the heat-up rate might go beyond 1 K/s). The zirconium-steam reaction is:

$$Zr + 2H_2O \rightarrow ZrO_2 + 2H_2 + \Delta H, \qquad \Delta H = -586.6\ \mathrm{kJ/kg}.$$

0.0442 kg of H_2 is produced when 1 kg of Zr is oxidized (IAEA, 2011).

3.2.2 Water Radiolysis

Radiolysis of water occurs during both normal operation and accidents. Radiolysis is the decomposition of water molecules by radiation (α, β, γ or n). Radiolysis of water can produce OH, H, HO_2, and H_2O_2 but most importantly H_2 and O_2. Afterwards, these products can react with either themselves or other chemicals present in the water to yield a variety of other products. Radiolysis can occur in the core, in the primary system, or in containment such as

in fuel pool. The rate of hydrogen and oxygen formation is controlled by three factors (Sandia National Laboratories, 1983):

I. the decay energy,
II. the fraction of the decay energy, which is absorbed by the water,
III. the effective rate of hydrogen and oxygen production per unit of energy absorbed by the water.

The G value, which could be defined as molecules of product formed per 100 eV of energy absorbed, provide information about the yield of a product species due to the radiolysis of water. The effect of the radiolysis on hydrogen production depends on the following parameters (Sandia National Laboratories, 1983):

1. extent and distribution of fission-product release,
2. the temperature and pH of the water,
3. degree of bubbling and turbulence of the water,
4. the types and quantities of impurities dissolved in the water.

3.3 Hydrogen Distribution

After releasing from the source in the reactor coolant system hydrogen gas could disperse over the containment through designed pathways of the containment. If there is no forced flow inside the containment, convective loops dictate the transport of hydrogen due to the hot gas/steam mixture released and steam condensation on cold walls. The important part here is how well the hydrogen is mixed within the containment atmosphere since the flammability of the hydrogen gas is directly related to the concentration of the hydrogen in the region considered. Stratification of the hydrogen gas could lead to concentrations above the flammability limits and cause problems (NEA/CSNI, 2014).

The physical mechanisms that affect the mixing of the atmosphere and consequently hydrogen distribution inside the containment could be listed as follows:

I. gas flow,
II. molecular diffusion,
III. heat transfer between various containment structures (walls, pipes, or other equipment, mostly made of steel or concrete) and the containment atmosphere,

IV. mass transfer (steam condensation in the context of LOCA).

The flow of gas in the containment atmosphere may result from the two driving forces, inertial forces, and buoyant forces. The inertial forces may bring about the gas flow because of steam discharge from the breach in the reactor coolant system into the containment atmosphere. The flow of the steam or the flow of other gases which are entrained by steam flow could be given as an example of inertial flow. The gas flow resulting from the buoyant forces happens when there is a density difference due to the difference in gas temperature or to intrinsic gas property (molecular mass). As a lighter gas inside the containment atmosphere, hydrogen is expected to be accumulated just below the dome of the containment after a certain period since the buoyancy factor forces the gas with lower density to move upwards. Following a pipe break, inertial effects near the break dictate the flow against the buoyant effects, at the initial stages of the accident. However, subsequently, or in some parts of the containment far from the break location, buoyant forces could become dominant in effect on the flow of gases inside the containment.

Heat transfer occurs between the containment atmosphere and structures of the containment such as walls, pipes, and equipment. If the structures are hotter compared to the gases nearby, then they heat the containment atmosphere, whereas if the structures are colder relative to the gases around, then they act as a heat sink. The change in density due to the temperature increase or decrease of the gases around a structure also triggers buoyant flow between those gases and adjacent gases away from the structure.

Steam condensation is the way of mass transfer inside the containment following a LOCA. Steam condensation takes place on surfaces of structures mainly, but experiments suggest that steam condensation is possible in the bulk of the atmosphere too. Steam condensation could trigger gas transport within the containment atmosphere in two ways basically:

a) The local gas density due to the condensation of the steam changes and that promotes a flow due to the density difference with the neighbouring gases. For steam-air mixture, the condensation makes the density of the gas mixture higher, it moves downwards along the surface carrying hydrogen to lower elevations.

b) The local steam concentration decreases due to condensation. It provokes Steam diffusion and Stefan flow towards the condensation surface and the moving gas could entrain hydrogen.

It should be noted that noncondensable gases such as hydrogen and carbon dioxide, inside the gas mixture, strengthen the resistance to steam diffusion and affect the steam condensation on the surfaces (Kljenak et al., 2012).

Some safety systems could change the distribution of hydrogen gas in the containment atmosphere. Air coolers and spray systems for controlling pressure and temperature within the containment might promote the mixing of the hydrogen gas better inside the atmosphere. However, these safety systems might reduce the steam concentration substantially as well leading to a reduction in the inerting effect of the steam on the gas mixture (IAEA, 2011; NEA/CSNI, 2014).

The net free volume within the containment and the reactor design changes the hydrogen distribution as well. In Figure 3-3, fans mix the hydrogen in the containment atmosphere to the extent that a uniform mixture is achieved, and then the average hydrogen concentrations of some reactors from various safety reports are shown. While the average mole fraction of the hydrogen in BWR Mark I containment is above 70%, the same fraction is less than 10% in the larger PWR dry-type containment. Since a BWR-type containment has a lower net free containment volume and more Zirconium in its core to be oxidized, the BWR design is more susceptible to higher hydrogen concentrations (Heising-Goodman et al., 1981).

The general layout of the containment also affects the hydrogen distribution within the atmosphere. With an energy source (a pipe break in a LOCA), the gases released flow upwards in the inner parts and downwards in the outer parts due to the cooling effect of the containment walls, and a convective motion in the atmosphere is formed. However, if there is not enough connection between the inner and outer regions inside the containment, then dead-end rooms might be observed where the hydrogen concentration might exceed the flammability limit and provoke hydrogen burn, especially, after the initial stages of the accident when condensation of the steam starts to dominate the other physical phenomena inside the containment (Figure 3-4) (IAEA, 2011).

The interaction of various physical phenomena and how the hydrogen distributes within the containment is difficult to be assessed in a straightforward way. In order to evaluate whether hydrogen stratification occurs within the containment, some experimental investigations have been conducted to increase the knowledge base and develop methods which will be explained in next section.

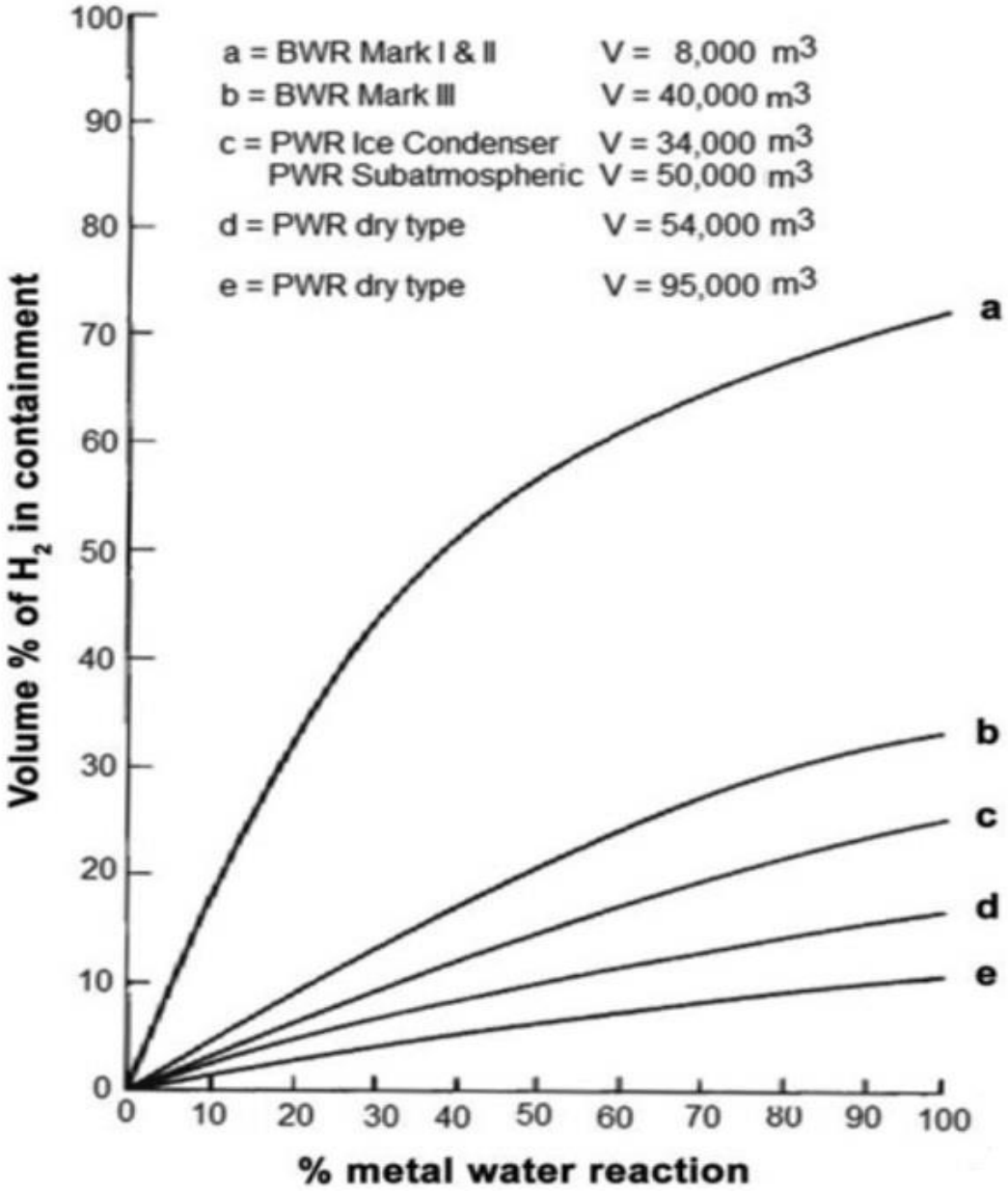

Figure 3-3. Average volumetric hydrogen concentration related to the amount of zirconium water reaction inside different containments of reactor designs in an accident scenario involving core degradation (Heising-Goodman et al., 1981).

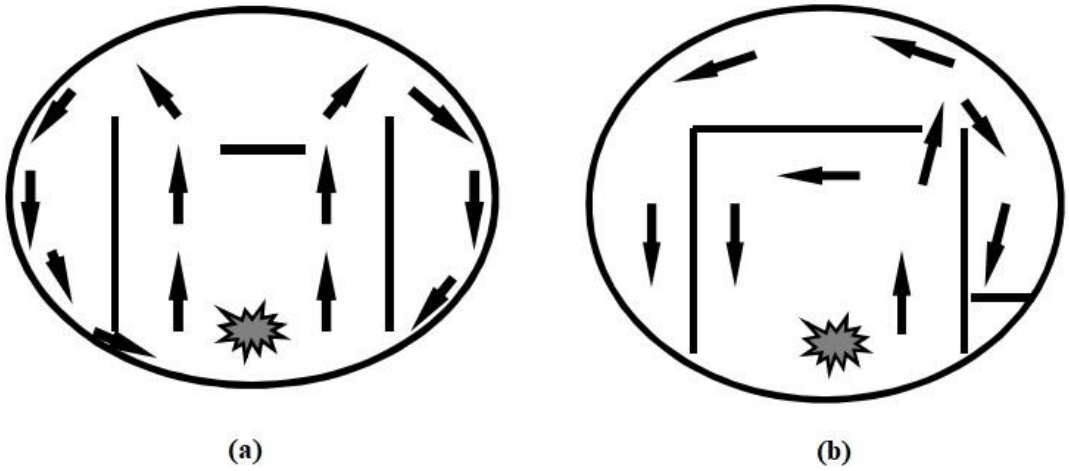

Figure 3-4. The convective motion within a containment with the energy source located in the lower part: (a) with and (b) without sufficient connection between inner and outer regions (IAEA, 2011).

3.3.1 Experimental Investigations on Hydrogen Distribution

The investigations on hydrogen distribution are carried out in containment experimental facilities. Those facilities examine the mixing of the atmosphere within a large enclosure. A homogenous or non-homogeneous (stratified) atmosphere is set initially, comprising air-steam, air-helium, or air-steam-hydrogen gas mixture. The reason for using helium instead of hydrogen in these facilities is related to the similarity of helium in behaviour to hydrogen despite being incombustible, ensuring the safety of the experiment. After setting the initial conditions, a gas is injected into the system (generally steam to simulate the flow through a pipe break in a LOCA), in a horizontal or vertical direction, with low momentum (plume) or high momentum (jet), at specific locations (upper or lower part of the facility). Then, the containment response is monitored typically over a period of several hours. Various parameters are measured to understand how a hydrogen cloud could disperse into the containment during an accident under various conditions and influences, such as:

I. pressure,
II. global and local temperatures, the latter especially important to investigate thermal stratification,
III. wall temperatures,
IV. flow velocities to investigate gas circulation patterns,

V. local compositions of the atmosphere, to examine whether there is a non-homogeneity of the atmosphere at different locations.

The volumes of large-scale containment experimental facilities are indeed a hundred or thousand times lower compared to the containments of nuclear power plants. Even though the experimental results received from the facilities could demonstrate qualitatively similar behaviour of hydrogen in mixing and combustion, the application of the results to the actual plants produces uncertainty to be dealt with.

The most important experimental containment facilities that have been operated could be divided into three groups (Kljenak et al., 2012):

I. Recently employed single-compartment facilities: TOSQAN (IRSN) (Malet et al., 2010) and MISTRA (CEA) (Studer et al., 2007) before the modification into a simple multicompartment facility,
II. Simple multicompartment facilities: MISTRA (after the modification), PANDA (PSI) (Paladino and Dreier, 2012), THAI (Becker Technologies GmbH, Germany) (OECD/NEA, 2007),
III. Complex multicompartment facilities: Heissdampf Reaktor or HDR (Kahlstein, Germany) (Bernardin et al., 2001), Battelle Model Containment or BMC (Battelle Ingenieurtechnik, Germany) (Wilkening et al., 2008), NUPEC (Japan) (OECD/NEA, 1994).

3.4 Hydrogen Combustion

Hydrogen is a burnable gas, in other words, it reacts chemically with oxygen to form water:

$$2H_2 + O_2 \rightarrow 2H_2O$$

This chemical reaction releases energy in the form of heat. The lower heat of combustion released due to the above reaction is 120 kJ per gram of hydrogen. The prerequisites of substantial hydrogen combustion are a flammable gas mixture and an ignition source. The initiation of the combustion might not sustain and eventually disappears. The dominant factor that shapes the conditions in a gas cloud for sustainable hydrogen combustion is its composition. The pressure and the temperature also affect flammability albeit their effect is secondary (Kljenak et al., 2012). The flammability limit is defined as the limiting concentration of a fuel in which a flame can be propagated indefinitely at a given temperature

and pressure. These limits are set by combustion experiments. Limiting values for hydrogen flammability for hydrogen-air mixtures at room temperature and pressure are presented in Table 3-1. The lower limit for upward flame propagation demands the least amount of hydrogen in concentration in the gas mixture. The downward flame propagation is less likely to be observed due to the stricter limitations on its occurrence.

Table 3-1. Hydrogen concentration limits for different flame propagation types at room conditions (Coward and Jones, 1952).

	Lower limit (vol.%)	Upper limit (vol.%)
Upward propagation	4.1	74
Horizontal propagation	6.0	74
Downward propagation	9.0	74

The lower flammability limit is the minimum concentration of hydrogen required to propagate a flame, while the upper limit is the maximum concentration. At the lower limit, the hydrogen is scarce, and the oxygen is abundant. At the upper limit of flammability for hydrogen, the reverse is true: oxygen is scarce (around 5% by volume). The upper limit of the flammability of hydrogen could be seen as the lower flammability limit for oxygen, emphasizing its deficit. In large PWR containments, hydrogen risk analysis is more focused on the lower limit of flammability since the oxygen is in excess inside the large volume of the containment.

The temperature and pressure of the containment atmosphere are unlikely to be at room conditions during a LOCA. In addition, there will be an ingress of steam into the system. Those parameters influence the flammability limits presented in Table 3-1. For example, temperature rise results in the widening of the flammability domain. At 100°C, the lower limit of flammability for downward flame propagation decreases to 8.8%. The effect of temperature on the hydrogen flammability limits for downward flame propagation is presented in Figure 3-5 (Sandia National Laboratories, 1983).

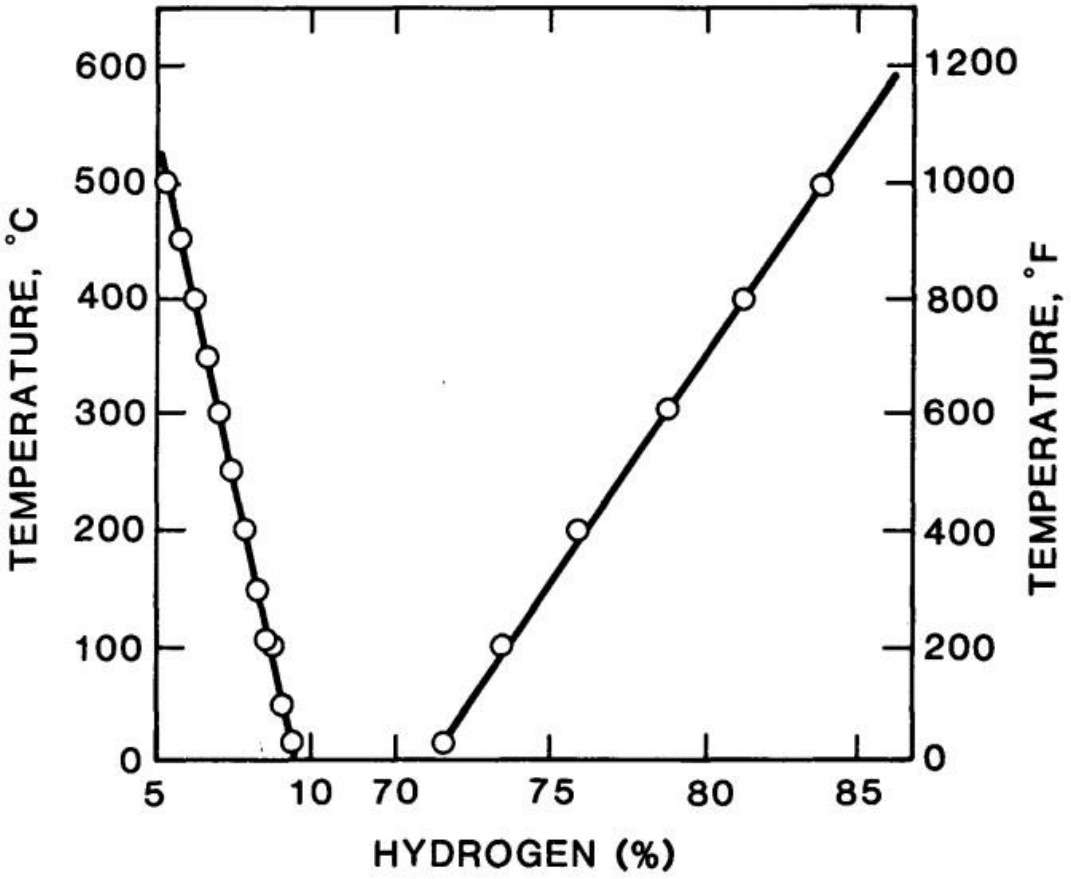

Figure 3-5. The effect of temperature on the flammability limits for downward flame propagation in hydrogen-air mixtures (Sandia National Laboratories, 1983).

The propagation of the flame depends on hydrogen concentrations in a mixture. A flame propagates preferentially in the upward direction around the lower flammability limit since hydrogen gas is a very light combustible (also hot during the release) and the flame in this domain is very weak and buoyancy is the dominant factor on the propagation. On the contrary, higher initial hydrogen concentration causes a more energetic flame that could propagate in all directions as could be seen in Table 3-1. The upward propagation occurs with the impact of the initial buoyant force when hydrogen concentration is between 4.1–6%. When hydrogen concentration is between 6–9%, combustion propagates in both, the upward and horizontal direction. For hydrogen concentration above 9%, combustion propagates in all directions with upward propagation being faster than downward propagation. Figure 3-6 shows the values of maximum combustion pressure in hydrogen-air mixture at initial conditions of 100 kPa and 27°C, comparing experimental measurements to theoretical calculations based on adiabatic isochoric combustion. As it could be deducted from the

figure, for the hydrogen concentration between 4% and 9%. The experimental maximum combustion pressure is lower than the theoretical one. The reason for that is related to the fact that flame could not propagate all over the volume under quiescent conditions. Starting from 9% of hydrogen concentration the experimental values are getting more in line with the theoretical values that show flame propagation occurs over the entire volume (IAEA, 2021).

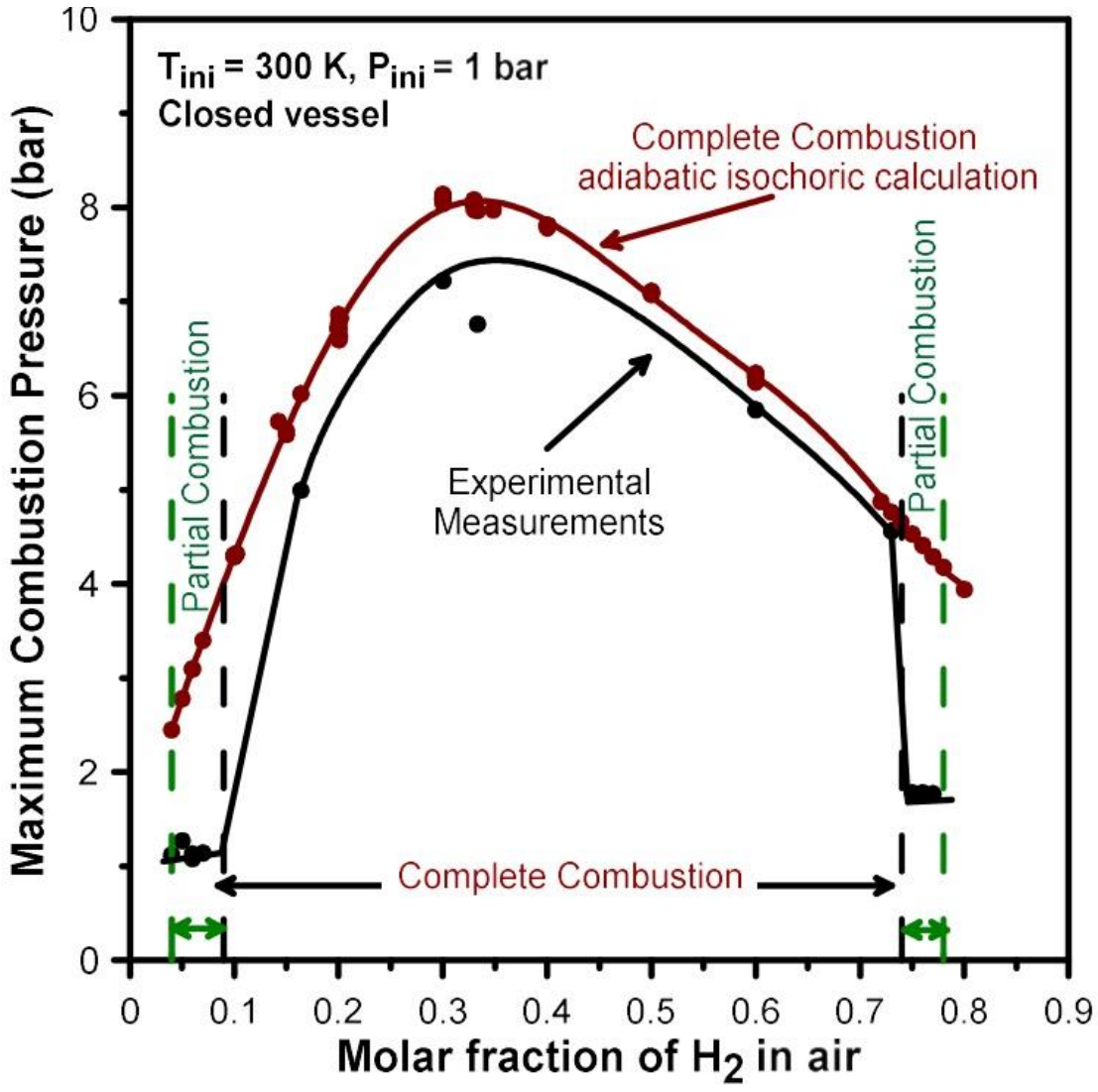

Figure 3-6. Experimental and theoretical maximum combustion pressures in a hydrogen-air mixture initially at 100 kPa and 27 °C (Grosseuvres et al., 2017).

With the presence of diluents inside the gas mixture such as carbon dioxide, nitrogen, steam or other diluent, the upper flammability limit decreases quickly, whereas the lower flammability limit rises slowly when the concentration of the diluents increases within the gas mixture. The amount of the diluent within the mixture might reach a point where the lower and upper limit of flammability equals each other, and the atmosphere becomes inerted. The inerted atmosphere prevents the propagation of the flame away from the reaction

source by a significant distance. The nitrogen concentration in the gas mixture for making it inerted is around 75%. This corresponds to 5% oxygen at the limit of flammability which is the same concentration at the upper limit of flammability of the hydrogen-air mixture. It might be deduced that a hydrogen-oxygen-nitrogen mixture will be flammable if the volumetric hydrogen concentration is above approximately 4% and the volumetric oxygen concentration is above approximately 5%. When the carbon dioxide concentration reaches roughly around 60%, the atmosphere is inerted. This corresponds to volumetric oxygen concentration at around 8%. The larger specific heat of the carbon dioxide reduces the flame temperature and flame velocity; therefore, carbon dioxide restrains flammability more than nitrogen. For the steam, the inerting effect could be observed at around 60% in hydrogen-air-steam mixtures (Sandia National Laboratories, 1983).

Shapiro diagram could be used in practical applications to understand whether a mixture is flammable or not (Figure 3-7). The triangular diagram has three sides which correspond to hydrogen, steam and air concentrations that are dominant gases inside the containment in a LOCA scenario. The diagram is prepared according to the empirical results. The diagram demonstrates the region of sustainable hydrogen combustion could occur with the burn limit curve and the region of hydrogen detonation could start with the detonation limit curve. Steam acts as an inerting gas as mentioned above. The Shapiro diagram is only an indicator and provides basic information about whether the mixture is flammable or not since the limits are also dependent on the geometry and shape of the vessel and also temperature and pressure (Kljenak et al., 2012). If a severe accident develops into an MCCI, the interaction of corium and basemat could produce a significant amount of carbon monoxide and dioxide released into the containment. Then, the containment atmosphere would also include carbon monoxide as a flammable gas and carbon dioxide as a diluent gas. The modified version of Shapiro would then be used the evaluate the possibility of hydrogen combustion, shown in Figure 3-8 (IAEA, 2021).

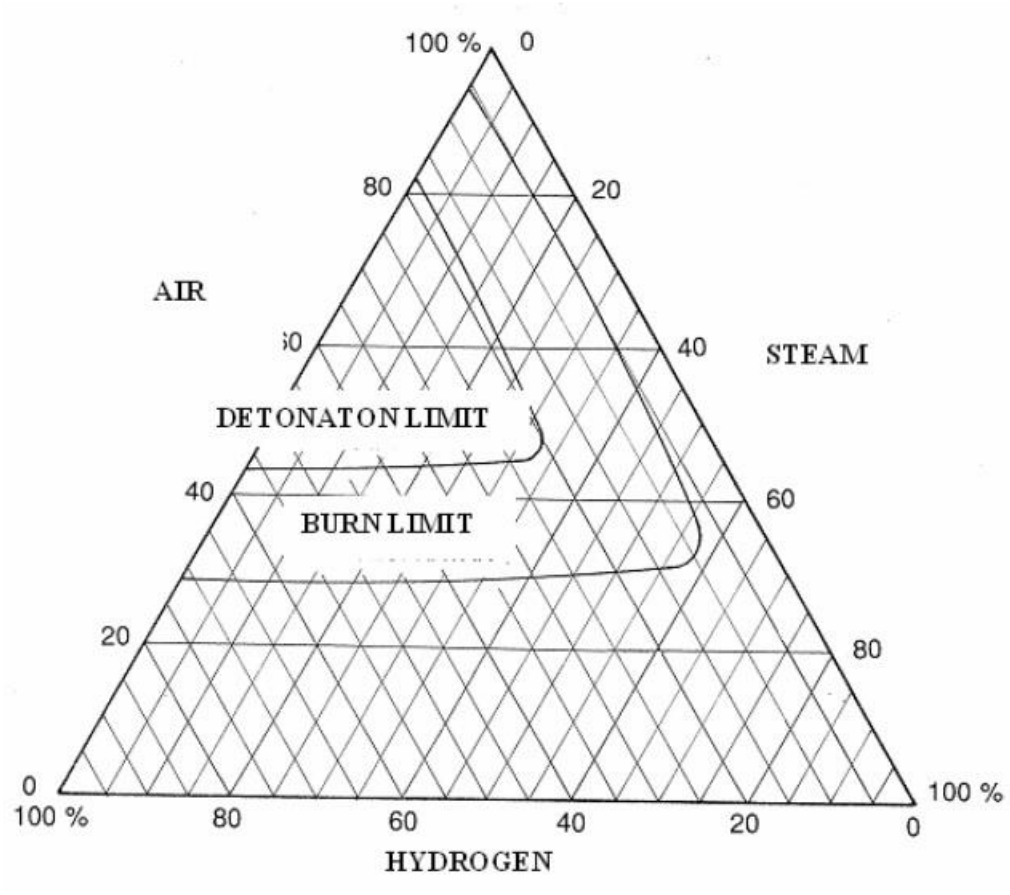

Figure 3-7. The Shapiro diagram for hydrogen-air-steam mixture (IRSN/CEA, 2007).

There are two types of combustion modes: detonation and deflagration. Deflagrations are flames that generally travel at subsonic speeds relative to the unburned gas. Deflagrations propagate essentially by thermal conduction from the hot burned gas into the unburned gas, increasing its temperature high enough for a rapid exothermic chemical reaction to occur. Deflagrations normally lead to quasi-static (nearly steady state) loads on containment. A detonation is a flame that travels at supersonic speeds relative to the unburned gas in front of it. Detonations are combustion waves in which the heating of the unburned gases is due to compression from shock waves. Detonation waves produce dynamic or impulsive loads on containment in addition to quasi-static loads (Sandia National Laboratories, 1983). If the mixture is in flammable region, a few mJ energy source is enough to trigger a deflagration. Hot points and electrical power devices could be given as igniter examples in an accident scenario. However, to trigger a stable detonation, much more energy (at least 100 kJ) is required. That is why direct detonation is not an expected outcome in accident scenarios. However, detonation could still occur through flame acceleration (flame speed is around a few hundred m/s) and deflagration-to-detonation transition (DDT) phenomena.

Hydrodynamic instabilities and turbulence caused mainly by obstacles on the flame path could lead to an acceleration of a deflagration as slow as 1 m/s. This acceleration might increase the speed of the flame to the flame acceleration, DDT or detonation (flame speed is over 1000 m/s) level (NEA/CSNI, 2014). Higher combustion speed brings higher pressure peak. Flame acceleration, DDT and detonation are the most dangerous mechanisms that threaten the containment integrity (Jacquemain, 2015).

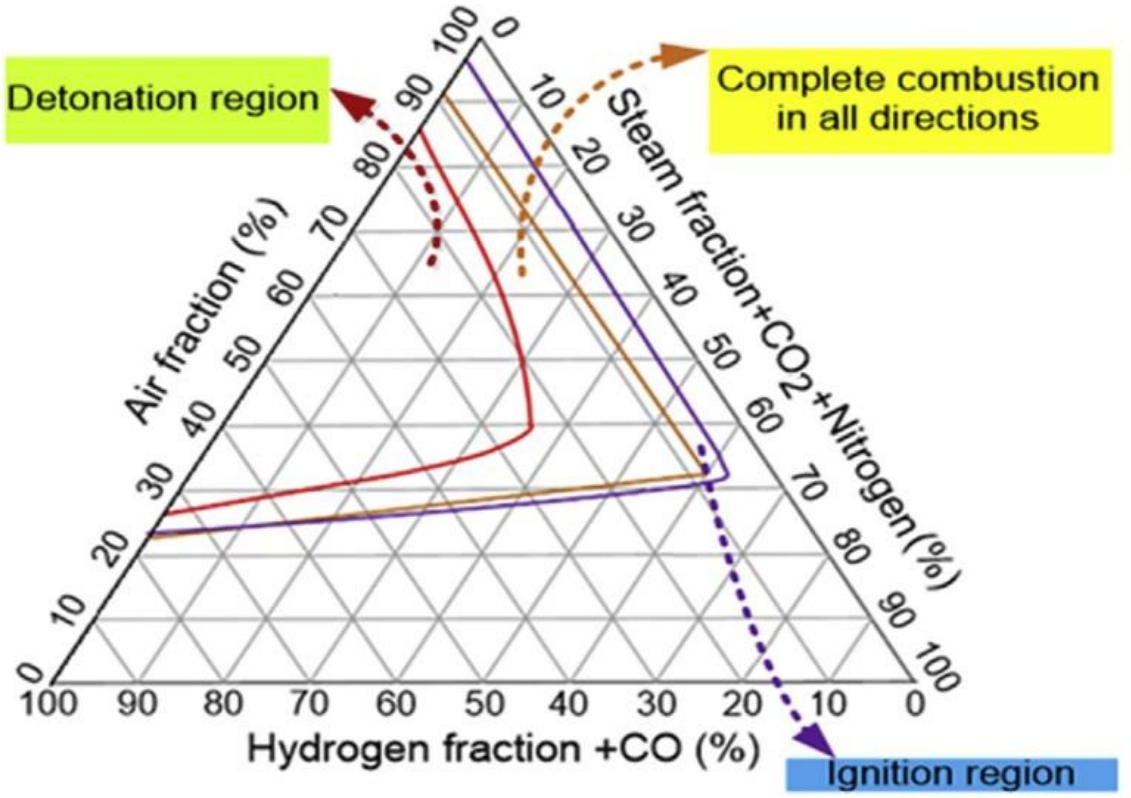

Figure 3-8. The Shapiro diagram with additional gases that could be emerged in the containment atmosphere during a severe accident (Gharari et al., 2018).

3.5 Hydrogen Mitigation

Mitigation of hydrogen risk deals with the prevention of severe thermal and pressure loads that could jeopardize the containment integrity or safety components. The aim is not the avoidance of hydrogen combustion, in fact, hydrogen might be burned deliberately in the early stages of the accident to prevent its accumulation to cause more threats later. To mitigate the hydrogen combustion risk in containment during an accident progression, the following techniques might be used (Kljenak et al., 2012):

- to inert the containment atmosphere, that is, removing or diluting oxygen,

- to mix the containment atmosphere to prevent stratification of hydrogen in local regions,
- to consume hydrogen by recombining or deliberate ignition.

3.5.1 Inertization of the Containment Atmosphere

The pre-inertization of the containment is the mitigation strategy most of the BWRs have employed. Many of the BWR plants have a small containment, which is not accessible during normal operation. Therefore, inertization with nitrogen during normal operation does not harm any staff and disrupt the plant operation. The small containment free volume enables to do the inertization and deinertization processes in hours and the costs are acceptable.

Reducing the oxygen concentration in the containment below 5% could nearly make the risk of hydrogen combustion zero. The cold stored nitrogen is heated by an air heated vaporizer for the ingress of additional nitrogen. It is fed into the containment by using the existing ventilation system.

For the large PWR containments, an inertization during normal operation is not practicable specifically if they are accessible. However, some investigations on inerting the atmosphere after the accident initiation that might lead to a significant amount of hydrogen production are made. Post-inertization involves the injection of non-combustible or combustion-inhibiting gases into the containment atmosphere (IAEA, 2011). The plant personnel should act at an early stage of the accident rapid enough to inert before the flammability limit of the gas mixture is exceeded in the containment. Setting regulations for operator actions on post-inertization is also a factor that should be considered. Another issue that needs to be taken into account is to design a diluent distribution system that could mix the diluent well over the containment rapidly (OECD/NEA, 1996). Since the quantity of diluent gas needed to inert the containment could be quite large due to the size of PWR containments, there is a risk of containment pressurization. Nitrogen and carbon dioxide have been considered as candidate diluent gases. There is no plant which utilizes this strategy yet to mitigate hydrogen (IAEA, 2011).

3.5.2 Mixing the Containment Atmosphere

Hydrogen combustion probably could not occur if all the generated hydrogen could be distributed uniformly, considering the large net free volume of a PWR containment. The

mixing of the containment atmosphere prevents hydrogen stratification and causes the hydrogen more uniformly distributed inside the containment.

The arrangement of compartments and various equipment is significant to accomplish proper mixing of the gases. Large openings in the containment compartments and the disposition of walls and equipment should permit flow paths. Mixing could be achieved either by promoting passive mixing through the containment in the design stage or by actively mixing the atmosphere by utilizing safety systems such as cooling fans (Kljenak et al., 2012).

3.5.3 Early Venting

The filtered containment vent system (FCVS) is designed to keep the containment pressure below the design limit to prevent containment failure in case of an accident. The filtration system could also significantly reduce the radioactive materials and limits the radiological impact of the accident. Specifically, caesium and iodine releases can be expected to be much less with filtration in comparison to a situation with unfiltered releases. Apart from the depressurization of the containment and confinement of radioactivity, FCVS could also be used in diminishing the hydrogen combustion risk as well as in decay heat removal of some small BWRs (OECD/NEA, 2014).

Early venting strategy is about the reduction of oxygen concentration prior to hydrogen ingress into the system. After the actuation of the venting system, steam and oxygen inside the containment atmosphere are replaced by injected steam into the containment possibly by a pipe break. Since steam acts as an inerting gas and there is less oxygen for hydrogen to react within the atmosphere, this leads to a reduction in hydrogen combustion risk. FCVS also changes the local hydrogen concentrations within the containment after the onset of the accident. Since hydrogen tends to accumulate on the top of the containment because of its density, venting through the top of the containment or placed near the hydrogen source is efficient for hydrogen migration during the accident (Fernández-Cosials, 2017).

if a sufficient amount of hydrogen is accumulated within the FCVS, combustible mixtures could be formed in the presence of oxygen because of air ingress from vent actuation. This situation can be worsened by steam condensation (if the vent line is cold) and pose a risk when an FCVS has not been initially designed to maintain its integrity against the dynamic loads that would be caused by hydrogen combustion (OECD/NEA, 2014).

3.5.4 Igniters

Igniters are triggering agents that initiate a slow deflagration deliberately to reduce the concentration of the hydrogen. They are installed within the containment and used to burn the hydrogen in a controlled way to prevent at least a mild deflagration that might develop into a fast acceleration or DDT. Resulting temperature and pressure peaks will be within containment design limits and hence could not cause any problem. Since the source will continue to produce hydrogen, they may need to be active on entire duration of the accident. If slow deflagration conditions are not met, they cannot be actuated and become useless.

The placement of the igniters are quite important to control the hydrogen concentration, path of the hydrogen could be foreseen in the containment starting from the source term, for example, it is generally concentrated more around the dome due to low density of the hydrogen (Fernández-Cosials, 2017).

There are three types of igniters. Glow plug igniters need a separate power source due to the high-power requirement (typically 150 to 200W each) to be actuated by the operator or itself automatically when LOCA signals received (IAEA, 2021). They are simple electrical resistance heaters that produce a surface temperature of 800 to 900°C, which is a positive ignition source for flammable hydrogen-air-steam mixtures. Hydrogen requires the least energy for the spark ignition among combustible materials. Therefore, spark igniters have reduced power need hence could be used with batteries. The main problem that poses a challenge in the use of spark igniters is about compatibility with other electronic equipment, in relation to electromagnetic interference or spurious signals arising from spark discharges. Interference effects are likely to be small but need to be assessed specifically for the plant and might affect igniter placement. They are used in Canadian reactors. Finally, catalytic igniters utilize the heat of the reactions of $H_2 - O_2$ at a spatial catalytic element to produce surface ignition temperatures sufficient enough to ignite and therefore they do not need any power supply. Those igniters could actuate itself without any operator intervention (IAEA, 2011). The disadvantages of catalytic igniters are their operation over a narrow range of mixture compositions in comparison to other type of igniters. They actuate beyond absolute flammability limits and if the gas mixture includes hydrogen concentration high enough, the margin between the flammability limit and detonation limit might be quite small. In addition, the catalytic igniters do not respond immediately since it takes time to react and produce heat.

Moreover, potential poisoning or fouling of the catalytic surface might reduce the effectiveness of these igniters (IAEA, 2021).

3.5.5 Passive Autocatalytic Recombiners

After the TMI-2 accident in 1979, nuclear safety community start to extensively investigate on hydrogen combustion phenomena following an accident. In the 1980s, several research programmes commenced to examine the hydrogen behaviour and control under postulated accident conditions. During these years, the prevailing methods to deal with hydrogen risk in containment were the dilution of the containment atmosphere with an inert gas and igniters.

In the 1990s, a new mitigation strategy based on the catalytic oxidation of hydrogen using oxygen from the containment atmosphere and a metal catalyst was proposed: the passive autocatalytic recombiner (PAR). For hydrogen recombination with oxygen, there is an activation energy to be surmounted to initiate the reaction. Only temperature values reaching 600 – 650°C could provide suitable conditions for the reaction to occur autonomously in the air. However, the activation energy that is needed for the recombination of hydrogen and oxygen can be substantially lowered using catalytic substances, so that the reaction can initiate at low temperatures automatically without spreading the reaction to the atmosphere nearby. The mechanism of a catalyst (platinum or palladium) is to decrease the bounding of the hydrogen molecules and to form radicals that will react more easily with the oxygen radicals. The catalytic oxidation of hydrogen on metals acts in accordance with the Langmuir-Hinchelwood mechanism. The two main steps are the diffusion of the reactants on the catalyst and the reaction of absorbed reactants on the catalyst (Arnould et al., 2001). A catalytic recombiner acts as a passive instrument which means it is actuated on itself, it has no moving parts and requires no external energy. They come into action automatically as soon as the hydrogen concentration starts to increase in the containment atmosphere (Fineschi et al., 1996). In practice, recombiners are actuated when the hydrogen concentration reaches around 1% and perform their operation if sufficient hydrogen and oxygen are available nearby (Rozeń, 2015).

A PAR includes a vertical channel (stack) equipped with a catalyst bed in the lower part as could be seen in Figure 3-9. In case of accident, the catalyst bed is in contact with the gas mixture of the containment. Hydrogen molecules encountering catalyst surface are reacted with oxygen in air. The heat of the reaction at the catalyst surface creates a convective flow, without mechanical assistance or power source. The heat release of the reaction in the lower

part of the recombiner causes buoyancy (chimney effect) which increases the inflow rate. Thus, the catalyst is supplied by a large amount of hydrogen gas mixture which ensures high efficiency of recombination. The natural convective flow currents around the PAR improve mixing of combustible gases in the containment, in other words, prevent hydrogen stratification on local regions.

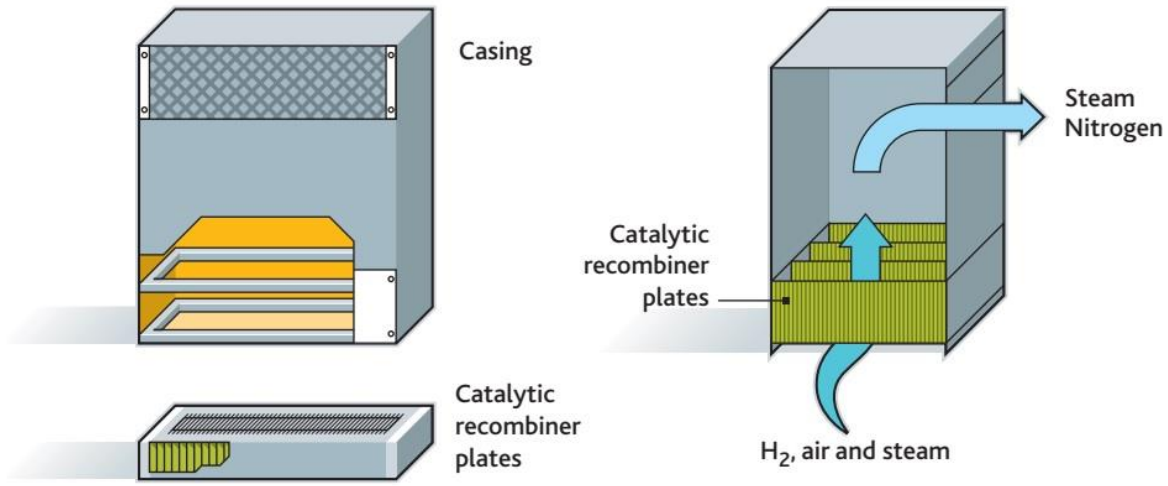

Figure 3-9. Diagram of a PAR (Jacquemain, 2015).

Apart from its passive features, the advantages of PARs could be listed as follows (Arnould et al., 2001):

I. A catalytic recombiner could operate under severe accident and design-basis accidents conditions,
II. A catalytic recombiner actuates at low hydrogen concentration, well below the lower hydrogen flammability limit (unlike igniters),
III. The recombiner physical phenomenology is well known,
IV. A recombiner does not induce operational constraints in normal operation (unlike inerting),
V. The passive autocatalytic recombiner technology is simple and does not need complex system (unlike post-inerting).
VI. Lowered cost in comparison to other mitigation techniques.

One of the issues that challenge the use of PARs as a hydrogen mitigation strategy is the autoignition phenomenon. The catalyst, heated by the exothermal H_2–O_2 reaction, is known to be a potential ignition source to cause hydrogen burns. The PAR catalyst temperature rises with exposure to elevated hydrogen concentrations. Hydrogen deflagration can be triggered at

higher hydrogen concentrations (typically above 6 vol%) because of the resulting catalyst temperatures (above 600 °C) (Gardner et al., 2021). Most commercial PARs have a very high probability of inducing a spontaneous ignition at a hydrogen concentration of about 8% or more (Kim et al., 2022). Currently, spontaneous ignition of PARs is recognized as an unavoidable phenomenon when a PAR is installed in a high-concentration hydrogen atmosphere. However, the upper concentration limit for PAR operation could be improved. The developer of the Russian manufactured RVK recombiners determined that the most probable source of autoignition are the metal structural members of the recombiner that are in contact with the catalyst, not the catalyst itself. They have modified the design of PARs in a way that the metal elements were made thicker to increase their heat capacity. In addition, heat transfer conditions were improved from the construction to the environment. Experiments revealed that these alterations increased the upper recombination threshold from 7% to 17% in new models (Keller, 2007).

When the volumetric hydrogen concentration triggers a PAR to function, it is not immediately in full effect, a certain time period needs to be passed for the PAR to heat up the catalyst by exothermic H_2–O_2 reactions. Chimney flow should be established around the PAR by the heat released during PAR operation at the initial stages. This is called start-up delay mechanism of the PAR and this inertial quality of the PAR is one of the problematic features of PAR operation. The start-up delay time of a commercial PAR reaches several minutes under normal conditions. However, this start-up delay time may be longer contingent upon the composition of the atmosphere and thermal-hydraulic conditions around the PAR location. Furthermore, the condition of the catalyst surface also influences the start-up time. Examples of the substances that increase the start-up of a PAR could be given as carbon monoxide (oxidation on the catalyst), volatile organic compounds, water (liquid film formation), soot etc. When these substances attach to the surface of the catalyst, they hinder the diffusion of hydrogen molecules to the surface of the catalyst or delay the catalytic reaction (Kim et al., 2022).

PARs could also induce thermal stratification inside the containment. The hot exhaust gas at the outlet of a PAR due to its lower density could accumulate at the top of the containment and prevent the natural convection inside the containment. In this case, the hydrogen released into the system from lower points of the containment could not penetrate the upper hot gas layer with lower density and accumulate below it as it depicted in Figure 3-10. It could be seen in Figure 3-10, that hydrogen injected mixes inside the containment of a small modular

reactor and be able to rise to the top of the containment. After conversion of the PARs within the containment, the stagnation of the hydrogen gas could be seen below the top layer on the right side of the figure (Kim et al., 2020). Hydrogen conversion rate of PARs is limited because of the speed of natural circulation flows and diffusion, and the availability of reacting species (e.g., O_2 starvation might happen) (Kljenak et al., 2012). In an accident scenario with a massive hydrogen release, installed PARs inside the containment would not be efficient enough to prevent hydrogen combustion (Reinecke et al., 2004).

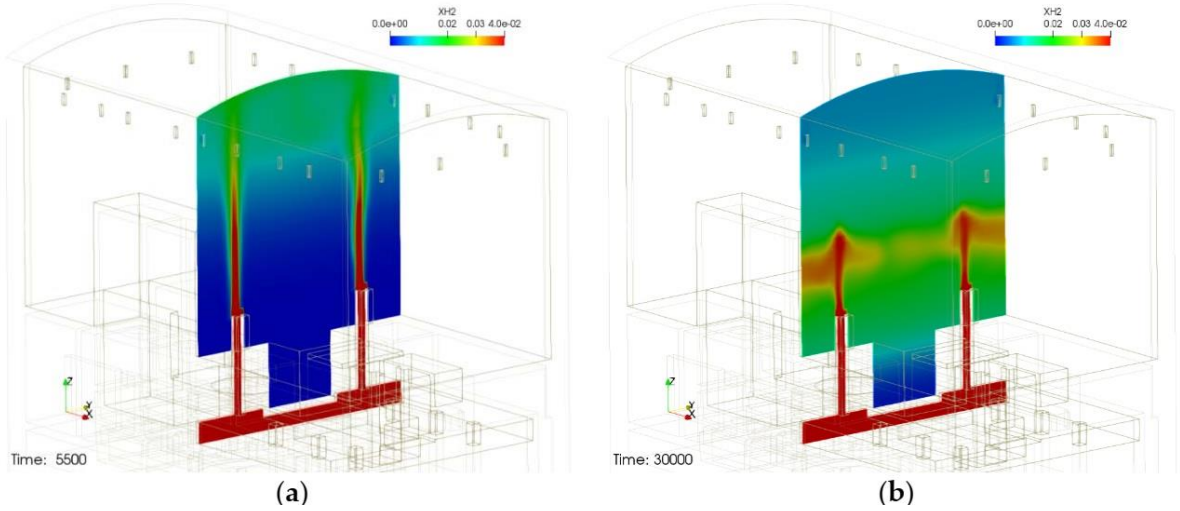

Figure 3-10. Hydrogen distribution inside a small modular reactor containment: (a) mixing of hydrogen by natural convection, (b) hydrogen stratification could be observed after the operation of PARs (Kim et al., 2020).

CHAPTER 4
METHODOLOGY

4.1 Introduction

In this chapter, first, GOTHIC code, which was utilized in this thesis, will be introduced. Next, modelling steps of VVER-1000 containment will be explained in detail from building the containment geometry in AutoCAD to transferring of the 3D built model to GOTHIC environment, including providing information about various components defined in the transferred model in GOTHIC. The conservation equations that are solved in GOTHIC solver for a finite volume in the computational grid are stated in Appendix B.

4.2 GOTHIC Code

GOTHIC (Generation of Thermal-Hydraulic Information for Containments) is a general-purpose thermal-hydraulic analysis code that solves the mass, energy and momentum conservation equations for multi-component and multi-phase flow, developed by Zachry Nuclear Engineering, Inc. The code could be used in the design, safety, operating and licensing analysis of nuclear containments and confinements, auxiliary buildings and equipment performance. The conservation equations are solved for three main fields: continuous liquid, liquid droplets and steam/gas mixture. GOTHIC code calculates temperatures and velocities for each field separately, thermal non-equilibrium between fields is also allowed in the same computational unit. GOTHIC is a hybrid code that allows a computational unit defined as a lumped parameter or a multi-dimensional volume where the volume could be subdivided into 1, 2 or 3 dimensions. The subdivision of the volume could be made in orthogonal coordinates. A cell, which is an output of the volume subdivision, interacts with adjoining cells through the parameters defined by the discretization of governing equations (EPRI, 2018a).

Being a hybrid code, GOTHIC can perform as LP code and a CFD code simultaneously. It utilizes the advantages of both types of severe accident codes and provides great flexibility to model the containment since the user could adjust the balance between computational cost and accuracy by defining various regions as control volumes of either CFD or LP code. The user can classify the regions inside the containment in terms of importance and model the lower impact regions as LP control volumes to save the time and effort to build the geometry needed to simulate the accident. The 3D capabilities of a CFD code were recently integrated into the code, previously it was only an LP code (NEA/CSNI, 2014).

GOTHIC uses a porous media approach for cell volumes and cell faces. The porosity of a cell defines the openness of the volume to be occupied by the fluid which means the porosity factor could be manipulated to change the free volume within a cell. This factor is a number between 0 and 1. Blockages are objects that displace fluid or solid. They could be used to model complex geometries by pre-defined geometric forms. GOTHIC includes full treatment of momentum transport terms in 3D simulations (EPRI, 2018a). The code also enables the user to model various components such as pumps, valves, fans, filters and igniters. More advanced systems could be defined in containment through the combination of those components (Ofstun and Scobel, 2006).

GOTHIC has a graphical user interface to draw and represent geometries in the model. Whenever a control volume is drawn, the user could select subdivided volume option in the menu and switch the volume to 3D. The user only defines the placements of the grid lines in the mesh geometry, in other words, it is like cutting a big LP volume into smaller LP volume pieces. Moreover, there is no need for modelling boundary layers as most of the other CFD codes require. Therefore, meshes are coarser than other CFD codes and simulation time is shorter and yet GOTHIC still could compete with the other CFD codes and produce accurate results. In OECD/NEA's third international benchmark activity, performances of the CFD codes for a given scenario are compared to the experimental data. The results show that a GOTHIC simulation with only 8000 meshes provides very good results in comparison to many other simulations which have more than millions of meshes. Moreover, the equivalent CPU time of the GOTHIC simulation is significantly shorter. A CFX simulation which produces similarly good results lasts 11680 hours, while the GOTHIC model runs only 48 hours in the same computational settings for nearly the same results (Andreani et al., 2016).

In this thesis, three simulations have been made; a) short-term and b) long-term analysis of thermal-hydraulic parameters and c) hydrogen distribution inside the containment. Effects of ESFs on mitigation of parameters have been completely evaluated. All the simulations are performed with GOTHIC version 8.3(QA). In this chapter, first, the steps for preparing the 3D model from AutoCAD to the GOTHIC environment will be explained. Then, after transferring the geometry, the completion of the VVER-1000/V446 containment modelling for the simulations will be described in detail.

4.3 3D Modelling of VVER-1000/v446 Containment

4.3.1 Development of a Detailed CAD Model of the Containment

A Computer-Aided Design (CAD) software provides a more user-friendly and easier-to-interact environment for 3D modelling in comparison to the GOTHIC graphical interface. Therefore, 3D as-built geometry of the containment was developed in AutoCAD. VVER-1000/V446 containment structure has been designed/formed by 10 different horizontal cross-section sketches (10 different elevations) that are shown in Figure 2-11 to Figure 2-21. Each of these cross-sections makes one of the 10 vertical slices of the containment and keeps the same compartment design along with its height. These elevations are distributed along -6.00 m, -1.50 m, 2.00 m, 6.00 m, 9.00 m, 10.50 m, 12.00 m, 16.40 m, 21.50 m and finally 26.80 m. The containment rooms have been developed as 2D in the first step and then turned into 3D volumes by extruding their cross-section along with their height according to their elevation in AutoCAD, three layers of the whole model at 10.50/12.00 m and 21.50 m could be seen in Figure 4-1 and Figure 4-2. Those vertical 3D sections from bottom to top are integrated to demonstrate the whole containment building as shown in Figure 4-3. Control volumes, indeed, are made of one or multiple designation rooms in the reactor building that are connected by doors, corridors, staircases and sometimes flow paths. In other words, they are enclosing sets of various rooms of the containment plan. A unique colour was assigned to each control volume set to distinguish them in the model as shown in Figure 4-3.

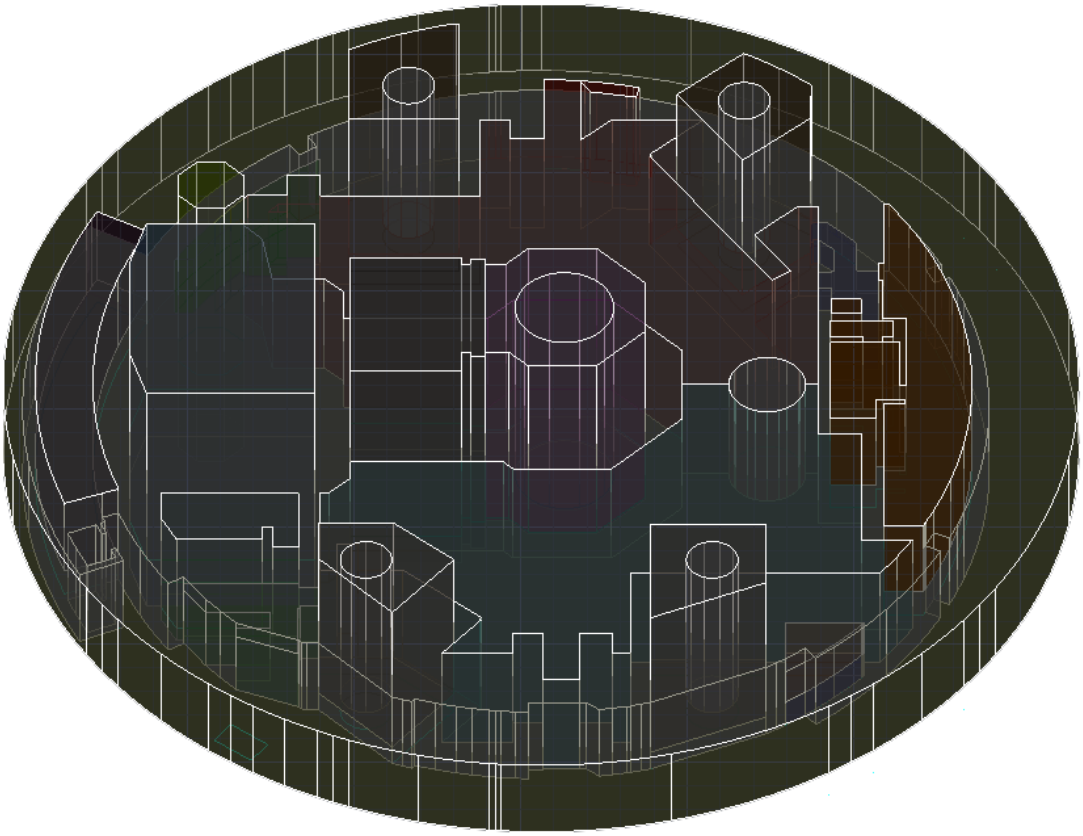

Figure 4-1. The 3D extruded cross-section of the containment at 10.50/12.00 m.

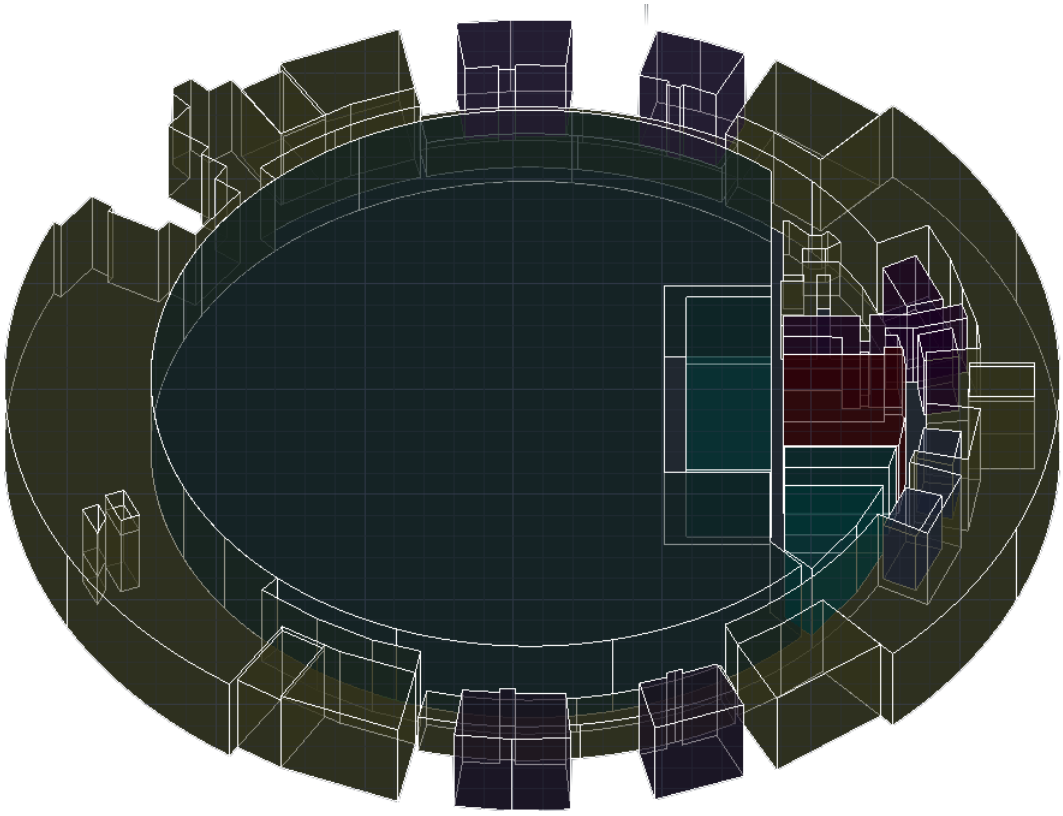

Figure 4-2. The 3D extruded cross-section of the containment at 21.5 m.

4.3.2 Preparing a CAD Simplified Model and GOTHIC Geometrical Input

Geometrical information in the detailed CAD model could not be transferred into the GOTHIC environment directly, since GOTHIC only uses simple geometrical forms like blocks, cylinders, cones, wedges and caps (allowed blockage geometry types). Therefore, an intermediate step should be taken here to ‘translate’ the geometrical ‘language’ of the detailed CAD geometry to the simplified GOTHIC geometrical ‘language’. This approach gives a tool to investigate different sub-regions inside the containment in terms of TH parameters.

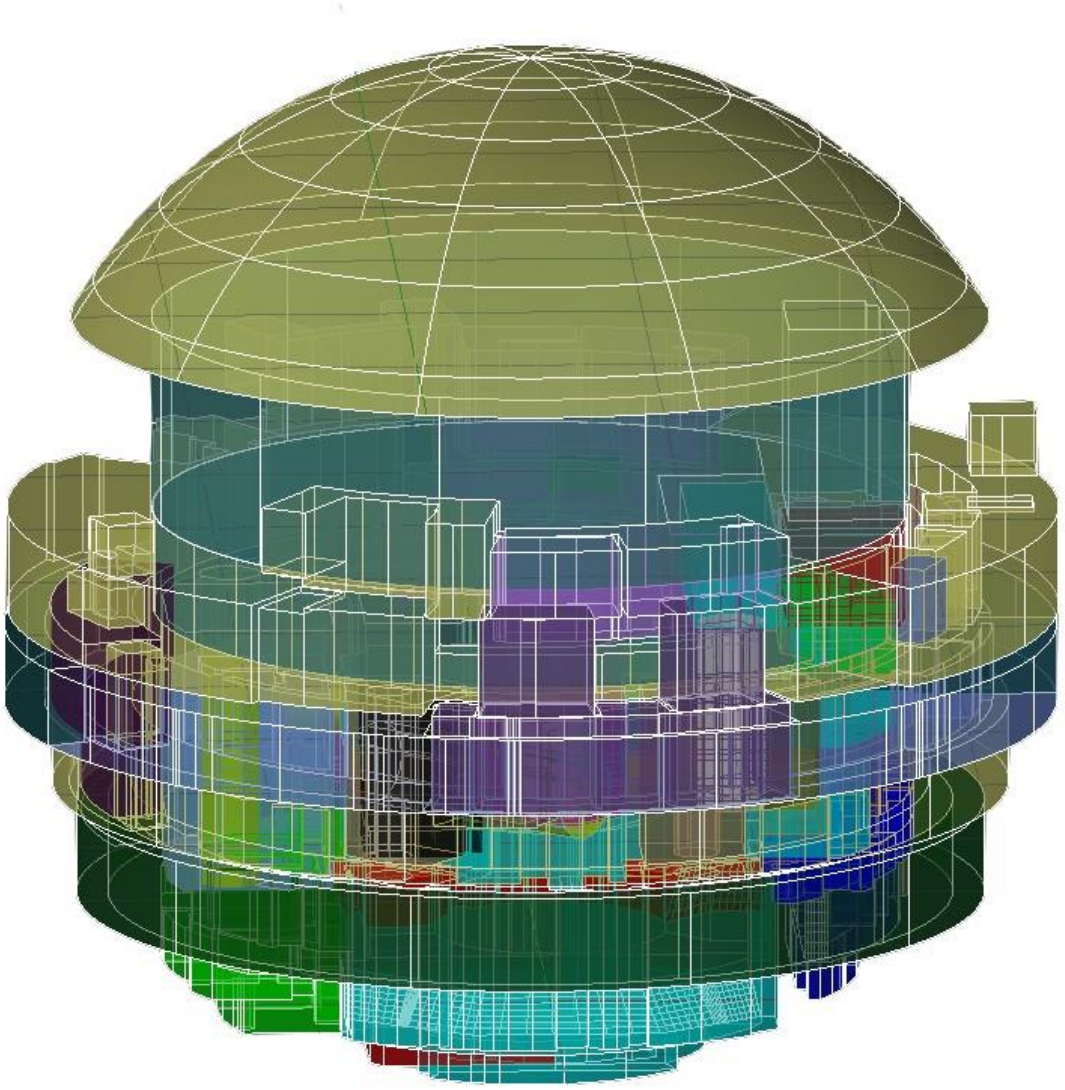

Figure 4-3. The Detailed VVER-1000/V446 containment model in AutoCAD.

There are two different modelling approach in GOTHIC 3-D modelling. One is detailed integral model and the other one is multi-zone model. In detailed integral model, only one control volume is defined, and that control volume resembles the whole containment. There is no need to define flow paths or 3D connectors (name of the flow path used if one of the control volumes is subdivided) since there is only one control volume and all the mass and energy transferred from one region to another inside the containment is enclosed in that one control volume. A detailed integral model is better when desiring to get temperature and pressure profiles within the containment. Multi-zone model (MZM) divides the whole containment into several rectangular prism compartments and the user carves the real geometry of the control volume out of the prism by using blockages, an example of the methodology is shown in Figure 4-4 (Bocanegra et al., 2016). In Figure 4-4, the real

geometry is enclosed by a cube, the region between the real geometry and the boundaries of the cube with blockages with porosity factor 0 is filled in MZM approach so GOTHIC will not include those cells into the solution matrix only the carved hole (real geometry) will be considered. This approach is better for hydrogen distribution analysis inside the containment and was selected for this work since it gives a better tool to investigate local regions inside the containment.

The diameter of the VVER-1000/V446 containment is 56 meters and the whole containment is subdivided into 60×60×60 grid lines. Cell size is selected as 5×5×5 meters, based on a previous work that shows around 1700 cells in a GOTHIC 3D MZM model could simulate temperature and pressure evolution during an LB-LOCA reasonably well in comparison to another model with the same approach but having approximately 7 times higher cells (Bocanegra et al., 2016). An enclosing rectangular prism is built according to the mesh system for each control volume as could be seen in Figure 4-4. The fitting of the geometry to the mesh as early as this stage is necessary due to the problems that might emerge in later phases in terms of maintaining thermal independence between two fluid regions (Bocanegra et al., 2016).

Wedge has been selected as the blockage type to use as the basic allowed geometrical shape to span the region needed, since it provides the easiest and most consistent way to achieve the goal of transferring the geometrical information of the detailed CAD containment model. The entire free volume inside each rectangular prism breaks into small wedges through triangulation of the surface and specifying the height. Each corner of a wedge is assigned a unique number (Figure 4-5). Each number has its x, y, z coordinates with respect to the control volume origin. Thus, a user could extract all the data (x, y, z coordinates of three corners of the triangle and the height) necessary to transfer the position of each wedge to GOTHIC 3D format. First, the raw data was extracted from the CAD software (corner coordinates) and then grouped for each wedge for each control volume in MS EXCEL. Moreover, the GOTHIC interface demands a certain data arrangement to describe each wedge according to its position. A specific Visual Basic Applications (VBA) macro was written for the task in MS Excel to transfer the data accordingly**.**

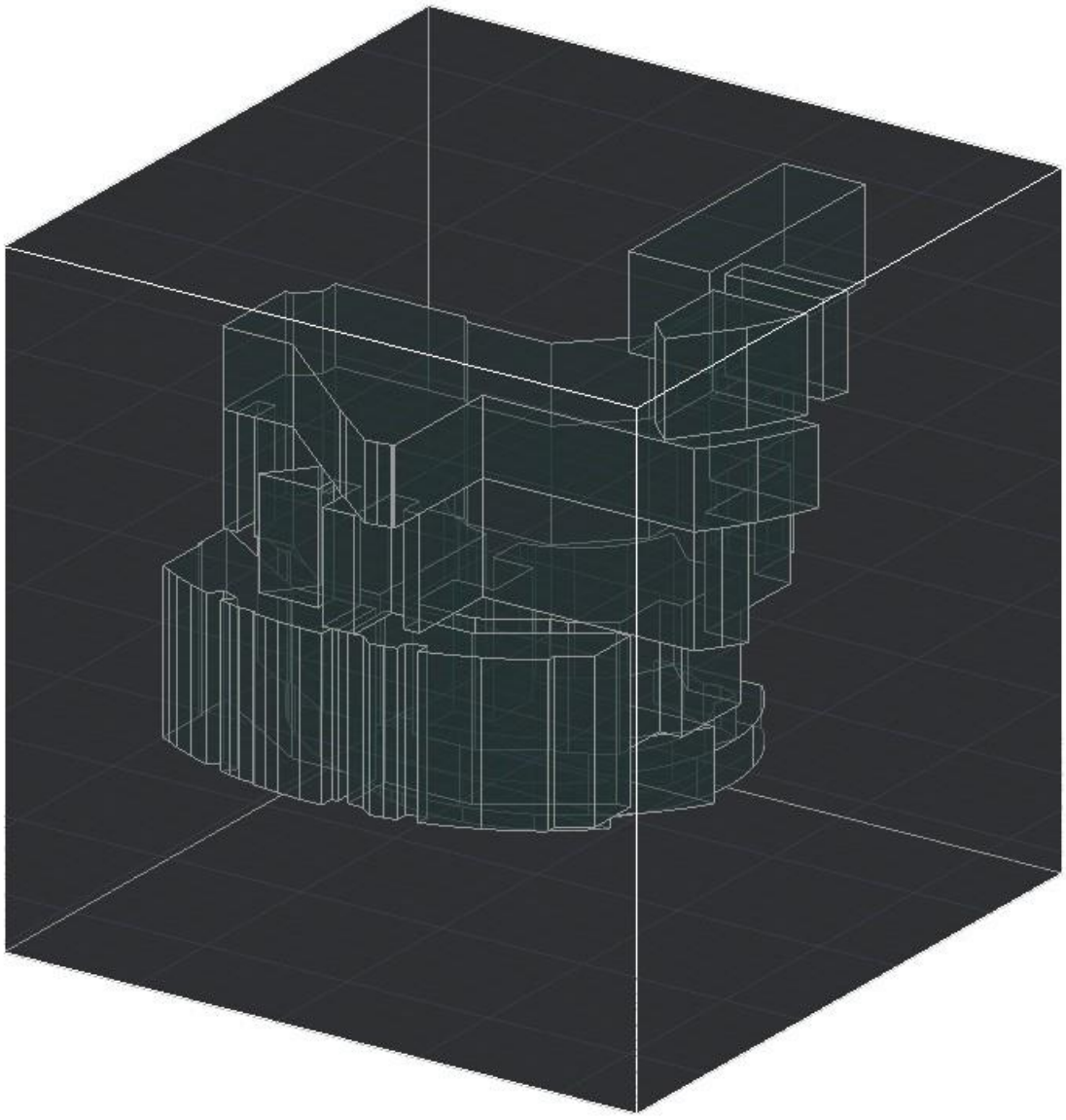

Figure 4-4. Control Volume 2 (Steam Generator 2) in the rectangular prism that is prepared according to the mesh created.

4.3.3 GOTHIC 3D Modelling with the Transferred Geometry

Figure 4-6 shows the GOTHIC 3D graphical user interface (GUI) after selecting the subdivided volumes option for the typical control volume No 6 as it was also shown in Figure 4-5 to demonstrate the transfer of the geometry. Each cell in the figure has a dedicated porosity factor to define the free volume inside the cell. The average thermal-hydraulic

parameters of the whole cell are stored in its centre which means each cell acts like a point that stores the information.

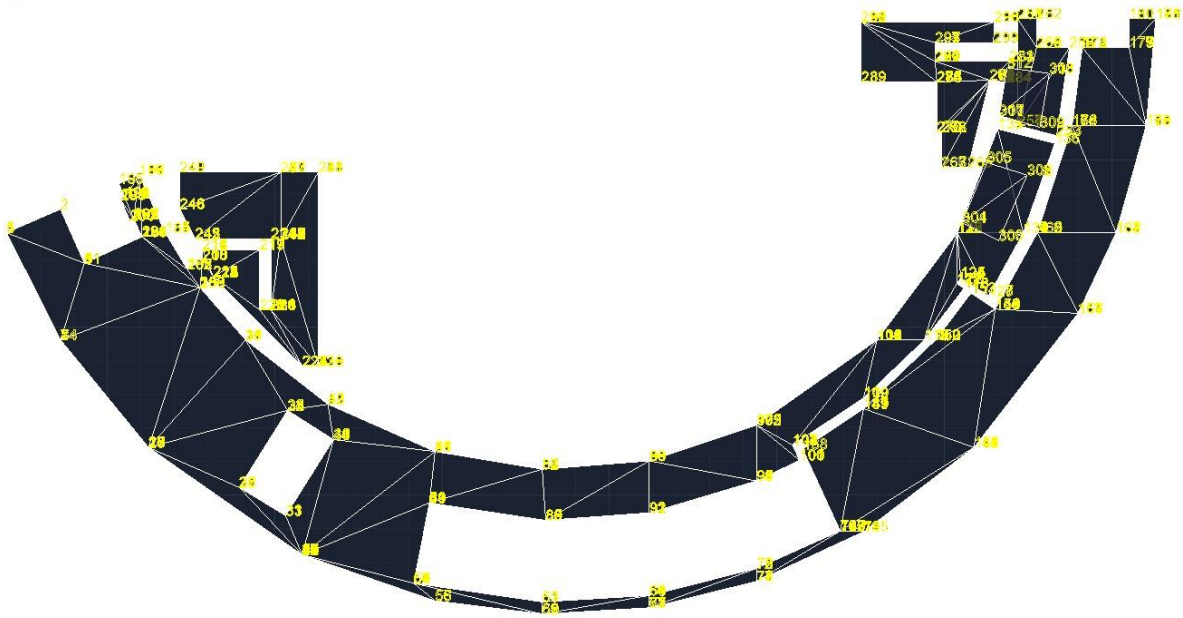

Figure 4-5. Triangulation and numbering of wedge corners of Control Volume No. 6 in AutoCAD.

Control volumes are subregions of the containment that could be occupied by ice or a fluid such as water, steam, non-condensing gases (hydrogen, air) or a mixture of these fluids. If the control volume is subdivided, mass and energy equations are solved for each cell to obtain mass and energy distribution and the momentum equations are solved at the cell faces to produce flow patterns within the control volume by the code. Some basic physical characteristics such as height, bottom elevation and net free volume are required to specify a control volume in GOTHIC (EPRI, 2018a). The 3D VVER-1000 containment is divided into 29 control volumes. The control volumes with their descriptions could be seen in Table 4-1. The layout of the control volumes within the steel containment is shown in Figure 4-7 and Figure 4-8.

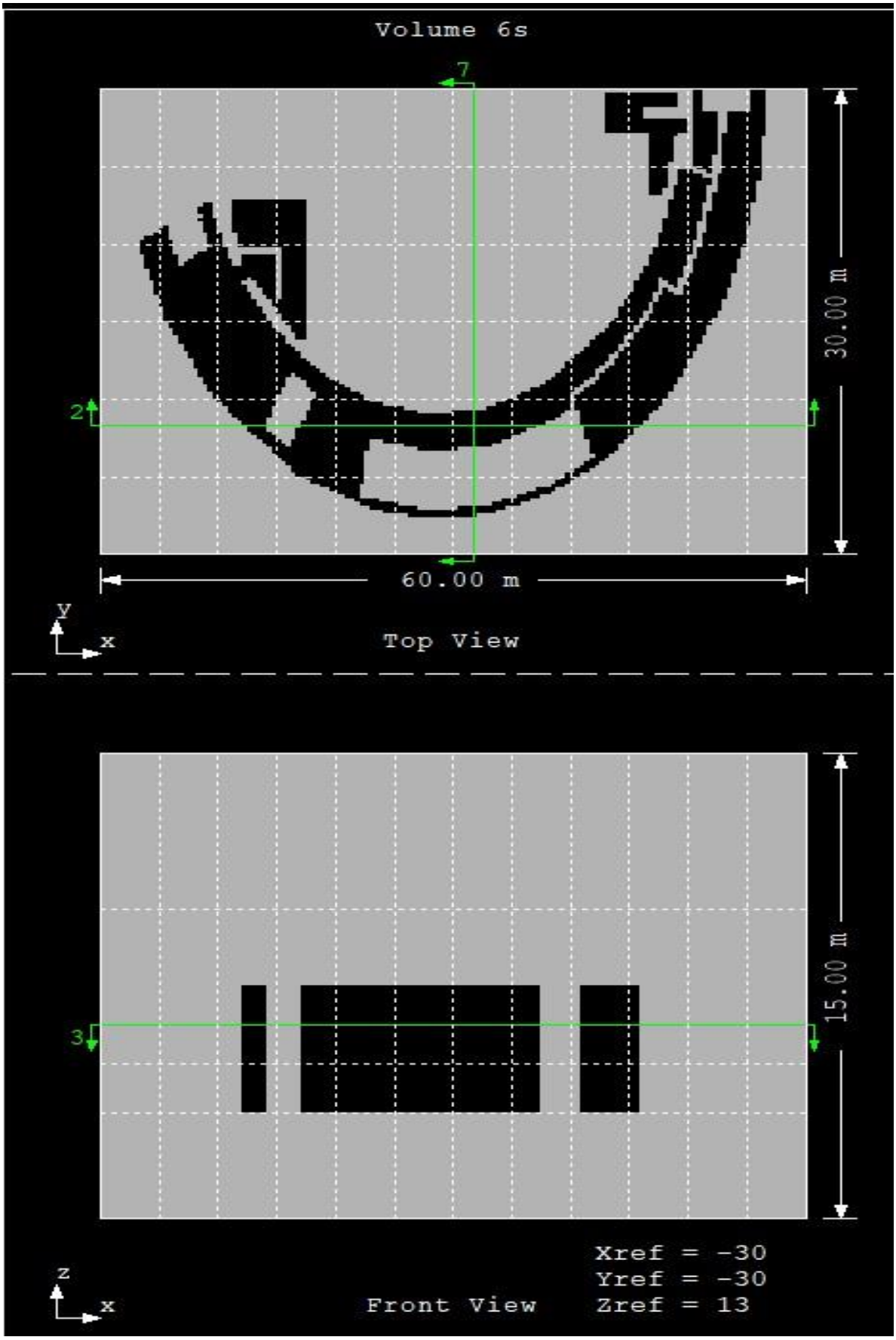

Figure 4-6. 3D model of control volume No 6 in GOTHIC 3D GUI on x-y and x-z planes.

Table 4-1. Containment control volume descriptions.

No	Description of the control volume	Volume (m^3)
1	Rooms of Steam Generator 1-2 and their loops	4870
2	Rooms of Steam Generator 3-4 and their loops	4830
3 and 4	Reactor Vault	458 and 1100
5	Annular corridor from 0 to 180 degrees, Shafts of steamlines of loops 1 and 2	699
6	Annular corridor from 180 to 360 degrees, measurement chamber, Shafts of steamlines of loops 3 and 4	787
7-10	Main coolant pump rooms	≈ 260 (each)
11	Fuel Pool	1380
12	New Fuel Storage	677
13	Reactor internals inspection pool	541
14	Cask pool	130
15 and 16	Ventilation system rooms	917 (each)
17-21	Active water treatment filter rooms and filter-container room	≈ 50 (each)
22	Valve chamber of nuclear component cooling system	278
23	I&C rooms, spare rooms and stairs	905
24	I&C rooms, spare rooms and stairs	847
25	Annular pipeline corridors from 0 to 360 degrees	784
26	Heat exchanger cooler rooms	135
27	Recuperative heat exchanger room	35
28	Central hall above the upper desk until 31.7 m	16949
29	Hall volume above the cylindrical wall (the dome) and between the cylindrical wall and containment (annular space)	26335

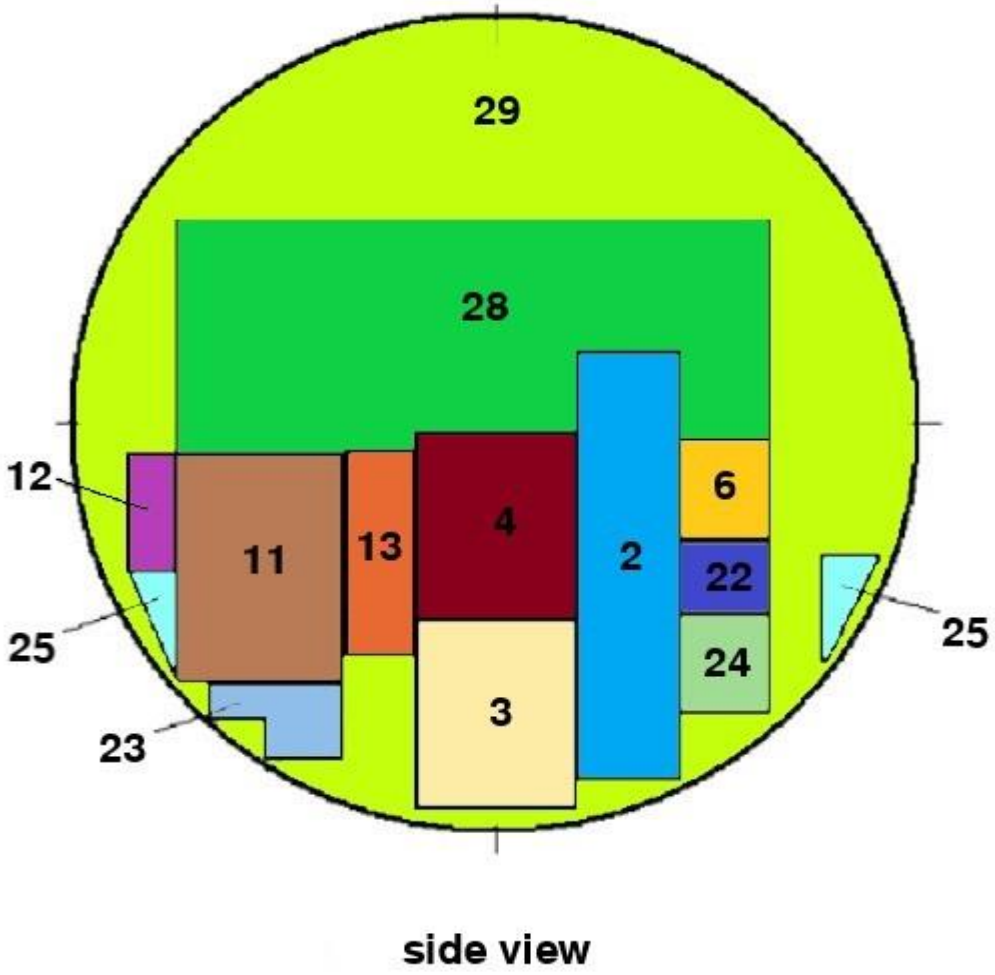

Figure 4-7. Control volume layout of the containment, vertical cross-sections; side view.

The hydraulic connections between control volumes are maintained by flow paths and 3D connectors. Flow paths could also be used to connect a boundary condition to a control volume. Momentum equations are solved for the liquid, vapour/gas mixture and droplets considering separate velocities for each phase. Hydraulic diameter, flow area, friction length, inertia length, loss coefficient, flow path end elevation and flow path height need to be specified to model a flow path in the code. 3D connectors could connect two adjacent ranges of cells while flow paths could only connect one cell to another between two subdivided volumes. 3D connectors could also establish a connection between an LP control volume and a subdivided volume. Mass and energy are stored in control volumes, not in flow paths or 3D connectors (EPRI, 2018a). 66 flow paths and 46 3D connectors are built within the model. In addition, 24 flow path connections in the model are described as valves that are closed until the pressure gradient between two adjacent control volumes that are connected through the flow path reaches 0.01 MPa.

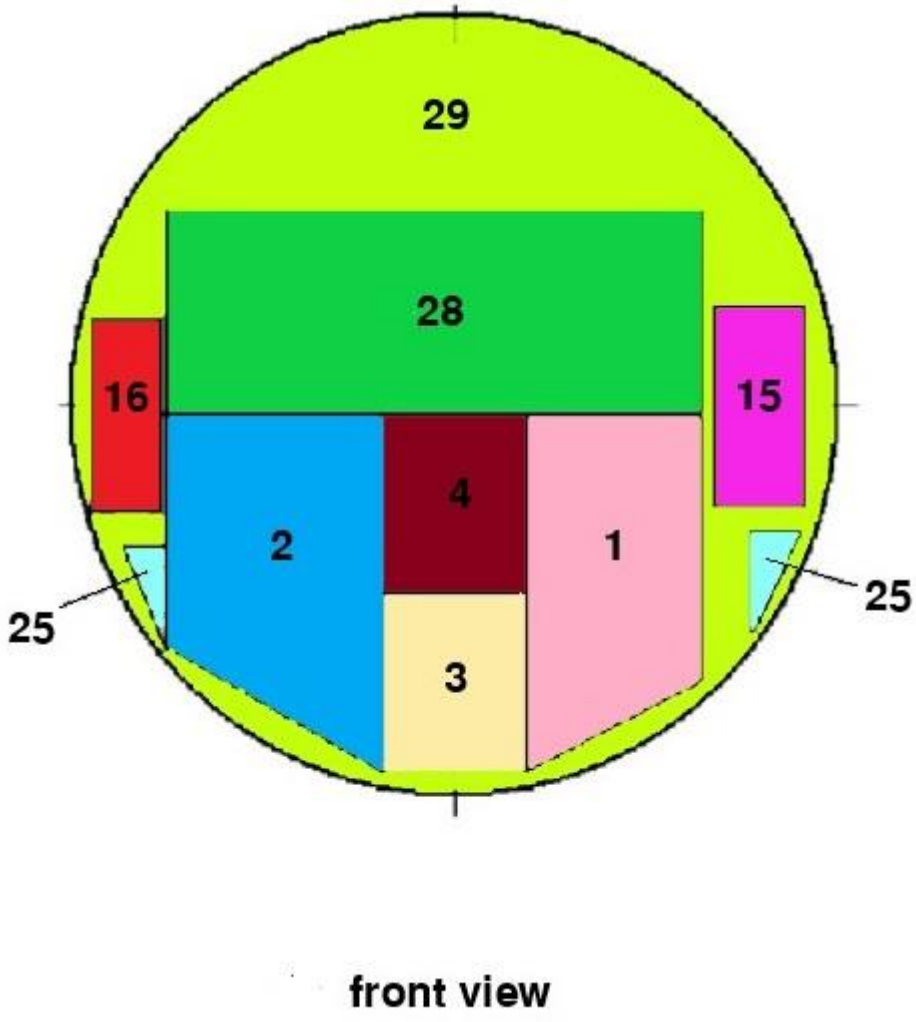

Figure 4-8. Control volume layout of the containment, vertical cross-sections; front view.

Thermal conductors are solid structures like internal concrete walls used for modelling the heat sink phenomena inside the containment in GOTHIC. Heat capacity of solid structures, heat transfer between volumes separated by a solid structure or between the fluid and the solid structure and radiative heat transfer between structure surfaces are modelled through thermal conductors. One-dimensional heat transfer is used to model conduction through the conductors. A conductor is modelled by dividing it into multiple temperature nodes with the thickness and the material assigned by the user. The spacing of the node boundaries should be closer to each other near the surfaces to adequately capture the steep temperature profiles through the conductor (EPRI, 2018a). Utilising this principle, the auto-divide option is used on the subdivision of all the thermal conductors in GOTHIC. There are several heat transfer coefficient options in GOTHIC such as film, direct and Tagami. The direct heat transfer

coefficient option is recommended by the code's manual in general condensation and blowdown cases and therefore selected in the modelling process. Available condensation options in GOTHIC are UCHIDA, GIDO-KOESTEL, MAX and four different variants of DLM. The diffusion layer model (DLM) condensation option is based on well-established principles for heat and mass transfer analogy (EPRI, 2018a) and accepted by NRC for LOCA and MSLB peak containment thermal-hydraulic response analysis (NRC, 2003). An enhanced version of DLM with film roughening and mist formation in the boundary layer (DLM-FM) is used as the condensation option for thermal conductors. Overall, 143 thermal conductors are defined to represent energy sinks inside the model.

Flow boundary conditions establish communication between the model and the known fluid conditions connected to the boundaries of the model (EPRI, 2018a). The known fluid conditions such as mass flow rate and water temperature could be specified to model CSS in the containment model. There are two boundary conditions defined for each spray header. Each boundary condition is connected to the control volume 29 (the upper dome) by a flow path. The mean spray droplet diameter, spray cone angle and the Geometric Standard Deviation for droplets are also specified in spray header modelling. Trips are set to trigger the actuation of the spray system when the pressure inside the containment reaches 130 kPa. Although the spray droplet temperature is specified between 20 to 60 °C in FSAR due to the variable temperatures of the sump water during the accident, the temperature for spray droplets is selected as 55 °C since this value is the predominant spray temperature in the long term (AEOI, 2003). In addition to CSS, break sources could also be modelled by using flow boundary conditions in GOTHIC. The mass and energy data taken from TECH-M-97 code results in FSAR are changed to mass flow rate and enthalpy data to put into GOTHIC in the modelling of LOCA discharge. 4 boundary conditions are defined, two for each break by separating water and steam sources, on the cold leg of the loop 4 in the control volume 2.

Figure 4-9 shows the central part of the whole containment model in GOTHIC 2D GUI. The yellow rectangles with dashed lines that have their number on the left upper corner represent control volumes. 5F and 6F cyan boxes, which are boundary conditions, represent the rest of the containment spray system that carries water to the spray nozzles 1N and 2N. Green lines, 63 and 64 that link boundary conditions to spray nozzles are called flow paths. Some flow paths have a valve defined on themselves, the number is written in red on the white tag such as 5V and 6V. Whereas yellow connections such as 12 and 13 that connect control volumes 23 to 29 on the left side are called 3D connectors. 1F and 2F on the lower left part are

boundary conditions that are linked to the control volume 2 and they are break sources releasing mass and energy to the containment during the accident. Red connections are thermal conductors and there are two types of them: internal and external. For internal thermal conductors, both surfaces are connected to the same cell. Whereas for external thermal conductors, surfaces are assigned to different cells and are usually used for modelling of walls between two control volumes. In this diagram, only external thermal conductors can be seen except the 40s in control volume No. 29. The 40s is the thermal conductor that connects the dome of the containment to the environment.

Russian ANGAR code has been used by FSAR to analyse thermal-hydraulic parameters and hydrogen distribution inside the containment. Since ANGAR is an LP code, a direct comparison of the simulation results with the GOTHIC 3D model is not appropriate due to the fundamentally different assumptions and calculation methods between the two codes. Therefore, an equivalent GOTHIC LP model needs to be developed from the GOTHIC 3D one to validate the results in short-term simulation by using the `revert to lumped' feature of the code. This conversion to an LP model also adds the capability of investigating LP and 3D code strength by comparing the results, in addition to validating the developed model in GOTHIC. The conversion included several steps to match two different models such as remodelling of 3D connectors as flow paths, since the former is not allowed in GOTHIC LP mode or consideration of changes in the inertia length of flow paths. It should be noted that the same layout of control volumes shown in Figure 4-7 and Figure 4-8 was considered in the GOTHIC LP simulation.

The long-term simulation runs for 100000 seconds while short-term simulation runs for 200 seconds to analyse the behaviour of the VVER1000 containment following the LB-LOCA.

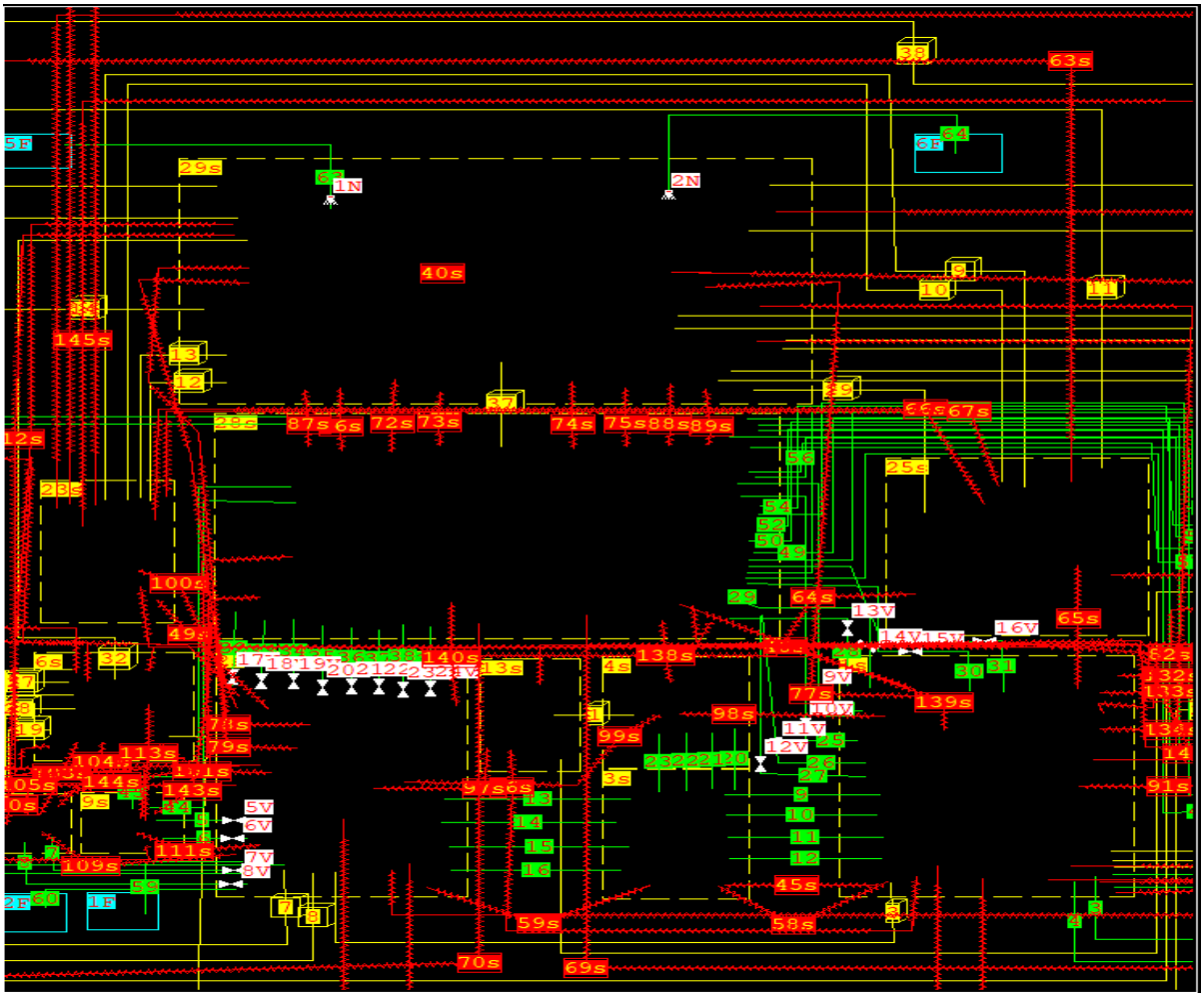

Figure 4-9. Display of the central segment of GOTHIC short-term and long-term containment model in 2D GUI of the code.

4.3.3.1 Modelling of Passive Autocatalytic Recombiners (PARs)

There are generally two types of numerical modelling of the PARs. One of them is black-box model, the simpler and widely used approach that is based on hydrogen recombination rate or efficiency calculated by using empirical correlations and implemented through volumetric sinks and sources of mass, energy, and momentum. Large-scale experiments were conducted to investigate the PAR behaviour under realistic conditions to obtain the PAR recombination rate. Apart from the black-box approach, mechanistic models could be used to model PAR behaviour, including the details of the convection flow through the PAR, and the reaction kinetics on the catalyst (Papini et al., 2019). A buoyancy model that explains the production and dissipation of turbulence and the radiative heat transfer between the plates of the instrument and between plates and the environment should also be considered in mechanistic models. Moreover, mechanistic models consider convective and diffusive transport of

hydrogen and oxygen in the bulk flow, the film diffusion through the boundary layer, and the pore diffusion to the reactive surface of the catalyst (Kelm et al., 2008). An example of such mechanistic models could be REKO-DIREKT which has been implemented in COCOSYS (Sonnenkalb et al., 2015) and the CFD code ANSYS-CFX (Kelm et al., 2010).

GOTHIC implements the black-box approach to model the PARs within the containment. The characteristics of the PAR instrument are not modelled, the effects of the PAR on the containment atmosphere while being active are introduced as mass, energy and momentum sources in the downstream cell. For example, the buoyancy force is calculated by GOTHIC using the density difference between inlet and outlet of the PAR and defined as a momentum source for the gas mixture (Papini et al., 2019).

A PAR utilized in the containment could be defined on a flow path in GOTHIC to simulate the hydrogen depletion through the flow path by converting a specific amount of the incoming hydrogen inside the gas mixture to steam. In other words, for each PAR component defined in GOTHIC, there needs to be a flow path that represents the inside of the metallic box where the gas mixture moves from below to above due to the chimney effect. Oxygen inside the incoming flow is depleted according to the stoichiometric ratio as well.

In FSAR, the set design parameters for the hydrogen removal system are such that during the LOCA (first 24 h), the volumetric concentration of hydrogen should not exceed 2% and in the post-accident period, the volumetric hydrogen concentration should be kept below 0.5%. Although the redundancy principle is not required for passive instruments by the regulatory authorities, the number of installed PARs within the system is more than 20% of the calculated design value against a DBA, associated with coolant leakage, caused by rupture of the pipeline of maximum nominal diameter 850 mm (variant 2) as discussed in section 2.4.1. Consequently, the amount of PARs installed within the containment in total equals 80 in design. The distribution of PARs is based on the possible hydrogen pathways and the volumes of the control volumes. Table 4-2 shows the control volumes and the number of PAR units installed within it (AEOI, 2003). To match the same conditions within the containment during the accident to compare hydrogen distribution results with FSAR, the design number of PAR units and the locations are implemented in the GOTHIC model as well. The location of PAR units is described as how many PARs are installed in which control volume without any specification on the exact position of them within the control volume in Table 4-2 because of the LP code limitations. In a 3D model, each control volume

consists of several cells that allow the user to place a PAR wherever it performs more appropriately in depleting the hydrogen amount. Therefore, a preliminary hydrogen distribution simulation was performed to investigate hydrogen stratification within each control volume to spot cells with higher hydrogen concentrations for the determination of the exact location of PAR units. All the cells within the GOTHIC containment model are checked and considered in the PAR installation process.

Table 4-2. The number of installed PARs in each control volume (AEOI, 2003).

Control Volume number	Number of installed PARs
1	7
2	7
3	1
4	1
5	2
6	1
7	1
8	1
9	1
10	1
11	0
12	1
13	0
14	1
15	1
16	1
17	1
18	1
19	1
20	1
21	1
22	1
23	3
24	2

25	2
26	1
27	1
28	0
29	38

Hydrogen recombination efficiency is a fraction of the flowing hydrogen through the PAR that will be converted to steam if a sufficient amount of oxygen is available, this value is between 0 and 1 (EPRI, 2018a). In addition, it could be defined as the recombination rate of hydrogen gas (the fraction of hydrogen that is converted per unit of time) divided by the hydrogen mass flow rate within the incoming gas mixture (the total amount of hydrogen that passes through the recombiner per unit of time). Hydrogen recombination efficiency is required as an input in GOTHIC to model a PAR. However, this efficiency is a function which depends on the recombination rate of the PAR could be derived from empirical correlations. The recombination rate formula for RVK-500 recombiners that are used in VVER-1000/V446 containment is based on the experiments performed at the All-Russia Research Institute for Thermal Engineering (VTI) and as follow:

$$R_{H_2} = n \cdot 10^{-3} x[a_0(p, T_C) + a_1(p, T_C)(x - 2) + a_2(p, T_C)(x - 2)^2]$$

Where R_{H_2} is the mass (g) of the hydrogen reacting in 1 sec, x is the hydrogen molar fraction, %, at the inlet into the recombiner. T_C is the temperature, °C, of the gas at the inlet, p is the pressure, 10^5 Pa. n is a constant equal to 7.7 for RVK-500 recombiner. The coefficients a_0, a_1, and a_2 are equal to:

$$a_0(p, T_C) = 1.43 + 0.24(p - 1) + 0.005(T_C - 20),$$

$$a_1(p, T_C) = 0.12 + 0.0031(p - 1) + 3.0 \cdot 10^{-4}(T_C - 20),$$

$$a_2(p, T_C) = 0.0099(p - 1) + 1.08 \cdot 10^{-4}(T_C - 20) - 1.54 \cdot 10^{-5}(p - 1)(T_C - 20).$$

The above recombination rate formula is valid for the condition, $x > 2$. For the condition $0.1 < x < 2$, the following linear interpolation is used:

$$R(x) = R(2)(x - 0.1)/1.9.$$

The relations above were obtained for pressure $10^5 < p < 5 \cdot 10^5$ Pa for hydrogen molar fraction up to 10%, providing that there is a sufficient amount of oxygen nearby (Tarasov et al., 2017).

The implementation of the formula to each PAR individually could be made through control variables in GOTHIC. Control variables are a specific class of GOTHIC variables that are calculated based on a set of defined functional forms, or operators, for which the arguments are also GOTHIC variables. In general, a control variable, Y, is calculated from an operator for which the generic function is:

$$Y = Gf(X_1, X_2, \dots, X_n).$$

Where G is a constant multiplier, and f is a defined operator having arguments X_i which are also GOTHIC variables such as cell pressure or mass flow rate of a junction. The function f could be defined by any specific pre-defined numerical operation such as division, integration, or multiplication. A control variable could also be an argument for another control variable (EPRI, 2018a). The GOTHIC variables that are used as an argument for the defining function of the control variables could only be selected at a specific cell or a flow path which means the variables should be defined for each PAR separately since the location of individual units is different. For example, if a PAR is defined on a flow path, to define the mass flow rate of the gas through that particular unit, that flow path should be selected as the location for that variable. In the case of another PAR, the flow path of that PAR would be different. Therefore, a set of control variables that defines the recombination efficiency are iterated for each PAR unit. Consequently, 1761 control variables are created to model 80 PARs within the containment.

Hydrogen sources that were given in Table 9 are modelled by using boundary conditions that were placed at the specific location of the source concerned, that are namely, the break at the reactor inlet, the fuel pool, the sump and under the dome (for the radiolysis of the steam and decomposition of hydrazine-hydrate). The hydrogen amount which is presented within the containment prior to the accident is included within the model as an initial condition. The hydrogen distribution simulation runs for 10^6 seconds (~275 hours). The solution method that is used to solve the pressure matrix equation at each time step during the run is ‘Direct’ which is the recommended method in the code manual (EPRI, 2018a). The differencing scheme is selected mostly First order upwind scheme (FOUP) but due to the instabilities in

the code, for some short periods, bounded second order upwind scheme (BSOUP) has also being applied.

CHAPTER 5
RESULTS AND DISCUSSIONS

5.1 Introduction

Three simulations were carried out through this research study; 1) short-term containment response analysis to evaluate peak pressure and temperature profiles whether they are below the design limit or not, 2) long-term containment response analysis to investigate the cool-down response of the containment, along with the influence of CSS on TH parameters, and finally, 3) the hydrogen distribution inside the containment following the DBA and the effectiveness of the PARs in mitigating the hydrogen risk.

One of the acceptance criteria to fulfil the requirement of the NRC's regulations is the duration to reach half of the peak pressure of the containment should be less than 24 hours following a LOCA (requirement of long-term simulation). Moreover, the containment structure and its internal compartments need to withstand the calculated TH conditions resulting from any loss-of-coolant accident without exceeding the design leakage rate and with sufficient margin (requirement of short-term simulation) (NRC, 2007). In addition, the lower flammability limit for hydrogen in air saturated with water vapour at room temperature and atmosphere pressure is assumed to be 4.1 percent. The components of the emergency hydrogen removal system have been designed so that they will operate successfully to maintain the maximum hydrogen concentration in the containment at or below 2 (two) % by volume during LOCA and below 0.5 % by volume in the post-accident period. The limit equal to 2 (two) percent by volume was selected conservatively to reflect a reasonable limit to avoid problems like nonuniform mixing etc (AEOI, 2003). In order to check whether these design parameters are exceeded, hydrogen distribution analysis should be conducted through the containment under the postulated accident explained in section 2.4.2. The TH parameters studies are based on the accident described in section 2.4.1.

5.2 VVER-1000/V446 Containment Short-term Response to the LB-LOCA

The temperature and pressure profiles of the containment extracted from the results of the GOTHIC LP simulation were compared to the FSAR for selected control volumes to validate the simulation procedures and inputs. After the first comparisons, numerous test runs were performed for sensitivity analysis and to increase the accuracy of the results. The inconsistency of model results were mainly about some undefined parameter values in FSAR such as initial pool water temperature, spray droplet diameter and temperature, and spray

header configuration. Another source of discrepancies was a result of intrinsic GOTHIC features such as different heat transfer correlations between containment and environment and its effects on the results. GOTHIC LP and 3D results (3D results have been averaged over the relevant volume) and FSAR results are shown in Figure 5-1 to Figure 5-6 for ease of comparison.

Figure 5-1 to Figure 5-5 show the short-term temperature profiles of control volumes 8, 10, 23, 25, and 28 respectively. Table 4-1 gives a description for each control volume and Figure 4-7 and Figure 4-8 show the relative positions of these control volumes within the containment. This selection is based on considering the different regions of containment for results validation. Since control volumes 8 and 10 (two main coolant pump rooms) have small volumes and therefore relatively low thermal inertia and are located near the break source, larger discrepancies can be observed in their profiles. Even in the FSAR, the curve of the control volume 10 does not fit the general tendency of the curves of other control volumes at earlier stages. Nonetheless, the temperature profiles of both GOTHIC simulations (LP and 3D mode) are in agreement with FSAR results for all control volumes; the deviation is within a reasonable limit. The temperature rises as the coolant discharges into the containment from the break. After a certain point, the heat transfer (cooling) effects of the containment spray system, thermal structures, and the heat transfer between the containment and the environment lead to a declining trend of the temperature profile. GOTHIC 3D peak values are higher than the FSAR, but passing the first peak the heat loss of the containment is faster and as a result, the temperature drops below FSAR values. The main distinctive tendency of GOTHIC LP results is the slightly earlier peak time compared to FSAR and GOTHIC 3D results.

The change in the average pressure of the containment during the LOCA for the first 190 seconds is depicted in Figure 5-6. The behaviour of the average pressure curves of both GOTHIC LP and 3D simulations is significantly similar to FSAR results. The maximum average pressure of the GOTHIC LP mode is 390 kPa, almost the same as the FSAR maximum average pressure, 392 kPa at 20 seconds although the pressure peak’s time value is slightly shorter for the GOTHIC LP mode. The GOTHIC 3D model predicts a higher maximum average pressure of 431 kPa at 18 seconds. The result is in the acceptable range with a relative error of 10% in comparison to the FSAR result and below the design maximum average pressure of containment 460 kPa.

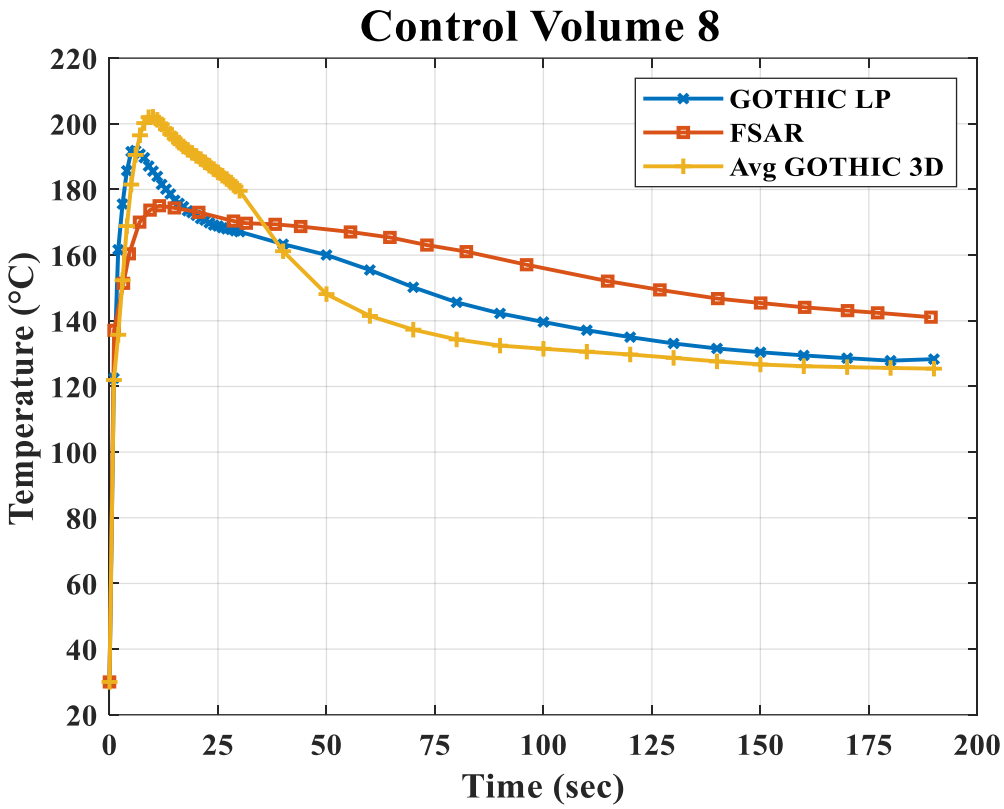

Figure 5-1. The short-term temperature profile of control volume 8 during the LB-LOCA.

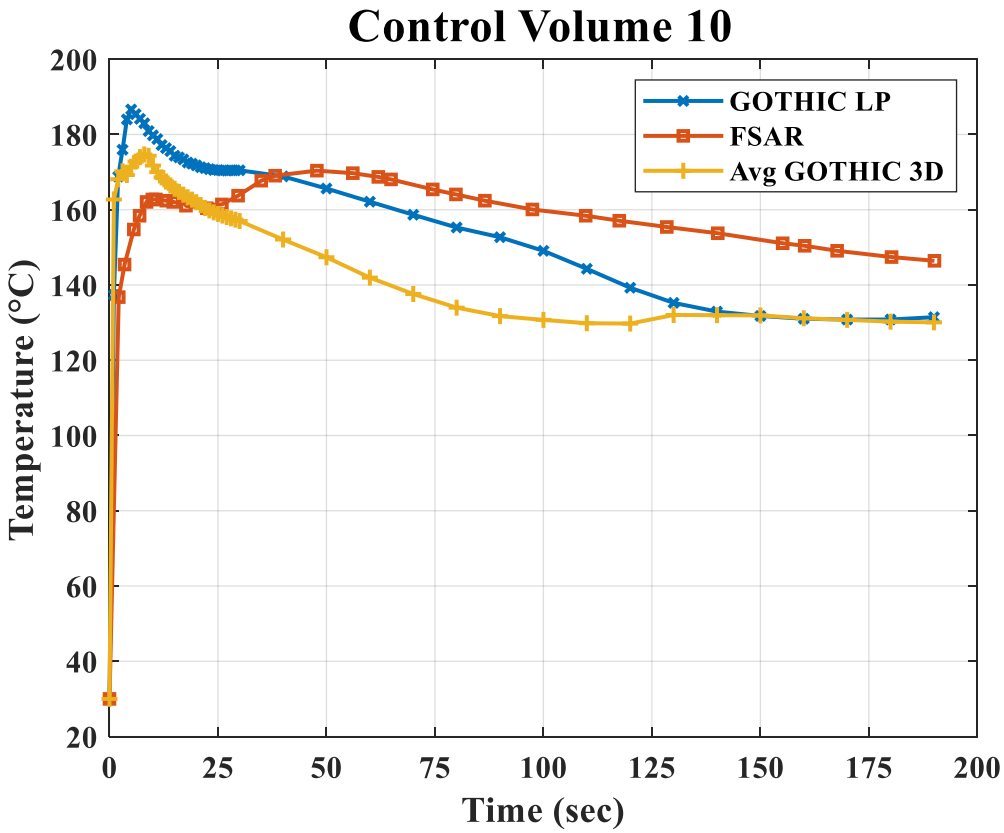

Figure 5-2. The short-term temperature profile of control volume 10 during the LB-LOCA.

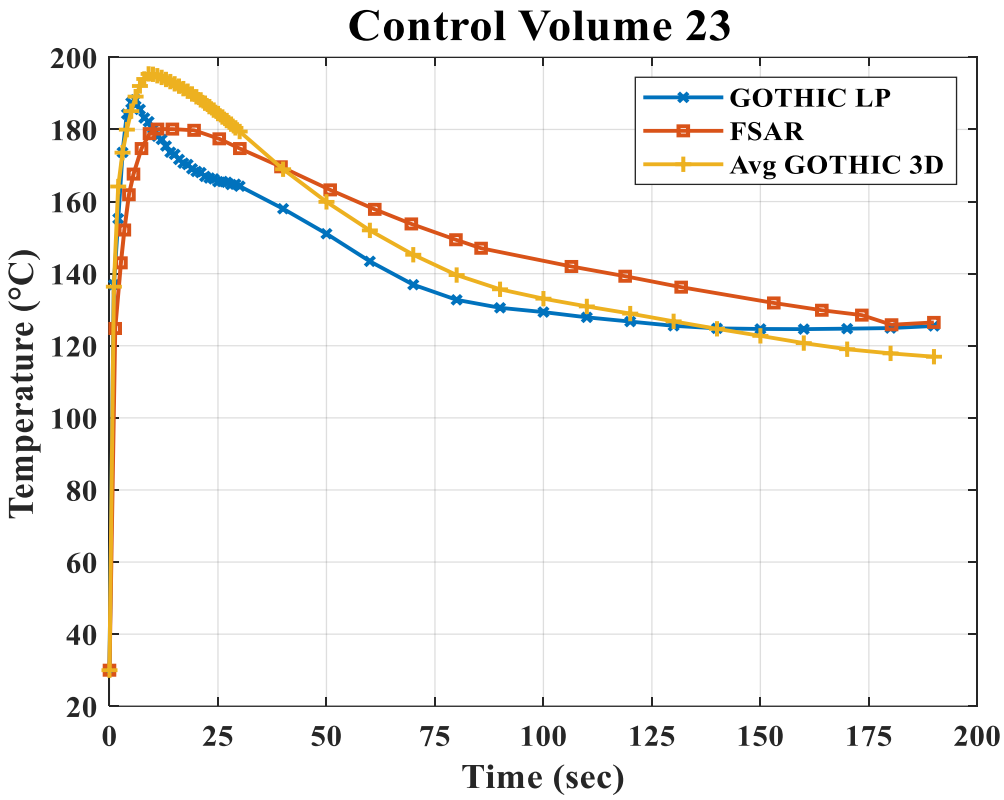

Figure 5-3. The short-term temperature profile of control volume 23 during the LB-LOCA.

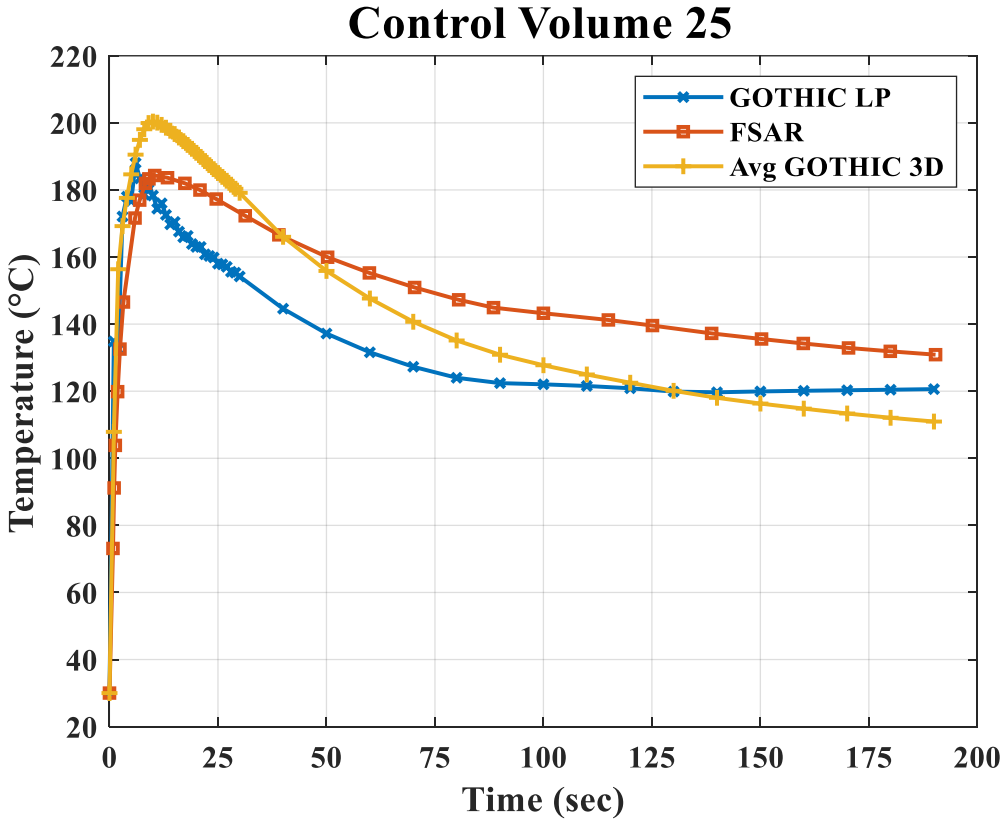

Figure 5-4. The short-term temperature profile of control volume 25 during the LB-LOCA.

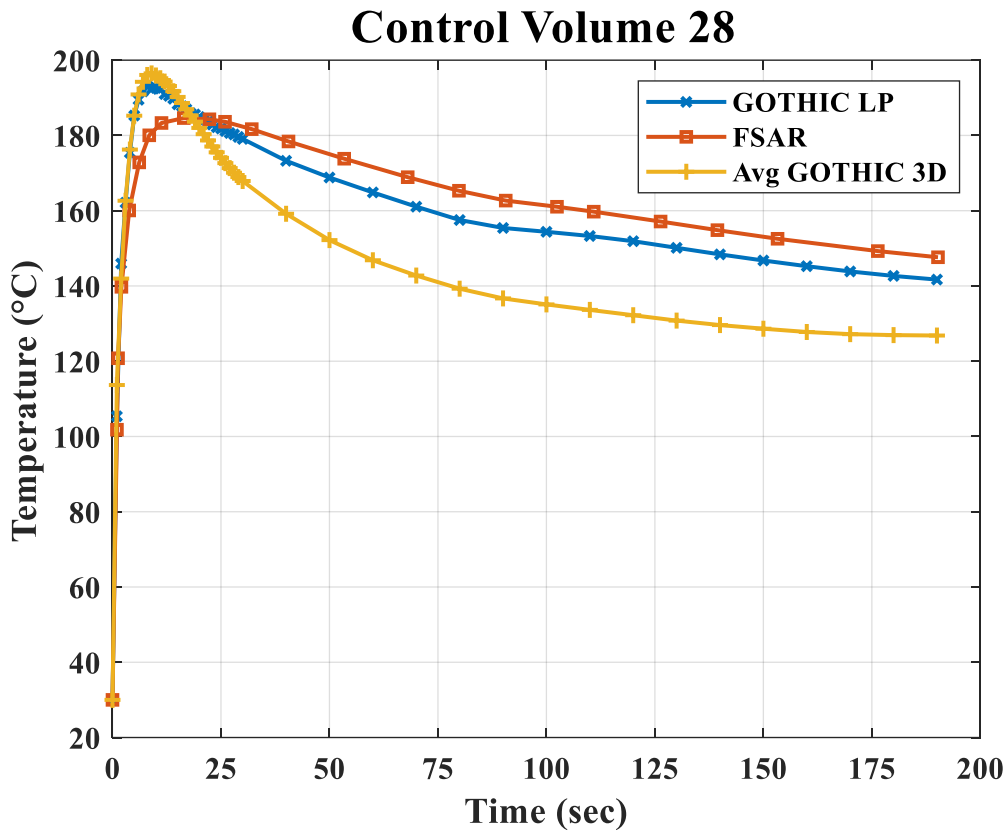

Figure 5-5. The short-term temperature profile of control volume 28 during the LB-LOCA.

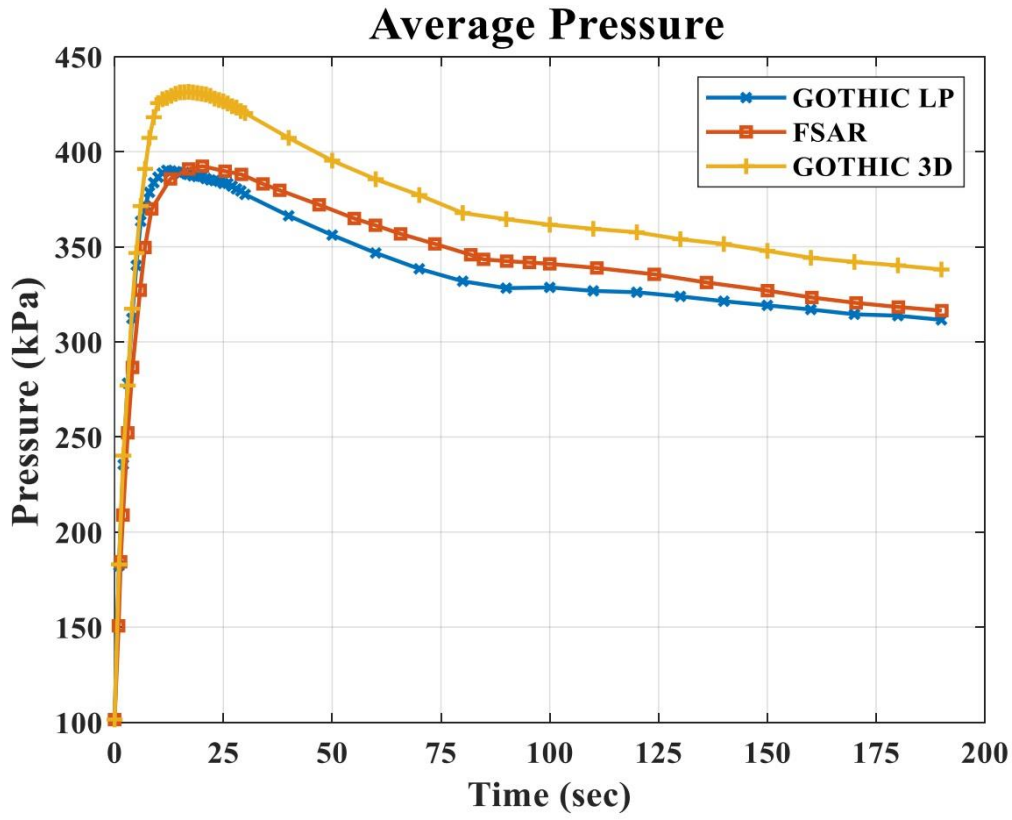

Figure 5-6. The average pressure profile of the containment during the LB-LOCA.

Pressure distribution inside the containment is more homogenous due to the dispersion of pressure at sonic speed from the pipe break, whereas temperature distribution is less homogenous. Figure 5-7 to Figure 5-13 show the 3D contours of the temperature profiles inside the containment for various elevations. The transient behaviour of contours has been presented at different times of 2, 5, 10, 15, 30 and 150 seconds. These time points were selected in a manner to cover all the alterations of temperature contours during short-term simulation. It is worth to be noted that all TH parameters inside containment are available at all points of the containment as a result of this simulation and these figures are just typical outcomes. These temperature contours are prepared in ParaView (Ahrens et al., 2005) data-visualization tool in the post-processing stage. The temperature rises through the first seconds rapidly and reaches its peak around 10 seconds after the break happens. Following its peak, it gradually decreases over time just as the temperature profiles demonstrated in Figure 5-1 to Figure 5-5. The same behaviour of GOTHIC LP and FSAR results versus time can be seen in these figures (3D results). The main advantages of these 3D contours regarding LP mode are; i) the capability of demonstrating the TH parameters in all coordinates of containment and ii) analyzing local hot spots inside the individual containment compartment for precise safety assessment. These figures can prove the contrast of temperature profile in individual volumes where this contrast has been omitted in LP mode because of its nature.

In addition to 3D temperature contours at different elevations, the 3D vertical temperature contours through the containment at x and y normal planes are shown in Figure 5-14 and Figure 5-15 respectively. These plots depict the blowdown of mass and energy released through the break source and its movement inside the containment. It is important to mention, in these figures, the temperature of the control volumes adjacent to the break source increases rapidly at the initial stages after the accident in comparison to others. With progressing in accident time, as different factors of mass and energy transfer between control volumes, size of CVs, flow path, turbulent regimes, etc. come into play, it can clearly affect the contours and as can be seen the CVs under containment dome can get more intensive profiles. In addition, the major effects of the spray system as an ESF in NPPs can be obviously monitored in long-term analysis (as it has exactly been dedicated for this purpose). Although, in the DECL accident, there is an enormous blowdown to the containment, the spray system actuates almost from the initial seconds of the accident (the spray set point is 130 kPa in this study). So, the temperature reduction inside the containment passing the maximum point (around 10-15 seconds) that can be seen in Figure 5-14 and Figure 5-15 results from two

factors, a) the minor effect of spray actuation in the short term and b) major effects of break mass and energy profile behaviour. It should be noted that, in long-term analysis, the effects of spray in depressurization will be the dominant factor.

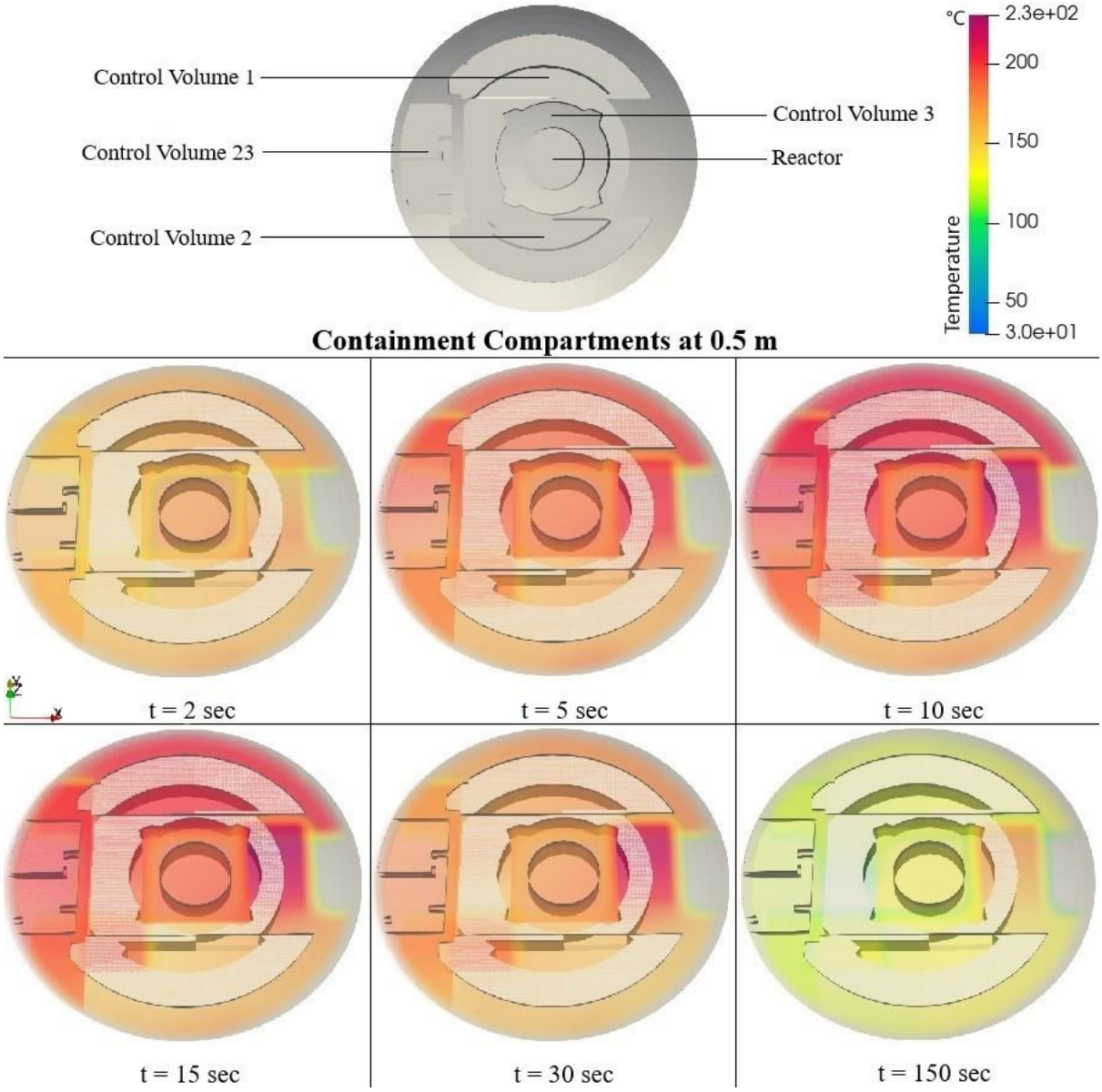

Figure 5-7. 3D temperature contours inside the containment at elevation z=0.5 m.

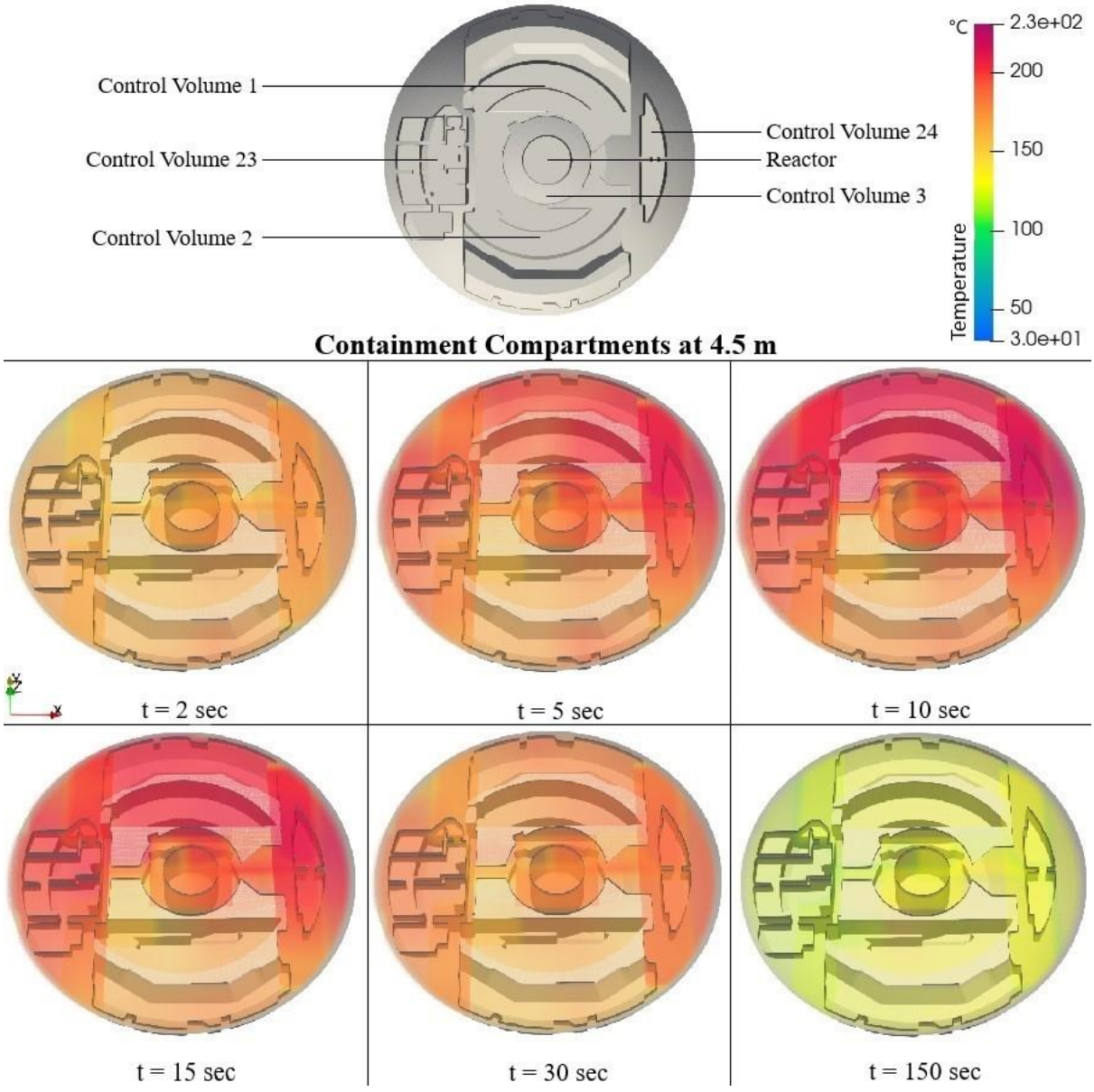

Figure 5-8. 3D temperature contours inside the containment at elevation z=4.5 m.

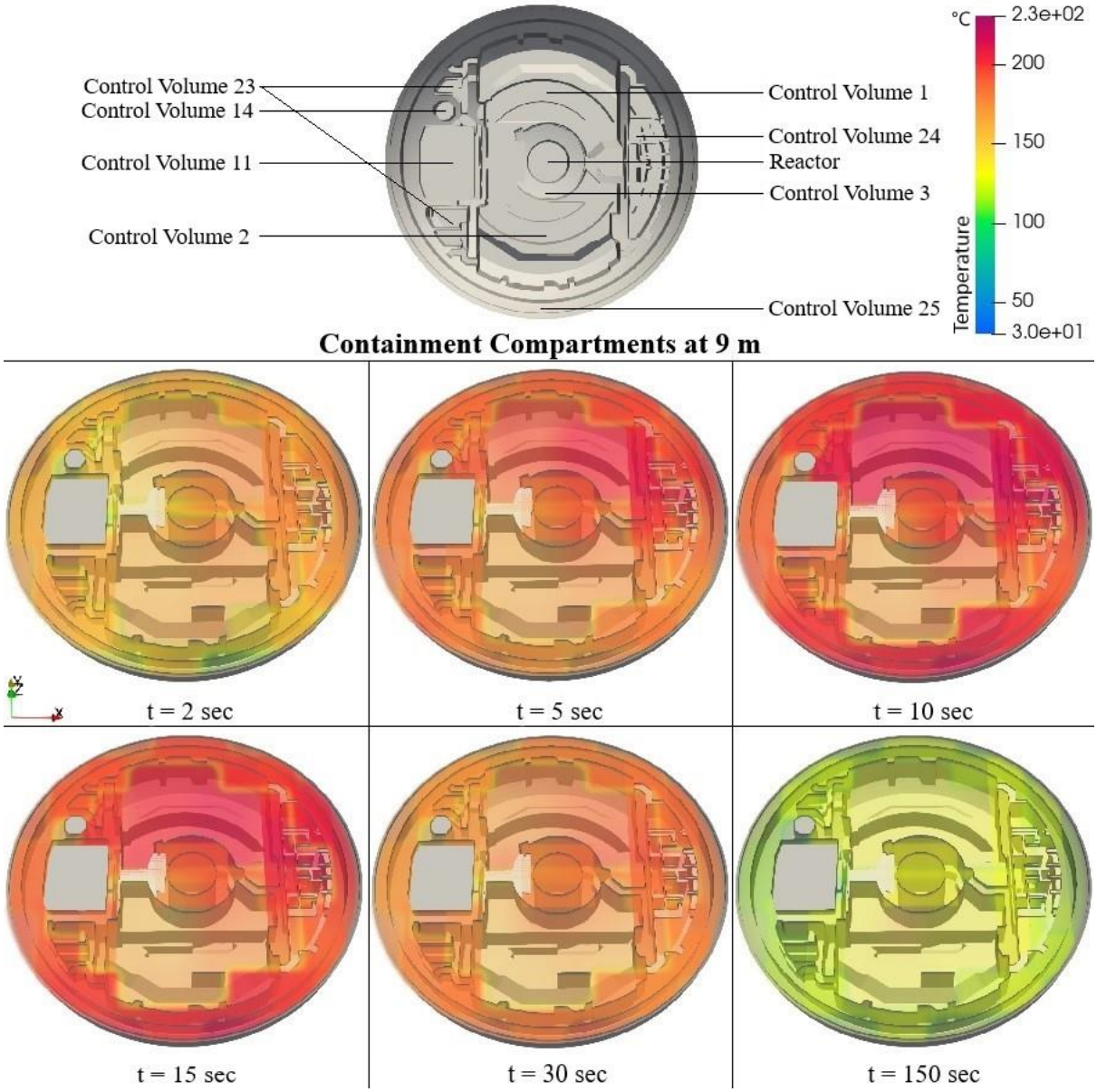

Figure 5-9. 3D temperature contours inside the containment at elevation z=9 m.

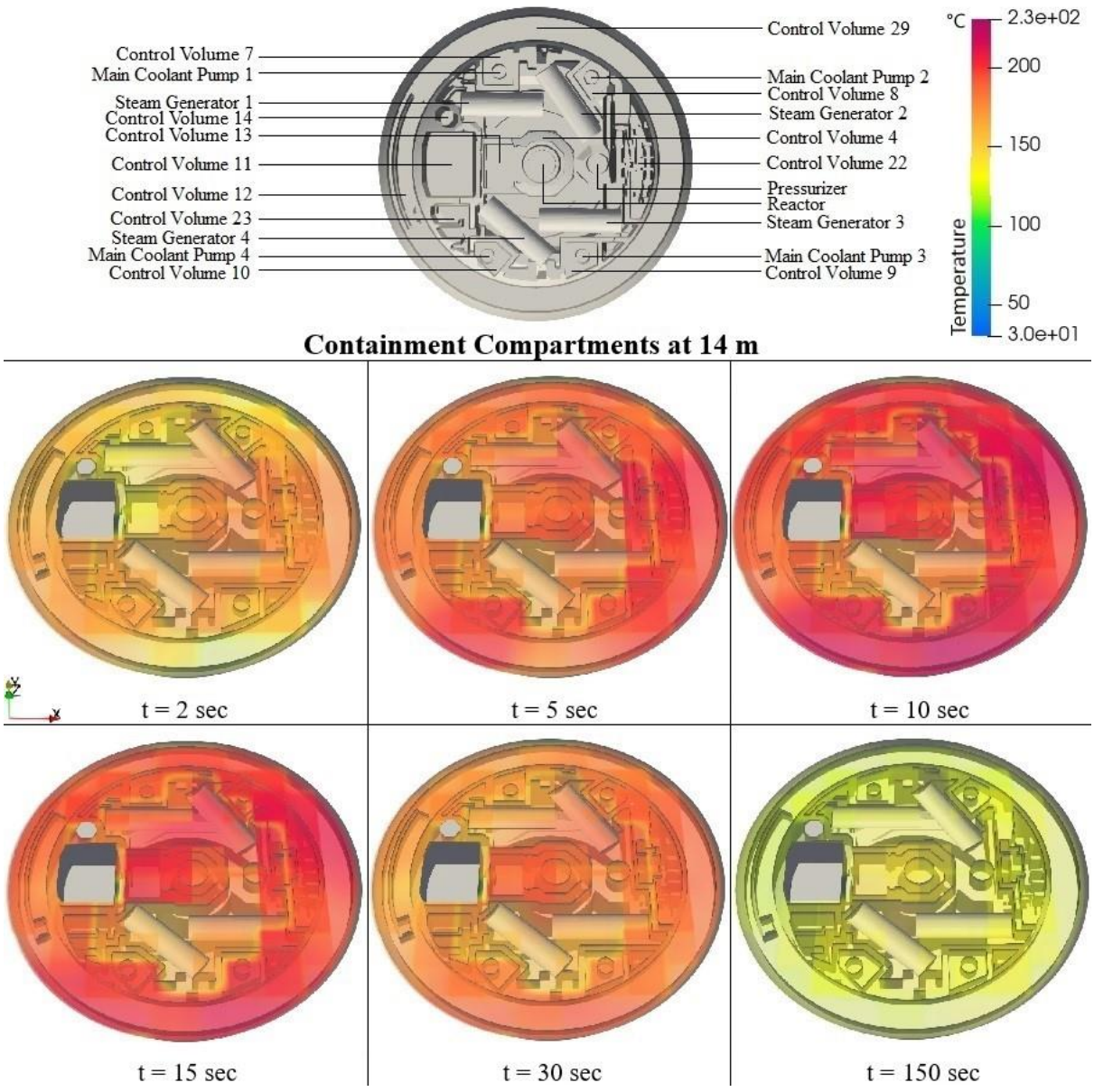

Figure 5-10. 3D temperature contours inside the containment at elevation z=14 m.

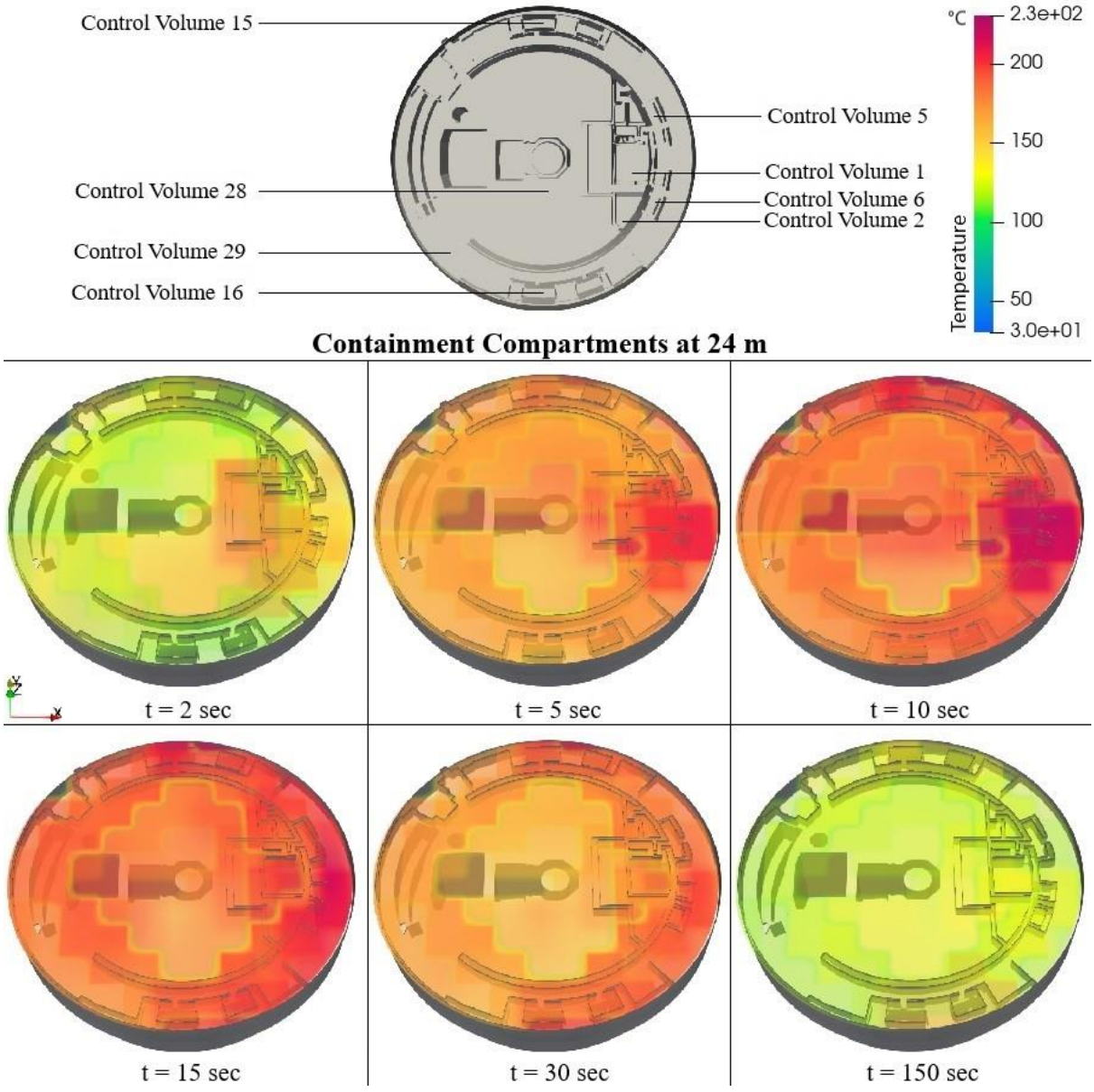

Figure 5-11. 3D temperature contours inside the containment at elevation z=24 m.

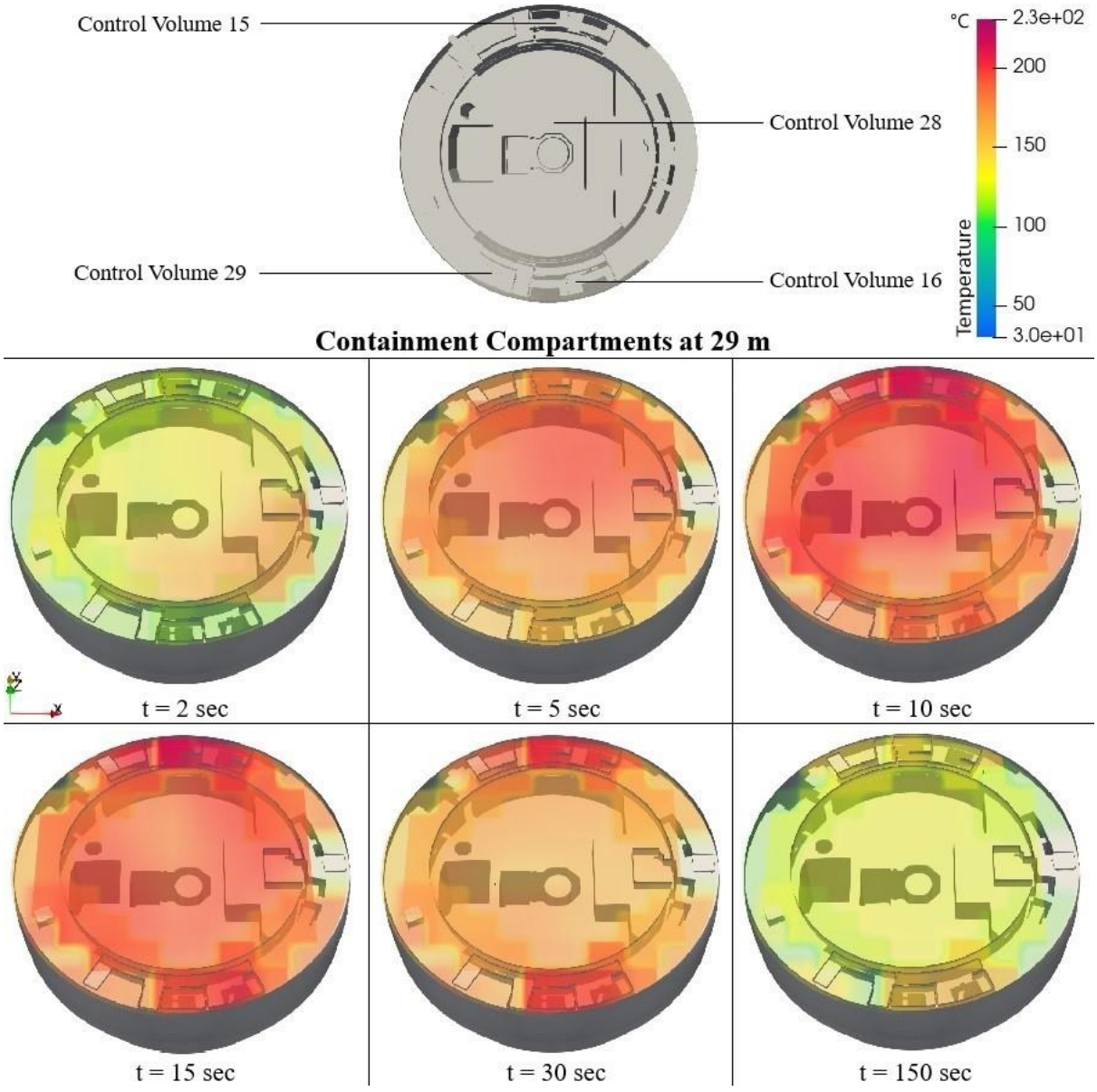

Figure 5-12. 3D temperature contours inside the containment at elevation z=29 m.

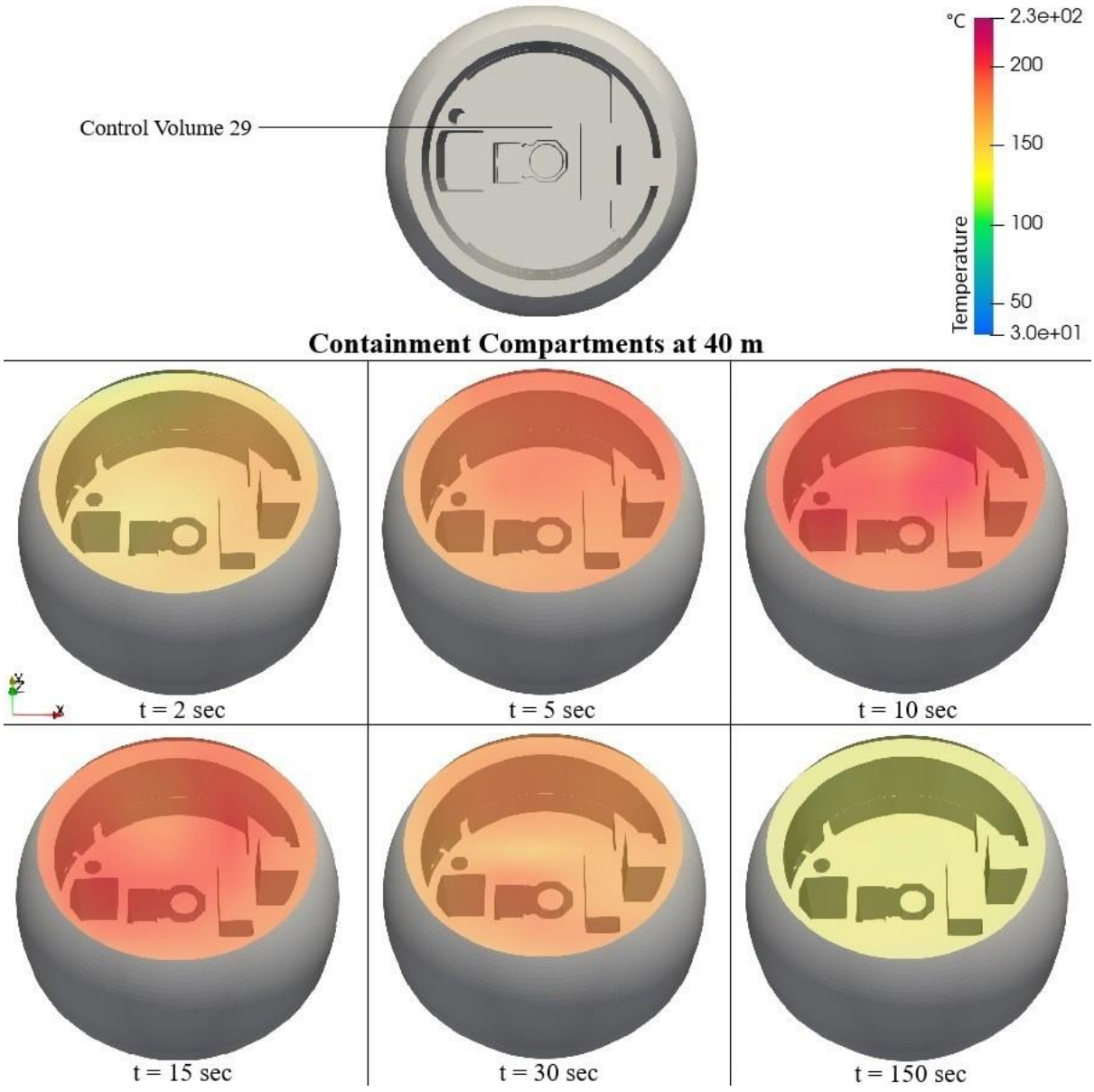

Figure 5-13. 3D temperature contours inside the containment at elevation z=40 m.

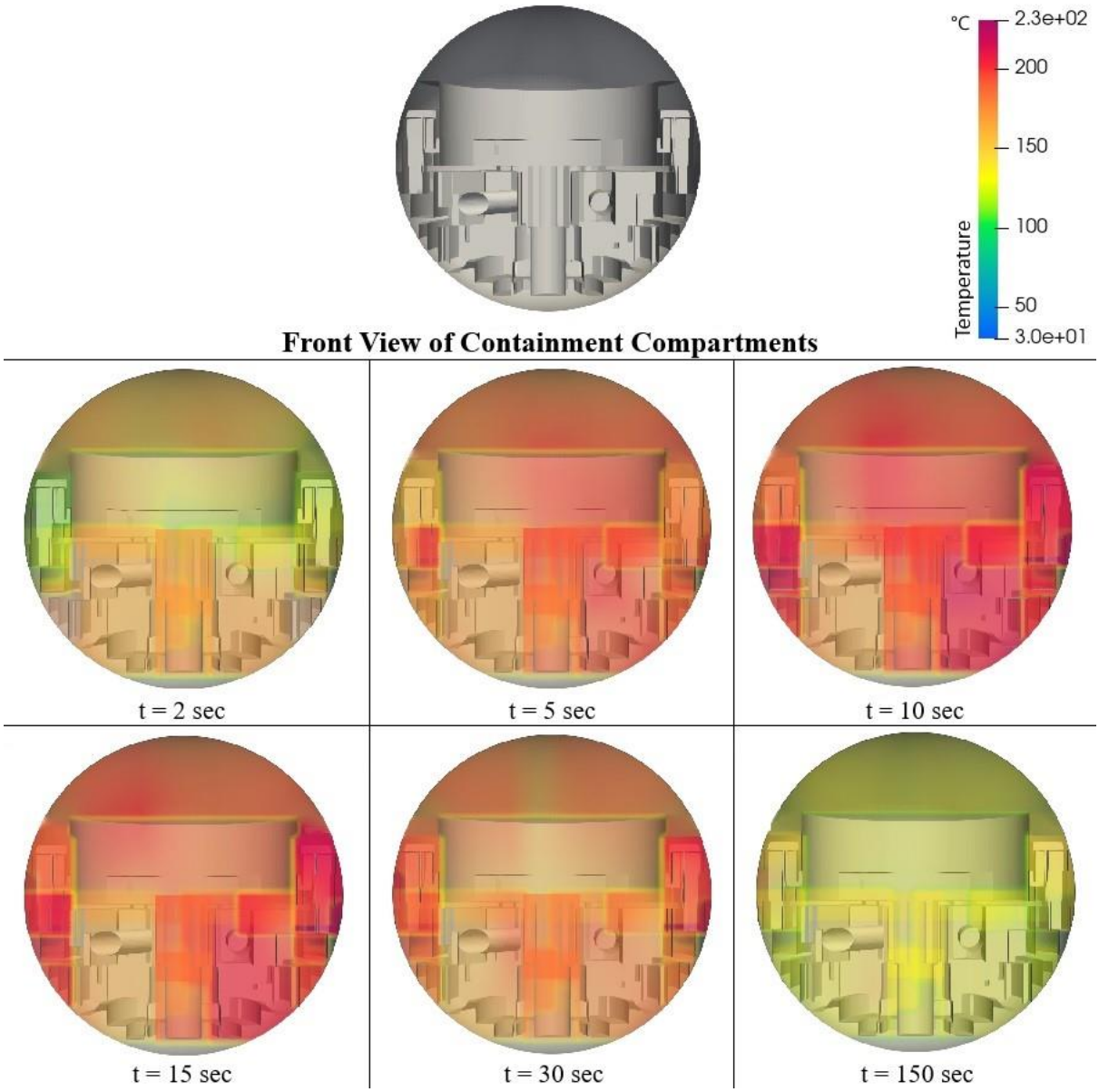

Figure 5-14. 3D temperature contours inside containment on the xz-plane cutting through the centre.

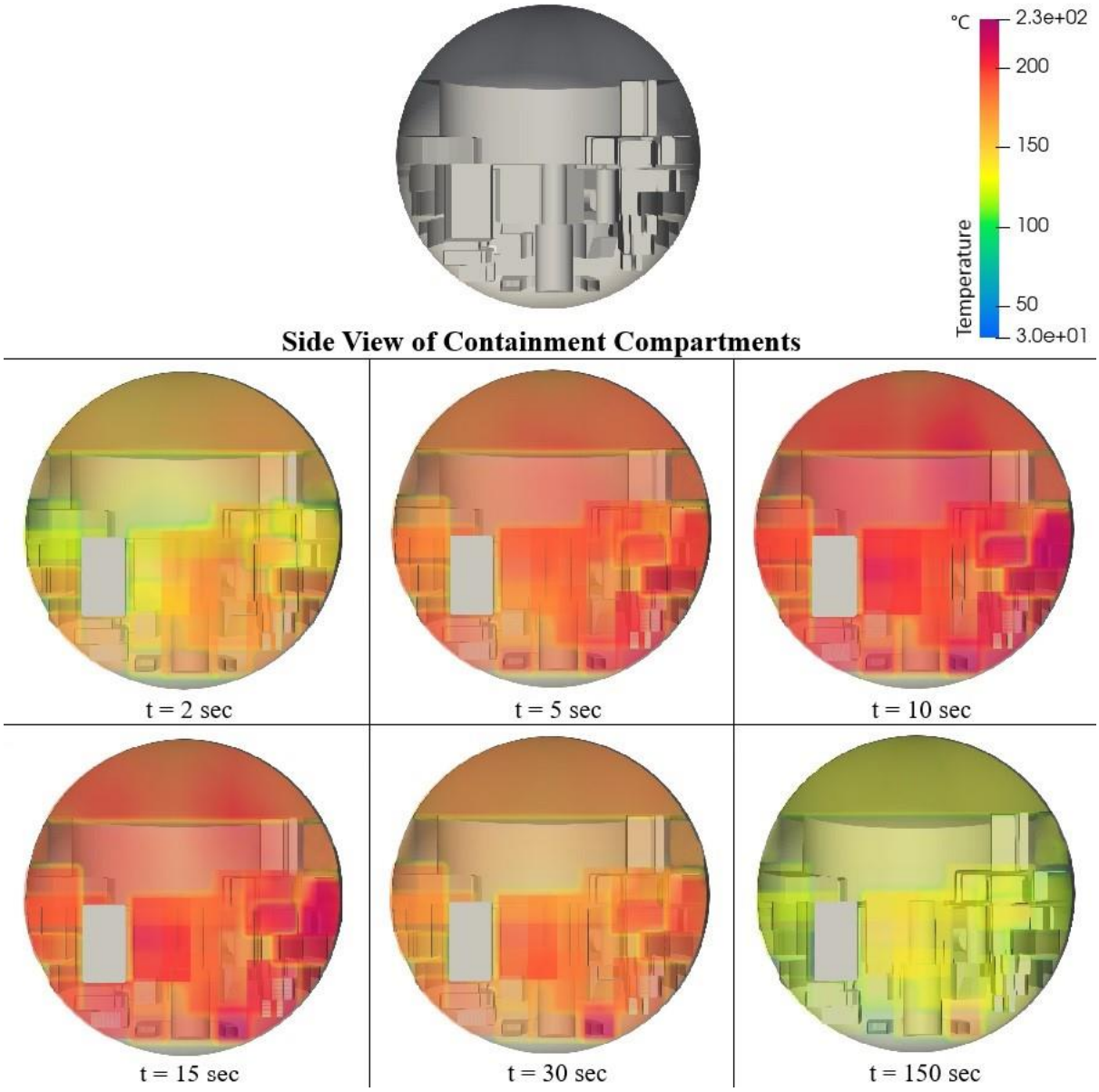

Figure 5-15. 3D temperature contours inside containment on the yz-plane cutting through the centre.

Demonstrating the water and steam flow path and velocity vectors through containment structure can clarify the pressurization procedure of different containment control volumes. Figure 5-16 and Figure 5-17 show the velocity vector resulting from the blowdown source and their flow directions at xz and yz plane respectively through the containment centre at the initial seconds of the accident (t=2 second). As it can be found in these pictures and could be expected, the highest velocity and flows of water and steam can be seen at the break source (CV 2) and its surrounding control volumes (large red arrows). The further we get far from the break source location, the size of the velocity vectors decreases due to smaller water and steam momentum and flows (smaller blue arrows). The high density of small blue vectors

under the containment dome in comparison to other coordinates can justify the higher temperature and pressure profiles for control volumes 28 and 29.

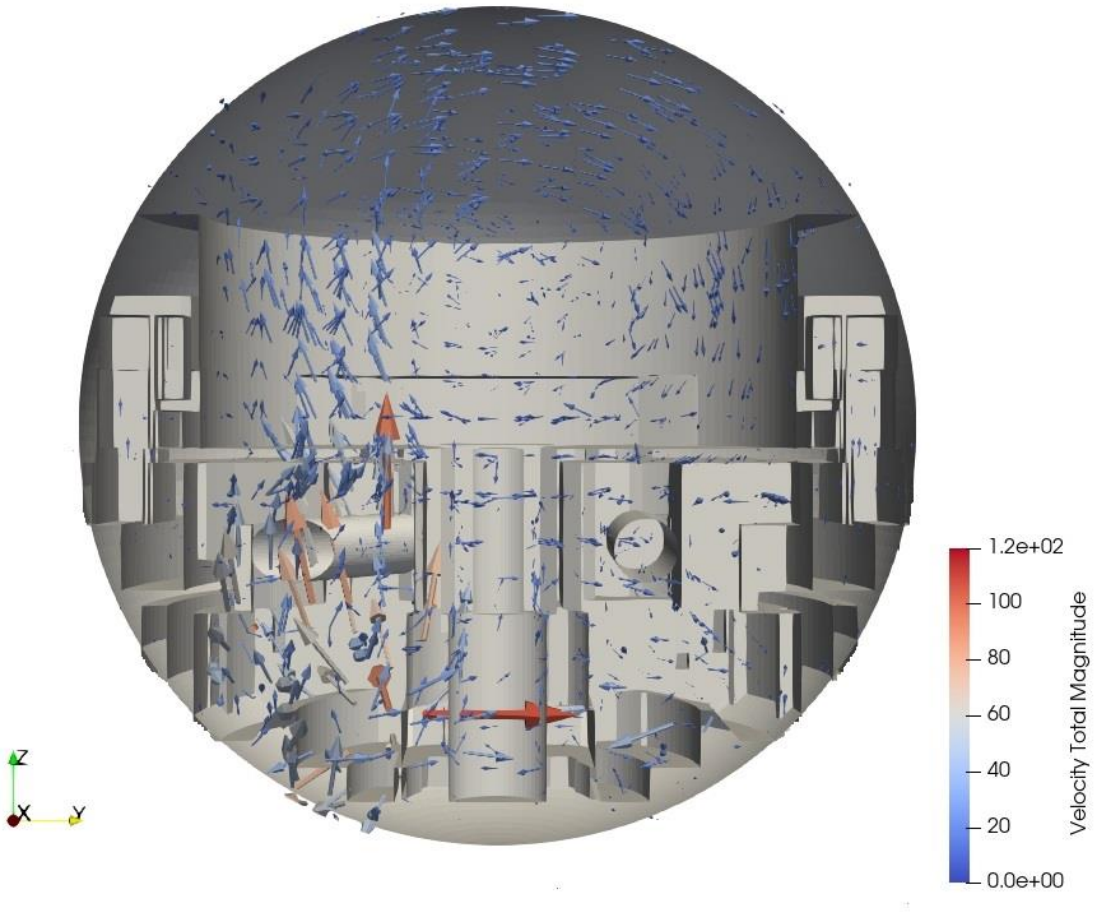

Figure 5-16. Velocity vectors inside containment on the xz plan, front view (t=2 second).

Since GOTHIC LP and 3D mode and ANGAR (FSAR results) use their dedicated methods, correlation, algorithms, etc. discrepancies in the simulation results were expected within a reasonable limit. LP codes assume when fluid enters a control volume it is immediately mixed and interacts with all thermal structures instantaneously. Moreover, 3D flow patterns are not considered in LP codes (Fernández-Cosials et al., 2017a). Even between two LP codes, the difference in code structures might cause discrepancies in the results.

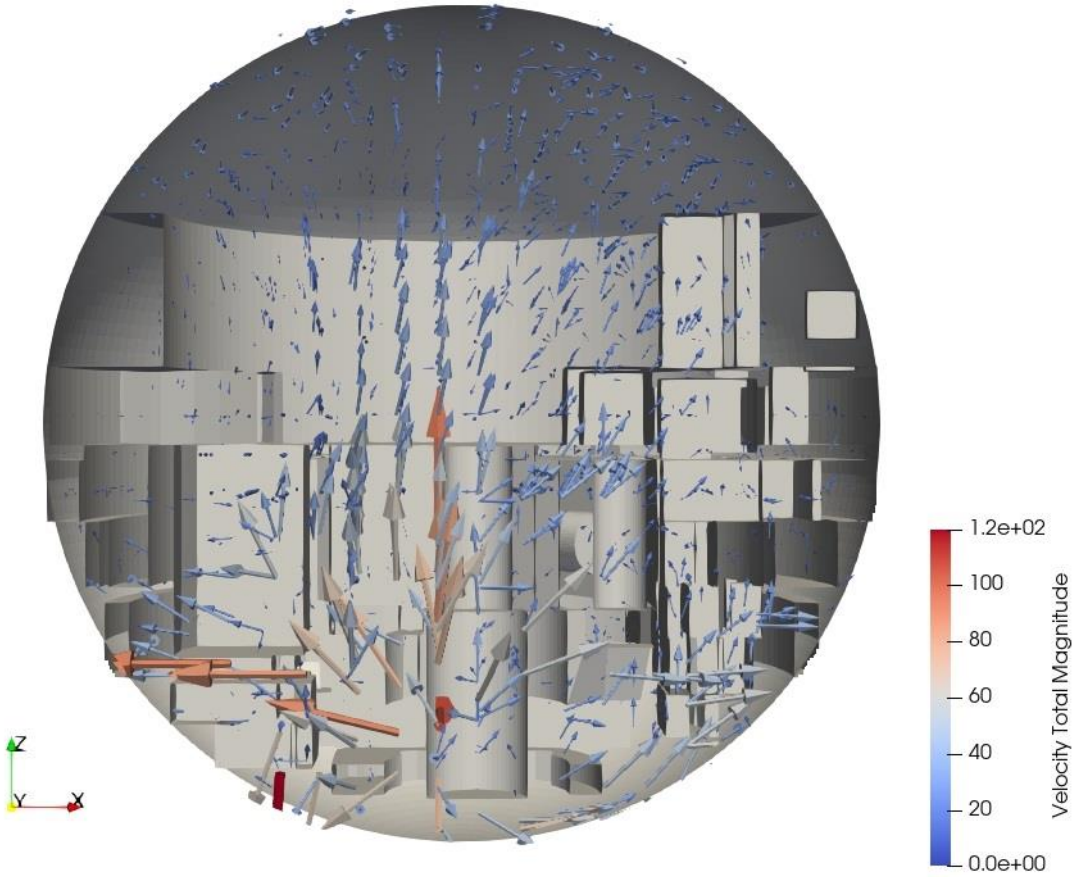

Figure 5-17. Velocity vectors inside containment on the yz plan, front side (t=2 second).

5.3 VVER-1000/V446 Containment Long-term Response to the LB-LOCA

The long-term thermal-hydraulic response of the containment is demonstrated in Figure 5-18 to Figure 5-23. The comparison is between FSAR LP results and two GOTHIC 3D model results (averaged over the volume), one is with the spray system modelled and the other is without the spray system modelled to show the effectiveness of the CSS. The compartments selected for the temperature analysis, control volumes 8, 9, 23, 25 and 28, are from different regions within the containment to demonstrate the overall thermal behaviour of the containment. The pressure data are volume-averaged over all the containment. The data set starts at 20 seconds, at around the peak temperature and pressure response of the containment and spans a long period of time up until 85000 seconds, the time that FSAR provides the latest value for its profile. The general trend of the three curves show a similar gradual decrease over time for both temperature and pressure profiles. The maximum average pressure value for the containment is 392 kPa in FSAR whereas it is 431 in GOTHIC 3D with

the CSS. The small gap between average pressure values of GOTHIC 3D with CSS and FSAR disappears over the period until 1000 seconds. After 1000 seconds, the pressure values are almost the same for the rest of the transient. The effectiveness of the CSS could not be observed clearly in the initial seconds following the LOCA. However, the peak average pressure is equal to 440 kPa at 20 seconds when the spray system is not present which is very near the design limits of the containment at 460 kPa. Therefore, the 9 kPa peak pressure difference between the models might be crucial in consideration of the containment safety during a LOCA. The pressure difference between the two GOTHIC simulations gets larger with time, reaches to a 15.9% reduction in pressure with the effect of the CSS at 1000 seconds. The pressure results of the two simulations become nearly the same when the containment cools down to a stable period from 20000 seconds onwards. The duration to reach half of the containment peak pressure is 2475 seconds in the FSAR simulation, whereas the same duration is 1380 and 2410 seconds for the GOTHIC simulations with or without the CSS model, respectively. The containment depressurization rate of the GOTHIC model with CSS is almost two times faster in comparison to the same model without the CSS actuation. This issue can demonstrate the effectiveness of the CSS on the cooling of the containment. On the other hand, the difference in containment depressurization rate between the GOTHIC simulation with CSS and the FSAR simulation might be explained by the difference in code structures, different heat transfer models within the codes and the fundamental differences between LP and CFD codes such as the characteristic length definition that could affect heat transfer phenomena within the containment. Characteristic length in LP models is the distance between control volumes which is much larger as opposed to the distance between cells in a 3D mesh system of a CFD code.

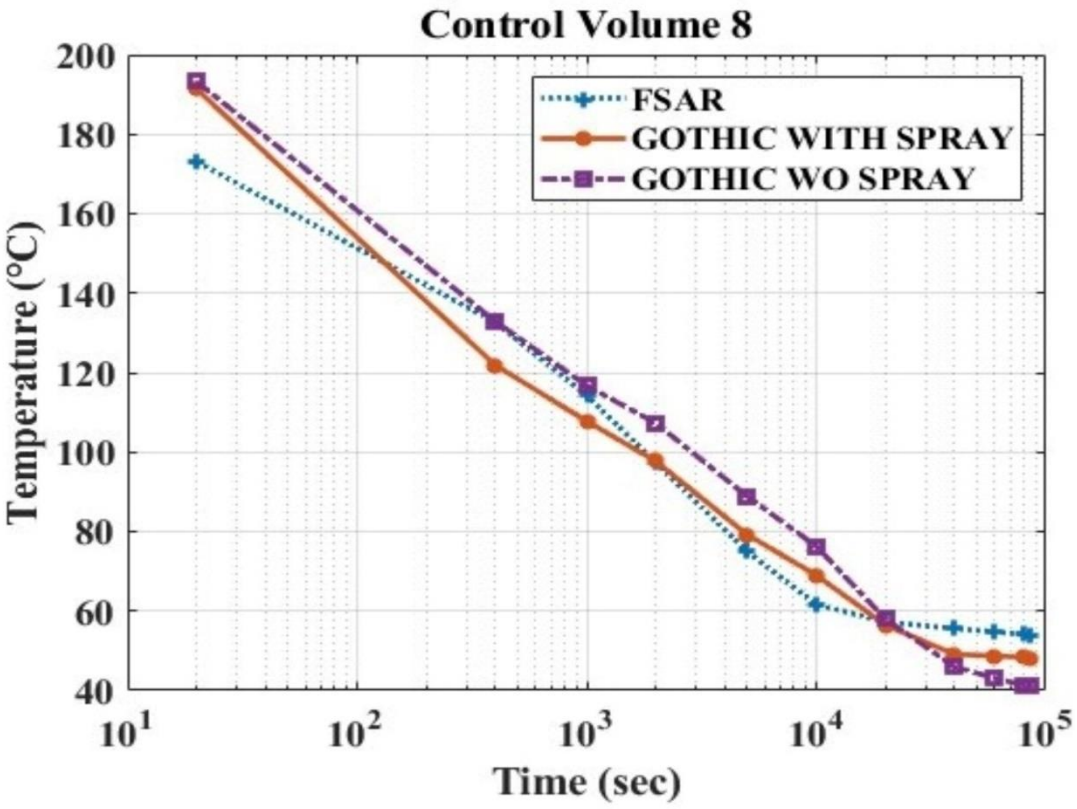

Figure 5-18. The long-term temperature profile of control volume 8.

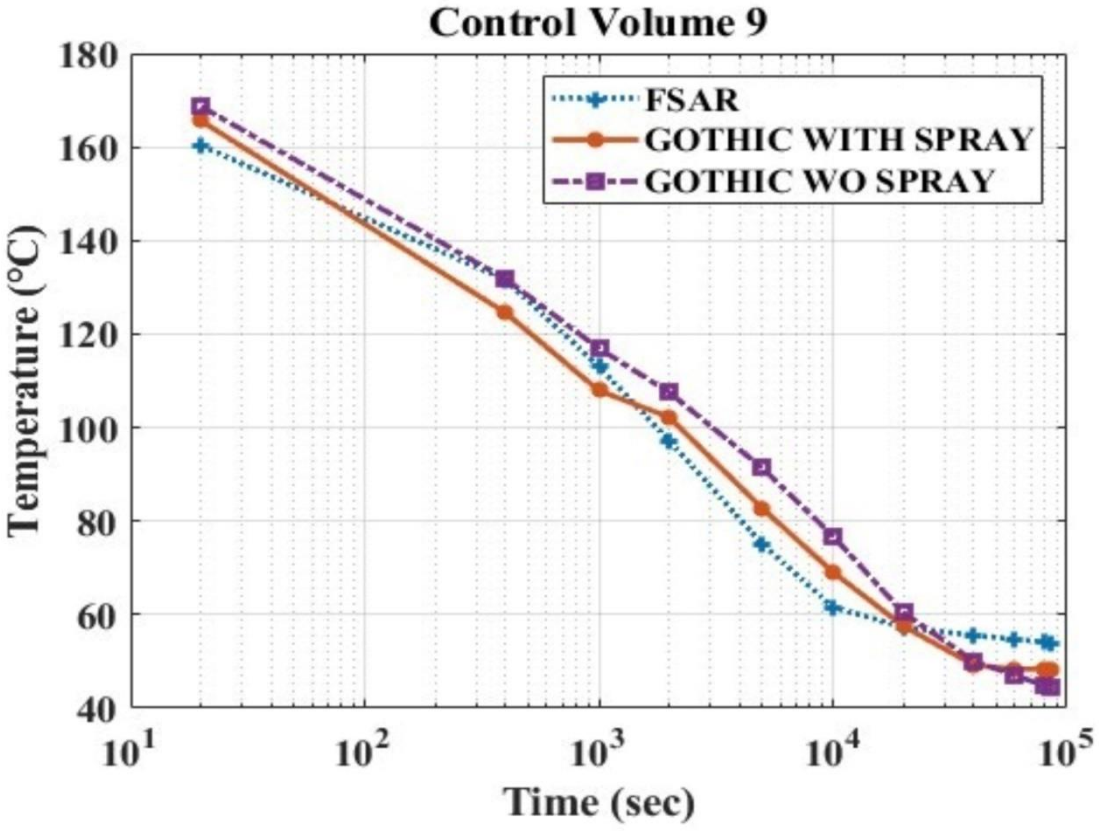

Figure 5-19. The long-term temperature profile of control volume 9.

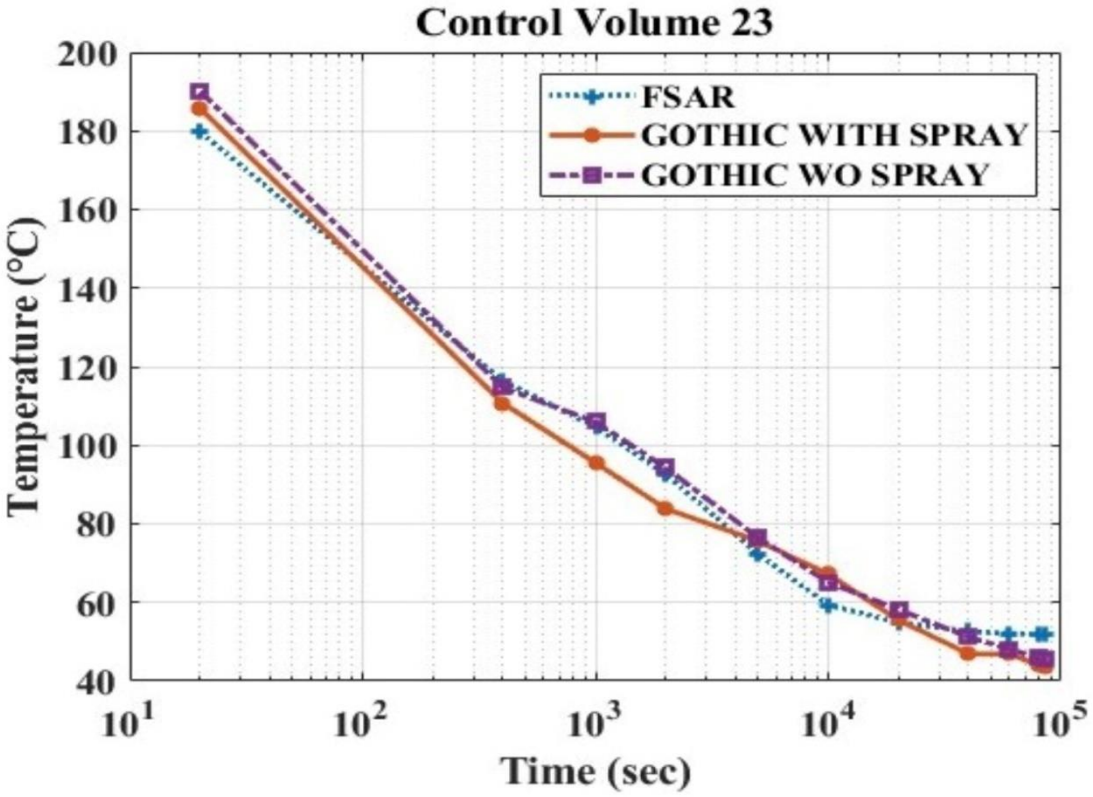

Figure 5-20. The long-term temperature profile of control volume 23.

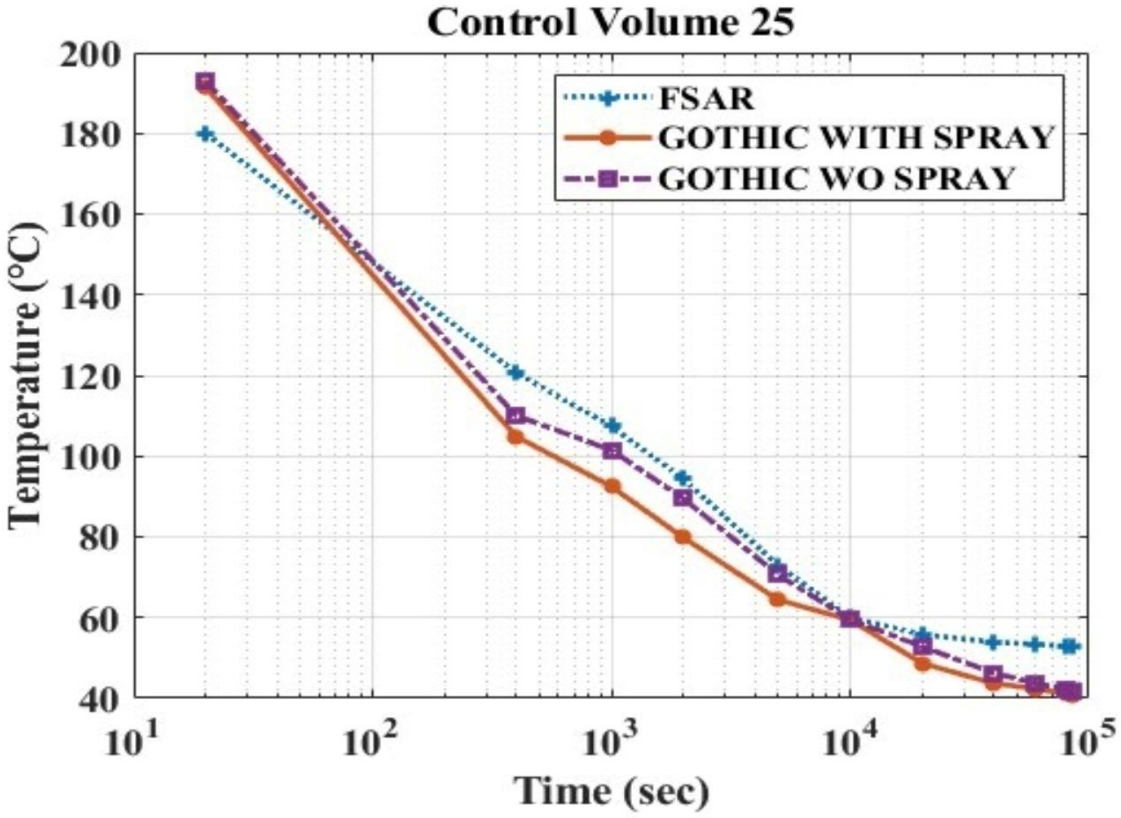

Figure 5-21. The long-term temperature profile of control volume 25.

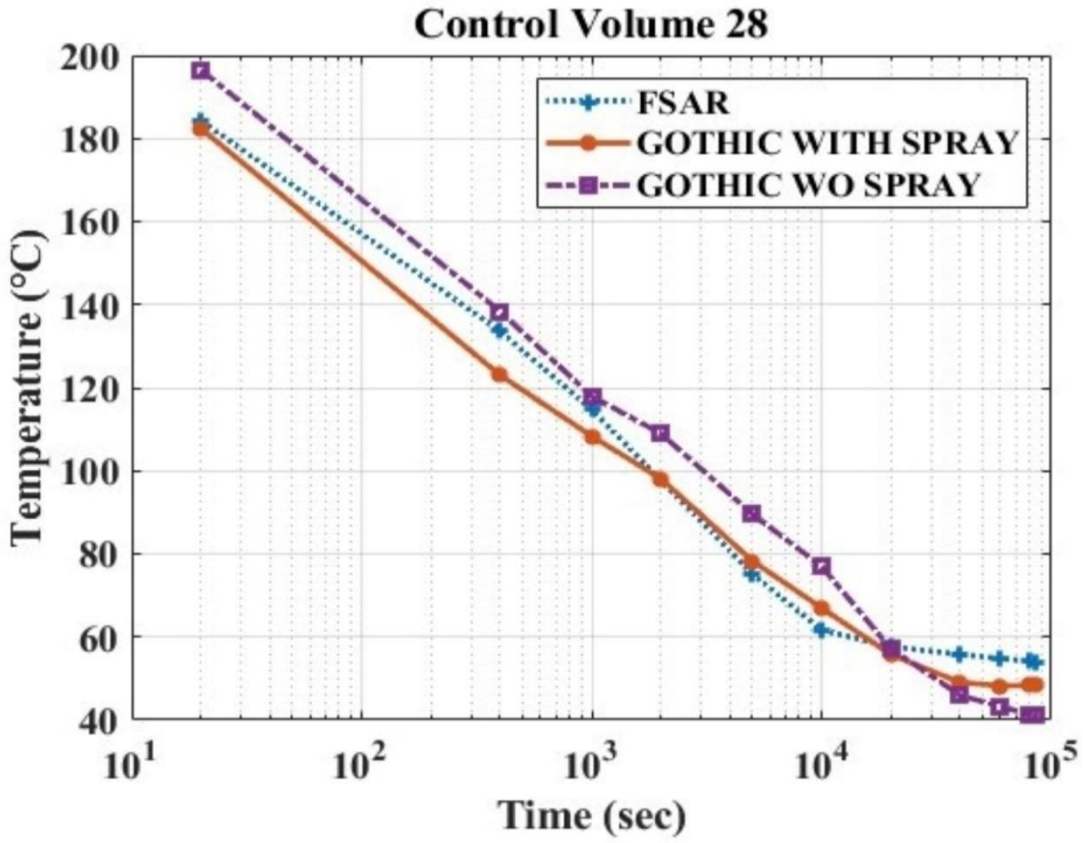

Figure 5-22. The long-term temperature profile of control volume 28.

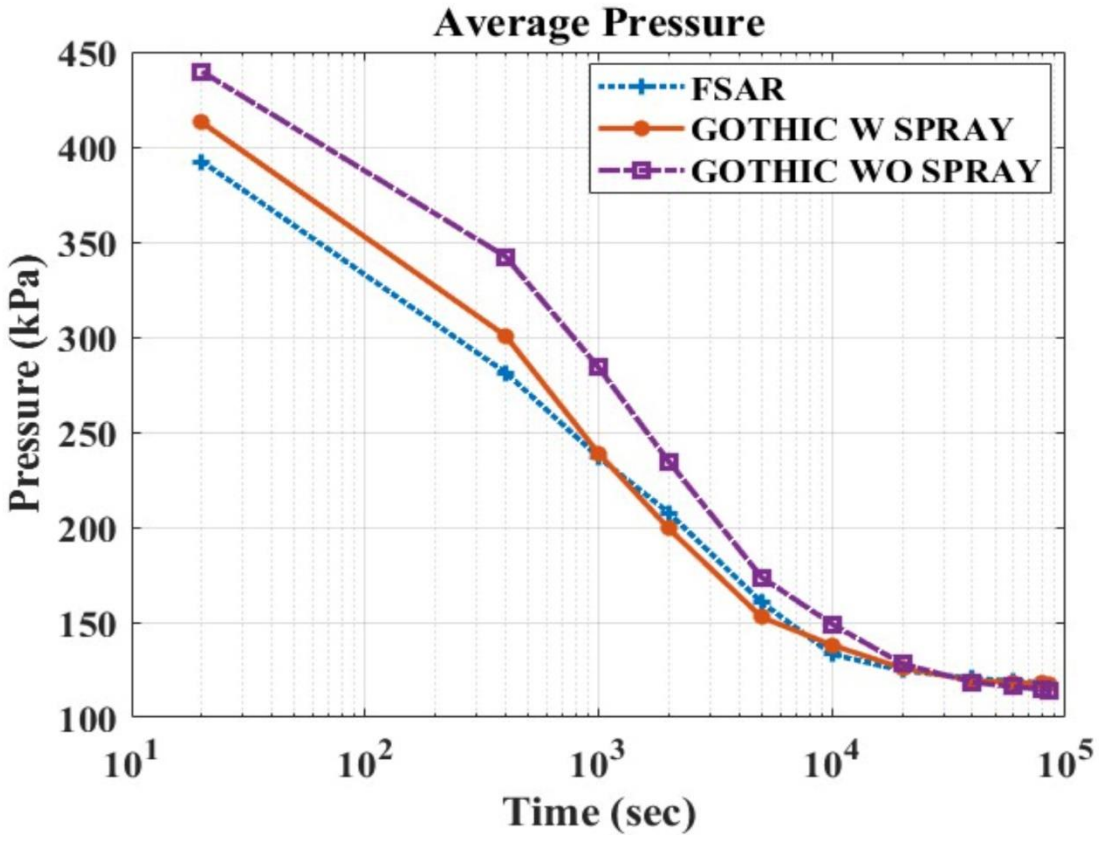

Figure 5-23. The average pressure profile of the containment.

As it can be seen, the GOTHIC simulation results with CSS are in agreement with the FSAR simulation results through the transient. The heat transfer between the containment and the environment and the cooling effect of the thermal conductors and the spray system lead to a gradual decrease in the temperature of all the control volumes. More effect of the CSS on the depressurization could be observed on the central control volumes (8, 9 and 28) in comparison to control volumes (23 and 25) where located on the periphery of the steel containment since the spray headers inject more droplets to the central regions of the containment. Especially, the difference in temperature between the two GOTHIC simulations is more prominent in control volume No. 28 (the lower part of the region between the dome and the upper desk) which is closer to the spray headers located below control volume No. 29. Some trends can be observed after 40000 seconds that GOTHIC results without the CSS reaching lower temperatures in comparison to GOTHIC results with CSS in the selected control volumes (exclude control volumes on the periphery of the containment). The main reason for this behaviour is that the spray temperature at 55 °C starts to heat the containment atmosphere since the temperature of the medium is lower than the droplets (reverse heat transfer from spray droplets to containment atmosphere). This explains the equilibrium temperature that GOTHIC with CSS simulation could reach around 55 °C while the temperature profile of the simulation without the CSS continues to decline at the final stages. Figure 5-24 demonstrates the same phenomenon by showing three simulation results with different spray temperatures and FSAR result for control volume 28. The spray temperature dictates the temperature within the control volume from 40000 seconds onwards, maintaining an equilibrium around spray droplets temperature. Heat transfer of containment to the environment in addition to the lower spray effectiveness, make the temperature behaviour of the peripheral control volumes dissimilar for the final stages of the simulation. Figure 5-25 shows the effect of the spray temperature on the depressurization of the containment. The gradual decrease in pressure profiles as the spray temperature drops could be seen in this figure. It also validates the assumption of the spray temperature as 55 °C by showing the correspondence of its results with FSAR. Moreover, the effect of spray droplet diameter on the depressurization of the containment is also investigated in Figure 5-26 and Figure 5-27. The difference in the thermal-hydraulic response of the containment between various spray droplet diameter cases is prominent only at 20 seconds when the peak temperature and pressure conditions emerged within the containment. Droplet-to-steam phase conversion within the system could be observed mainly in the first 40 seconds due to the higher temperature difference between the droplet and the medium. Smaller droplet diameter

means more heat transfer surface for the same mass ejected into the system resulting in lower temperature and pressure within the containment. The rest of the transient after the initial period shows almost the same trend regardless of the spray droplet diameters.

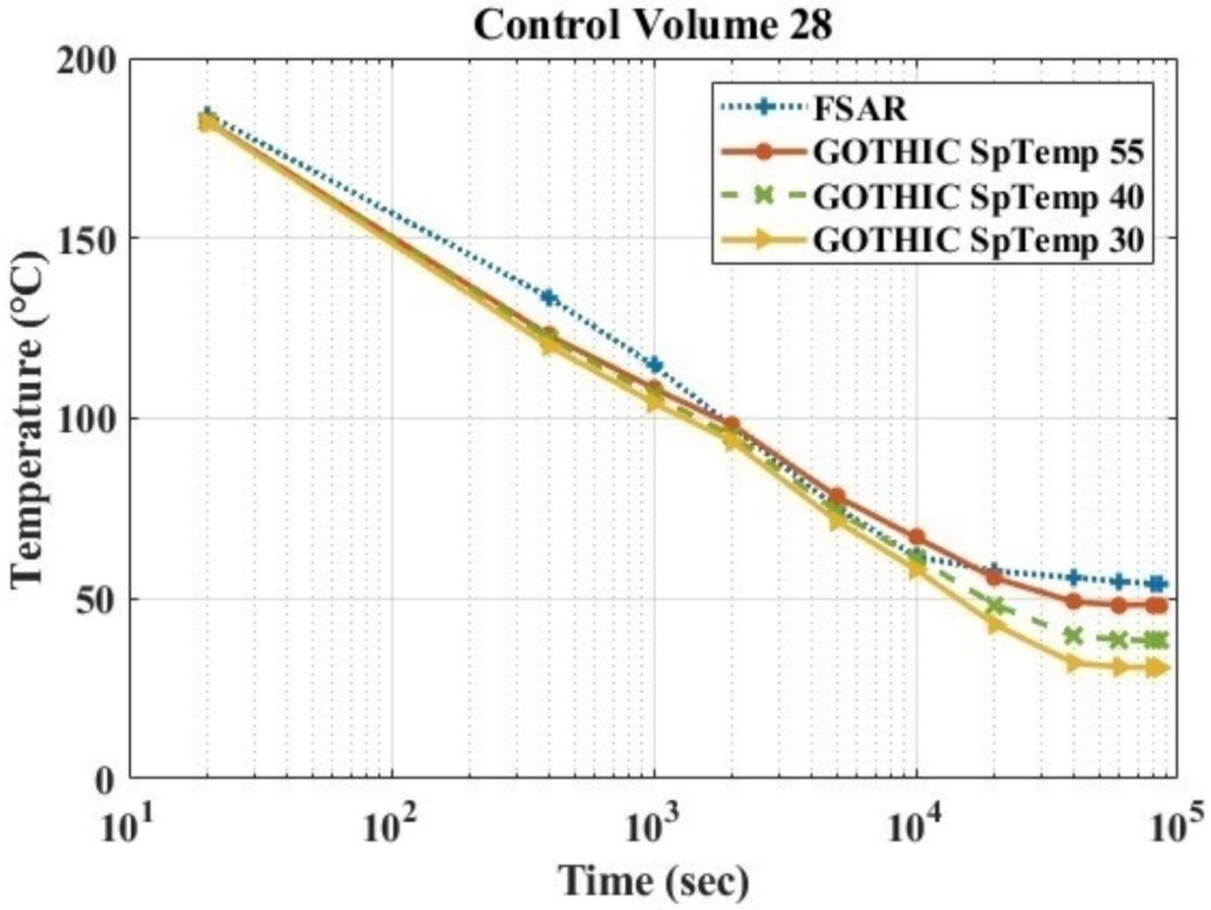

Figure 5-24. Sensitivity analysis of spray droplet temperature on the containment depressurization in control volume 28.

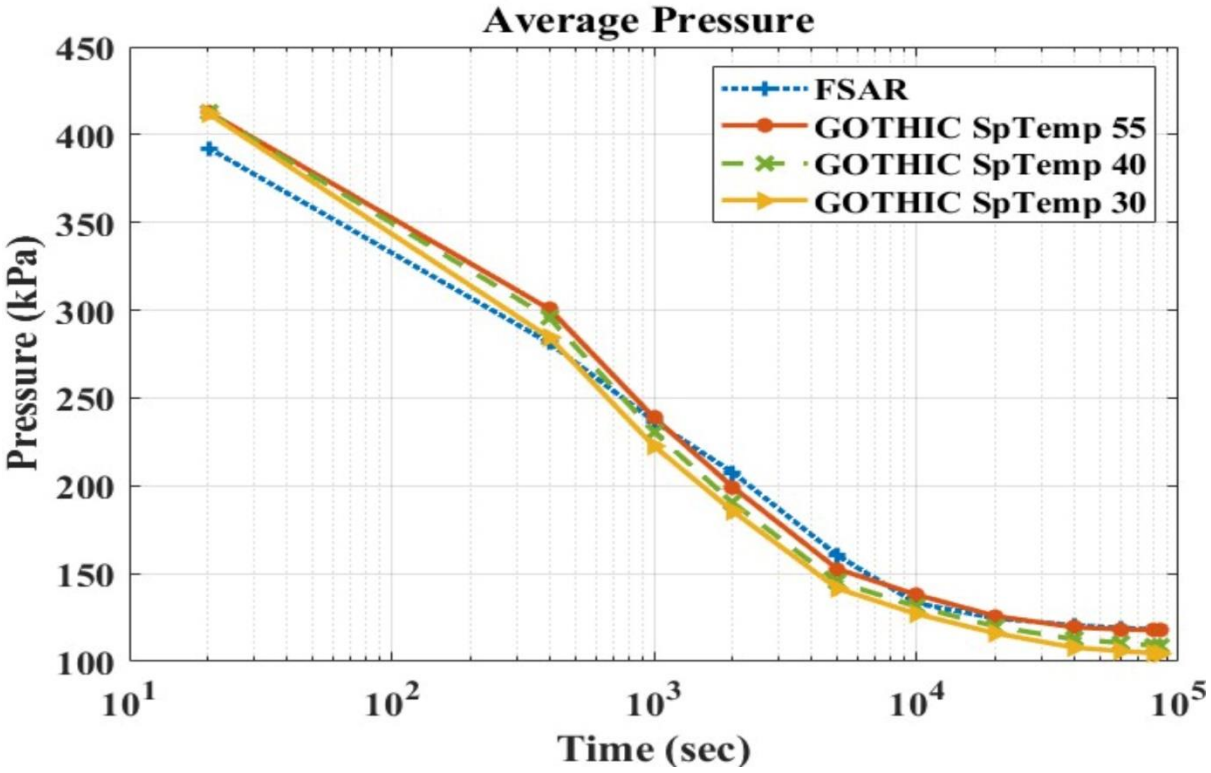

Figure 5-25. Sensitivity analysis of spray droplet temperature on the containment depressurization over the whole containment.

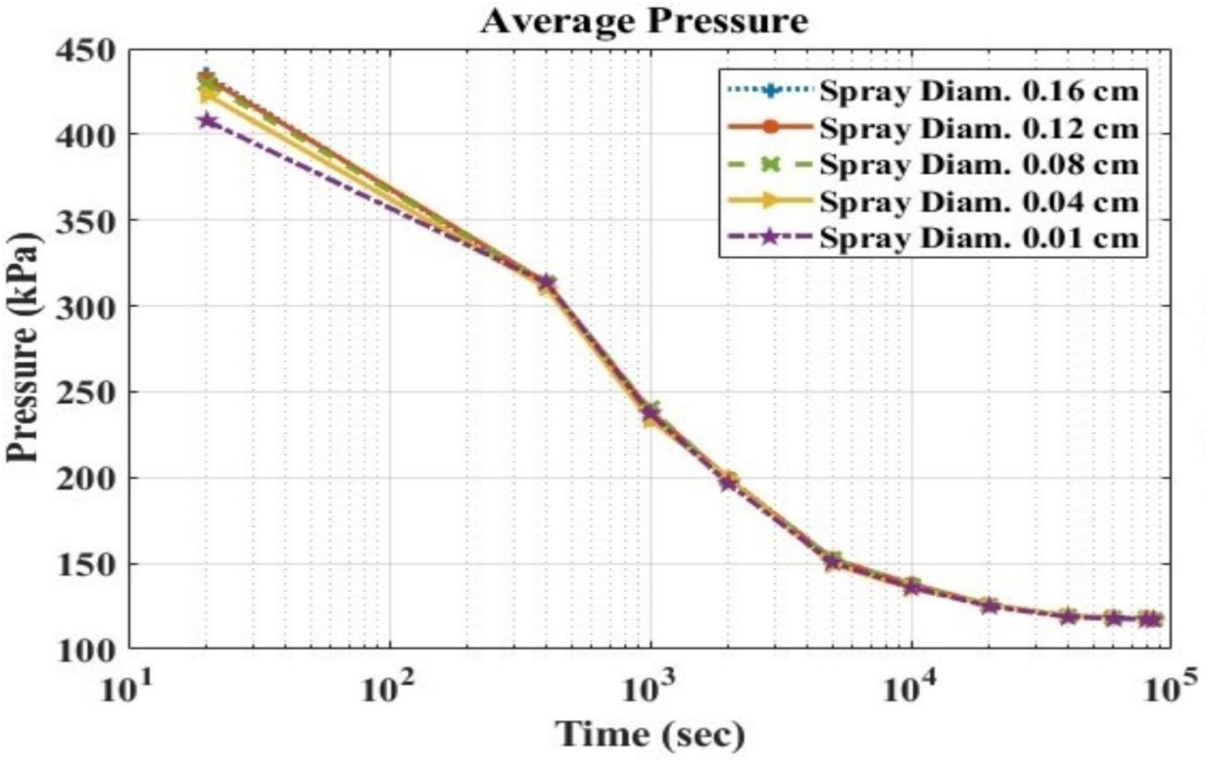

Figure 5-26. Sensitivity analysis of spray droplet diameter on the containment depressurization over the whole containment.

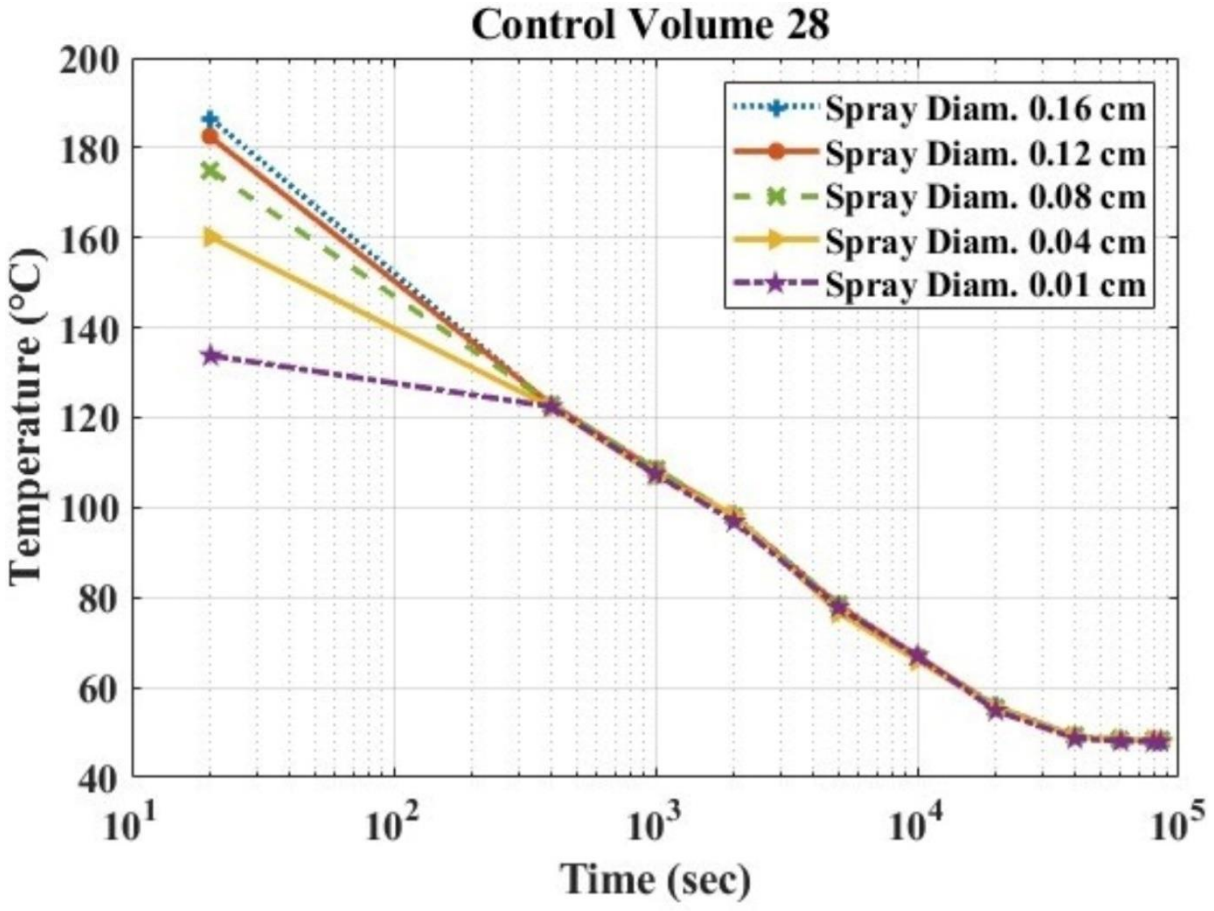

Figure 5-27. Sensitivity analysis of spray droplet diameter on the containment depressurization in control volume 28.

Since following a blowdown, the pressure wave disperses through the containment at sonic speed, its distribution is almost homogenous over the containment. However, temperature distribution over the containment is slower and heterogenous due to the convective-diffusive nature of its transmittance (Jimenez et al., 2017). This leads to local temperature differences and hotspots inside the containment. To investigate the heterogeneity of the temperature inside the containment, 3D contour maps are prepared in ParaView post-processing data visualization program by processing GOTHIC 3D results. Temperature contours of three different elevations of the containment, 4.5 m, 14 m and 25 m, are presented in Figure 5-28, Figure 5-29 and Figure 5-30 respectively. Since the focus of this part is on the long-term behaviour of the containment, the transients depicted in the figures range from 200 seconds to 80000 seconds. Local hot spots within control volumes could be observed in these figures and can be reviewed for more safety assessments. One particular local hot spot is located at the bottom left corner of the reactor pressure vessel which is the result of the break point in

the control volume 2. Since mass and energy releases from the break sources stop are terminated around 17000 seconds, the last two transient time steps (20000 and 80000) do not show the same hot region in Figure 5-28 and Figure 5-29. Although the elevation at 25 m is quite high concerning the break source location in Figure 5-30, the mark of the LOCA source is still there at 200 seconds.

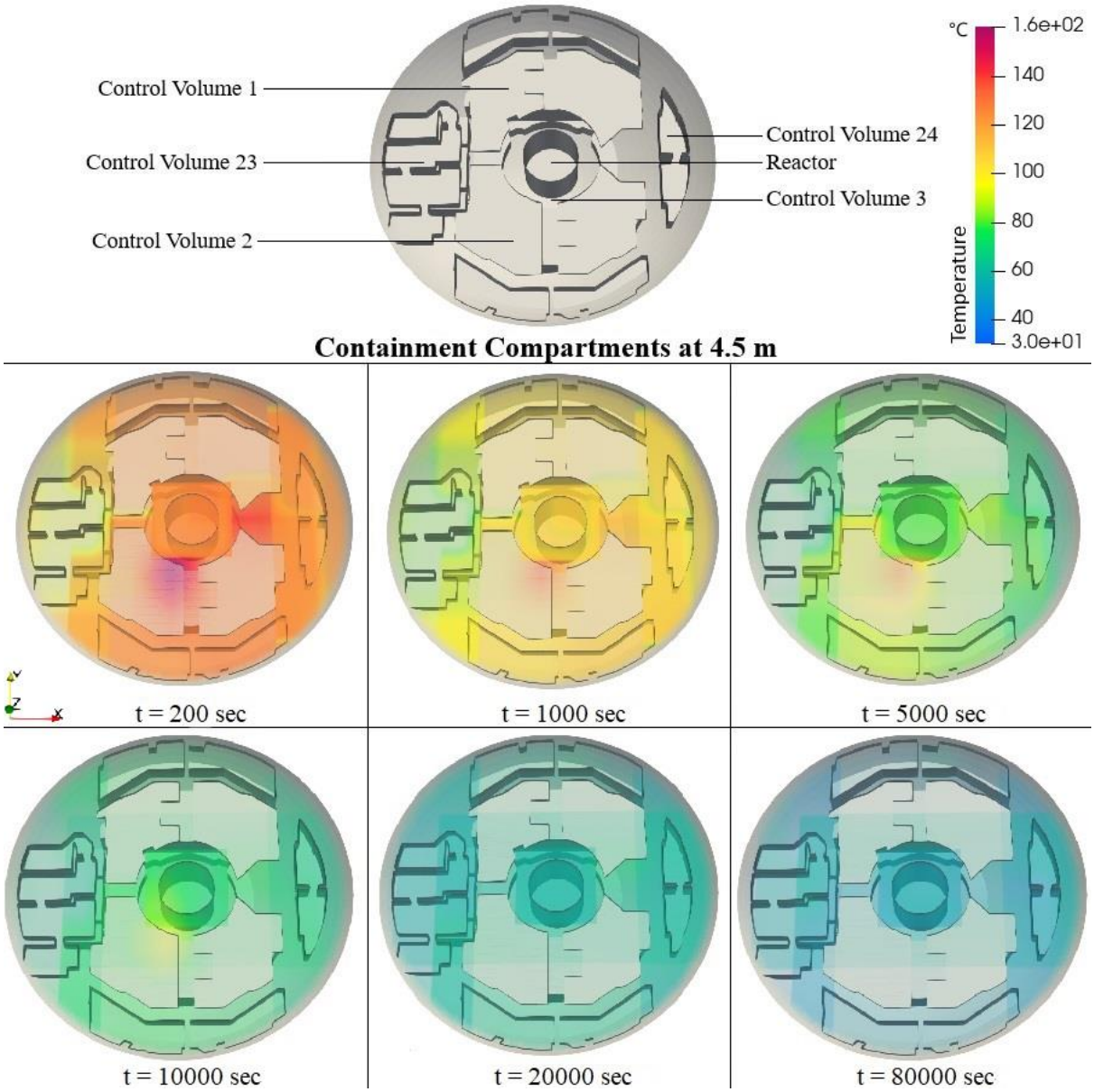

Figure 5-28. Temperature contour of the containment at 4.5 m.

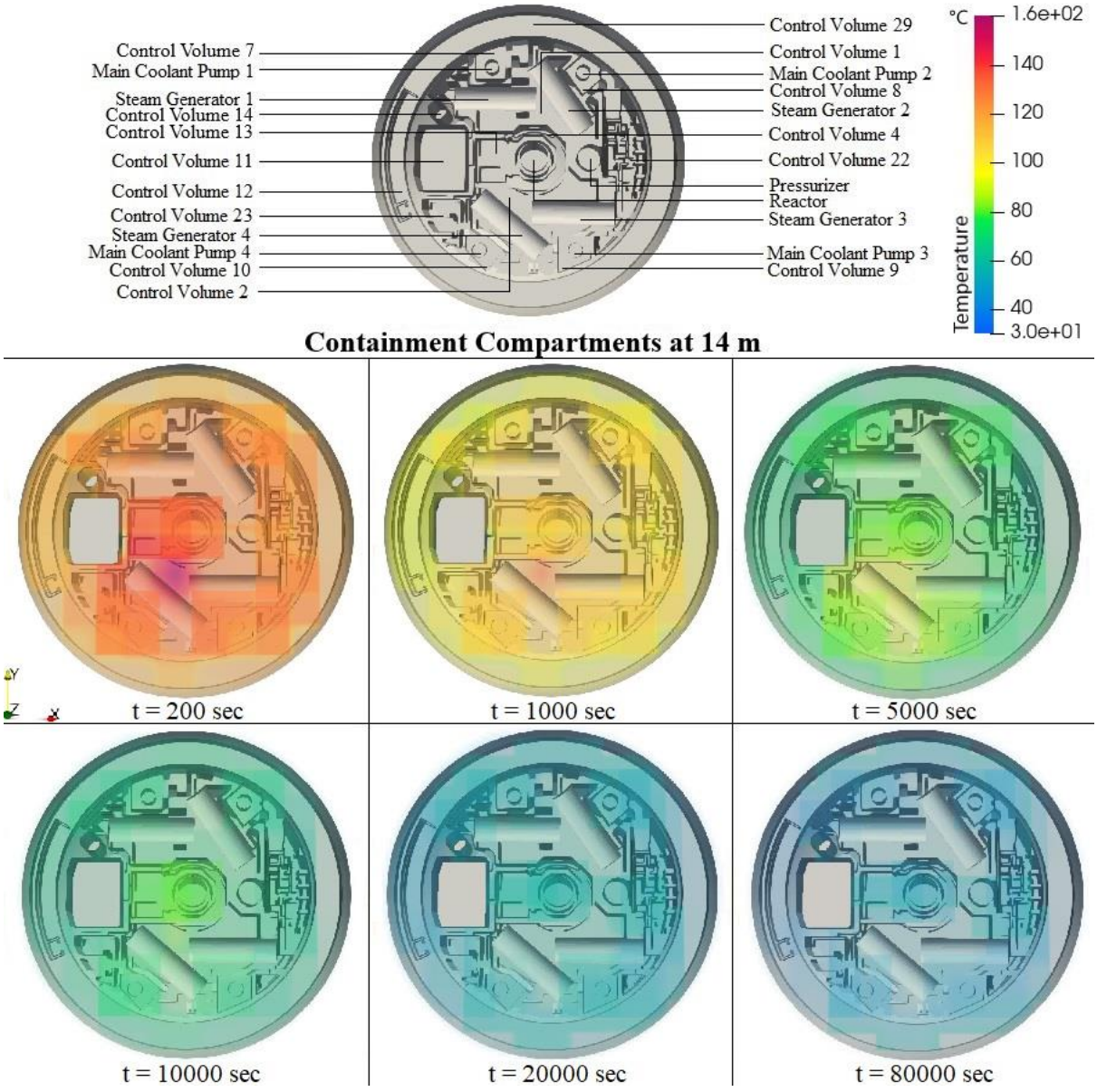

Figure 5-29. Temperature contour of the containment at 14 m.

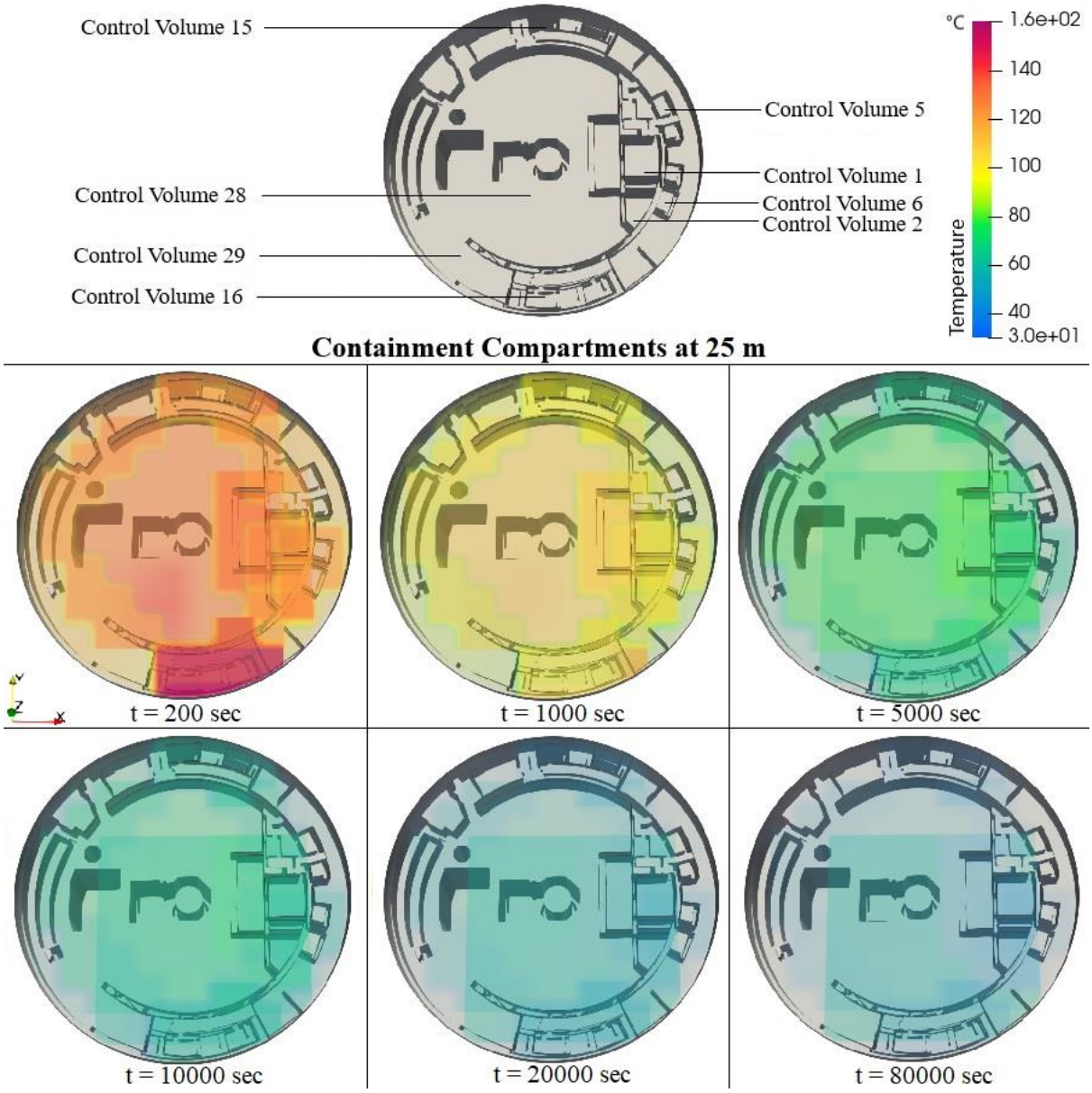

Figure 5-30. Temperature contour of the containment at 25 m.

Temperature contours on the yz and xz planes for the whole containment cross-section through the centre are shown in Figure 5-31 and Figure 5-32. The heterogeneous temperature distribution of the containment with its local hot regions could be observed and the 3D flow patterns could be visualized over time through these figures. They also show the lower effectiveness of the spray system drops as the elevation decreases, especially in the transients at 10000 and 20000 seconds, when the hot spots appear visibly at the bottom.

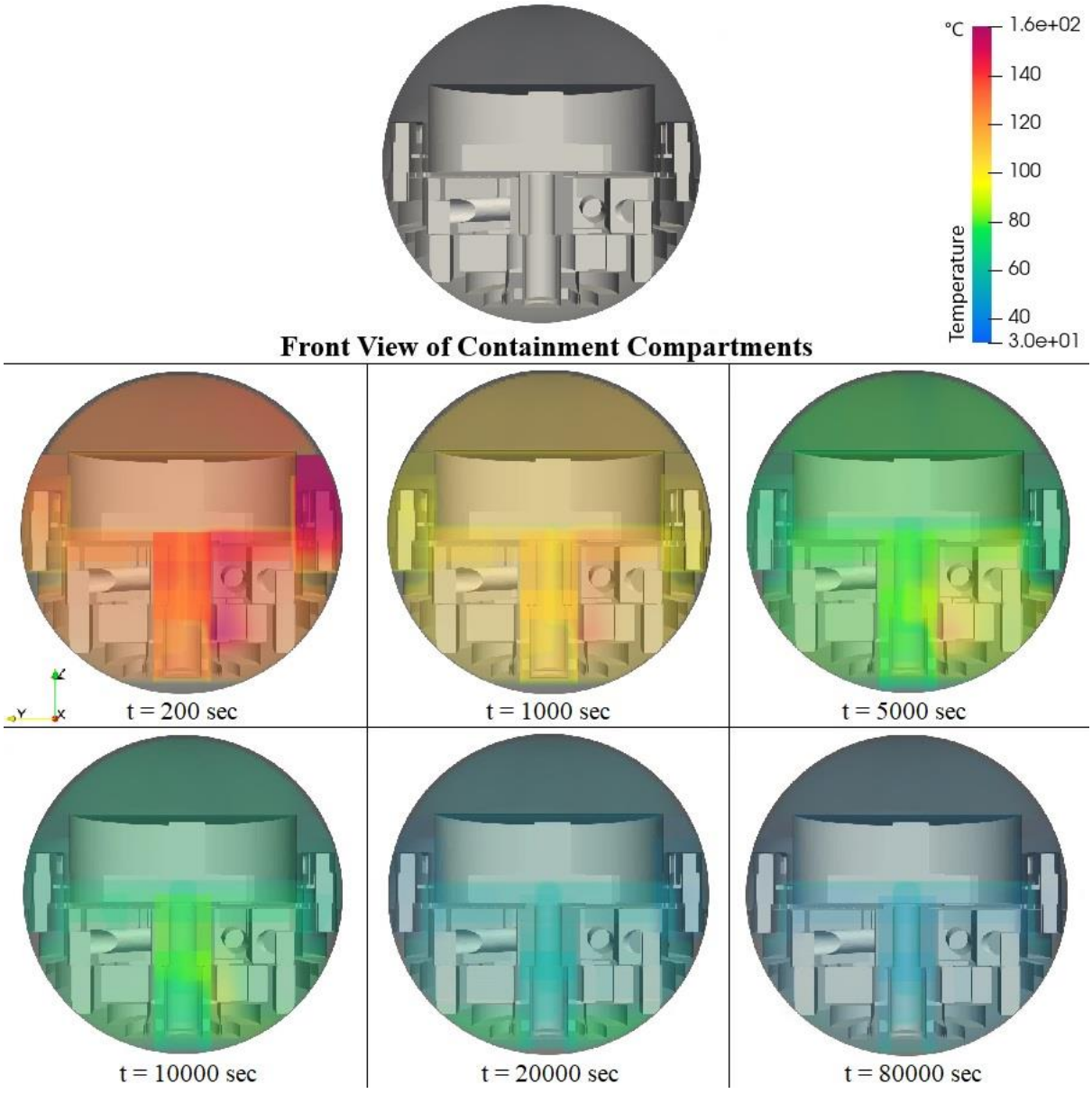

Figure 5-31. Temperature contour of the containment hemisphere: front view.

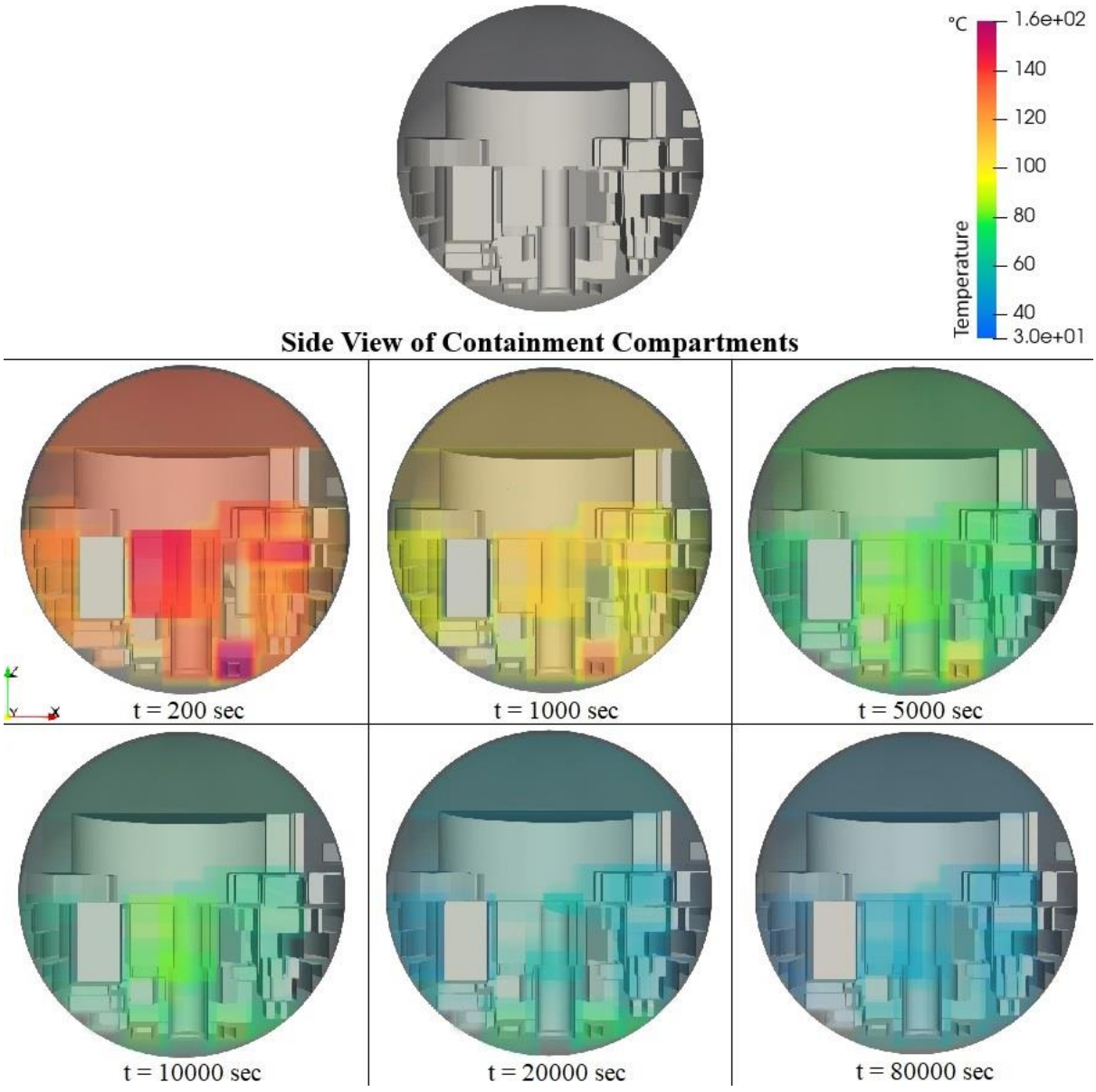

Figure 5-32. Temperature contour of the containment hemisphere: side view.

5.4 Hydrogen Distribution Inside the VVER-1000/V446 Containment during the LB-LOCA

Figure 5-33 to Figure 5-37 provide information of the change in average hydrogen concentration with time in several control volumes selected from different regions inside the containment. These figures can depict an overall picture of the hydrogen distribution during the LB-LOCA. The selected compartments are namely, control volume 8, 9, 23, 25 and 28 in these figures (nearly same in TH evaluation). The figures include four data sets of simulation outputs, namely, GOTHIC model without PAR installation, FSAR without PAR installation and GOTHIC and FSAR models with PARs installed. First, the comparison between FSAR and GOTHIC results without PARs are quite in agreement with each other. Although the trends of the two graphs are similar, the GOTHIC simulation provides slightly higher hydrogen concentration within all the selected control volumes after 5 hours. Since ANGAR code as an LP code was used in FSAR, the difference between code structures might explain this slight dissimilarity, moreover considering the break source also provides steam into the system and different approaches of the two codes on various heat transfer phenomena. The hydrogen flammability limit was assumed as 4.1% in FSAR, and it could be seen in the figures that GOTHIC results exceed this limit just passing 200 hours after the onset of the accident. The FSAR results reach this value at around 300 hours. Since the simulation ends at about 275 hours, the surpassing of the lower hydrogen flammability limit could not be seen in these figures for FSAR results. Therefore, a hydrogen removal method needs to be implemented (implemented in FSAR). 80 PARs were installed within the model, and the results of both FSAR and GOTHIC simulation with the PAR units could also be observed through these figures. The two GOTHIC simulations (with/out PARs) have nearly the same results for the first 5 hours following the LB-LOCA, since RVK-500 recombiners actuate when the volumetric hydrogen concentration reaches 0.45%. The recombiners continue to reduce the amount of hydrogen by converting it to steam until the volumetric hydrogen concentration at the inlet of the PAR drops to 0.45%. At this stage, the hydrogen concentration within the containment reaches an equilibrium at this value. It should be noted that the lower hydrogen flammability limit after PAR installation is set to 2% for the first 24 hours and during the post-accident period, it is set as 0.5% conservatively by taking into account non-uniform mixing that might emerge inside any control volume due to the

limitations of LP codes, in FSAR. The average hydrogen concentration in all the control volumes is lower than 1.5% through all the periods during the accident with the activity of installed PARs. Moreover, after 50 hours passed following the LB-LOCA, the GOTHIC model with PARs reaches a stable state at 0.45% in the post-accident period. Figure 5-38 demonstrates the evolution of average volumetric hydrogen concentration inside the containment atmosphere during the accident. It demonstrates the same trend discussed above regarding individual control volumes.

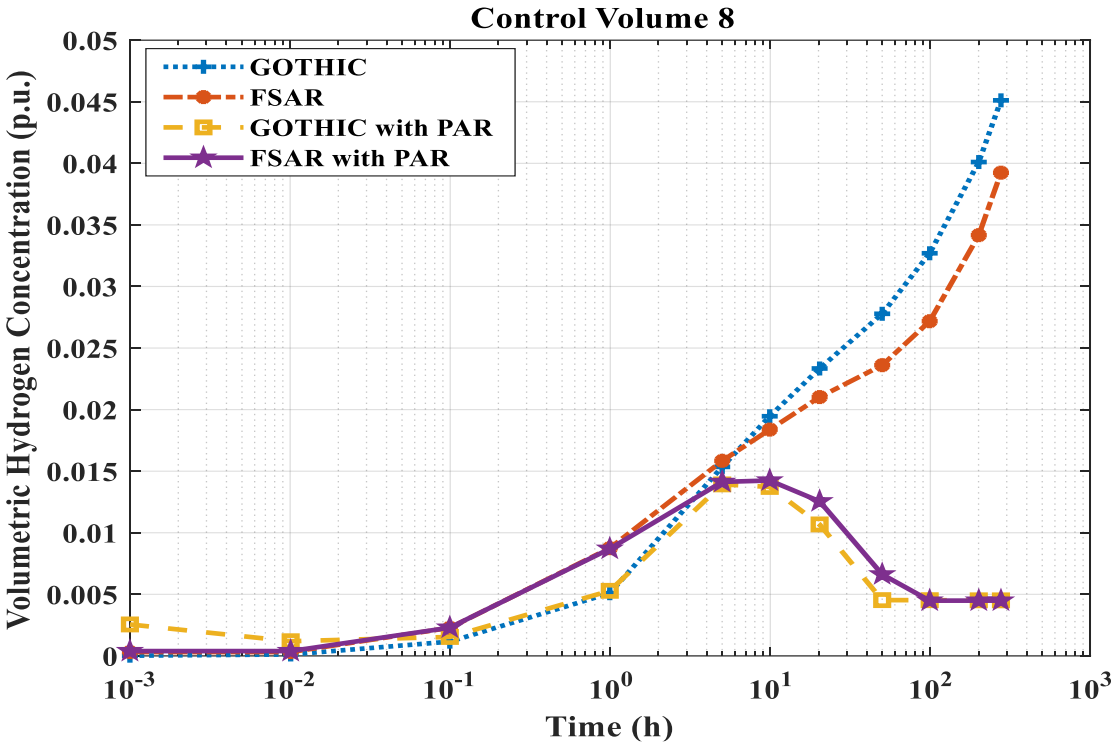

Figure 5-33. The volumetric hydrogen concentration with respect to time within the control volume 8.

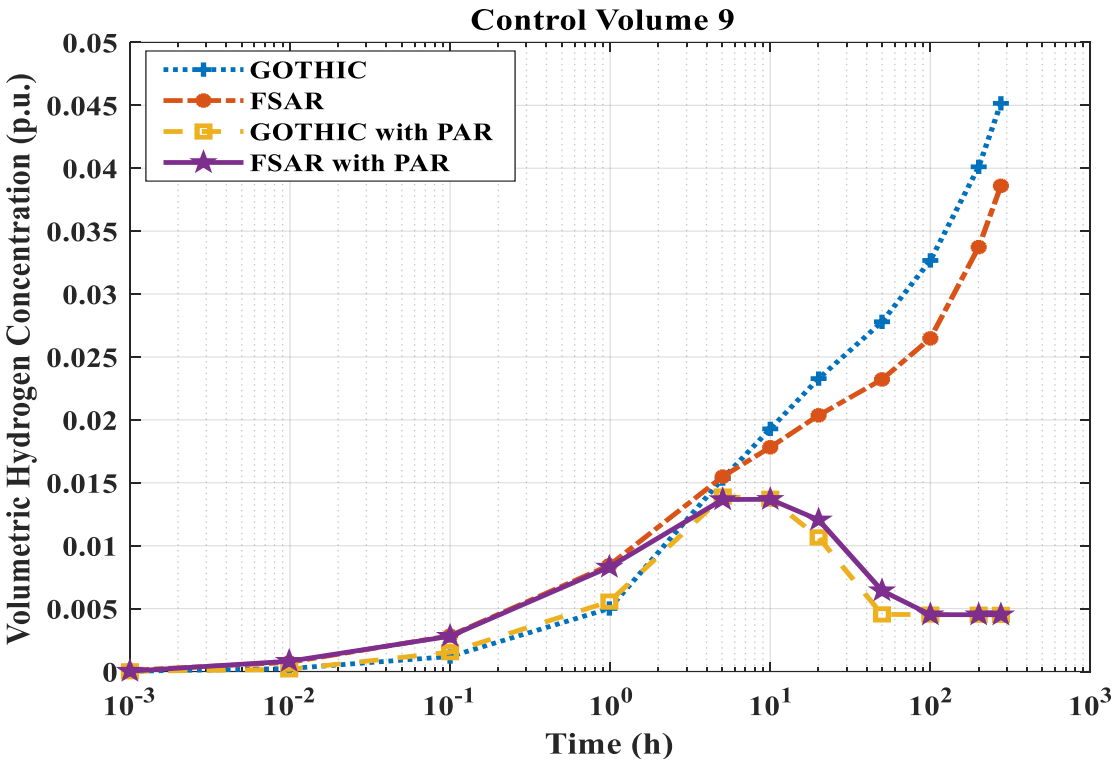

Figure 5-34. The volumetric hydrogen concentration with respect to time within the control volume 9.

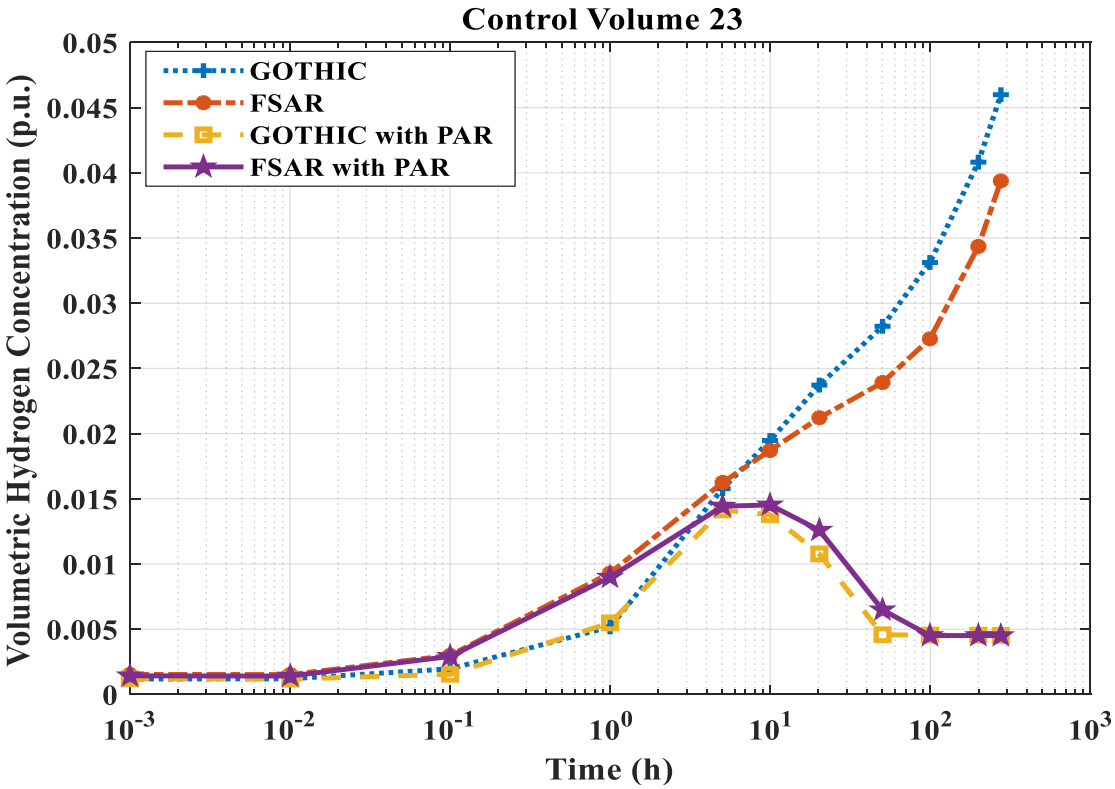

Figure 5-35. The volumetric hydrogen concentration with respect to time within the control volume 23.

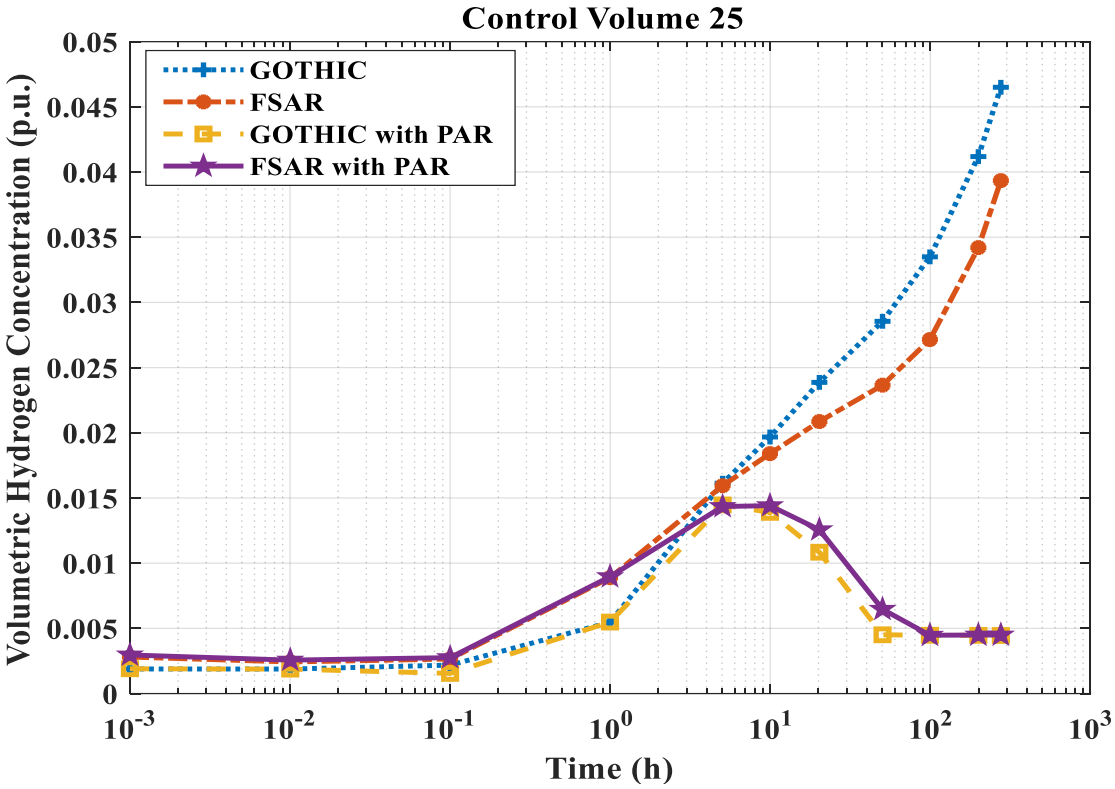

Figure 5-36. The volumetric hydrogen concentration with respect to time within the control volume 25.

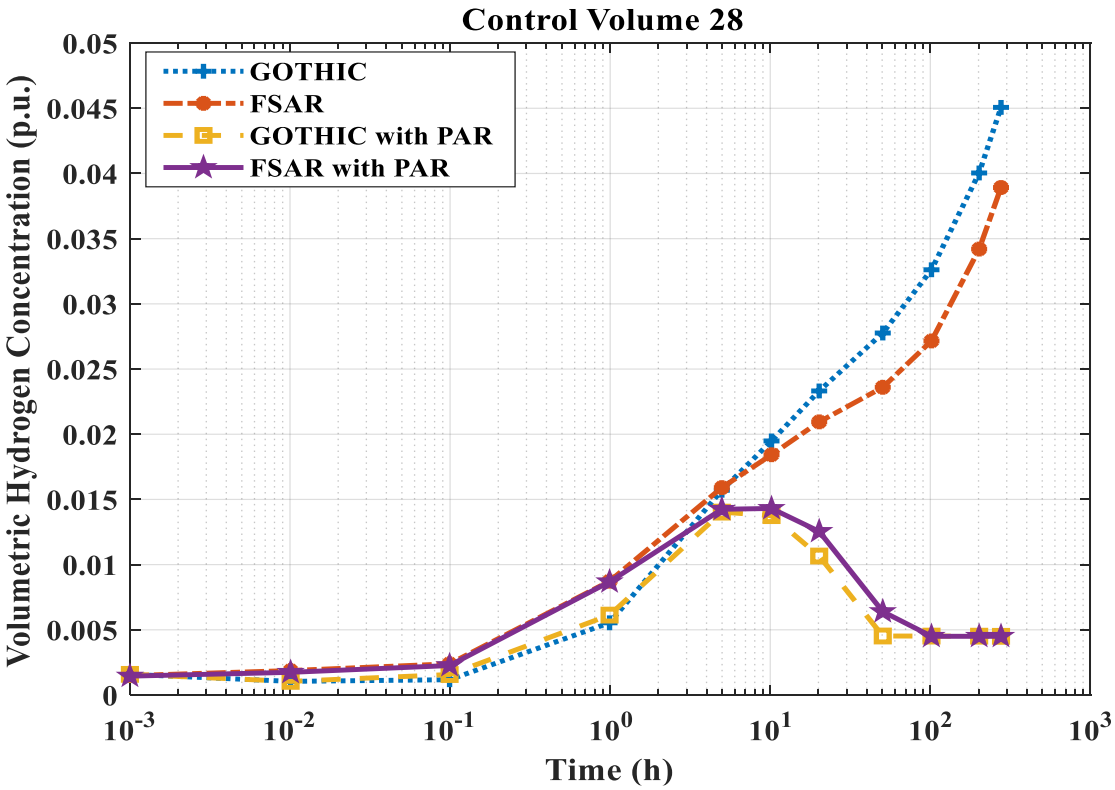

Figure 5-37. The volumetric hydrogen concentration with respect to time within the control volume 28.

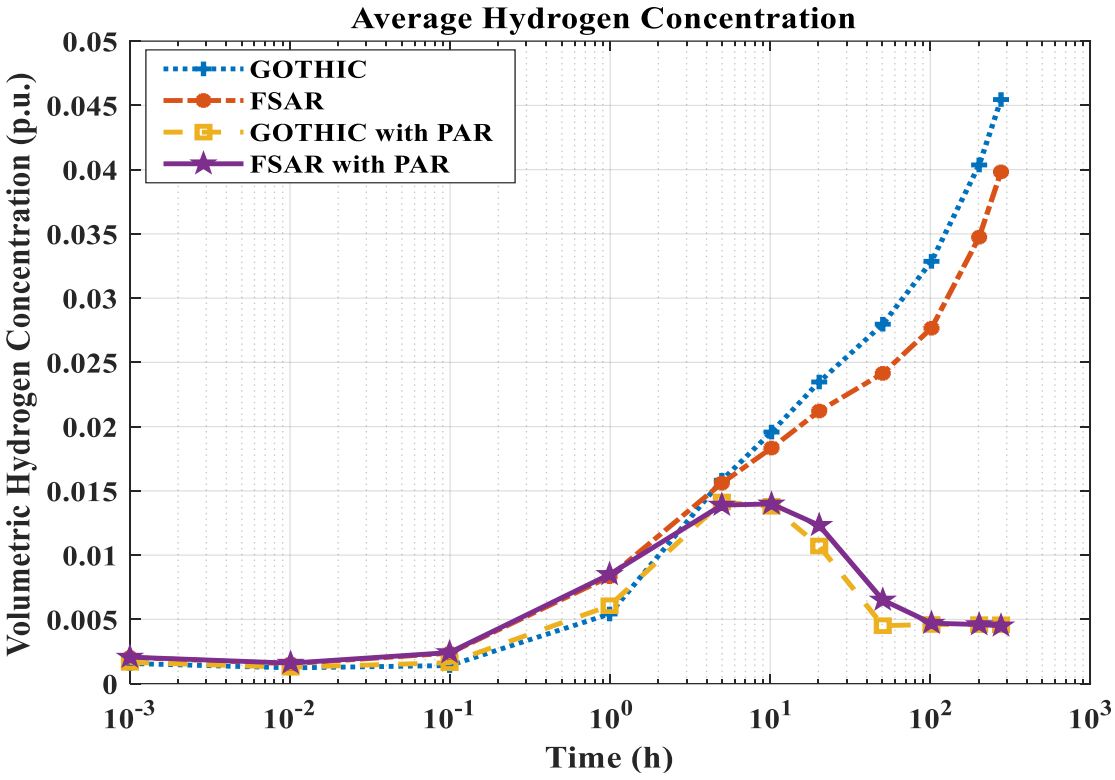

Figure 5-38. Average volumetric hydrogen concentration over the whole containment volume.

Apart from the investigation on average hydrogen concentration in each control volume, there should be an assessment within control volumes to check whether there is a hydrogen stratification within any control volume that contains hydrogen concentration more than the lower flammability limit. Unlike LP codes which FSAR utilized, the codes with 3D capabilities just like GOTHIC could give the necessary resolution to carry out such an investigation on its mesh system. The 3D contours of volumetric hydrogen concentration within the containment with and without the PAR influence are provided (produced in the post-processing stage of the study in ParaView as a data visualization tool) in Figure 5-39 to Figure 5-45. The time steps chosen for these figures are 1, 5, 10, 20, 50 and 100 hours (and 200 hours just on the onset of entering into the flammability region without PARs model) to represent different periods during the accident in terms of hydrogen distribution. At 1 hour, there is no difference between the two models due to the inactive PARs but starting from 5 hours, when the hydrogen concentration exceeds the 0.45% threshold, the divergence between the two models becomes more and more apparent with the effect of the recombiners. After 50 hours following the LB-LOCA, the containment reaches a stable state as it could be seen in Figure 5-43 and Figure 5-44, although the hydrogen concentration continues to rise inside the containment without PARs, and eventually, reach the lower flammability limit at

around 200 h (Figure 5-45). As it could be seen through the figures either with or without the PAR effect, the distribution of the hydrogen through the containment is almost homogenous. In a severe accident, the hydrogen release is quite intense and fast ejection of hot hydrogen gas into the system is observed through the break source due to the significant amount of zirconium reacting with steam, however, in DBAs, the amount of zirconium to react with steam is limited to 1%. This allows the consideration of other hydrogen sources like water radiolysis in a DBA since the amount of hydrogen released due to the zirconium oxidation is in the order of other sources, which is normally neglected in a severe accident case. The slow rate of hydrogen ingress into the containment provides better conditions for mixing inside the containment which leads to the homogenous distribution. It could be said that the 2% allowed hydrogen concentration limit set by FSAR considering the possibility of non-uniform mixing is a bit strict. Hydrogen stratification is not formed within the containment during the transient in the 3D code results.

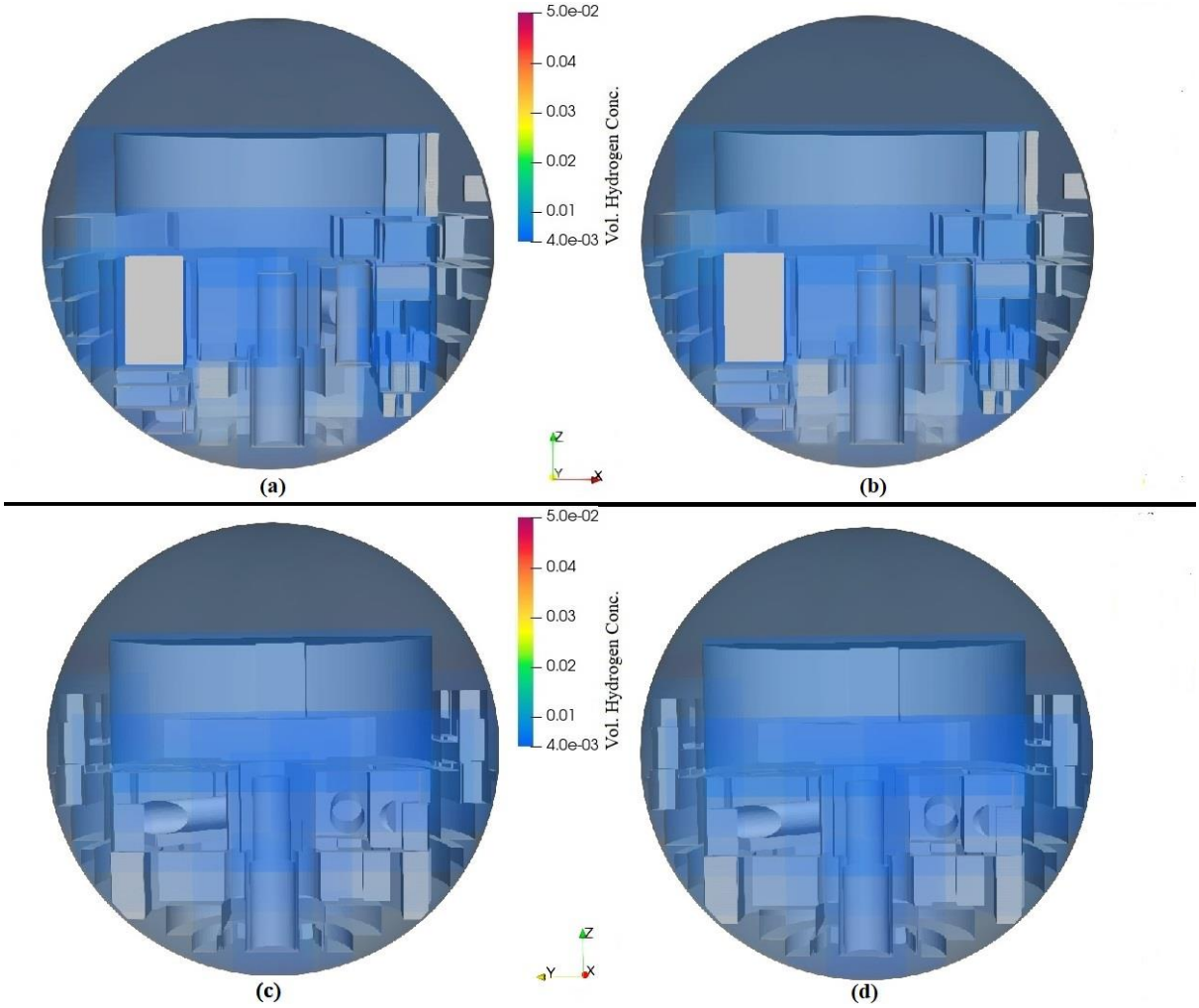

Figure 5-39. The 3D map of volumetric hydrogen concentration over the containment at 1 hour; (a) front view without PARs, (b) front view with PARs, (c) side view without PARs, (d) side view with PARs.

.

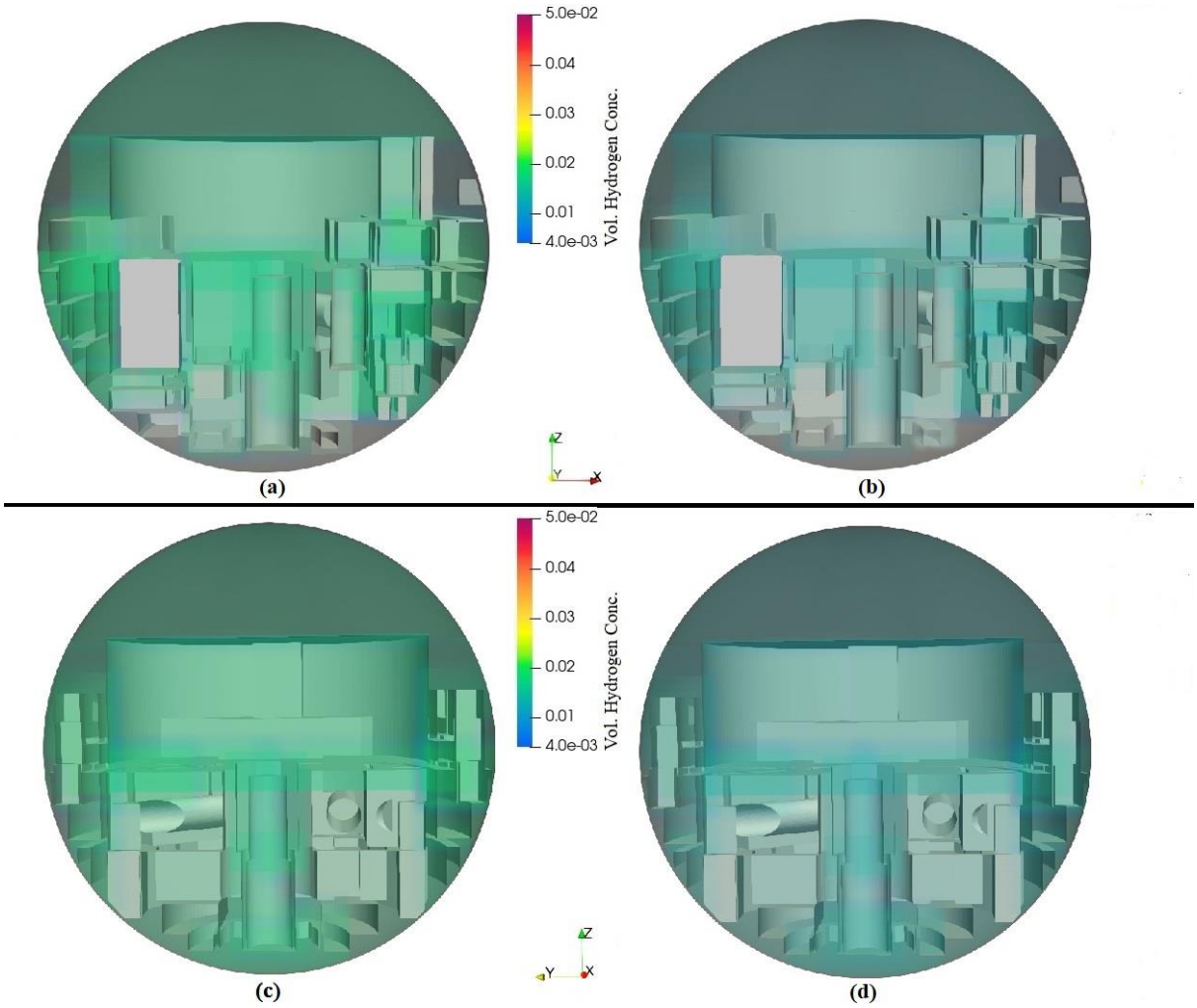

Figure 5-40. The 3D map of volumetric hydrogen concentration over the containment at 5 hours; (a) front view without PARs, (b) front view with PARs, (c) side view without PARs, (d) side view with PARs.

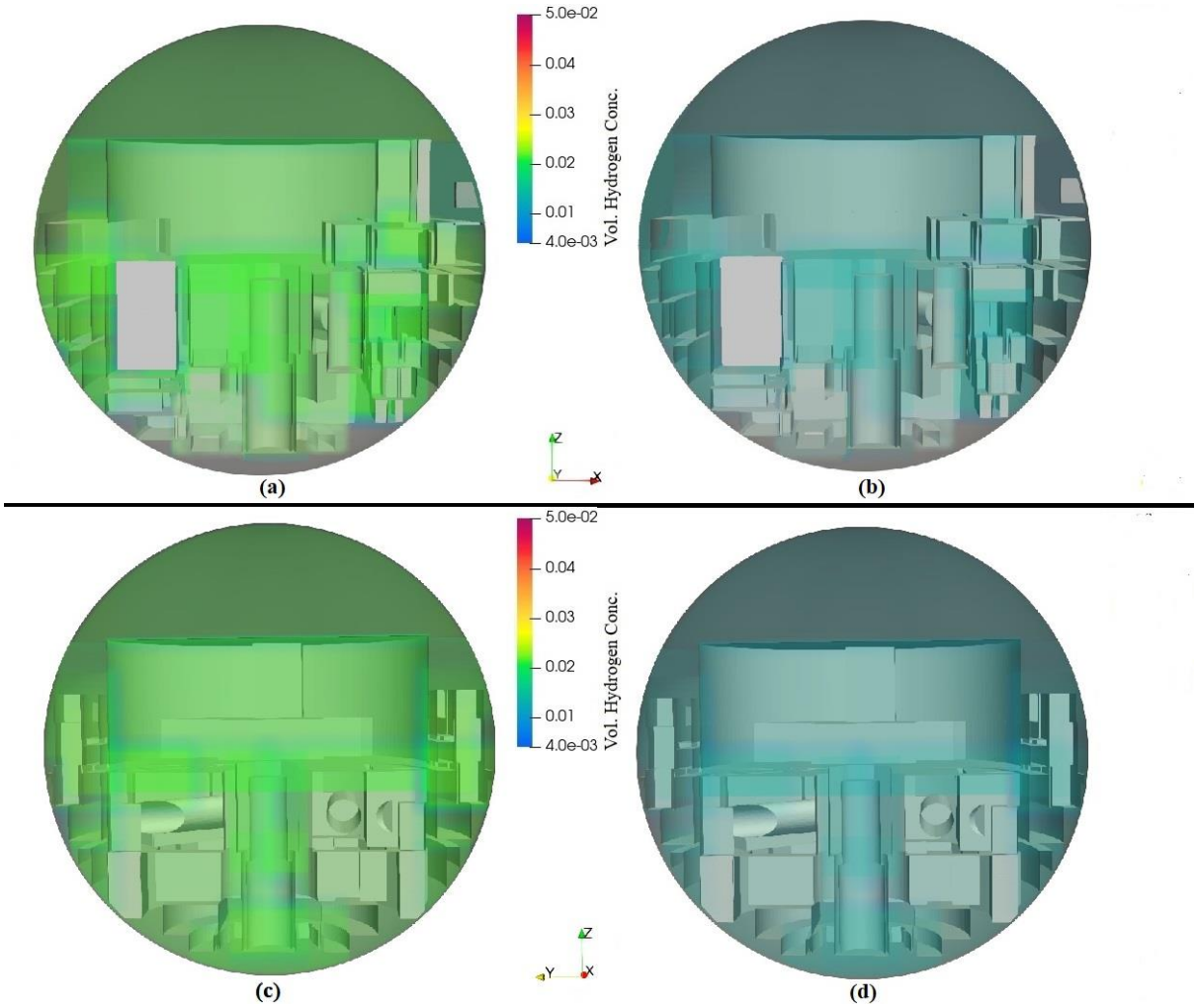

Figure 5-41. The 3D map of volumetric hydrogen concentration over the containment at 10 hours; (a) front view without PARs, (b) front view with PARs, (c) side view without PARs, (d) side view with PARs.

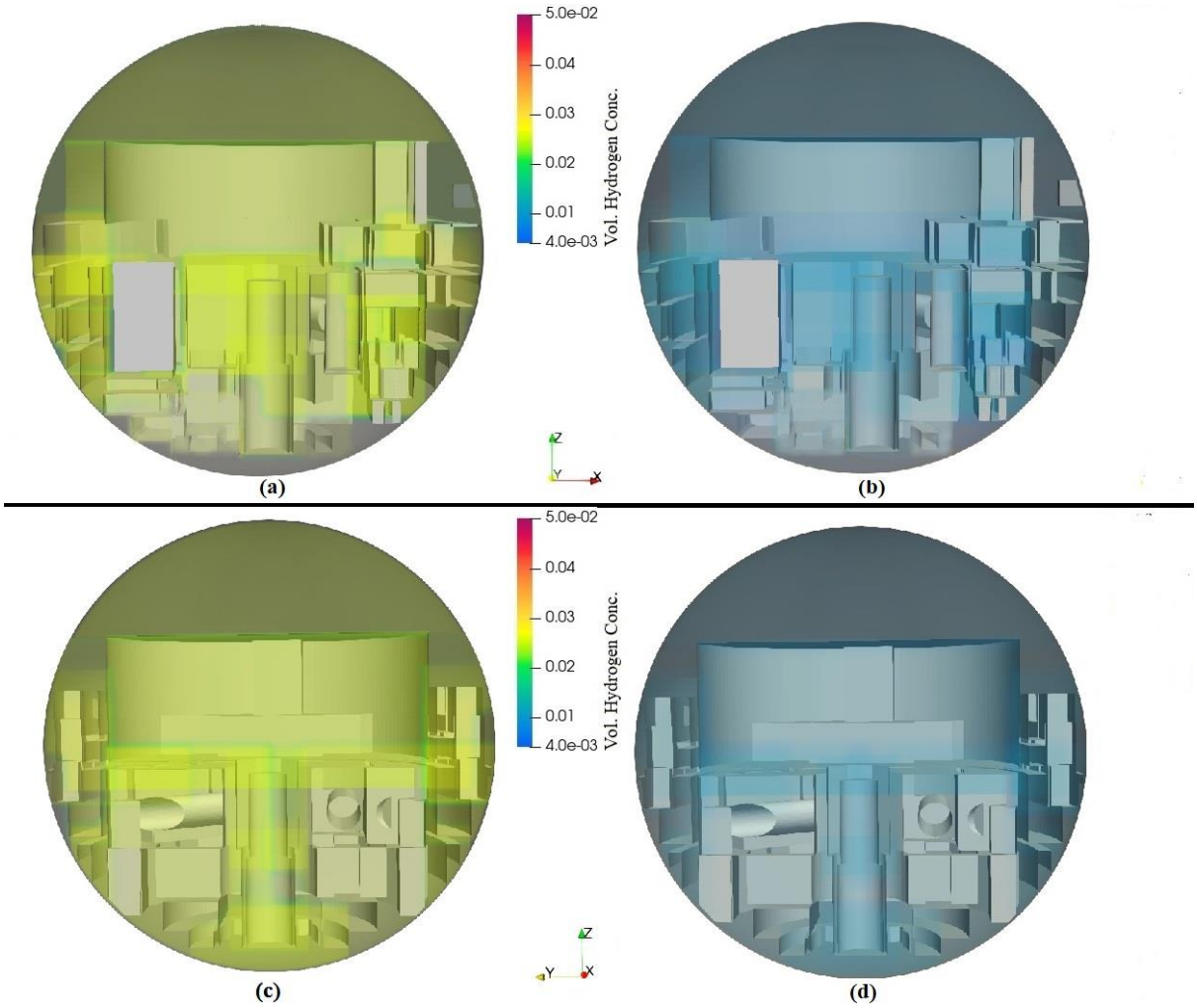

Figure 5-42. The 3D map of volumetric hydrogen concentration over the containment at 20 hours; (a) front view without PARs, (b) front view with PARs, (c) side view without PARs, (d) side view with PARs.

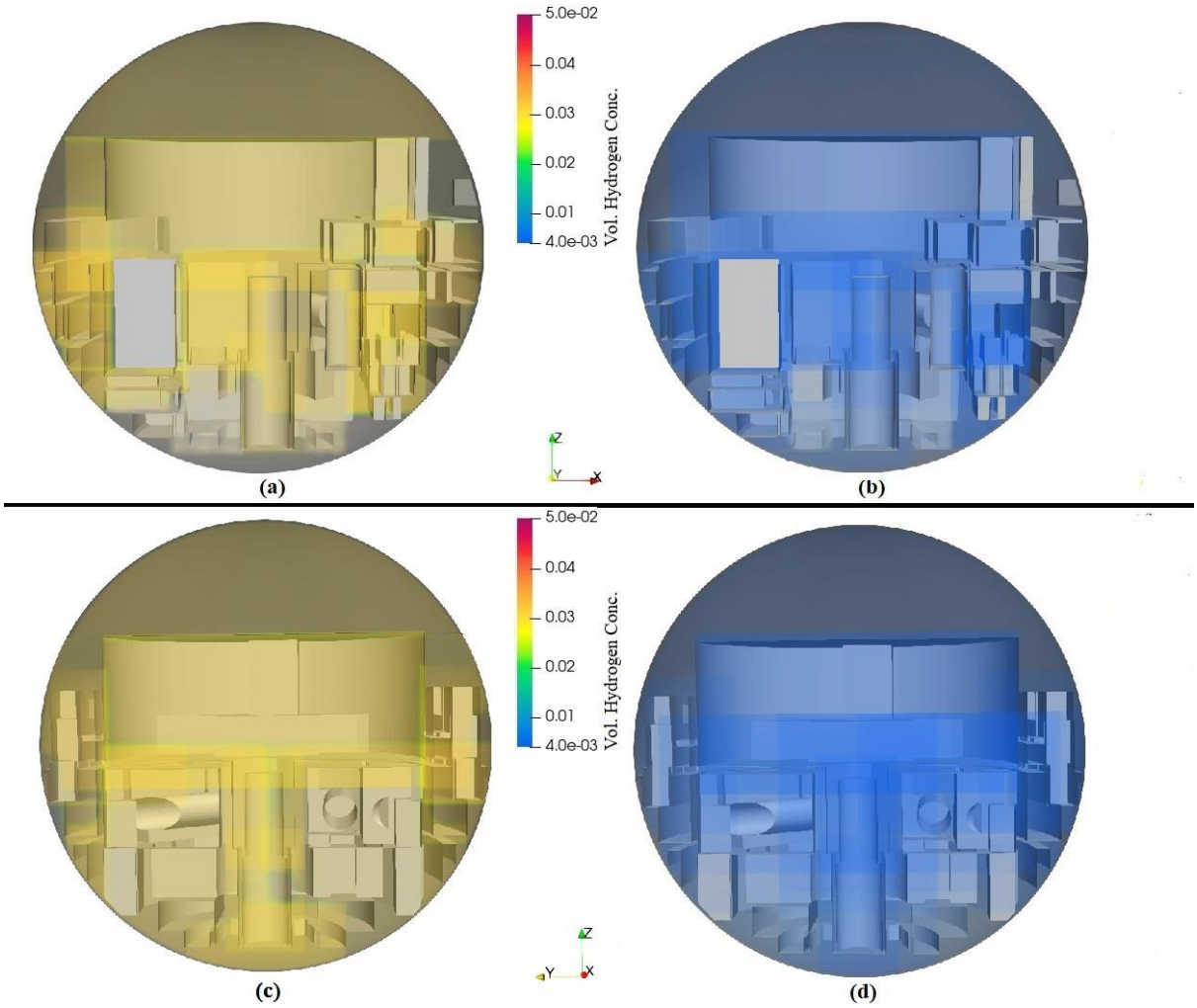

Figure 5-43. The 3D map of volumetric hydrogen concentration over the containment at 50 hours; (a) front view without PARs, (b) front view with PARs, (c) side view without PARs, (d) side view with PARs.

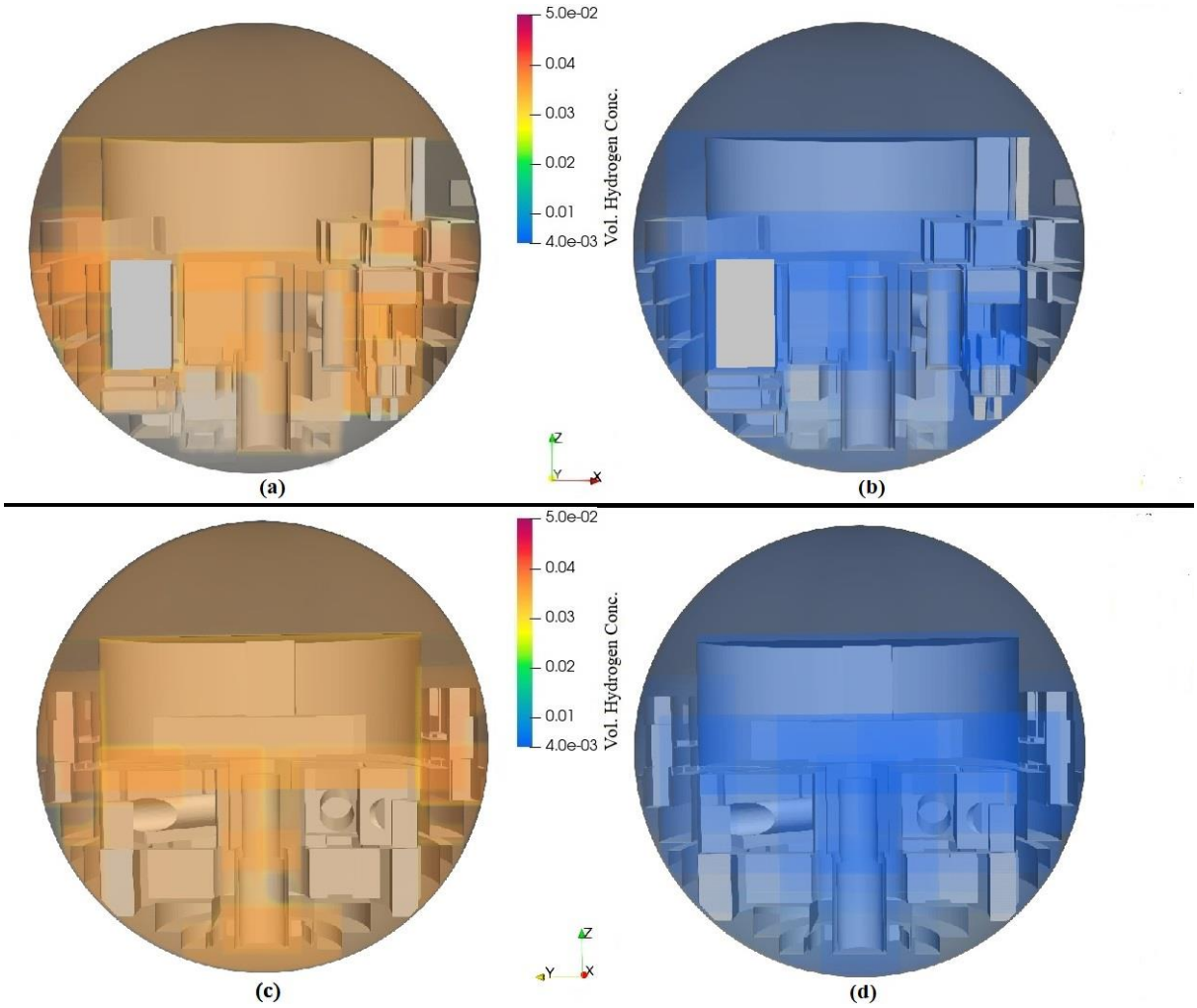

Figure 5-44. The 3D map of volumetric hydrogen concentration over the containment at 100 hours; (a) front view without PARs, (b) front view with PARs, (c) side view without PARs, (d) side view with PARs.

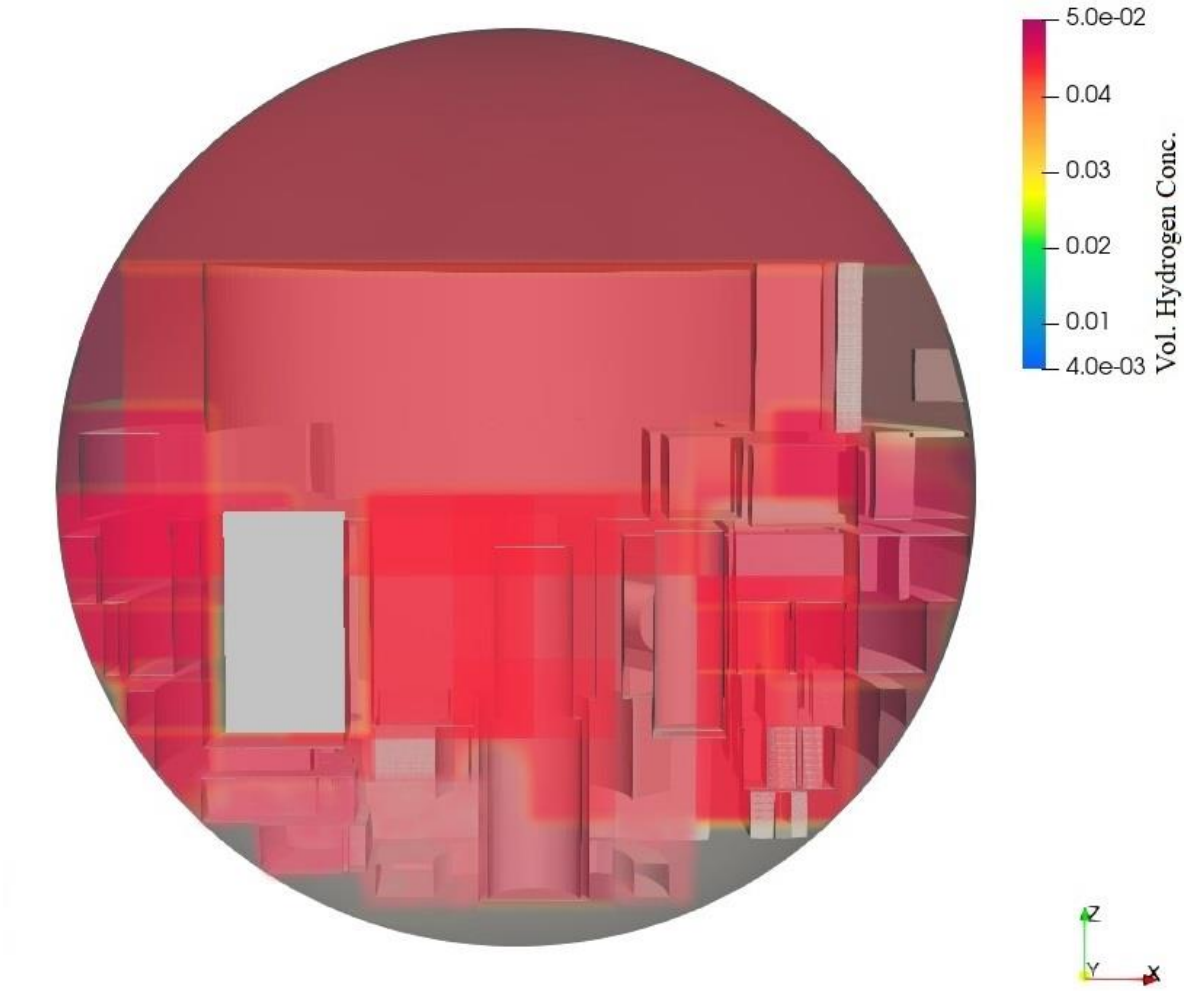

Figure 5-45. The 3D map of volumetric hydrogen concentration inside the containment at 200 hours, front view without PARs.

5.5 Conclusion

Maintaining containment integrity to avoid the release of radioactive material into the environment during nuclear accidents is one of the major goals of nuclear safety. Following a loss of coolant accident, the coolant discharges from the pipe break leading to a rise of the temperature and pressure inside the containment atmosphere and consequently hydrogen could be generated as result of water radiolysis and zircalloy-steam reaction in a design basis accident scenario. These phenomena pose a risk of containment failure and explosion and therefore investigation of containment thermal-hydraulic parameters, hydrogen distribution and relevant mitigation methods are one of the inseparable part of nuclear safety assessment. In this thesis, a detailed 3D simulation of a unique VVER-1000/V446 containment structure and the investigation of its short-term and long-term pressurization and hydrogen distribution

during the large-break loss of coolant accident have been conducted by using AutoCAD and GOTHIC code. Simulation results are presented in 3D contours of thermal-hydralic parameters and hydrogen distribution inside containment and can cover the whole coordinates of the structure. In the short-term analysis, an equivalent lumped parameter model has been developed in GOTHIC to validate the methods and simulation procedure and moreover to compare the accuracy of lumped parameter and 3D methodology. The long-term behaviour of the containment was also analysed by taking into account the containment spray system and sensitivity study of its parameters. A hydrogen distribution analysis has been carried out in GOTHIC by modifying the model with the installation of 80 passive autocatalytic recombiners in 3D. The 3D maps of volumetric hydrogen concentration through the containment with and without passive autocatalytic recombiner models at different time steps are also presented and the mixing of the hydrogen within the containment was investigated.

The author has not encountered a study which performs 3D containment analysis of VVER-1000 reactor in the literature, although there are works having lumped parameter analysis of the containment. Traditional method to carry out containment analysis for plant licensing purposes is employed by using lumped parameter codes. However, newly emerged 3D methodology provides better resolution inside the large and complex system of the containment, showing local stratification/hot spot phenomena which is not possible through lumped parameter codes due to intrinsic limitations of the codes. The method of constructing the geometry of the containment through AutoCAD to GOTHIC has been proposed by Bocanegra et al. and validated in performing a loss of coolant accident scenario for a PWR-W containment in their study (Bocanegra et al., 2016).

Although, the hydrogen distribution analysis has been considered for a design-basis large-break loss of coolant accident to compare with final safety analysis report, as it was done in thermal-hydralic parameter study in this thesis, a severe accident case would be investigated easily by using the same methodology described in this work by employing a code such as MELCOR to get mass, energy and hydrogen release data for the new case to put as boundary conditions inside the GOTHIC model. In such a case, the optimum number of passive autocatalytic recombiners with their placements to mitigate hydrogen risk inside the containment might be a topic in a further study. The effect of containment spray system on hydrogen distribution might also be valuable to investigate in a further study, since the spray system although boost the mixing of the hydrogen gas inside the containment to prevent local

stratification phenomenon, it decreases the steam concentration in the containment atmosphere by condensation which means reducing the diluting effect of steam in the gas mixture.

The following highlighted points can be concluded as a result of the short-term study:

- Although 2D temperature and pressure profiles have the same trend for all three methods (GOTHIC lumped parameter, average GOTHIC 3D and ANGAR for FSAR) reported in Figure 5-1 to Figure 5-6, different equations, correlations, turbulent regime, numerical methods etc. employed in these methods/codes can produce some difference between results.

- As expected, the results of 2D profiles for GOTHIC lumped parameter mode and ANGAR code are almost the same while the average GOTHIC 3D mode has agreed less with respect to the previous ones (Figure 5-1 to Figure 5-6). The main reason is related to the nature of GOTHIC 3D mode which uses a completely different methodology compared to the lumped parameter codes. Even volume averaging of 3D calculated parameters in each control volume to make it a 2D profile point can introduce some errors in the calculated outputs.

- 3D vertical temperature contours presented in Figure 5-14 and Figure 5-15 can give an overall view of containment parameters and how their location regarding the break source can affect their profile behaviour from both time and value points.

- This study can give a complete understanding of the importance of using 3D simulation for containment parameters because of the occurrence of some hot spots in individual control volumes - that can be seen in 3D contours (and hidden in 2D ones). As 3D contours give a detailed map of containment parameters in all coordinates, it can be used to upgrade the safety assessment, in addition, to improve the siting of the engineered safety features in the design and operation stage of nuclear power plants.

The following highlighted points can be concluded as a result of the long-term study:

- The overall trend of the temperature and pressure profiles as the result of the study are in agreement with the reference (final safety analysis report). The main discrepancies arise in the cooling rate of the containment at earlier stages of the simulation. The intrinsic differences between lumped parameter and computational fluid dynamics codes, differences in code structures and heat transfer models could be the distinguished reasons for this margin.

- The effect of containment spray system as one of the predicted engineered safety features in the depressurization of containment can be found clearly throughout Figure 5-18 to Figure 5-32. The subsequent long-term reducing effect could also be noticed in both pressure and temperature results.

- Sensitivity analysis on the spray droplet temperature and diameter were presented in Figure 5-24 to Figure 5-27 respectively. It could be expected, the lower spray temperature could result in more heat transfer from the containment atmosphere to the droplets and subsequently a higher depressurization rate. As it has been seen, higher spray droplet temperature leads to heat transfer equilibrium between droplet and containment atmosphere at the later stages by reversing the heat transfer direction (from spray droplets to containment as in Figure 5-24). So, controlling the spray droplet temperature through spray closed cooling system (heat exchanger, pumps etc.) is a vital point to get expected effects of the spray system as an engineered safety feature. Smaller spray droplets will increase the heat transfer surface for the same mass and as a direct result rises the depressurization capability for the initial seconds of the transient due to the droplet to steam phase conversion.

- The importance of 3D analysis can be realized in Figure 5-28 to Figure 5-32 where non-visible hot spots in 2D profiles, can be found easily in these 3D contours. This can provide the opportunity for more assessment, and modifying engineered safety features to avoid hot spots in the containment pressurization which can jeopardize its integrity.

Finally, for the hydrogen distribution analysis, the following results could be presented as a conclusion:

- Figure 5-33 to Figure 5-38 clearly show the effectiveness of passive autocatalytic recombiners in mitigating the hydrogen risk. The volumetric hydrogen concentration after passive autocatalytic recombiner activation drops to values below 0.5% which stabilizes/saves the containment structure in terms of hydrogen risk. Whereas it is clearly seen through the figures, if no hydrogen mitigation technique is applied, the hydrogen concentration surpasses the lower flammability limit and could jeopardize the containment integrity by auto-ignition/explosion.

- Figure 5-39 to Figure 5-45 demonstrate the 3D distribution of hydrogen concentration within the containment and provide information about the local regions where hydrogen stratification might occur within a control volume although could not be observed in lumped parameter averaged over the volume calculations. The hydrogen distribution within the containment is found homogenous because of the nature of the accident.

- Two percentage hydrogen lower limit set by the final safety analysis report might be too conservative. Non-uniform mixing concerns could be removed by using a code with 3D capabilities. Since it is found that the mixing inside the containment is homogenous, the number of passive autocatalytic recombiners installed might be decreased to optimize the system in the reduction of hydrogen concentration in a further study.

Appendix-A Hydrogen Generation within the Context of Severe Accidents

A severe accident progression consists of two phases, in-vessel, and ex-vessel. The in-vessel stage includes all the phenomena until the reactor pressure vessel breaches such as core relocation to the lower plenum and core melting. Zirconium, steel and B_4C oxidation contribute to hydrogen accumulated inside the containment as in-vessel sources. After the reactor vessel fails, the phenomena like molten core concrete interaction or direct containment heating are included in the ex-vessel phase and cause the ingress of hydrogen into the containment atmosphere. Moreover, water radiolysis and metal corrosion could also be regarded as ex-vessel hydrogen sources.

A.1 In-vessel Hydrogen Generation

A.1.1 Zirconium Oxidation and In-Vessel Severe Accident Progression

A severe accident starts with an initiating event like a LOCA. After that triggering incident, coolant becomes insufficient in amount with time and could not carry the necessary heat through the fuels hence fuel temperature rises. Increased fuel temperature makes the core uncovered by vaporizing the water around the core into steam. Since the heat transfer coefficient of steam flow is lower in comparison to water flow, core temperature increases further because of the decay heat (IAEA, 2011). When the temperature reaches 700-900 °C, higher than the maximum temperature of 350 °C which fuel cladding undergoes at normal operation, the mechanical properties of the fuel cladding start to degrade, and deterioration starts. Gases inside the fuel rod comprise inert gases added in the fuel rods during manufacture and noble gases like xenon and krypton produced during the fission of the fuel. As the temperature increases further, if the pressure of those gases inside the fuel cladding exceeds the pressure of the vessel, the clad swells until it is breached. Then, fission products escape into the reactor coolant system (Figure A-1). If the pressure of the vessel exceeds the inside pressure of the fuel rod, then cladding is pushed against the fuel due to the heat. The formation of UO_2-Zr liquid eutectic mixtures is also observed at later stages (Figure A-2).

(Jacquemain, 2015).

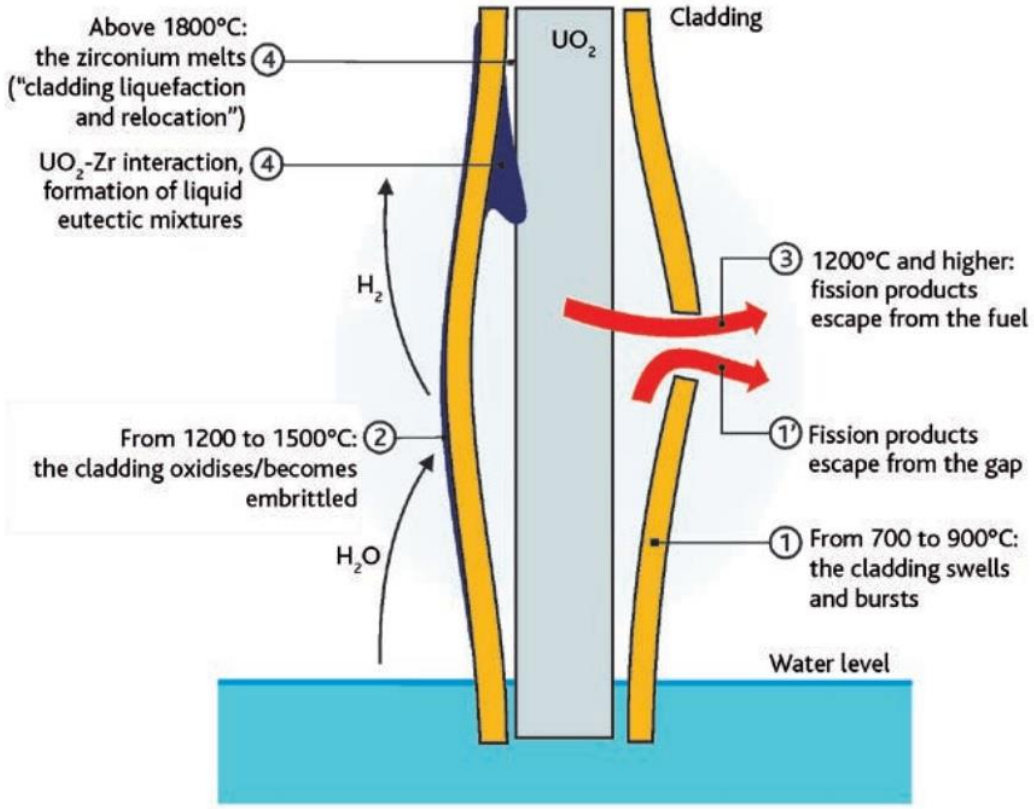

Figure A-1. Degradation of the fuel cladding in a severe accident when the inside pressure is higher than the outside pressure (Jacquemain, 2015).

At around 1000 °C, zirconium fuel cladding reacts with steam and is oxidized. The reaction is strongly exothermic and rapid, it intensifies the process of core degradation by further increasing the temperature rise in the core (the heat-up rate might go beyond 1 K/s). The zirconium-steam reaction is:

$$Zr + 2H_2O \rightarrow ZrO_2 + 2H_2 + \Delta H, \qquad \Delta H = -586.6\ \mathrm{kJ/kg}.$$

0.0442 kg of H_2 is produced when 1 kg of Zr is oxidized (IAEA, 2011).

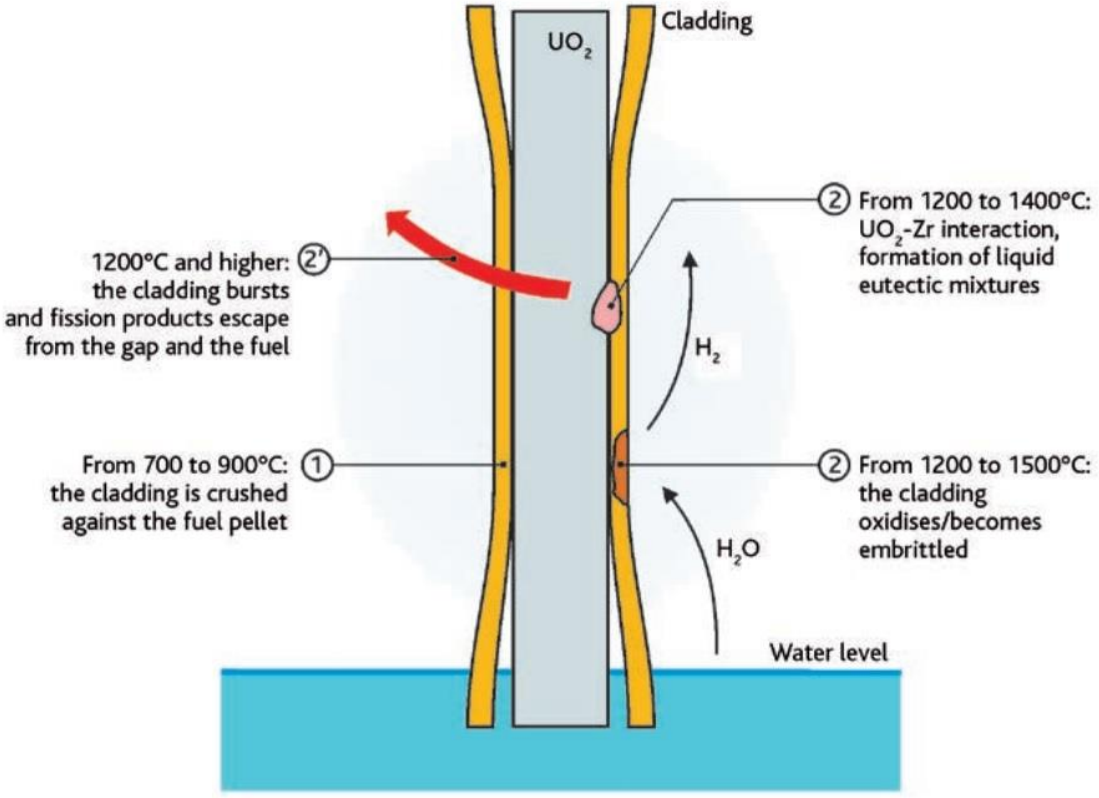

Figure A-2. Degradation of the fuel cladding in a severe accident when the outside pressure is higher than the inside pressure (Jacquemain, 2015).

Table A-1. Approximate values of zirconium and hydrogen gas produced in case of total zirconium oxidation for typical BWR and PWRs (IAEA, 2011).

	Typical BWR, kg (3800 MWth)	Typical PWR, kg (3600 MWth)	VVER-1000, Russian fuel, kg	VVER-1000, Westinghouse fuel, kg
Zirconium	76000	26000	22630	24765
Hydrogen gas	3360	1150	1000	1095

The total amount of hydrogen that could be produced in a severe accident is different for PWRs and BWRs especially considering the hydrogen generated through the zirconium oxidation. If the total amount of the zirconium in a typical PWR core were reacted with steam, this would generate around 1150 kg of hydrogen. If the total amount of zirconium in a typical BWR core were exposed to the same reaction, the total amount of hydrogen produced would be around 3360 kg, as stated in Table A-1. Typically, large BWR cores contain about

58% greater initial uranium mass than large PWR cores and this greater mass is divided into approximately 45% more fuel rods than in a PWR. Moreover, BWR fuel assemblies have channel boxes surrounding the fuel rods with each having a mass greater than 100 kg, unlike PWRs. Overall, the zirconium amount within a BWR core is significantly larger in comparison to PWRs, which leads to a much higher generation of hydrogen during a severe accident (Leyse and Paine, 2014).

Further continuing the in-vessel severe accident progression, components of the core such as control rods, structured steel, and unoxidized zirconium left in the cladding melt or vaporize between 900 – 1800 °C. Other core components begin to melt above 1800 °C. Those melted materials lead to the formation of a corium, a molten mixture consisting of fuel and structural materials within the core. Residual heat because of the fission products within the corium retains the molten state of the mixture (Jacquemain, 2015). Corium relocates downwards to the lower plenum of the reactor pressure vessel gradually and causes RPV breach either by reacting with water there and causing a steam explosion or through thermal decomposition (Hashim et al., 2013).

A.1.2 Steel Oxidation

Large quantities of steel are contained within the walls of the reactor vessel such as control-rod cladding, core barrels, control-rod guide tubes, and core support plates. This steel may be oxidized to produce hydrogen when it is heated to high temperatures and exposed to steam. Oxidation of steel by high-temperature steam is highly complex, and several different oxide forms are possible. Like the zirconium oxidation, these reactions are exothermic, the heat released depends upon the composition of the steel. Normally, steel oxidation is not important below temperatures of about 1200 °C and core uncovery would require remaining for a long period of time to reach these temperatures following the accident. Nevertheless, as the melting point of steel is approached between 1370 °C and 1500 °C, the steel oxidation rate can become significant and exceed the zirconium oxidation rate (Sandia National Laboratories, 1983). However, a general estimation of the proportion of the hydrogen produced due to the steel-steam reaction during a severe accident may be around 10% to 15% of the total amount of hydrogen generated (OECD/NEA, 2001).

A.1.3 Boron Carbide (B_4C) Oxidation

B_4C, as a neutron absorber material, is utilized in BWR, VVER and some western-type PWR designs. When steam interacts with the B_4C inside control rods, boron carbide is likely to react rapidly with the steam during the core melting. The gases produced after the reaction include H_2, CO, CO_2 and CH_4. Moreover, vapours of B_2O_3 and various acids of boron are produced. B_4C reactions with steam contribute to the hydrogen source term and these oxidation reactions under steam are more exothermic and produce more hydrogen per gram material in comparison to zirconium oxidation. The consequence of such an effect depends on the mass of B_4C in each reactor type. Table A-2 shows the order of magnitude of hydrogen gas produced by boron carbide oxidation compared to hydrogen gas produced by zirconium oxidation for several PWRs. The situation for BWRs is different since they used 2 to 3 times more B_4C mass than PWRs or VVERs so the contribution to the total amount of hydrogen produced during a severe accident is larger (IAEA, 2011).

Table A-2. The amount of produced hydrogen gas due to the boron carbide oxidation and the comparison to Zr oxidation (IAEA, 2011).

Reactor type	Hydrogen gas generated by B_4C oxidation with steam	Hydrogen gas produced by B_4C oxidation versus hydrogen gas produced by Zr oxidation, with steam
French P4-P'4 PWR	between 45 kg and 95 kg	less than 10%
French N4 PWR	between 50 kg and 100 kg	less than 10%
Russian VVER-1000	between 40 kg and 80 kg	at most around 8%

A.2 Ex-vessel Hydrogen Generation

A.2.1 Molten Core Concrete Interaction (MCCI)

If the reactor coolant system is depressurized and the RPV is failed to contain the corium, gravitational corium drop is observed. If the reactor cavity where corium falls is dry, then MCCI happens. When corium contacts the basemat of the containment, a violent gas release penetrates the corium. H_2O and CO_2 (emerging from the thermal decomposition of the concrete basemat) in this gas release react with Cr and Zr contained within corium and

oxidize them rapidly. It is assumed that all the remaining Zr and Cr within the corium undergo oxidation in one hour after MCCI starts. Then, other metals like Fe oxidize for days at a rate of 4g/s until the corium penetrates the basemat completely. H_2 amount released after the interaction between corium and concrete basemat depends on the initial amount of Cr and Zr. A substantial amount of H_2 gas release could be observed in this stage, for example, 2000 kg of H_2 gas could be produced during MCCI in a VVER-1000 reactor.

Basemat concrete composition is important because of the amount of CO released during MCCI. Combustion of the CO + H_2O mixture should be considered when the flammability of the hydrogen is concerned. In other words, CO poses an additional threat to the containment safety. There are two types of concrete used in containment basemat one is siliceous type and the other one is limestone type. For a siliceous concrete, the amount of gas produced during MCCI is not significant enough to lead pressure peaks which threaten the containment integrity. Moreover, it includes very low amount of $CaCO_3$ concentration which lowers the amount of CO that could be produced in MCCI process. Volumetric hydrogen concentration could be at least 10 times higher than the volumetric CO concentration. This means the effect of CO could be assumed as negligible in siliceous-type concrete. Whereas the reaction between corium and limestone concrete basemat could produce a significant amount of CO within less than 1 hour, approximately 40% of the volume around the reactor pit might be filled with combustible gas by volume, mostly carbon monoxide (IAEA, 2011).

A.2.2 Direct Containment Heating

If the reactor coolant system is pressurised when the vessel is breached, corium may spread into the containment while it leaves the reactor vessel and leads to a pressure spike as the heat contained in the molten corium is transferred to the gases in the containment atmosphere rapidly. This phenomenon is called direct containment heating. Corium dispersion enables a very efficient heat exchange between the corium and the gases present, along with oxidation of metallic components of corium, producing hydrogen consequently. The oxidation is mainly due to the steam present in the reactor coolant system but also steam inside the containment contributes to reaction as well. The temperatures reached by the gases in the containment and the presence of very hot corium particles then provokes the combustion of the hydrogen generated through oxidation of the dispersed corium. If the hydrogen concentration is sufficient enough, this combustion could cause the hydrogen already present

in the containment to ignite as soon as the reactor vessel ruptures. These phenomena rise the temperature and pressure of the containment atmosphere sharply in a very fast way (in a few seconds), leading to the failing of the containment integrity.

Figure A-3 shows a diagram of the phenomena during direct heating of the gases inside the containment. When the reactor vessel ruptures, it includes a mixture of steam and hydrogen, some corium in the lower head and structural elements that are still in place, and possibly some water under a pressure ranging from the operating pressure of the reactor coolant system (approximately 160 bar) to a pressure near the containment pressure (a few bar) if the reactor coolant system is depressurized. If the reactor vessel is pressurized, the corium, the steam, and possibly hydrogen are discharged into the reactor pit in different phases (single phase liquid corium jet, followed by a two-phase corium and gas jet and a gaseous jet). The characteristics of the discharge depend on the size, location and shape of the break in the reactor vessel wall (Jacquemain, 2015).

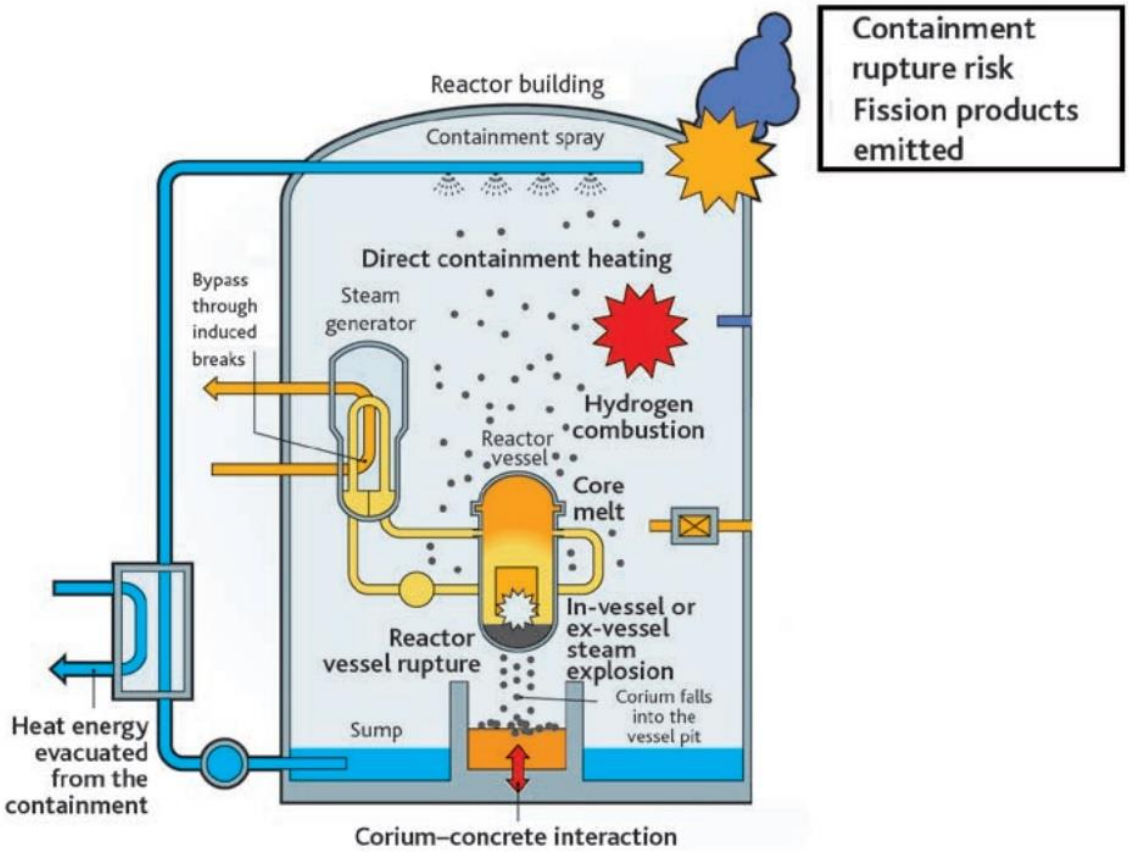

Figure A-3. The diagram of the physical phenomena occurring during direct containment heating inside the containment (Jacquemain, 2015).

A.2.3 Corrosion of Metals

Zinc and Aluminium could also produce hydrogen by corrosion reactions. Zinc could be found on some paints and galvanized steel in a containment. Corrosion of Zinc based material is a function of temperature, composition, surface area, and pH of the spray solution. For a typical PWR, the amount of hydrogen produced could be estimated around 106 kg of hydrogen for corrosion of zinc-based paint and 52 kg of hydrogen for corrosion of galvanized steel, which is quite lower in amount compared to other sources mentioned above like Zr oxidation during a severe accident (Sandia National Laboratories, 1983).

Appendix-B General Conservation Equations Solved by GOTHIC

The information provided here is taken from the GOTHIC's technical manual (EPRI, 2018b). The conservation equations for mass, energy and momentum which are used in GOTHIC will be described on here. The equations are written in integral form related to the finite volume numerical method that applied for a fixed volume to solve those equations. Figure B-1 illustrates a control volume (one of the finite volumes on the computational grid) with a fixed volume V, bounded by area A. All the equations written below are stated for multi-dimensional analysis. For lumped parameter analysis, there are some simplifications on the equations which are not explained here.

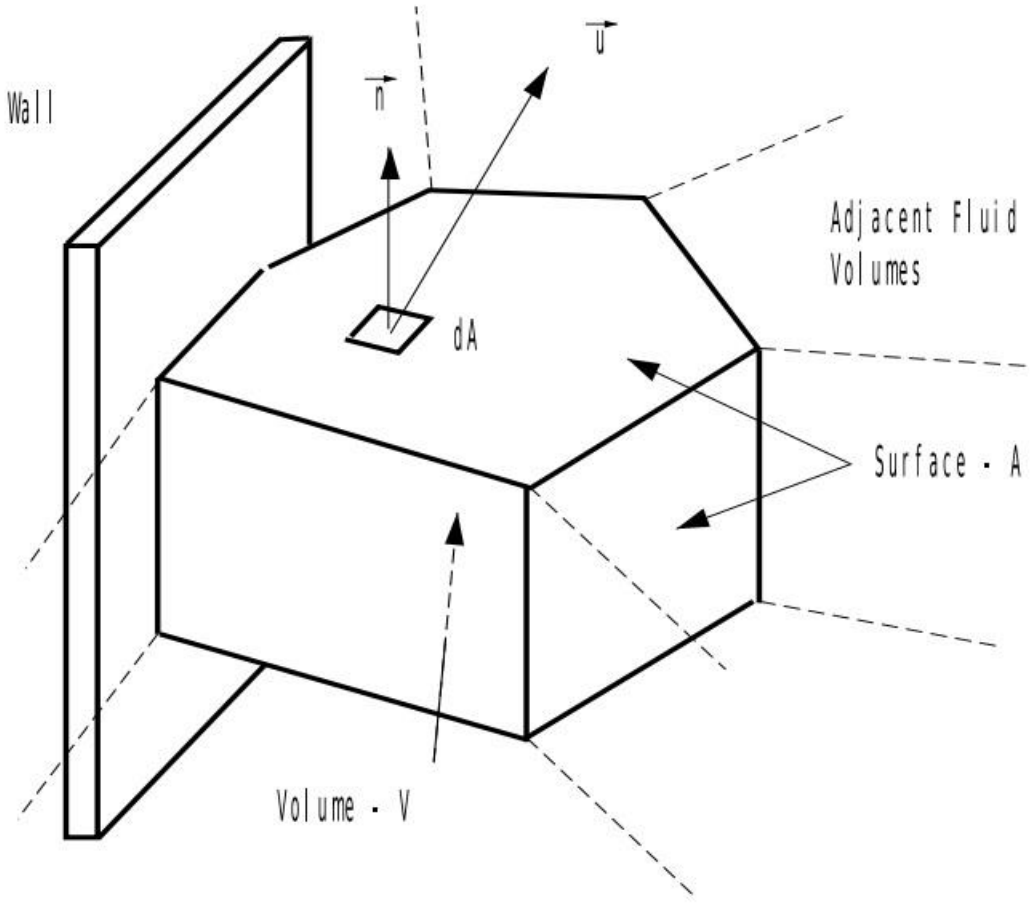

Figure B-1. The control volume for conservation equations (EPRI, 2018b).

Mass Conservation:

Mass conservation equations are solved for liquid, each drop field, steam and each noncondensing gas component, ice and mist.

$$\frac{\partial}{\partial t}\int_V \Theta\alpha_\phi \rho_{\phi\zeta} dV = -\int_{A_f} \psi\alpha_\phi\rho_{\phi\zeta}\vec{u}_\phi \cdot \vec{n} dA + \int_{A_f} \psi\alpha_\phi\rho_\phi D_\phi^C \vec{\nabla}\left(\frac{\rho_{\phi\zeta}}{\rho_\phi}\right)\cdot \vec{n} dA + \int_{A_w} s_{\phi\zeta}^C dA + S_{\phi\zeta}^C + E_{\phi\zeta}^C + C_{\phi\zeta}^C$$

This is the general form of mass balance equation where ϕ refers to phase: vapor, liquid, drop field or ice. ζ refers to component of the vapor: steam, noncondensing gas mixture or a component of the noncondensing gas mixture. Θ is the volume porosity and ψ is the area porosity factor. α refers to volume fraction, ρ is the density, $\vec{u}$ is the velocity vector, $\vec{n}$ is the outward normal vector to the surface dA (as it could be seen in Figure B-1), A_f is the portion of the total surface area that connects the control volume to an adjacent control volume where fluid could move in, D^C is the mass diffusion coefficient (including turbulence effects), s^C is the mass source per unit area generated or passed through the bounding wall A_w. S^C is the mass source because of the interactions between phases such as evaporation or condensation. E^C is the mass source term comes from engineered safety equipments, and lastly, C^C is the mass source term comes from the hydrogen combustion. The term on the left side of the equation refers to storage, whereas, the first three terms on the right side in order: convection, diffusion and boundary source.

Energy Conservation:

Energy conservation equations are written for enthalpy and solved for liquid, drops, and vapor/mist. The fluid energy balance equation is:

$$\frac{\partial}{\partial t}\int_V \Theta\alpha_\phi(\rho_\phi(h+ke)_\phi - P)dV = -\int_{A_f}\psi\alpha_\phi\rho_\phi(h+ke)_\phi\vec{u}_\phi\cdot\vec{n}dA - \int_V P\frac{\partial}{\partial t}(\Theta\alpha_\phi)dV + \int_{A_f}\psi\alpha_\phi\rho_\phi c_{p\phi}D_\phi^e\vec{\nabla}T_\phi\cdot\vec{n}dA + \sum_\zeta\int_{A_f}\psi\alpha_\phi\rho_\phi D_\phi^C\vec{\nabla}\left(\frac{\rho_{\phi\zeta}}{\rho_\phi}\right)h_{\phi\zeta}\cdot\vec{n}dA + \sum_k\int_V \Theta\lambda_k q_k\alpha_\phi\Phi_{k\phi}dV + \int_{A_w} s_\phi^e dA + S_\phi^e + E_\phi^e + C_\phi^e$$

In this equation h refers to enthalpy and ke refers to kinetic energy. Kinetic energy is included or excluded according to the user choice and all other energy forms that are not explicitly represented in the equation is neglected. The kinetic energy is defined as $ke_\phi = \frac{u_\phi^2}{2}$. Each drop field has its own energy balance. P is the static pressure, D^e is the thermal diffusion coefficient, λ_k is the decay rate for tracer k (fission/s-mol), q_k is the decay energy

release per fission event, s^e is the energy source per unit wall area, S^e is the interphase energy source, E^e is the energy source comes from engineered safety equipments, C^e is the energy source term comes from the hydrogen combustion. The left side of the equation is the storage, the first six terms of the right side of the equation starting from the left, in order, are related to: convection, work, thermal diffusion, gas component diffusion, tracer decay and boundary source.

Momentum Conservation:

Momentum conservation equations are solved for liquid, drops and vapor and the general form of the equation is:

$$\frac{\partial}{\partial t}\int_V \Theta\alpha_\phi \rho_\phi \vec{u}_\phi dV = -\int_{A_f} \psi\alpha_\phi\rho_\phi \vec{u}_\phi(\vec{u}_\phi \cdot \vec{n})dA + \int_{A_f} \psi\alpha_\phi \underline{\sigma}_\phi \cdot \vec{n}dA + \int_V \Theta\vec{g}\alpha_\phi\rho_\phi dV + \int_{A_w} \overrightarrow{s_\phi^m} dA + \overrightarrow{S_\phi^m} + \overrightarrow{E_\phi^m}$$

$\underline{\sigma}$ refers to static pressure and Reynolds and viscous stress terms, $\vec{g}$ is the gravitational acceleration, $\overrightarrow{s^m}$ is the momentum source per unit wall area, $\overrightarrow{S^m}$ refers to momentum source due to interphase interactions such as phase transition and $\overrightarrow{E^m}$ refers to momentum source comes from safety equipments. The left side of the equation is the storage, the first four terms of the right side of the equation starting from the left, in order, are related to: convection, surface stress, body force and boundary source.

References

AEOI, 2003. Final Safety Analysis Report (FSAR) for BUSHEHR VVER-1000 Reactor. Tehran.

Ahrens, James, Geveci, Berk, Law, Charles, 2005. ParaView: An End-User Tool for Large Data Visualization, Visualization Handbook. Elsevier.

Allardice, C., Trapnell, E.R., 1946. THE FIRST PILE.

Allelein, H.J., Arndt, S., Klein-Heßling, W., Schwarz, S., Spengler, C., Weber, G., 2008. COCOSYS: Status of development and validation of the German containment code system. Nuclear Engineering and Design 238, 872–889. https://doi.org/10.1016/j.nucengdes.2007.08.006

Andreani, M., Badillo, A., Kapulla, R., 2016. Synthesis of the OECD/NEA-PSI CFD benchmark exercise, in: Nuclear Engineering and Design. Elsevier Ltd, pp. 59–80. https://doi.org/10.1016/j.nucengdes.2015.12.029

Arnould, F., Bachellerie, E., Auglaire, M., De Boeck, B., Braillard, O., Eckardt, B., Ferroni, F., Moffett, R., Van Goethem, G., 2001. State of the art on hydrogen passive auto-catalytic recombiner (european union Parsoar project), in: 9 International Conference on Nuclear Engineering.

Avdeenkov, A. V, Kalyakin, S.G., Soloviev, S.L., Duong Quang, H., 2022. On the scalability of the operating capacity of hydrogen recombiners. Nuclear Energy and Technology 8, 143–152. https://doi.org/10.3897/nucet.8.83223

Bachellerie, E., Arnould, F., Auglaire, M., De Boeck, B., Braillard, O., Eckardt, B., Ferroni, F., Moffett, R., 2003. Generic approach for designing and implementing a passive autocatalytic recombiner PAR-system in nuclear power plant containments. Nuclear Engineering and Design 221, 151–165.

Bernardin, H., Škerlavaj, A., Mavko, B., Kljenak, I., Jožef, ", Institute, S.", 2001. Simulation of atmosphere stratification in the HDR test facility with the Contain Code, in: International Conference Nuclear Energy in Central Europe.

Bocanegra, R., Jimenez, G., Fernández-Cosials, M.K., 2016. Development of a PWR-W GOTHIC 3D model for containment accident analysis. Ann Nucl Energy 87, 547–560. https://doi.org/10.1016/j.anucene.2015.10.022

Broxtermann, P., Allelein, H.J., 2013. Simulation of AP1000's passive containment cooling with the German containment code system COCOSYS. Nuclear Engineering and Design 261, 326–332. https://doi.org/10.1016/j.nucengdes.2012.09.038

Chatelard, P., Reinke, N., Arndt, S., Belon, S., Cantrel, L., Carenini, L., Chevalier-Jabet, K., Cousin, F., Eckel, J., Jacq, F., Marchetto, C., Mun, C., Piar, L., 2014. ASTEC V2 severe accident integral code main features, current V2.0 modelling status, perspectives. Nuclear Engineering and Design 272, 119–135. https://doi.org/10.1016/j.nucengdes.2013.06.040

Coward, H.F., Jones, G.W., 1952. Limits of flammability of gases and vapors. Washington.

Díez Álvarez-Buylla, P., Estévez-Albuja, S., Jiménez, G., Gavilán, C., 2021. Analysis of venting strategies and hydrogen concentration evolution during a station blackout in a BWR-6 containment using GOTHIC 8.3. Progress in Nuclear Energy 141. https://doi.org/10.1016/j.pnucene.2021.103930

EPRI, 2018a. GOTHIC Thermal Hydraulic Analysis Package, User Manual, Version 8.3(QA). Palo Alto, CA.

EPRI, 2018b. GOTHIC Thermal Hydraulic Analysis Package, Technical Manual, Version 8.3(QA). Palo Alto, CA.

EPRI, 2013. MAAP5 - Modular Accident Analysis Program for LWR Power Plants. Palo Alto, CA.

Fernández-Cosials, K., 2017. Analysis and Improvement of Hydrogen Mitigation Strategies during a Severe Accident In Nuclear Containments (Doctoral Thesis). Technical University of Madrid, Spain.

Fernández-Cosials, K., Estévez-Albuja, S., Jiménez, G., Bocanegra, R., Vázquez-Rodríguez, C., Rey, L., Martínez-Murillo, J.C., 2019. 3D containment modeling of PWR-KWU Trillo NPP with the GOTHIC code. Ann Nucl Energy 133, 387–399. https://doi.org/10.1016/j.anucene.2019.05.041

Fernández-Cosials, K., Goñi, Z., Jiménez, G., Queral, C., Montero, J., 2017a. Three-dimensional simulation of a LBLOCA in an AP1000® containment building. Energy Procedia 127, 234–241. https://doi.org/10.1016/j.egypro.2017.08.124

Fernández-Cosials, K., Jimenez, G., Bocanegra, R., Queral, C., 2017b. Study of hydrogen risk in a PWR-W containment during a SBO scenario; Tau parameter definition and application on venting strategy analysis. Nuclear Engineering and Design 325, 164–177. https://doi.org/10.1016/j.nucengdes.2017.10.012

Fineschi, F., Bazzichi, M., Carcassi, M., 1996. A Study on the Hydrogen Recombination Rates of Catalytic Recombiners and Deliberate Ignition. Nuclear Engineering and Design 166, 481–494.

Gardner, L., Liang, Z., Clouthier, T., MacCoy, R., 2021. A large-scale study on the effect of ambient conditions on hydrogen recombiner-induced ignition. Int J Hydrogen Energy 46, 12594–12604. https://doi.org/10.1016/j.ijhydene.2020.06.132

Gharari, R., Kazeminejad, H., Mataji Kojouri, N., Hedayat, A., 2018. A review on hydrogen generation, explosion, and mitigation during severe accidents in light water nuclear reactors. Int J Hydrogen Energy 43, 1939–1965. https://doi.org/10.1016/j.ijhydene.2017.11.174

Glasstone, S., Sesonske, A., 1994. Nuclear Reactor Engineering, Nuclear Reactor Engineering. Springer US. https://doi.org/10.1007/978-1-4615-2083-2

Grosseuvres, R., Chaumeix, N., Bentaib, A., Goulier, J., 2017. The Flame “Curriculum Vitae” in the Framework of Safety Analysis, in: NURETH-17. Xian, China.

Hashim, M., Ming, Y., Saeed Ahmed, A., 2013. Review of Severe Accident Phenomena in LWR and Related Severe Accident Analysis Codes. Research Journal of Applied Sciences, Engineering and Technology 5, 3320–3335. https://doi.org/10.19026/rjaset.5.4574

Heising-Goodman, C.D., Prabhakar, A., Das, S.K., 1981. An evaluation of containment inerting and air dilution systems as methods for post-accident hydrogen control in BWRS. Nuclear Engineering and Design 64, 329–346. https://doi.org/10.1080/01457632.2015.965091

Henrie, J.O., Postma, A.K., 1987. Lessons Learned from Hydrogen Generation and Burning During the TMI-2 Event.

Humphries, L.L., Beeny, B.A., Gelbard, F., Louie, D.L., Phillips J., 2017. MELCOR Computer Code Manuals. Washington, DC.

IAEA, 2021. Hydrogen Phenomena during Severe Accidents in Water Cooled Reactors. Vienna.

IAEA, 2019. Safety Glossary 2018 Edition. IAEA Library Cataloguing in Publication Data 278.

IAEA, 2016. Safety Assessment for Facilities and Activities. Vienna.

IAEA, 2011. Mitigation of Hydrogen Hazards in Severe Accidents in Nuclear Power Plants, Iaea-Tecdoc-1661.

IAEA, 2005a. Assessment of Defence in Depth for Nuclear Power Plants. Austria.

IAEA, 2005b. WWER-1000 Reactor Simulator. Vienna.

IAEA, 2003. Safety margins of operating reactors : analysis of uncertainties and implications for decision making. Vienna.

IAEA, 2002. Accident Analysis for Nuclear Power Plants. Vienna.

IAEA, 2000. Safety of Nuclear Power Plants: Design.

IAEA, 1999. Basic safety principles for nuclear power plants : INSAG-12. International Atomic Energy Agency.

IAEA, 1996. Defence in Depth in Nuclear Safety INSAG-10. Vienna.

IAEA, 1995. Guidelines For Accident Analysis Of Wwer Nuclear Power Plants. Vienna.

IAEA, 1992. INSAG-6 Probabilistic Safety Assessment.

IRSN/CEA, 2007. Research and development with regard to severe accidents in pressurised water reactors: Summary and outlook.

Ivanov, B., Ivanov, K., Groudev, P., Pavlova, M., Hadjiev Nuclear Power Plant Kozloduy, V., 2002. VVER-1000 Coolant Transient Benchmark PHASE 1 (V1000CT-1) Vol. I: Main Coolant Pump (MCP) switching On-Final Specifications.

Jacquemain, D., 2015. Nuclear Power Reactor Core Melt Accidents, Current State of Knowledge, EDP Sciences.

Jimenez, G., Fernández-cosials, M.K., Bocanegra, R., Queral, C., 2017. Analysis of the equipment and instrumentation quali fi cation criteria using 3D containment models. Nuclear Engineering and Design 323, 28–38. https://doi.org/10.1016/j.nucengdes.2017.07.038

Kaltenbach, C., Laurien, E., 2018. CFD simulation of spray cooling in the model containment THAI. Nuclear Engineering and Design 328, 359–371. https://doi.org/10.1016/j.nucengdes.2017.12.030

Keller, V.D., 2007. Passive catalytic hydrogen recombiners for nuclear power stations. Thermal Engineering 54, 236–239. https://doi.org/10.1134/S0040601507030111

Kelm, S., Jahn, W., Reinecke, E.-A., 2008. Operational Behaviour of Catalytic Recombiners—Experimental Results and Modelling Approaches, in: Workshop on "Experiments and CFD Code Application to Nuclear Reactor Safety (XCFD4NRS)." Grenoble.

Kelm, S., Reinecke, E.-A., Jahn, W., Allelein, H.-J., 2010. Simulation of PAR operation within compartments - Coupling of REKO-DIREKT and CFX, in: 2nd International Topical Meeting on Safety and Technology of Nuclear Hydrogen Production, Control, and Management. pp. 135–140.

Kim, H.C., Pak, S.K., Lee, J.S., Cho, S.W., 2018. Validation of the MELCOR input model for a CANDU PHWR containment analysis by benchmarking against integrated leakage rate tests. Nuclear Engineering and Design 340, 201–218. https://doi.org/10.1016/j.nucengdes.2018.09.022

Kim, J., Hong, S., Park, K.-H., Kim, J.-H., Oh, J.-Y., 2022. Experimental Study on Hydrogen Recombination Characteristics of a Passive Autocatalytic Recombiner during Spray Operation. Hydrogen 3, 197–217. https://doi.org/10.3390/hydrogen3020013

Kim, J., Hong, S., Park, K.H., Kim, J.H., Oh, J.Y., 2020. Experimental study on a hydrogen stratification induced by PARs installed in a containment. Energies (Basel) 13. https://doi.org/10.3390/en13215552

Kim, J., Hong, S.W., Kim, S.B., Kim, H.D., 2005. Hydrogen mitigation strategy of the APR1400 nuclear power plant for a hypothetical station blackout accident. Nucl Technol 150, 263–282. https://doi.org/10.13182/NT05-A3621

Kim, J., Park, S.-Y., Ha, K.-S., Hong, S.-W., Kim, S.-B., 2009. Hydrogen Safety Analysis of the OPR1000 Nuclear Power Plant during a Severe Accident by a Small-Break Loss of Coolant, in: Transactions of the Korean Nuclear Society Spring Meeting Jeju.

Kljenak, I., Bentaib A., Jordan T., 2012. Early containment failure, in: Nuclear Safety in Light Water Reactors. Elsevier Inc., pp. 185–306. https://doi.org/10.1016/B978-0-12-388446-6.00003-4

Kostka, P., Techy, Z., Sienicki, J.J., 2002. ICONE10-22206 HYDROGEN MIXING ANALYSES FOR A VVER CONTAINMENT, in: 0th International Conference on Nuclear Engineering (ICONE 10).

Leyse, M., Paine, C., 2014. Preventing Hydrogen Explosions In Severe Nuclear Accidents: Unresolved Safety Issues Involving Hydrogen Generation And Mitigation, NRDC Report.

Li, Y., Zhang, H., Xiao, J., Jordan, T., 2019. Numerical study of thermal hydraulics behavior on the integral test facility for passive containment cooling system using GASFLOW-MPI. Ann Nucl Energy 123, 86–96. https://doi.org/10.1016/j.anucene.2018.09.014

Lopez-Alonso, E., Papini, D., Jimenez, G., 2017. Hydrogen distribution and Passive Autocatalytic Recombiner (PAR) mitigation in a PWR-KWU containment type. Ann Nucl Energy 109, 600–611. https://doi.org/10.1016/j.anucene.2017.05.064

Malet, J., Porcheron, E., Vendel, J., 2010. OECD International Standard Problem ISP-47 on containment thermal-hydraulics - Conclusions of the TOSQAN part. Nuclear Engineering and Design 240, 3209–3220. https://doi.org/10.1016/j.nucengdes.2010.05.061

Mathworks, 2022. MATLAB Primer R2022a, Book.

NEA/CSNI, 2014. Status Report on Hydrogen Management and Related Computer Codes. Nea/Csni/R(2014)8.

Nichols, B., Necker, G., Travis, J., Spore, J., Lam, K., Royl, P., Wilson, T., 1998. GASFLOW: A Computational Fluid Dynamics Code for Gases, Aerosols, and Combustion, Volume 2: User's Manual. https://doi.org/10.2172/1222

Noori-kalkhoran, O., Jafari-ouregani, N., Gei, M., Ahangari, R., 2019. Simulation of hydrogen distribution and effect of Engineering Safety Features (ESFs) on its mitigation in a WWER-1000 containment. Nuclear Science and Techniques 30, 1–16. https://doi.org/10.1007/s41365-019-0624-0

Noori-Kalkhoran, O., Minuchehr, A., Rahgoshay, M., Shirani, A.S., 2014a. Short-term and long-term analysis of WWER-1000 containment parameters in a large break LOCA. Progress in Nuclear Energy 74, 201–212. https://doi.org/10.1016/j.pnucene.2014.03.007

Noori-Kalkhoran, O., Rahgoshay, M., Minuchehr, A., Shirani, A.S., 2014b. Analysis of thermal-hydraulic parameters of WWER-1000 containment in a large break LOCA. Ann Nucl Energy 68, 101–111. https://doi.org/10.1016/j.anucene.2014.01.009

Noori-Kalkhoran, O., Shirani, A.S., Ahangari, R., 2016. Simulation of Containment Pressurization in a Large Break-Loss of Coolant Accident Using Single-Cell and Multicell Models and CONTAIN Code. Nuclear Engineering and Technology 48, 1140–1153. https://doi.org/10.1016/j.net.2016.03.008

NRC, 2022. Code of Federal Regulations. Title 10 Energy.

NRC, 2007. NUREG-0800, Standard Review Plan for the Review of Safety Analysis Reports for Nuclear Power Plants: LWR Edition.

NRC, 2003. NRC Letter from Anthony C. McMurtray (NRC) to Thomas Coutu (NMC),Enclosure 2, Safety Evaluation.

NRC, 1997. Perspectives on Reactor Safety.

NRC, 1979. Standard Format and Content of Safety Analysis Reports for Nuclear Power Plants (LWR Edition), Regulatory Guide 1.70. Washington, DC.

NRC, 1975. Reactor Safery Study.

OECD/NEA, 2014. Status Report on Filtered Containment Venting.

OECD/NEA, 2007. International Standard Problem ISP-47 on Containment Thermal Hydraulics: Final Report.

OECD/NEA, 2001. In-Vessel and Ex-Vessel Hydrogen Sources.

OECD/NEA, 1999. VVER-Specific Features Regarding Core Degradation.

OECD/NEA, 1996. The Implementation of Hydrogen Mitigation Techniques. Paris.

OECD/NEA, 1994. Final Comparison Report on ISP-35: NUPEC Hydrogen Mixing and Distribution Test (Test M-7-1).

Ofstun, R.P., Scobel, J.H., 2006. Westinghouse Containment Analysis Methodology.

Oslick, H., 1976. Safety Aspects Of Containment System Design For Nuclear Power Plants, in: Rust, J.H., Weaver Lynn E. (Eds.), Nuclear Safety. Pergamon, pp. 1–32. https://doi.org/https://doi.org/10.1016/B978-0-08-021744-4.50005-1

Ozdemir, O.E., George, T.L., Marshall, M.D., 2015. Fukushima Daiichi Unit 1 power plant containment analysis using GOTHIC. Ann Nucl Energy 85, 621–632. https://doi.org/10.1016/j.anucene.2015.06.017

Paladino, D., Dreier, J., 2012. PANDA: A multipurpose integral test facility for LWR safety investigations. Science and Technology of Nuclear Installations 2012. https://doi.org/10.1155/2012/239319

Papini, D., Andreani, M., Ničeno, B., Prasser, H.M., Steiner, P., Klugel, J.U., 2015. Simulation of hydrogen distribution in the containment during a severe accident with fast hydrogen-steam release. International Topical Meeting on Nuclear Reactor Thermal Hydraulics 2015, NURETH 2015 2, 1474–1487.

Papini, D., Andreani, M., Steiner, P., Ničeno, B., Klügel, J.U., Prasser, H.M., 2019. Evaluation of the PAR Mitigation System in Swiss PWR Containment Using the GOTHIC Code. Nucl Technol 205, 153–173. https://doi.org/10.1080/00295450.2018.1505356

Papini, D., Grgić, D., Cammi, A., Ricotti, M.E., 2011. Analysis of different containment models for IRIS small break LOCA, using GOTHIC and RELAP5 codes. Nuclear Engineering and Design 241, 1152–1164. https://doi.org/10.1016/j.nucengdes.2010.06.016

Park, J.S., Kim, Y., Lim, K., 2022. 3D simulation of hydrogen distributions affected by a passive auto-catalytic recombiner in an oxygen-starved condition. Int J Hydrogen Energy 47, 38395–38406. https://doi.org/10.1016/j.ijhydene.2022.08.311

Petrangeli, G., 2006. Nuclear Safety, First Edition. ed. Butterworth-Heinemann.

Philipov, S., Filipov, K., 2014. Hydrogen Distribution Assessment With Cfd Tool in Help of Severe Accident, in: 22nd International Conference on Nuclear Engineering ICONE22. pp. 1–5.

Reinecke, E.A., Kelm, S., Jahn, W., Jäkel, C., Allelein, H.J., 2013. Simulation of the efficiency of hydrogen recombiners as safety devices. Int J Hydrogen Energy 38, 8117–8124. https://doi.org/10.1016/j.ijhydene.2012.09.093

Reinecke, E.A., Tragsdorf, I.M., Gierling, K., 2004. Studies on innovative hydrogen recombiners as safety devices in the containments of light water reactors. Nuclear Engineering and Design 230, 49–59. https://doi.org/10.1016/j.nucengdes.2003.10.009

Royl, P., Rochholz, H., Breitung, W., Travis, J.R., Necker, G., 2000. Analysis of steam and hydrogen distributions with PAR mitigation in NPP containments, Nuclear Engineering and Design.

Rozeń, A., 2015. A mechanistic model of a passive autocatalytic hydrogen recombiner. Chemical and Process Engineering 36, 3–19. https://doi.org/10.1515/cpe-2015-0001

Ryzhov, S.B., Mokhov, V.A., Nikitenko, M.P., Bessalov, G.G., Podshibyakin, A.K., Anufriev, D.A., Gado, J., 2010. VVER-Type Reactors of Russian Design, in: Handbook of Nuclear Engineering. Springer .

Šadek, S., Grgić, D., Šimić, Z., 2017. Application of ASTEC, MELCOR, and MAAP Computer Codes for Thermal Hydraulic Analysis of a PWR Containment Equipped with the PCFV and PAR Systems. Science and Technology of Nuclear Installations 2017. https://doi.org/10.1155/2017/8431934

Saghafi, M., Yousefpour, F., Karimi, K., Hoseyni, S.M., 2017. Determination of PAR configuration for PWR containment design: A hydrogen mitigation strategy. Int J Hydrogen Energy 42, 7104–7119. https://doi.org/10.1016/j.ijhydene.2017.01.110

Sandia National Laboratories, 1983. Light Water Reactor Hydrogen Manual, Nureg/Cr-2726.

Sehgal, B.R., 2012. Light water reactor safety. A historical review, in: Nuclear Safety in Light Water Reactors. Elsevier Inc., pp. 1–88. https://doi.org/10.1016/B978-0-12-388446-6.00001-0

Sonnenkalb, M., Band, S., Nowack, H., Schwarz, grsde S., 2015. RE-EVALUATION OF PAR CONCEPT IN GERMAN PWR WITH REVISED PAR MODEL, in: 16th International Topical Meeting on Nuclear Reactor Thermal Hydraulics (NURETH-16) . Chicago.

Stubley, G.D., 2009. ME 566 Computational Fluid Dynamics for Fluids Engineering Design ANSYS CFX STUDENT USER MANUAL Version 11. Fluid Dynamics.

Studer, E., Magnaud, J.P., Dabbene, F., Tkatschenko, I., 2007. International standard problem on containment thermal-hydraulics ISP47. Step 1-Results from the MISTRA exercise. Nuclear Engineering and Design 237, 536–551. https://doi.org/10.1016/j.nucengdes.2006.08.008

Sun Microsystems, 2001. Fortran USER'S Guide; Forte Developer 6 update 2.

Tarasov, O. V., Kiselev, A.E., Filippov, A.S., Yudina, T.A., Grigoruk, D.G., Koshmanov, D.E., Keller, V.D., Khristenko, E.B., 2017. Development and Verification of a Model of RVK-500, -1000 Recombiners for Modeling the Containment Shells of NPP with VVER by Computational Hydrodynamics. Atomic Energy 121, 166–172. https://doi.org/10.1007/s10512-017-0178-3

Tsubakizaki, S., Masaharu, T., Hideji, G., Kenji, M., Nobuo, I., 2009. Alternatives to Hydrazine in Water Treatment at Thermal Power Plants, Mitsubishi Heavy Industries Technical Review.

Visser, D.C., Siccama, N.B., Jayaraju, S.T., Komen, E.M.J., 2014. Application of a CFD based containment model to different large-scale hydrogen distribution experiments. Nuclear Engineering and Design 278, 491–502. https://doi.org/10.1016/j.nucengdes.2014.08.005

Vryashkova, P., 2013. Investigation of oxygen depletion during hydrogen recombination for VVER1000 of Kozloduy NPP, in: 22nd International Conference Nuclear Energy for New Europe. pp. 1–10.

Wilkening, H., Baraldi, D., Heitsch, M., 2008. CFD simulations of light gas release and mixing in the Battelle Model-Containment with CFX. Nuclear Engineering and Design 238, 618–626. https://doi.org/10.1016/j.nucengdes.2007.02.042

Williams, K.M.D., Tills, J., Griffith, R.O., Gido, R.G., Tadios, E.L., Davis, F.J., Martinez, G.M., Washington, K.E., 1997. Code manual for CONTAIN 2.0: A computer code for nuclear reactor containment analysis. Sandia National Laboratories.

Xiao, J., Breitung, W., Kuznetsov, M., Zhang, H., Travis, J.R., Redlinger, R., Jordan, T., 2017. GASFLOW-MPI: A new 3-D parallel all-speed CFD code for turbulent dispersion and combustion simulations: Part I: Models, verification and validation. Int J Hydrogen Energy 42, 8346–8368. https://doi.org/10.1016/j.ijhydene.2017.01.215

Xiao, J., Travis, J.R., Royl, P., Necker, G., Svishchev, A., Jordan, T., 2016. Three-dimensional all-speed CFD code for safety analysis of nuclear reactor containment: Status of GASFLOW parallelization, model development, validation and application. Nuclear Engineering and Design 301, 290–310. https://doi.org/10.1016/j.nucengdes.2015.12.033

Xiong, J., Yang, Y., Cheng, X., 2009. CFD application to hydrogen risk analysis and PAR qualification. Science and Technology of Nuclear Installations 2009. https://doi.org/10.1155/2009/213981

Zhu, J., Zhang, X., Cheng, X., 2016. Assessment of Prediction Capabilities of COCOSYS and CFX Code for Simplified Containment. Science and Technology of Nuclear Installations 2016. https://doi.org/10.1155/2016/9542121